EFFECT OF LIQUID AND GAS PHYSICAL PROPERTIES ON THE HYDRODYNAMICS OF PACKED COLUMNS

by

Ulrich Ludkin Minne

Thesis presented in partial fulfilment
of the requirements for the Degree

of

MASTER OF ENGINEERING
(CHEMICAL ENGINEERING)

in the Faculty of Engineering
at Stellenbosch University

Supervisor

Professor C.E. Schwarz

Co-Supervisor/s

Professor A.J. Burger

December 2017

DECLARATION

By submitting this thesis electronically, I declare that the entirety of the work contained therein is my own, original work, that I am the sole author thereof (save to the extent explicitly otherwise stated), that reproduction and publication thereof by Stellenbosch University will not infringe any third party rights and that I have not previously in its entirety or in part submitted it for obtaining any qualification.

Date: December 2017

Abstract

To fully utilise the higher capacity and separation efficiency of modern random packings, models are required that are capable of accurately predicting the capacity and separation efficiency of these packings. Since the capacity and separation efficiency in packed columns are influenced by the physical properties of liquids and gases, experimental data with varied liquid and gas physical properties are required for both the development and validation of these models.

The aim of this project was to investigate the effect of liquid and gas physical properties on the hydrodynamic behaviour of Intalox Ultra A and O random packing with nominal sizes of 1.5" and 2.5", respectively. This was achieved experimentally by measuring the pressure drop, liquid hold-up and liquid entrainment for four liquids with different viscosities, densities and surface tensions, and two gasses with different densities, at different liquid flow rates over the entire hydrodynamic range.

The pilot plant in which the experimental work was performed had a column diameter of 400 mm and a packed bed height of 3 m. Liquid flow rates of 6, 37, 73, 98 and 122 $m^3/(m^2.h)$ were investigated. The small open area of the existing pan type distributor restricted the accurate measurement of liquid entrainment. Therefore, it was replaced with a channel-type distributor, doubling the available open area for gas flow to 60 %.

A method was developed to identify the loading and flooding points when presented with the experimental pressure drop data, based on the statistical approach of prediction intervals of regressed curves. Overall, this method provides relatively accurate identification of the loading and flooding points at high liquid flow rates, while the use of entrainment data in identifying the flooding point was found to over-predict the flooding point at high liquid flow rates.

The high viscosity of silicone oil and ethylene glycol resulted in these liquids having higher pre-loading liquid hold-up compared to that of water and Isopar G. For silicone oil and ethylene glycol, the ratio of viscous forces over the gravitational forces is much larger than for water and Isopar G. Despite the difference in their physical properties, Isopar G and silicone oil produced very similar flooding velocities, which were lower than that of water and ethylene glycol. While the high viscosity of silicone oil resists the flow of liquid down the column, resulting in low capacity, the low density of Isopar G allows the upward drag force of the gas to counteract the gravitational force on the liquid at a lower gas flow rate than the other liquids with higher densities.

At the same superficial gas velocity, carbon dioxide, with a higher gas density, produced a higher pressure drop than air/nitrogen, as well as a higher liquid hold-up above the loading point. This is a

result of the higher gas kinetic energy of carbon dioxide compared to air/nitrogen at the same superficial gas velocity.

The general effect of increasing the packing size from 1.5" Intalox Ultra A to 2.5" Intalox Ultra O is a reduction in both pressure drop and liquid hold-up, as well as an increase in capacity of approximately 11 % at a liquid flow rate of 6 $m^3/(m^2.h)$, increasing to approximately 37 % at a liquid flow rate of 122 $m^3/(m^2.h)$.

A comparison of the Billet and Schultes, Maćkowiak and Stichlmair model predictions for the experimental data showed that in general all three models predict the pre-loading pressure drop for both packings with all four liquids poorly. Overall, the Maćkowiak model predicts flooding points better than the other two models. The Maćkowiak model is the only model based on the droplet entrainment modelling approach, whereas the Billet and Schultes and Stichlmair models are based on the liquid film modelling approach. The Maćkowiak model is the only model that takes into account the surface tension of the liquid. The experimental pressure drop was also compared to the pressure drop predicted with KG-Tower. The predicted and experimental pressure drop were in good agreement in the pre-loading region, with some deviation at higher gas flow rates. Overall, KG-Tower predicted the pressure drop better than the Billet and Schultes, Maćkowiak and Stichlmair models.

The project created an extensive data set of experimental hydrodynamic data, for a range of physical fluid properties, which can be used in both the verification of existing hydrodynamic models and the development of new models.

Samevatting

Om die verhoogde kapasiteit en skeidingsdoeltreffendheid van moderne ongeordende pakking ten volle te benut, word modelle benodig wat in staat is om die kapasiteit en skeidingsdoeltreffendheid van hierdie pakking akkuraat te voorspel. Aangesien die kapasiteit en skeidingsdoeltreffendheid in gepakte kolomme beïnvloed word deur die fisiese eienskappe van vloeistowwe en gasse, word eksperimentele data met gevarieerde vloeistof en gas fisiese eienskappe benodig vir beide die ontwikkeling en validering van hierdie modelle.

Die doel van hierdie projek was om die effek van vloeistof en gas se fisiese eienskappe op die hidrodinamiese gedrag van Intalox Ultra A en O ongeordende pakking, met nominale groottes van onderskeidelik 1.5” en 2.5”, te ondersoek. Dit is behaal deur eksperimenteel die drukval, vloeistof inhoud en vloeistof meesleuring van vier vloeistowwe met verskillende viskositeite, digthede en oppervlaktespannings, en twee gasse met verskillende digthede, by verskillende vloeistof vloeitempo’s, oor die hele hidrodinamiese gebied te meet.

Die lootsaanleg waarin die eksperimentele werk uitgevoer is, het 'n kolom deursnee van 400 mm en 'n gepakte bedhoogte van 3 m. Vloeistof vloeitempo’s van 6, 37, 73, 98 en 122 $m^3/(m^2.h)$ is ondersoek. Die klein oop area van die bestaande pan-tipe verspreider het die akkurate meting van vloeistof meesleuring beperk. Daarom is dit vervang met 'n kanaal-tipe verspreider, wat die beskikbare oop area vir gasvloei verdubbel het tot 60 %.

'n Metode is ontwikkel om die ladingspunte en vloedpunte te identifiseer. Die metode maak gebruik van die eksperimentele drukvaldata en is gebaseer op die statistiese benadering van voorspellingsintervalle van regresseerde kurwes. Oor die algemeen bied hierdie metode relatief akkurate identifisering van die ladingspunte en vloedpunte by hoë vloeistof vloeitempo's, terwyl die gebruik van vloeistof meesleuring data vir die identifisering van die vloedpunt, die vloedpunt oorvoorspel by hoë vloeistof vloeitempo's.

Die hoë viskositeit van silikoonolie en etileenglikol het daartoe gelei dat hierdie vloeistowwe hoër vloeistof inhoud in die ladingsgebied het in vergelyking met die van water en Isopar G. Vir silikoonolie en etileenglikol is die verhouding van viskosekragte oor die gravitasiekragte veel groter as vir water en Isopar G. Ten spyte van die verskil in hul fisiese eienskappe het Isopar G en silikoonolie baie soortgelyke vloedpunt snelhede opgelewer, wat laer is as die van water en etileenglikol. Terwyl die hoë viskositeit van silikoonolie die afwaartse vloei van vloeistof in die kolom weerstaan, en gevolglik lae kapasiteit veroorsaak, veroorsaak die lae digtheid van Isopar G dat die opwaartse sleurkrag van

die gas die gravitasiekrag op die vloeistof by ‘n laer gasvloeitempo teen werk as vir die ander vloeistowwe met hoër digthede.

By dieselfde oppervlakte-gassnelheid het koolstofdioksied, met 'n hoër gasdigtheid, 'n hoër drukval as lug/stikstof ervaar, as ook 'n hoër vloeistof inhoud bo die ladingspunt veroorsaak. Dit is as gevolg van die hoër gaskinetiese energie van koolstofdioksied in vergelyking met lug/stikstof by dieselfde oppervlakte-gassnelheid.

Die algemene effek van die verhoging van die pakkingsgrootte van 1.5" Intalox Ultra A tot 2.5" Intalox Ultra O is 'n afname in beide drukval en vloeistof inhoud, sowel as 'n toename in kapasiteit van ongeveer 11 % teen 'n vloeistof vloeitempo van 6 $m^3/(m^2.h)$, wat verhoog na ongeveer 37 % teen 'n vloeistof vloeitempo van 122 $m^3/(m^2.h)$.

'n Vergelyking van die Billet en Schultes, Maćkowiak en Stichlmair modelvoorspellings vir die eksperimentele data het getoon dat in die algemeen al drie modelle die voor-ladings-drukval, vir beide van die pakking, met al vier vloeistowwe, swak voorspel. Oor die algemeen voorspel die Maćkowiak model die vloedpunte beter as die ander twee modelle. Die Maćkowiak model is die enigste model wat gebaseer is op die drupel-meesleuring-modellerings-benadering, terwyl die Billet en Schultes en Stichlmair modelle gebaseer is op die vloeistoffilm-modellerings-benadering. Die Maćkowiak model is ook die enigste model wat die oppervlakspanning van die vloeistof in ag neem. Die eksperimentele drukval is ook vergelyk met die drukval wat deur KG-Tower voorspel is. Die voorspelde en eksperimentele drukval het goed vergelyk in die voor-ladingsgebied, met 'n mate van afwyking by hoër gasvloeitempo’s. Oor die algemeen het KG-Tower die drukval beter as die Billet en Schultes, Maćkowiak en Stichlmair modelle voorspel.

Die projek het 'n omvattende datastel van eksperimentele hidrodinamiese data, vir ‘n uitgebreide omvang van fisiese vloeistof eienskappe, geskep, wat gebruik kan word in beide die verifikasie van bestaande hidrodinamiese modelle en die ontwikkeling van nuwe modelle.

Acknowledgements

When we achieve, we usually do so because others have helped. I would like to extend my sincere gratitude to:

- My supervisors, Prof. C.E. Schwarz and Prof. A.J. Burger, for their guidance through my ignorance, encouragement when it was needed, and immense patience throughout this project.
- Sarel Lamprecht, L.J. Du Preez and Jamie Cripwell for their help and guidance.
- The workshop staff, oom Anton, oom Jos and Brent, because taking a packed column apart and putting it back together is not a one-man job.
- The laboratory staff, Alvin, Linda, Ollie and the late Vincent Carolissen, for always willing to lend a hand when needed.
- The analytical laboratory staff, Mrs. Botha, Levine and Jaco, for their help with all analytical work.
- The friends that were always there when needed.
- My family, for their unconditional love and support.
- Johanné Kleinhans, who stood beside me throughout this journey, for sacrificing so much through your continuous support.

This project was supported by the **Department of Process Engineering, Stellenbosch University, Koch-Glitsch, LP., Sasol (Pty) Ltd.** and the **National Research Foundation (NRF).**

Table of Contents

Nomenclature

Symbol	Definition	Units
a	Specific surface area of random packing	$\frac{m^2}{m^3}$
A_0	Venturi contraction area	m^2
a_h	Billet and Schultes hydraulic surface area	$\frac{m^2}{m^3}$
B_L	Dimensionless irrigation density	-
C_1, C_2, C_3	Stichlmair packing-specific constants	-
C_D	Venturi discharge coefficient	-
$C_{Fl,0}$	Maćkowiak flood factor for packings	
$C_{Fl,P}$	Billet and Schultes flooding point packing-specific constant	-
C_h	Billet and Schultes liquid hold-up constant	-
C_p	Billet and Schultes pressure drop constant	-
$C_{S,P}$	Billet and Schultes loading point packing-specific constant	-
D	Column diameter	m
d_h	Hydraulic diameter of packed bed	m
d_p	Particle diameter	m
d_p'	Stichlmair particle diameter including surface liquid	m
d_T	Droplet diameter	m
f_0	Stichlmair friction factor for flow past a single particle	-
f_0'	Stichlmair friction factor for wet particle	-
F_G	Vapour flow factor	$\left(\frac{m}{s}\right) \cdot \left(\frac{kg}{m^3}\right)^{0.5}$
$F_{G,Fl}$	Vapour flow factor at flooding	$\left(\frac{m}{s}\right) \cdot \left(\frac{kg}{m^3}\right)^{0.5}$
F_p	Packing Factor	-

Fr_L	Liquid Froude number	-
g	Gravitational constant	$\frac{m}{s^2}$
G	Gas mass flow rate	$\frac{kg}{h}$
H	Packed bed height	m
h_L	Total liquid hold-up	$\frac{m^3}{m^3}$
$h_{L,Fl}$	Liquid Hold-up at flooding	$\frac{m^3}{m^3}$
$h_{L,S}$	Liquid hold-up below loading point	$\frac{m^3}{m^3}$
K	Wall factor	-
K_A	Maćkowiak lift force	N
K_g	Maćkowiak gravitational force	N
K_ψ	Maćkowiak thrust force	N
L	Liquid mass flow rate	$\frac{kg}{h}$
L'	Liquid entrainment rate	$\frac{kg}{h}$
LRV	Lower range value	-
n_{Fl}	Billet and Schultes flooding point exponent	-
n_S	Billet and Schultes loading point exponent	-
Q	Liquid volume flow rate	$\frac{m^3}{h}$
R_G	Gas Reynolds number	-
R_L	Liquid Reynolds number	-
u_0	Effective falling velocity of droplet	$\frac{m}{s}$
u_G	Superficial gas velocity	$\frac{m^3}{m^2 \cdot s}$
$u_{G,Fl}$	Superficial gas velocity at the flooding point	$\frac{m^3}{m^2 \cdot s}$
$u_{G,S}$	Superficial gas velocity at the loading point	$\frac{m^3}{m^2 \cdot s}$
u_L	Superficial liquid velocity	$\frac{m^3}{m^2 \cdot s}$

$u_{L,S}$	Superficial liquid velocity at the loading point	$\frac{m^3}{m^2 \cdot s}$
URL	Upper range limit	kPa
URV	Upper range value	-

Greek Symbols

Symbol	Definition	Units
ΔH	Height difference	m
ΔP	Pressure drop	Pa
ΔP_{dry}	Dry bed pressure drop	Pa
ΔP_{irr}	Irrigated pressure drop	Pa
ε	Packing void fraction	$\frac{m^3}{m^3}$
ε'	Stichlmair irrigated packing void fraction	$\frac{m^3}{m^3}$
θ	Maćkowiak packing-specific constant	-
λ_0	Maćkowiak phase flow ratio at flooding point	-
μ_G	Dynamic gas viscosity	$\frac{kg}{m \cdot s}$
μ_L	Dynamic liquid viscosity	$\frac{kg}{m \cdot s}$
μ_w	Dynamic viscosity of water	$\frac{kg}{m \cdot s}$
ν_L	Kinematic liquid viscosity	cSt
ρ_G	Gas density	$\frac{kg}{m^3}$
ρ_L	Liquid density	$\frac{kg}{m^3}$
ρ_w	Density of water	$\frac{kg}{m^3}$
ψ_{dry}	Billet & Schultes dry bed resistance coefficient	-
ψ_{Fl}	Billet and Schultes resistance coefficient at flooding	-
ψ_{Fl}^*	Maćkowiak drag coefficient of dry packing at flooding	-

ψ_{irr}	Billet and Schultes irrigated bed resistance coefficient	-
ψ_S	Billet and Schultes resistance coefficient at the loading point	-
ψ_T	Maćkowiak drag coefficient of falling droplet	-

Glossary

Absolute Average Relative Error (AARE)

The average of the absolute difference between all predicted and experimental values.

$$: \boldsymbol{AARE}\ [\%] = \frac{\mathbf{100}}{\boldsymbol{N}} \cdot \sum_{\boldsymbol{i=1}}^{\boldsymbol{N}} \left| \frac{\boldsymbol{x_i}^{\boldsymbol{calc}} - \boldsymbol{x_i}^{\boldsymbol{Exp}}}{\boldsymbol{x_i}^{\boldsymbol{Exp}}} \right|$$

Where:

N : is the number of data points

x_i : is the parameter that is evaluated

Average Relative Error (ARE)

The average of the difference between all predicted and experimental values.

$$: \boldsymbol{AARE}\ [\%] = \frac{\mathbf{100}}{\boldsymbol{N}} \cdot \sum_{\boldsymbol{i=1}}^{\boldsymbol{N}} \frac{\boldsymbol{x_i}^{\boldsymbol{calc}} - \boldsymbol{x_i}^{\boldsymbol{Exp}}}{\boldsymbol{x_i}^{\boldsymbol{Exp}}}$$

Where:

N : is the number of data points

x_i : is the parameter that is evaluated

1. Introduction

1.1 Background

Despite the high capital cost and energy-intensive nature of distillation, it is still one of the most widely used separation technologies in the process industry (Górak and Olujić, 2014). With the current demand for more sustainable processes, development in the field of distillation has been focussed on improving equipment and integrating processes in an attempt to increase separation efficiency and capacity. For a large industrial company to stay competitive, development and implementation of innovative separation technology is necessary. Also required is the minimization of capital expenditures and operating costs while production capacity is increased (Olujić *et al*. 2009). To pursue this goal one focus area has been the improvement of performance characteristics associated with the liquid vapour contacting devices. This has led to a number of different modern random and structured packings being developed.

To utilise these modern packings in either newly designed columns or retrofitting existing columns, accurate predictions of the capacity and separation efficiency is required to take full advantage of improved performance of these modern packings. The separation efficiency and capacity of packed columns are influenced by both thermodynamic and hydrodynamic characteristics. The hydrodynamic behaviour in packed columns is again influenced by the physical liquid and gas properties, the type, size and material of packing, column size and operating conditions. Most of the models found in literature that are used for predicting hydrodynamic behaviour are semi-empirical. These models require experimentally determined constants that are dependent on the type, size and material of packing that is used. As a result, the predictions of hydrodynamic behaviour in packed columns are still dependent on experimental pressure drop and liquid hold-up data, obtained through pilot plant experimentation under industrial operating conditions.

Over the past 80 years a significant amount of research has been done on packed column hydrodynamics, building up data banks of experimental pressure drop and liquid hold-up data on different packings, fluid properties and column sizes (Piché *et al*. 2001-A, 2001-B). However, a great deal of this work consists of hydrodynamic data for mostly air/water systems, as well as older generation packings. The hydrodynamic models developed and validated with this data thus apply to the older generation packings for which they were developed and for which the required packing-specific constants are available (Kuźniewska-Lach, 1999). For modern lattice type packings, for which

the packing-specific constants for these models are not available, the validity of these models is unknown and experimental data are required for further investigation.

The focus of this project is on the hydrodynamic behaviour of Intalox Ultra, a fourth generation random packing manufactured by Koch-Glitch. The influence of liquid and gas physical properties, as well as the nominal packing diameter on the pressure drop and liquid hold-up are investigated, while liquid entrainment is used as an additional measure to determine hydrodynamic capacity. The experimental data, trends and observations obtained through this project will provide a better understanding of the influence of these parameters on the hydrodynamic behaviour of modern lattice type packings and support the development of more accurate hydrodynamic models.

1.2 Objectives

The aim of this project was to **investigate the effect of physical liquid and gas properties on the hydrodynamic behaviour of random packing of the same type, but different nominal size**. The stated aim was pursued by setting the following objectives:

1. Design and build a new liquid distributor with an open area larger than the available distributor, which was unable to measure liquid entrainment accurately.
2. Validate the experimental data by comparison with the experimental data measured by Lamprecht (2010) under similar conditions.
3. Measure the pressure drop, liquid hold-up and liquid entrainment for:
    - Intalox Ultra A and O random packing with nominal sizes of 1.5” and 2.5” respectively
    - Four liquids with different physical properties
    - Two gasses with different physical properties
    - Five different liquid flow rates
    - Different gas flow rates covering the entire hydrodynamic spectrum from loading to superflood breakpoint
4. Develop a method to accurately identify the loading and flooding points from the experimental data.
5. Examine and draw conclusions on the effect of liquid density, viscosity and surface tension and gas density and viscosity, as well as the packing nominal size, on the pressure drop and liquid hold-up and ultimately the different operating regions.
6. Compare the experimental pressure drop and liquid hold-up data to pressure drop and liquid hold-up predicted with the semi-theoretical hydrodynamic models available in literature

1.3 Scope

1.3.1 Liquid Flow Rates

The liquid flow rates that were investigated for this project were chosen to correspond with those used by Lamprecht (2010). Lamprecht (2010) conducted a large amount of experimental work on different random packings in the same experimental setup. By investigating corresponding liquid flow rates this project builds on the experimental data set already established and allows for comparison under similar conditions. The liquid flow rates investigated by Lamprecht (2010) were chosen to cover the range used in the validation of hydrodynamic models for previous generations of packing, but also to go beyond this range by investigating even higher liquid flow rates.

The liquid flow rates selected in this project are: 6, 37, 73, 98, and 122 $m^3/(m^2.h)$.

1.3.2 Liquid and Gas Physical Properties

The liquids and gasses used in this project were selected to ensure that the investigated range of physical properties extend as far as possible. The selection was also influenced by these liquids already being available in the department from previous hydrodynamic studies.

The factors initially accounted for when selecting the liquids and gasses included safety concerns and minimization of mass transfer. If a flammable liquid with a high vapour pressure and a low flashpoint is chosen, there is a risk of an explosion. To cover a wide range of liquid properties, the use of flammable liquids is however necessary. To minimize this risk, pure inert gasses (nitrogen and carbon dioxide) were used when working with flammable liquids. When choosing a liquid with a high vapour pressure, evaporation of the liquid is inevitable, meaning that mass transfer will take place. To avoid the evaporation of liquid as far as possible, an operating temperature of 25^{o}C was chosen.

While the operating pressure when working with air was at atmospheric pressure, the pressure was slightly above atmospheric when working with nitrogen and carbon dioxide to prevent air from entering the system.

Table 1.1 and Table 1.2 list the liquids and gasses that were used in this study, together with their physical properties. The physical liquid property values of the different liquids are the average values measured for these properties throughout the project. The physical gas property values were obtained from Perry & Green (2008).

Table 1.1: Liquid physical properties at 25°C and 1 atm

Liquid	Density [kg/m³]	Dynamic Viscosity [mPa.s]	Surface Tension [mN/m]
Silicone Oil	958	57	20
Ethylene Glycol	1095	11	34
Isopar G	736	0.84	23
Water	995	0.89	62

Table 1.2: Gas physical properties at 25°C and 1 atm

Gas	Density [kg/m³]	Dynamic Viscosity [mPa.s]
Air	1.18	$1.84x10^{-2}$
N_2	1.15	$1.78x10^{-2}$
CO_2	1.81	$1.49x10^{-2}$

1.4 Thesis Outline

Section 2 of this thesis start with an overview of the development of different generations of random packing, followed by a discussion on liquid distribution and the different liquid distributor designs that are used in packed columns. The different parameters (pressure drop, liquid hold-up and entrainment) by which hydrodynamic behaviour is characterized are discussed, along with the different hydrodynamic operating regions that can be identified from these parameters. The effects of different physical fluid properties on these parameters, as described in literature, are discussed, followed by the effect of random packing nominal size. Lastly in this section, the different hydrodynamic models available in literature are studied.

Section 3 describes the experimental setup that was used in this project and the required modifications that were made. An overview of the experimental procedures and the measurement accuracy are also provided.

In ***Section 4*** the experimental data measured in this project are verified and a method is developed by which the different hydrodynamic operating regions can be identified. The effect of the physical liquid

and gas properties on the parameters (pressure drop and liquid hold-up) characterizing hydrodynamic operating regions are discussed with regard to the experimental data. The effect of packing size is also discussed.

In ***Section 5*** the available hydrodynamic models, discussed in ***Section 2***, are compared to the experimental data.

Sections 6 and ***Section 7*** provide the conclusions and recommendations, respectively, while the cited literature can be found in ***Section 8***. ***Section 9*** provides the data on the calibration and verification of different measured parameters, as well as a more detailed analysis of measurement accuracy. Also provided in this section are step-by-step experimental procedures. Lastly graphs of all the experimental data are provided.

2. Literature Review

This section provides the required background on packed column hydrodynamics and the different parameters affecting hydrodynamic behaviour. It also highlights the importance of hydrodynamic operating regions with regard to the operation of a packed column.

2.1 Distillation, Absorption & Stripping

The separation processes in which chemical species are either transferred from a gas phase mixture to a liquid phase or removed from liquid phase mixture and transferred to a gas phase are known respectively as absorption and stripping (Henley et al. 2011). The distillation process consists of both absorption and stripping processes occurring in the same separation column. The mass transfer, or mass or molar flux, is a function of both the concentration difference of species between the two phases as well as the contact area between the two phases (Henley et al. 2011). To increase the mass or molar flux thus requires either an increase in the concentration difference between the species or an increase in the contact area between the liquid and gas phase available for mass transfer.

2.2 Column Internals

It is the function of the column internals to provide a large interfacial area for liquid and gas contact, as well as appropriate distribution over the cross sectional area of the column. According to Olujić *et al*. (2009) the key to successful implementation of energy and cost saving configurations in distillation columns lies in the development of novel and better performing liquid-vapour contacting devices, designed for particular separation tasks. The most common contacting devices used in industrial distillation processes can be classified into two categories, namely trays and packing; with each having features that makes one more appropriate than the other for particular separation applications. This project focuses on packing. For more information on trays as contacting devices the reader is referred to Uys (2012) who studied the effect of physical liquid and gas properties on the hydrodynamic behaviour in a tray column.

2.2.1 Packing

The contacting devices known as packing can be classified as random packing, structured packing or grid packing. Although random packing is the most common packing type in commercial use, structured packing has seen continuous increase in market share. Grid packing is primarily used in heat transfer and wash services where high fouling resistance is necessary (Kister, 1992). While tray columns can be divided into distinct liquid-vapour contacting stages, columns containing random,

structured and grid packings have a continuous liquid-vapour contacting interface throughout the column. The liquid-vapour contact is established through the flow of liquid down the column as films, rivulets or droplets on the packing elements, while the vapour flows up through the wetted packing, contacting the liquid (Henley *et al.* 2011).

To date the development of both random and structured packing can be divided into four distinct phases, also referred to as generations. Even though the focus of improvement of each successive generation was on increasing capacity and efficiency, a recurring aspect of packed columns mentioned in literature is the trade-off between capacity and efficiency (Bessou *et al*. 2010; Kister, 1992; Nieuwoudt *et al*. 2010; Olujić *et al*. 2009). The objective of any packing is thus to maximize efficiency for a given capacity, or vice versa. The following quote from Nieuwoudt *et al*. (2010) highlights the problem and attitude that packing manufacturers had to take on in the development of a new generation of packing:

"It becomes evident that the refiner had to make a choice when it came to revamping a tower: give up some efficiency for extra capacity or give up some capacity to get extra efficiency. But why can we not have both?"

To develop an effective packing and thus maximize both capacity and efficiency, Kister (1992) lists the following objectives that should be pursued (Kister, 1992):

- Maximizing the packing surface area
- Uniform spread of surface area
- Create an even distribution of vapour and liquid flow throughout the packed bed
- Minimize stagnant liquid pockets by allowing liquid to freely drain from the packing
- Promote maximum wetting of the packing surface area
- Maximize the packing voidage
- Provide uniform resistance to both liquid and vapour flow throughout the packed bed, while the friction to gas flow is minimized
- Allow easy vapour-liquid disengagement
- Minimize mechanical deformation under the weight of the packed bed

Structured packing

Structured packing typically consists of multiple layers of either corrugated sheets or crimped wire mesh, arranged in an orderly manner to form packing elements (Kister, 1992). The corrugated sheets or crimped wire mesh are arranged vertically and parallel, while the triangular corrugations are

inclined with respect to the column axis (Schultes *et al*. 2010). Typically the inclination angle is either 45° or 60° with respect to the horizontal. The packing elements are also rotated 90° with respect to its top or bottom element, ensuring a uniform spread of liquid and vapour in all radial planes. With regard to surface features, the corrugated sheets or crimped wire mesh may have perforations, while the surface of corrugated sheets may be grooved, textured or smooth (Kister, 1992).

Random packing

Random packing, also referred to as dumped packing, are discrete packing elements with a specific geometric shape. These packing pieces are dumped or randomly packed in the shell of a column, providing the surface area required for liquid-vapour contact. The first generation of packing (1907 – 1950s) produced the Raschig ring and the Berl saddle. The better aerodynamic shape of the Berl saddle resulted in lower pressure drop and higher capacity compared to the Raschig ring, as well as larger surface area (Kister, 1992; Dutta, 2007). These two basic shapes became the ancestors of modern random packing from which successive generations were developed. Since these packings have all been superseded by more modern packings, first generation packings are seldom used in packed columns today (Kister, 1992).

Two popular geometries produced as the second generation of random packing (1950s – 1970s) are the Pall ring and the Intalox saddle, which respectively evolved from the first generation Raschig ring and Berl saddle (Kister, 1992). By cutting window-like shapes in the cylinder wall of the Raschig ring and bending these window tongues into the cylinder, the packing element was opened up. This newly open shaped Pall ring produced a lower pressure drop while capacity was also dramatically enhanced. The bent tongues resulted in better area distribution around the element, which improved separation efficiency (Kister, 1992). By modifying the shape of the Berl saddle in such a way as to prevent the formation of stagnant pools of liquid, trapping of vapour and abrupt changes in vapour flow direction, the newly formed Intalox saddles showed higher capacity and efficiency and a lower pressure drop (Kister, 1992).

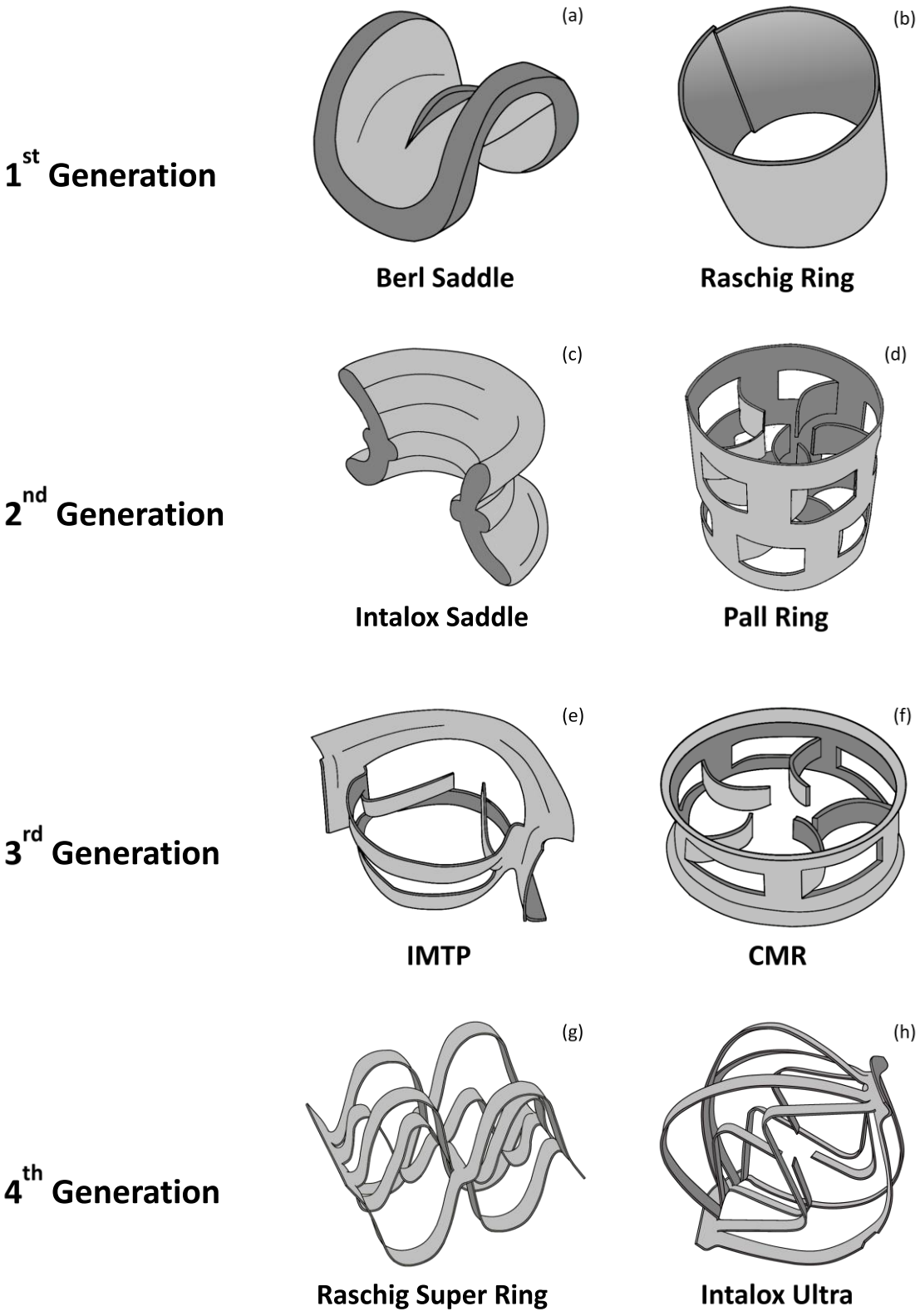

Figure 2.1: Generations of random packing – Redrawn from: (a) Schultes (2003); (c) and (f) Maćkowiak (2009); (g) Raschig-USA (n.d.); (b), (d), (e) and (h) author's photographs

The third generation of random packing (1970s – 1990s) produced a range of popular geometries, of which most evolved from the Pall ring and Intalox saddles (Kister, 1992). The most common random packings forming part of the third generation include the Cascade Mini Ring (CMR), Nutter-ring and the Intalox Metal Tower Packing (IMTP) (Schultes *et al*. 2010). The CMR is very similar to the Pall ring, but with a smaller height to diameter ratio. This is believed to better orient the packing elements so that the open sides of the packing face in the direction of gas flow. This results in reduced friction, while also increasing the surface area exposed for mass transfer (Kister, 1992; Nieuwoudt *et al*. 2010). The Nutter-ring and IMTP can be seen as ring/saddle hybrids, which incorporate both the ring and saddle shape for improved mass transfer and pressure drop, respectively (Schultes *et al*. 2010). The well distributed surface area and high voidage of the Pall ring is combined with the low aerodynamic drag of the saddle shape to produce IMTP. The Nutter-ring has an open structure with better liquid spread when compared to the second generation saddle shapes, while retaining the saddle shape's low pressure drop (Kister, 1992).

In general the second and third generation random packings utilized tongues in their packing shape that promote the formation of droplets. It was believed that the formation of droplets resulted in higher mass transfer rates, since the droplet surface provides a large surface area. However, Schultes *et al*. (2010) state that the droplets filling the packing element void space create resistance drag on vapour flow, resulting in high pressure drop. Liquid droplets are also entrained at much lower vapour flow rates compared to film-flows, resulting in lower capacity.

With the fourth generation of random packing (1990s - present) a departure from the ring, saddle and hybrid shape packings are seen (Nieuwoudt *et al*. 2010; Schultes *et al*. 2010). The Raschig Super Ring (RSR), known as the first fourth generation random packing, has an open structure with uniform material distribution in the form of sinusoidal waves (Schultes *et al*. 2010). This structure promotes the formation of turbulent liquid films over the packing element while droplet formation is minimized. This leads to a high capacity for the RSR, while the evenly wetted packing results in excellent mass transfer efficiency (Schultes, 2003; Schultes *et al*. 2010).

When considering RSR as well as the first, second and third generation random packings discussed, it can be noted that from certain vantage points it is not possible to see through these packing elements, if at all possible from another angle. Depending on the orientation of the packing element the available vapour flow path will thus be different (Nieuwoudt *et al.* 2010). A characteristic of packing elements where the performance depends on a preferential orientation presents a number of disadvantages. It can be reasoned that if the packing elements are preferentially orientated so that downstream

surfaces are shielded by upstream surfaces, mass transfer on the downstream surfaces can be negatively affected, as well as generating a higher pressure drop (Nieuwoudt, 2010).

One of the primary requirements in the development of the fourth generation Intalox Ultra was a packing that has both high capacity and mass transfer, as well as low pressure drop, regardless of the packing element orientation (Nieuwoudt, 2010). The Intalox Ultra random packing consists of a pair of curved side strips, which are flanged for added strength. Extending from these side strips are the inner and outer arched ribs with different heights and shapes forming the inner area of the packing (Nieuwoudt, 2010). The continuous outer ribs are dented to provide strength, while the smooth inner ribs are either continuous between the two side strips or discontinuous (Nieuwoudt *et al*. 2010). Both the inner and outer ribs are shaped to minimize nesting, since nesting can promote liquid and vapour channelling within the packed bed, reducing mass transfer efficiency (Nieuwoudt *et al*. 2010). Even though the inner and outer ribs are oriented to create an even distribution of available surface area inside the volume of the packing element, the outer shell of the element is relatively open from all angles to allow access to the inner surface area (Nieuwoudt, 2010). The performance of Intalox Ultra can thus be regarded as element orientation independent (Nieuwoudt *et al.* 2010).

2.2.2 Liquid and Gas Distribution

An aspect of concern in packed columns is the distribution of liquid and vapour throughout the radial area of the column, since this directly influences packing efficiency (Kister, 1992). To achieve a uniform distribution, liquid and gas distributors are used. The liquid distributor is located at the top of the column distributing the feed or reflux uniformly over the packing material. An ideal liquid distributor has the following characteristics (Koch-Glitch LP., 2010):

- Uniform liquid distribution
- Resistance to plugging or fouling
- A wide operating range in terms of liquid flow rate
- Low vapour phase pressure drop
- Minimal use of vessel height

While a central open feed pipe or a spray nozzle may be adequate for a small diameter column, more elaborate designs are used for larger diameter columns (Sinnott & Towler, 2009). Different distributor designs that are used, each with certain advantages in specific applications, include:

- Pan Distributor
- Deck Distributor
- Channel Distributors
- Trough Distributors
- Annular/Lateral Pipe Distributors

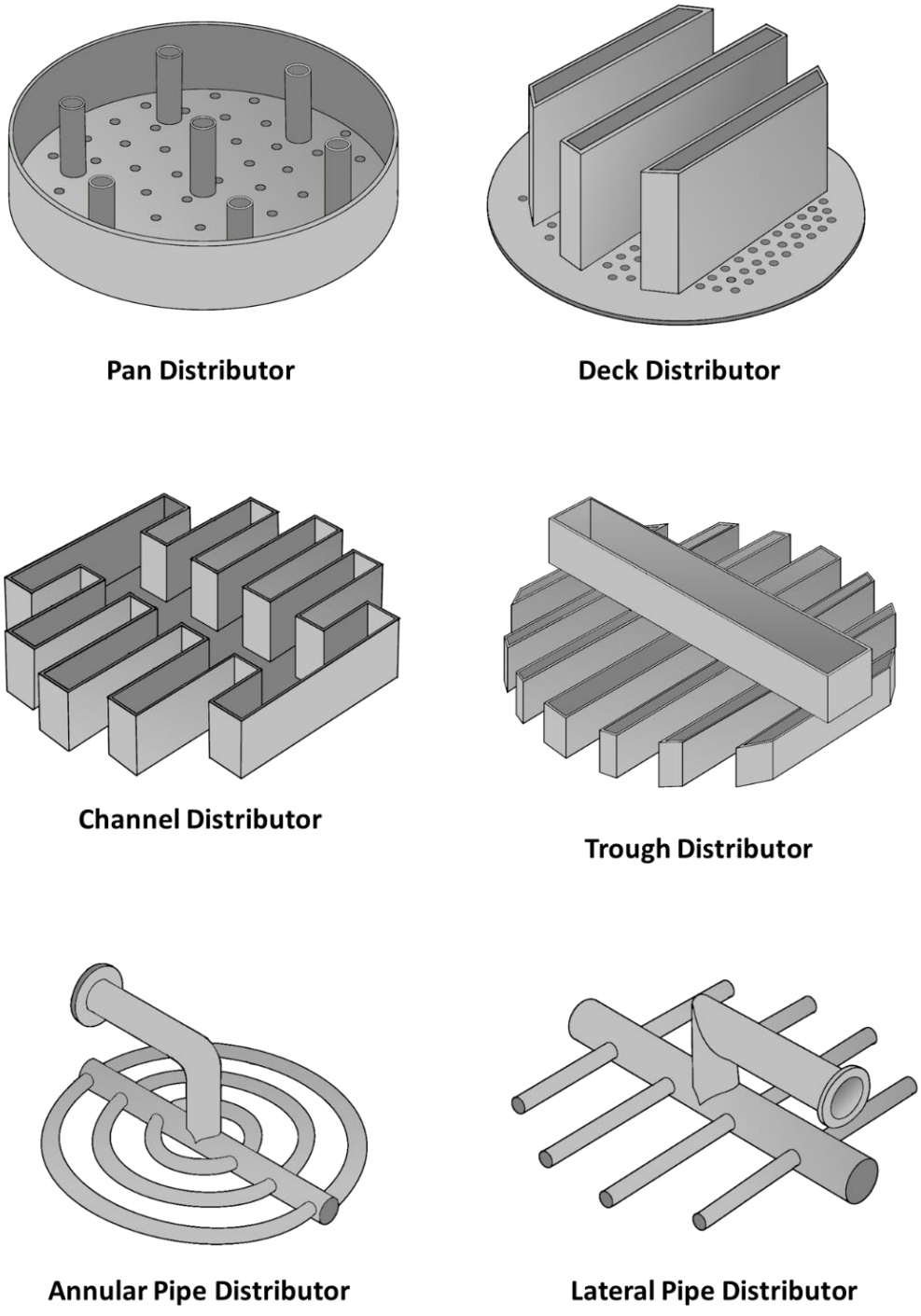

Figure 2.2: Distributor Designs [Redrawn from BTS Engineering (2015)]

In most of these designs the liquid is fed from the distributor to the column by gravity. The flow rate is thus determined by the liquid level that is maintained in the distributor. Liquid flow is either through orifices in the bottom of the distributor base, or conductor tubes passing up through the distributor base. When conductor tubes are used, the orifices are usually located in the side of the tubes, above the distributor base. Drip pipes extending down through the bottom of the distributor base are also used. A parameter used in characterising liquid distributors is the drip point density, the number of drip points per unit area.

In pan and deck type distributors the flow of gas past the distributor is facilitated by gas risers extending up through the distributor base, positioned between distribution points, preventing liquid and gas contact. In trough or channel type distributors vapour passage is provided by the open space between the troughs or channels and the column wall. A similar design is seen in pan type distributors used in small diameter columns, where gas risers are not used and the passage of gas is provided by a gap between the pan and the column wall.

While a liquid distributor can usually ensure a uniform distribution of liquid flowing down the column to a certain extent, a source of maldistribution in packed columns is the formation of liquid channels in the packed bed as the liquid flows down the column. According to Sun *et al.* (2000) the formation of these preferred paths of liquid flow is part of the intrinsic nature of random packing and is referred to as the natural flow pattern. For an initial liquid distribution that is better than the natural flow pattern, the liquid distribution will tend towards the natural liquid distribution over a certain packed bed height (Sun *et al,* 2000). The same phenomenon occurs for an initial liquid distribution worse than the natural flow pattern.

As the liquid flows down a packed column, a tendency for the liquid to flow radially outwards to the wall of the column develops (Kister, 1992; Sun *et al*. 2000). This is caused by the higher voidage in the wall region due to the large difference between the curvature of the column wall and the packing elements, resulting in a non-uniform liquid flow resistance. This radial flow of liquid decreases the amount of liquid flowing down the bulk of the packed bed and increases the amount of liquid wall flow.

Yin *et al*. (2000) investigated liquid maldistribution in a 0.6 m diameter column filled with Pall rings to a bed height of 3 m, using primarily water and air. They found that an increase in liquid flow rate reduced the relative wall flow slightly, and that the height for the liquid distribution to reach the natural flow pattern was also reduced. The effect of gas flow rate on liquid distribution in the bulk packing region was found to be insignificant. Liquid wall flow was also not influenced by the gas flow

rate in the pre-loading region. Above the loading point, liquid wall flow rapidly increased with an increase in gas flow rate. With regard to liquid physical properties, they found liquid surface tension had little or no effect on liquid distribution when comparing the results of water (72 mN/m) and a detergent solution (33 mN/m) having the same liquid density and viscosity. The effect of liquid viscosity was investigated with water (1 mPa.s, 1000 kg/m^3) and Isopar (2.46 mPa.s, 788 kg/m^3). It was concluded that liquid viscosity reduces radial liquid spread and that higher liquid viscosity results in lower liquid wall flow. According to Yin *et al*. (2000), turbulent liquid motion enhances the spread of liquid and, as a result of the reduction in liquid turbulence with an increase in liquid viscosity, the spread of liquid is reduced.

As a result of the maldistribution of liquid that develops in packed columns, redistributors are used to capture the liquid that has migrated to the column walls or formed flow channels and redistribute the liquid evenly over the packing below. Kister (1992) suggests that liquid redistribution is required approximately every six meters of bed height, while Sinnott & Towler (2009) suggest that the maximum bed height should not exceed 8 to 10 column diameters. Redistribution of the liquid is also typically required if the feed is introduced to, or product is drawn from an intermediate position in the column.

Compared to liquid maldistribution, much less information is available on how gas or vapour maldistribution affects the performance of packed columns (Olujić *et al.* 2004). The flow of gas or vapour through a packed column tends to follow the path of least resistance. This generally corresponds with the regions of lower liquid load and where lower liquid and gas interaction occurs. For this reason it can be concluded that the distribution of gas or vapour throughout the column is dependent on the liquid flow patterns (Sun *et al.* 2000). What can still be of concern is the initial maldistribution of gas or vapour when fed to the column, since the general opinion is that the gas or vapour is always more or less uniformly distributed if a good initial distribution is ensured (Olujić *et al.* 1991). Based on general experience however, it is suggested that even severe initial gas maldistribution quickly corrects itself within a rather short bed height and that initial gas maldistribution has no effect on packing efficiency (Olujić *et al.* 2004).

According to Olujić *et al*. (2009), the functionality of gas distributors, unlike liquid distributors, cannot be experimentally tested before installation. Consequently, CFD will become increasingly important when designing gas distributors in the future.

2.3 Hydrodynamic Behaviour

When designing a new packed column or retrofitting an existing column, predictive models are often used to predict the separation efficiency that can be expected from the column (Henley *et al*. 2011). However, the separation efficiency is influenced by a number of factors, which include: the interfacial area available for mass transfer, the thermodynamics of the system, as well as the hydrodynamic behaviour in the column. Since the focus of this project will be on the hydrodynamics of random packing, it will be discussed in more detail.

The hydrodynamic behaviour in packed columns are generally characterised by **the pressure drop over the column** and the **liquid hold-up in the column**, although **the rate of liquid entrainment** can also be used in the examination of the hydrodynamic behaviour.

2.3.1 Pressure Drop

The pressure drop over a packed column can be classified into two categories: the dry bed pressure drop and the irrigated pressure drop. The dry bed pressure drop is the gas phase pressure drop over the packed bed with no liquid load to the column. This pressure drop is the result of the resistance to gas flow by only the packing inside the column and proportional to the square of the gas flow rate for turbulent gas flow (Kister, 1992). This is an important parameter used in a number of models predicting the pressure drop in two phase counter current flow, as well as in assessing the operating regions of packed columns.

The irrigated or wet pressure drop is the drop in pressure over the packed column when the packing is subjected to a liquid load under counter current two-phase flow. The liquid load wets the packing as the liquid flows down the column as films, rivulets or droplets on the packing elements. This results in a reduced cross-sectional open area available for gas flow, leading to higher frictional losses in the gas phase (Maćkowiak, 2010). Consequently the irrigated pressure drop is higher than the dry bed pressure drop.

2.3.2 Liquid Hold-up

The liquid hold-up is defined as the volume fraction of the packed bed that is occupied by liquid for a given operating condition. The total liquid hold-up in a column consists of the static liquid hold-up and the operating or dynamic liquid hold-up. The static liquid hold-up is defined as the liquid that does not drain from the column and remain on the packing surface after liquid supply to the column (as well as the gas flow through the column) has been stopped for an extended period of time. The dynamic liquid

hold-up, on the other hand, is the volume of liquid that freely drains from the packed bed after the liquid supply is stopped for an extended period of time (Yin *et al*. 2002).

Since the liquid hold-up directly influences the pressure drop, the liquid hold-up plays an important role in modelling the irrigated pressure drop. The liquid hold-up is also an important parameter when working with systems where the liquid residence time in the column is of importance, i.e. when working with thermally unstable mixtures where a long residence time can lead to product degradation or fouling; or absorption processes with slow chemical reactions (Kister, 1992; Maćkowiak, 2010). The liquid hold-up is also taken into consideration when designing support devices for the column and packing since it represents the weight of liquid when in operation (Kister, 1992).

2.3.3 Liquid Entrainment

Liquid entrainment can be described as the upward movement of liquid droplets through the column carried by the flow of gas. The forces acting on droplets in two-phase counter current flow of liquid and gas in a packed column are the gravitational force and the drag force (Woerlee & Berends, 2001). When the gas flow rate is large enough so that the drag force becomes larger than the gravitational force, the liquid droplet is entrained. Besides the creation of liquid droplets as a result of the packing structure or shape (discontinuous tongues and ribs), two other mechanisms of droplet creation include the shearing of wave crests from roll-waves formed in the liquid film, and the wave undercut mechanism (Ishii and Mishima, 1989).

Liquid entrainment data in packed columns containing random packing are not common in literature. The reason for this, according to Spekuljak (1985), is because flooding, which will be discussed in the next section, occurs much more abruptly in random packing compared to structured packing. For this reason, columns with random packing are usually operated a safe distance away from the point where flooding occurs and as a result, the range of operation in which liquid entrainment occurs is very small.

2.3.4 Hydrodynamic Operating Regions

The hydrodynamic behaviour in a packed column can be characterised by the pressure drop, liquid hold-up and liquid entrainment. All three of these factors are dependent on the gas flow rate and generally expressed as a function of the vapour flow factor. For a particular liquid flow rate, the vapour flow factor is defined as the superficial gas velocity flowing upwards through a packed column, adjusted for gas density, and represents the square root of the gas kinetic energy. The vapour flow factor is expressed as:

$$F_G = u_G \cdot \sqrt{\rho_G} \qquad [2.1]$$

As the vapour flow factor increases the liquid hold-up and pressure drop in a packed column change in such a manner that three operating regions can be identified in the operation of the column. These regions are: the pre-loading, loading and flooding regions, with the transition from one region to another separated by the loading and flooding points. Each of these regions will be discussed next with regard to Figure 2.3, Figure 2.4 and Figure 2.5. These figures depict the typical trends in pressure drop, liquid hold-up and HETP (height equivalent to a theoretical plate) as the vapour flow factor increases.

The HETP expresses the separation efficiency of a packed column as the packed bed height required to achieve the same separation as one equilibrium (theoretical) stage in a tray column (Henley *et al*. 2011). The lower the HETP, the more efficient the separation.

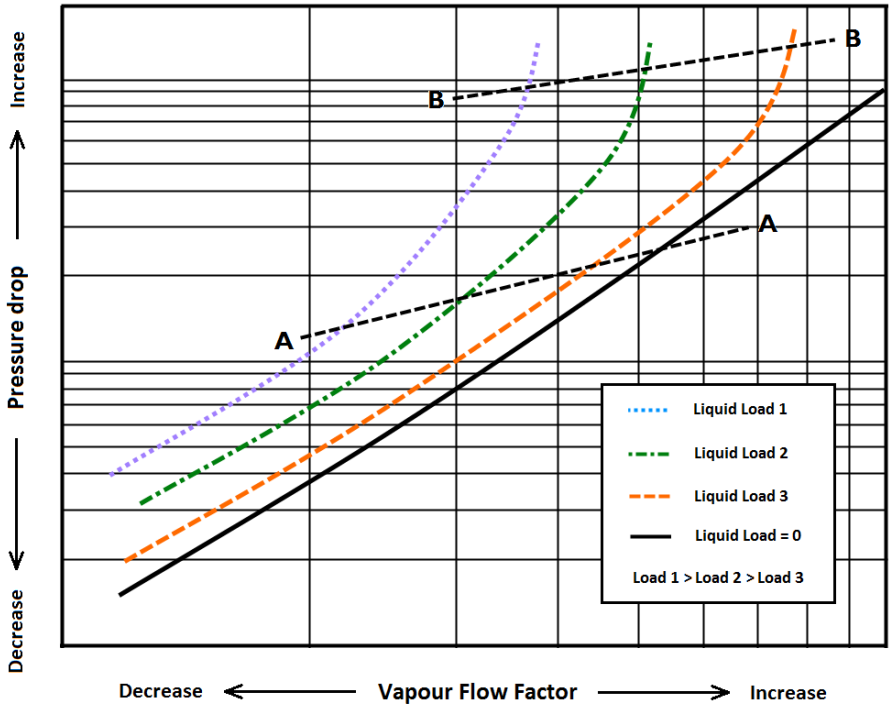

Figure 2.3: Log-log plot of the typical pressure drop versus vapour flow factor trends for packed columns

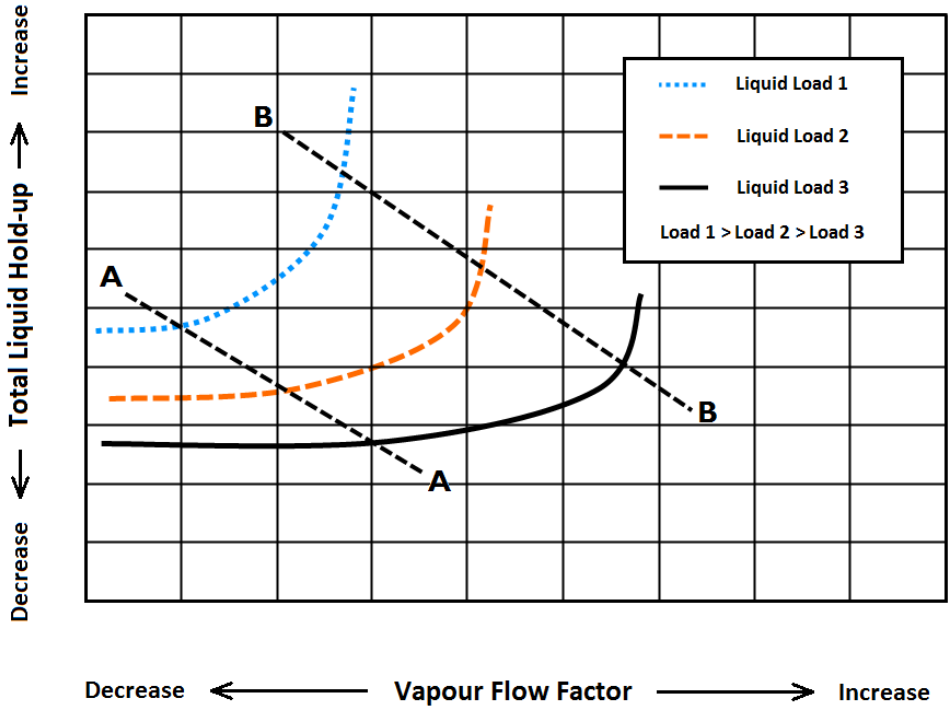

Figure 2.4: Typical liquid hold-up versus vapour flow factor trends for packed columns

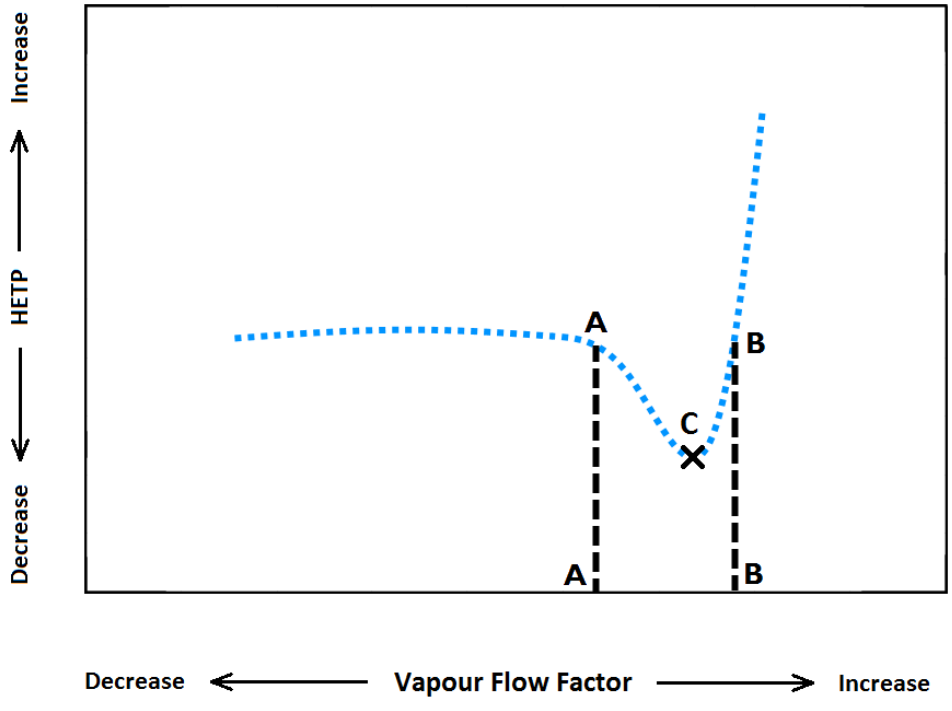

Figure 2.5: Typical HETP versus vapour flow factor trend for packed columns

Pre-loading

In the pre-loading region (below line A-A in Figure 2.3, Figure 2.4 and Figure 2.5) the liquid flowing down through the packed bed is not influenced by the flow of gas upwards through the column. Figure 2.4 shows that the liquid hold-up is independent of the vapour flow factor in the pre-loading region. As shown in Figure 2.3 on a log-log plot of pressure drop versus the vapour flow factor, the pressure drop increases uniformly and parallel to the dry bed pressure drop for each of the liquid loads as the vapour flow factor increases in the pre-loading region. In this region, separation efficiency is also relatively independent of the gas flow rate (Figure 2.5) (Kister, 1992).

Loading

As the gas flow rate increases, a point is reached when the flow of liquid down the column starts to be influenced by the gas flowing upwards through the column. This point is depicted by line A-A in Figure 2.3 and Figure 2.4, and is defined as the loading point. At this point the interfacial gas and liquid frictional forces start to counteract the gravitational force acting on the liquid, causing the liquid to start accumulating in the packed bed which increases the liquid hold-up. Above the loading point, the pressure drop starts to increase more rapidly for all liquid loads and moves away from the linear trend of the dry bed pressure drop. The deviation from the uniform increase in the pre-loading region is a result of the reduction in the cross-sectional area available for gas flow, caused by the accumulation of liquid in the packed bed (Kister, 1992).

The accumulation of liquid in the packed bed is also accompanied by an increase in separation efficiency in the loading region (Figure 2.5). The increase in efficiency arises due to the increase in contact area between the liquid and gas as a result of increased liquid hold-up (Billet & Schultes, 1999). However, the efficiency reaches a maximum (point C in Figure 2.5) and starts to decrease as the flooding point is approached (line B-B in Figure 2.3, Figure 2.4 and Figure 2.5). The decrease in efficiency is a result of back-mixing in the liquid phase as liquid is entrained up the column, counteracting the positive effect of the larger liquid-gas interface (Billet & Schultes, 1999; Kister, 1992).

Flooding

Although different definitions of the flooding point exist (Kister, 1992), it can generally be regarded as the point where the pressure drop and liquid hold-up start to rapidly increase with a slope tending towards infinity as the gas flow rate increases (line B-B on Figure 2.3, Figure 2.4 and Figure 2.5) (Kister, 1992). As the gas flow rate increases beyond the loading point the frictional forces of the gas acting

on the liquid films, rivulets and droplets start to counteract the gravitational force acting on the liquid, leading to an increase in the liquid hold-up. The increased liquid hold-up leads to a decrease in packed bed voidage and, as a result, a decrease in the free cross-sectional area available for gas to pass through the packed bed. With a smaller cross-sectional area for the gas to pass through, the velocity of the gas relative to the liquid flowing down the column increases. This increased gas velocity further increases the frictional forces between the gas and liquid, resulting in the liquid hold-up increasing even more. The end result is the exponential increase in liquid hold-up and pressure drop, characterizing the flooding phenomenon. Beyond the flooding point, the flooding region is characterized by unstable pressure drop and liquid hold-up, entrainment and poor separation efficiency (Kister, 1992).

While the liquid generally flows down the column as liquid films, rivulets and droplets, liquid film flow applies to non-perforated, smaller packings, with low voidage and high specific packing area, characteristic of first generation packings in particular. For these types of packing, flooding is also associated with an increase in the liquid film thickness and the dead space in these packings filling up with liquid (Maćkowiak, 2010; Górak and Olujić, 2014). In the case of the more modern lattice type packings, developed as the third and fourth generation of packings with a much more open structure, these packings have very little, if any, dead space that can fill up with liquid. While these packings also have liquid flowing down the packed bed as liquid films, they have a much higher tendency for droplet formation as a result of liquid dripping from individual packing elements or the shearing of droplets from the liquid films and runlets (Maćkowiak, 2010; Górak and Olujić, 2014). As a result, the contribution of droplet entrainment to the cause of flooding is much larger for these types of packing.

Beyond the flooding zone a fourth hydrodynamic region exists, which Lerner and Grove (1951) call the superflood zone. The flooding region and the superflood zone is separated by the superflood brake point. This region is associated with gas bubbling though the column and extreme liquid entrainment, with the effective liquid load to the column decreasing. Beyond the superflood brake point, the pressure drop trend breaks from the drastic increase seen in the flooding region, with a decrease in the slope of the pressure drop trend (Lerner and Grove, 1951).

Packed columns are generally operated at a gas flow rate equal to 70-80 % of that at the flooding point (Billet & Schultes, 1999; Maćkowiak, 1991). This ensures that advantage can be taken of the increase in efficiency experienced in the loading region, which is at about 70 % of the flooding gas flow rate (Billet & Schultes, 1999). Since the efficiency drastically drops again as the flooding point is approached, accurate prediction of the loading and flooding points are very important. If the flooding point is over-predicted, the column will be operated closer to the true flooding point and at a much

higher pressure drop than what was intended, possibly resulting in a lower efficiency. If under-predicted, the column will not be operated at its full capacity.

2.4 Fluid Physical Properties

Over the past 80 years a large amount of research has been done on packed column hydrodynamics. Although the majority of this work consists of hydrodynamic studies of different packings with primarily water/air systems, extensive work has also been done on systems with varying liquid and gas physical properties (Piché *et al*. 2001-B). Not only did these studies provide a better understanding of the effects of different physical liquid and gas properties, they also provided the data required for the development of better hydrodynamic models and correlations. The influence of different physical fluid properties on the hydrodynamic behaviour, recognised by these studies, is discussed in the following sections.

2.4.1 Liquid Viscosity

Viscosity is a measure of a fluid's tendency to resist deformation or more generally, the resistance to flow, with higher viscosities having a higher resistance. In a packed column, liquid viscosity influences the flow of liquid through the packed bed so that liquids with high viscosities drain poorly from the packed bed. As a result higher liquid viscosities lead to more accumulation of liquid in the packed bed. Böcker and Ronge (2005) described this as a type of plugging that occurs. Higher liquid viscosities thus result in higher liquid hold-up, which again leads to an increase in pressure drop as a result of the decreased open area available for gas flow (Böcker and Ronge, 2005; Brunazzi *et al*. 2002; Fourati *et al.* 2012; Zakeri *et al*. 2011). As a result, higher liquid viscosities lead to column flooding at lower gas flow rates. Piché *et al*. (2001-B) point out that liquid viscosity has a larger effect on pressure drop at high gas flow rates where the shearing force of the gas becomes prominent. According to Strigle (1994), when compared to the liquid hold-up of an air/water system, which has a liquid viscosity of approximately 1 cP, an increase in liquid viscosity to 2 cP would result in a 10 % increase in liquid hold-up. With an increase to 16 cP, the liquid hold-up would be about 50 % larger. For liquid viscosities of about 0.45 cP, the liquid hold-up would reduce by about 10 %, while a viscosity of 0.15 cP would result in a 20 % decrease in liquid hold-up.

2.4.2 Surface Tension

Surface tension is a measure of a liquids tendency to contract to a minimum surface area as a result of the tension on the interface between two phases. In the scope of this project these two phases are the liquid and gas phase. Liquids with low surface tension have the tendency to spread out over a

surface, while liquids with high surface tension tend to clump together (Kister, 1992). In a packed column, surface tension is an important parameter with regard to the wetting of packing, with lower surface tension leading to improved surface wetting (Alekseenko *et al*. 2008). According to Strigle (1994), surface tension has little influence on the liquid hold-up when working with high surface tension liquids such as water. However, at low liquid flow rates liquids with a surface tension of about 27 mN/m will have a liquid hold-up of about 12 % lower than that of water. For liquids with a surface tension as low as 13 mN/m, a 20 % decrease in liquid hold-up can be expected compared to water at low liquid flow rates. At higher liquid flow rates, above 17 $m^3/(m^2.h)$, the effect of surface tension on liquid hold-up weakens.

Strigle (1994) states that there is no general agreement on what the effect of surface tension is on the capacity of packed columns. In air/water tests where the surface tension was lowered through the addition of surfactants, a decrease in column capacity was observed. However, it was concluded that the reduced capacity was a result of liquid foaming. Studies in which surfactants were used in an aqueous system to reduce surface tension show a substantial increase in pressure drop. However, with the addition of an antifoaming agent, the pressure drop was reduced to a level comparable to what was achieved with a methanol solution with the same surface tension. It was concluded that the increase in pressure drop was a result of foaming and that surface tension has no effect on capacity when working with non-foaming liquids (Strigle, 1994).

2.4.3 Liquid Density

In a packed column where liquid flows down the column by means of gravity, liquid density provides a measure of the gravitational force acting on the liquid, as well as the inertial force of the liquid as a result of its mass. For a certain mass of liquid hold-up, and thus also a certain gas flow rate to induce this liquid hold-up, a reduction in liquid density will result in a reduction in the packed bed void fraction due to the increased volume of liquid occupied by the mass of liquid held up (Strigle, 1994). The result is an increase in both liquid hold-up and pressure drop as the liquid density is lowered.

In the presence of a gas environment, liquid density also provides a measure of buoyancy of the liquid in this environment when compared to the density of the gas making up the environment. The liquid buoyancy results from the static head produced by the gas. When operating a packed column at atmospheric pressures, the density difference between the liquid and gas is relatively large, with the liquid having a much higher density. In this case the influence of the buoyancy force on the liquid is negligible (Stichlmair *et al*. 1989; Strigle, 1994). At high pressures the density difference is much smaller and the influence should be accounted for (Strigle, 1994).

2.4.4 Gas Density

Considering the flow of gas through a packed column without a liquid load, the pressure drop over the packed column results from the presence of the packing elements creating resistance to the flow of gas. Under laminar flow conditions, thus low Reynolds numbers, this resistance is primarily a function of viscous forces (Ergun and Orning, 1949). Strigle (1994) states that under these conditions, form drag loss accounts for most of the pressure drop. In the turbulent flow regime, thus high Reynolds numbers, the resistance is dominated by inertial forces. Ergun and Orning (1949) describe this resistance as a result of the kinetic effect. In addition to the gas velocity, the inertial forces are a function of the gas density, where an increased gas density results in an increased resistance, and thus increased pressure drop. This conclusion is also applicable to irrigated packed beds.

Another way in which the gas density affects the hydrodynamic behaviour in an irrigated packed column is through the buoyancy force, described in Section 2.4.3, acting on the liquid as a result of the static head produced by the gas. This is however mostly applicable at high operating pressures where the density difference between the gas and liquid is relatively small.

2.4.5 Gas Viscosity

As mentioned in Section 2.4.4, under laminar flow conditions the resistance to gas flow is primarily a function of viscous forces (Ergun and Orning, 1949), where the drag coefficient is inversely proportional to the gas phase Reynolds number (Strigle, 1994). An increase in gas viscosity thus results in an increase in pressure drop. Since the flow of gas through packed columns is turbulent for most applications, the influence of gas viscosity is very limited. Woerlee and Berends (2001) state that the influence of gas viscosity on packed column capacity is seldom over 5 %.

2.5 Packing Nominal Size

Manufacturers of random packing generally produce a type of random packing in different nominal sizes. While the decision of which packing size to use depends on the diameter of the column being designed or retrofitted, the decision should also be based on the capacity and efficiency requirements, since there is usually a trade-off between the two (Perry & Green, 2008). According to Perry & Green (2008), a packing size should be chosen so that the column diameter to packing diameter ratio lies between 10 and 40, since very large ratios lead to loss of efficiency due to maldistribution and very small ratios lead to increased wall flow effects. While the bed void fraction for different sizes of packing from the same type is relatively constant, there is a large difference in the packing surface area (Nakov *et al*. 2012; Nakov *et al*. 2007).

Nakov *et al*. (2012) measured the pressure drop of IMTP for different nominal sizes (25, 40, 50 and 70 mm) in a packed column with a diameter of 470 mm and packed bed height of 2400 mm with an air/water system. They found that larger size packings had higher capacity, with a higher pressure drop measured for smaller packings at the same vapour flow factor.

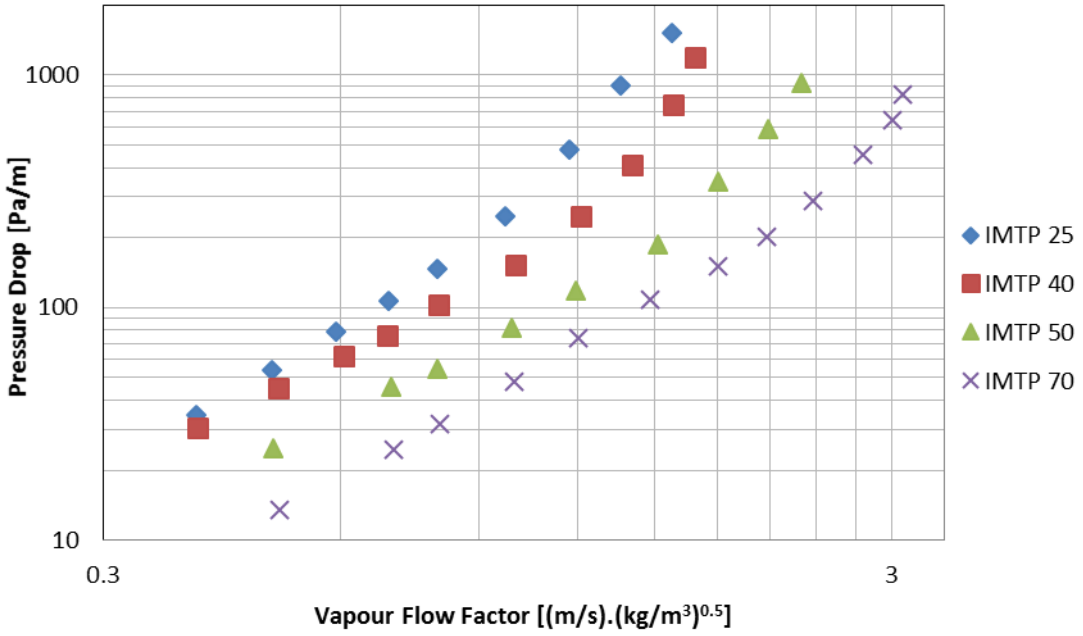

Figure 2.6: Pressure drop of different sizes of IMTP at a liquid flow rate of 120 $m^3/(m^2.h)$ with air/water – Data obtained from Nakov *et al*. (2012)

Smaller sized packing tends to have higher liquid hold-up compared to larger packings (Ludwig, 1997). The higher pressure drop with smaller packings can be explained by the reduced area open to gas flow as a result of the increased liquid hold-up.

2.6 Hydrodynamic Modelling

Over the years, numerous attempts had been made at predicting the hydrodynamic behaviour in packed columns (Maćkowiak, 2010). The initial graphical methods, based on the correlation chart of pressure drop over the packed column developed by Sherwood *et al*. (1938), focused on predicting flooding conditions based on droplet entrainment. This method was later extended to predicting the pressure drop over the entire hydrodynamic operating range and became known as the generalized pressure drop correlation (GPDC) chart (Kister, *et al*. 2007). Mersmann (1965) also developed a graphical correlation, but instead of the droplet entrainment approach used in the GPDC, Mersmann's correlation is based on the so-called film model. For more information on these graphical methods,

the reader is referred Kister (1992) and Maćkowiak (2010), who describe the development of these methods and also provide the required diagrams.

A number of empirical and semi-theoretical correlations have been developed for predicting the pressure drop, liquid hold-up and flooding conditions for random packing (Maćkowiak, 2010; Piché *et al*. 2001-B).

Both the graphical and semi-theoretical correlations were validated with different types of random packing and most of these require empirical constants specific to the packing under consideration. These empirical constants for first, second and third generation random packing are readily available in literature, while the lack of empirical constants for fourth generation random packing restricts the use of these correlations for predicting the hydrodynamic behaviour using these packings.

Three semi-theoretical hydrodynamic models for random packing will be investigated in this project. These are the Billet and Schultes model (Billet & Schultes, 1991; 1993; 1995; 1999), the Maćkowiak model (Maćkowiak, 1990; 1991; 2009) and the Stichlmair model (Stichlmair *et al*. 1989). The three models employ different approaches with regard to the modelling of the packing material inside the column, with the Billet and Schultes model and the Maćkowiak model employing the channel model approach, while the Stichlmair model uses the particle model approach. The models also differ with regard to their flooding mechanisms. While the Billet and Schultes model and the Stichlmair model employ a film model approach with regard to flooding, the Maćkowiak model uses a droplet entrainment approach.

In all three of the semi-theoretical models that will be investigated, the irrigated pressure drop is derived by first considering the dry bed pressure drop and then adding the effect of the liquid hold-up when irrigated. The modelling of the dry bed pressure drop is based on either the flow of gas through a pipe (channel model) or a fluidized bed (particle model).

The dimensionless numbers that are used in the semi-theoretical models that are discussed in Sections 2.6.1 and 2.6.2 are summarized in Table 2.1.

Table 2.1: Dimensionless numbers used in the different semi-theoretical models

Dimensionless Number	*Billet & Schultes Model*	*Maćkowiak Model*	*Stichlmair Model*
Gas Reynolds Number	$Re_G = \frac{u_G \cdot d_p \cdot \rho_G}{(1-\varepsilon) \cdot \mu_G} \cdot K$	$Re_G = \frac{u_G \cdot d_p \cdot \rho_G}{(1-\varepsilon) \cdot \mu_G} \cdot K$	$Re_G = \frac{u_G \cdot d_p \cdot \rho_G}{\mu_G}$
Liquid Reynolds Number	$Re_L = \frac{u_L \cdot \rho_L}{a \cdot \mu_L}$	$Re_L = \frac{u_L \cdot \rho_L}{a \cdot \mu_L}$	Not Used
Liquid Froude Number	$Fr_L = \frac{u_L^2 \cdot a}{g}$	Not Used	$Fr_L = \frac{u_L^2 \cdot a}{g \cdot \varepsilon^{4.65}}$

2.6.1 Channel Models

Two channel models are investigated, namely the Billet and Schultes model and the Maćkowiak model.

Billet & Schultes Model:

Billet & Schultes (1991; 1993; 1995; 1999) developed a hydrodynamic model for both random and structured packing based on the channel model approach. In their model, the empty space in random or structured packings is assumed, for theoretical considerations, to consist of vertical flow channels through which the evenly distributed liquid flows down, while the gas flows counter-currently upwards through these channels. In reality however these channels are not all vertical and are, in the case of random packing, determined by the shape and random orientation of packing elements. To account for the deviation of real flow behaviour from the assumed vertical channel flow of liquid and gas, packing-specific constants are introduced.

To calculate the pressure drop over an unirrigated packed bed, the following correlation is used, derived from the flow of gas through a pipe:

$$\frac{\Delta P_{dry}}{H} = \psi_{dry} \cdot \frac{a}{\varepsilon^2} \cdot \frac{F_G^2}{2} \cdot \frac{1}{K} \qquad [2.2]$$

$$\frac{1}{K} = 1 + \frac{2}{3} \cdot \frac{1}{1-\varepsilon} \cdot \frac{d_p}{D} \qquad [2.3]$$

$$\psi_{dry} = C_p \cdot \left(\frac{64}{Re_G} + \frac{1.8}{Re_G^{0.08}} \right) \qquad [2.4]$$

$$d_p = \frac{6 \cdot (1-\varepsilon)}{a} \qquad [2.5]$$

The wall factor, K, is included to account for the increase in the void fraction at the column wall.

To calculate the irrigated pressure drop, the decrease in the packed bed void fraction, and as a result the free cross-sectional area available for gas flow, caused by the liquid being held up in the packing is taken into account.

$$\frac{\Delta P_{irr}}{H} = \psi_{irr} \cdot \frac{a}{(\varepsilon - h_L)^3} \cdot \frac{F_G^2}{2} \cdot \frac{1}{K} \qquad [2.6]$$

$$\psi_{irr} = C_p \cdot \left(\frac{64}{Re_G} + \frac{1.8}{Re_G^{0.08}} \right) \cdot \left(\frac{\varepsilon - h_L}{\varepsilon} \right)^{1.5} \cdot \left(\frac{h_L}{h_{L,S}} \right) \cdot exp\left(C_1 \cdot \sqrt{Fr_L} \right) \qquad [2.7]$$

$$C_1 = \frac{13300}{a^{\frac{3}{2}}} \qquad [2.8]$$

The total liquid hold-up is calculated by the liquid hold-up in the pre-loading region, which is independent of the gas flow rate, together with the liquid hold-up at the flooding point, which is dependent on the gas flow rate at the flooding point.

$$h_L = h_{L,S} + (h_{L,Fl} - h_{L,S}) \cdot \left(\frac{u_G}{u_{G,Fl}} \right)^{13} \qquad [2.9]$$

$$h_{L,S} = \left(12 \cdot \frac{1}{g} \cdot \frac{\mu_L}{\rho_L} \cdot u_L \cdot a^2\right)^{\frac{1}{3}} \quad [\ 2.10\ ]$$

$$\left(h_{L,Fl}\right)^3 \cdot \left(3 \cdot h_{L,Fl} - \varepsilon\right) = \frac{6}{g} \cdot a^2 \cdot \varepsilon \cdot \frac{\mu_L}{\rho_L} \cdot \frac{L}{G} \cdot \frac{\rho_G}{\rho_L} \cdot u_{G,Fl} \quad \text{for} \quad \frac{\varepsilon}{3} \leq h_{L,Fl} \leq \varepsilon \quad [\ 2.11\ ]$$

Billet and Schultes (1999) found that the real column hold-up can be better predicted by taking into account non-uniform wetting of the packing material. This is achieved by a hydraulic surface area term in the calculation of the pre-loading liquid hold-up. Furthermore, at low liquid Reynolds numbers, the hydraulic surface area increases less than at larger liquid Reynolds numbers.

$$h_{L,S} = \left(12 \cdot \frac{1}{g} \cdot \frac{\mu_L}{\rho_L} \cdot u_L \cdot a^2\right)^{\frac{1}{3}} \cdot \left(\frac{a_h}{a}\right)^{\frac{2}{3}} \quad [\ 2.12\ ]$$

$$\frac{a_h}{a} = C_h \cdot \left(\frac{u_L \cdot \rho_L}{a \cdot \mu_L}\right)^{0.15} \cdot \left(\frac{u_L^2 \cdot a}{g}\right)^{0.1} \quad \text{for} \quad Re_L < 5 \quad [\ 2.13\ ]$$

$$\frac{a_h}{a} = 0.85 \cdot C_h \cdot \left(\frac{u_L \cdot \rho_L}{a \cdot \mu_L}\right)^{0.25} \cdot \left(\frac{u_L^2 \cdot a}{g}\right)^{0.1} \quad \text{for} \quad Re_L \geq 5 \quad [\ 2.14\ ]$$

Another adaption was introduced (Billet and Schultes 1993, 1999) with regard to the liquid hold-up at the flooding point. It was found that the theoretical liquid hold-up at flooding diverged erratically from the measured liquid hold-up when predicted with Equation [2.11]. As a result the following empirical equation is provided to calculate the real liquid hold-up at flooding.

$$h_{L,Fl} = 2.2 \cdot h_{L,S} \cdot \left(\frac{\mu_L \cdot \rho_w}{\mu_w \cdot \rho_L}\right)^{0.05} \quad [\ 2.15\ ]$$

However, to calculate the total liquid hold-up and thus the irrigated pressure drop, the flooding point gas velocity is required, as seen in Equation [2.9]. Provided below is the calculation procedure for both the loading and flooding point gas velocities as described by Billet and Schultes (1999).

To calculate the gas flow rate at the loading point, a loading point resistance coefficient is calculated.

$$u_{G,S} = \sqrt{\frac{g}{\psi_S}} \cdot \left[\frac{\varepsilon}{a^{\frac{1}{6}}} - a^{\frac{1}{2}} \cdot \left(12 \cdot \frac{1}{g} \cdot \frac{\mu_L}{\rho_L} \cdot u_{L,S} \right)^{\frac{1}{3}} \right] \cdot \left(12 \cdot \frac{1}{g} \cdot \frac{\mu_L}{\rho_L} \cdot u_{L,S} \right)^{\frac{1}{6}} \cdot \sqrt{\frac{\rho_L}{\rho_G}} \qquad [\ 2.16\ ]$$

$$\psi_S = \frac{g}{C_S^2} \cdot \left[\frac{L}{G} \cdot \sqrt{\frac{\rho_L}{\rho_G}} \cdot \left(\frac{\mu_L}{\mu_G} \right)^{0.4} \right]^{-2 \cdot n_S} \qquad [\ 2.17\ ]$$

$$u_{L,S} = \frac{\rho_G}{\rho_L} \cdot \frac{L}{G} \cdot u_{G,S} \qquad [\ 2.18\ ]$$

Where n_S is dependent on the flow parameter, which characterizes the load conditions when phase inversion occurs.

$$n_S = -0.326 \text{ and } C_S = C_{S,P} \text{ for } \frac{L}{G} \cdot \sqrt{\frac{\rho_G}{\rho_L}} \leq 0.4 \qquad [\ 2.19\ ]$$

$$n_S = -0.723 \text{ and } C_S = 0.695 \cdot C_{S,P} \cdot \left(\frac{\mu_L}{\mu_G} \right)^{0.1588} \text{ for } \frac{L}{G} \cdot \sqrt{\frac{\rho_G}{\rho_L}} > 0.4 \qquad [\ 2.20\ ]$$

For flow parameters smaller than 0.4, the liquid trickles down over the packing material as the dispersed phase, while for a flow parameter larger than 0.4, the liquid flows down as the continuous phase.

Billet and Schultes (1999) state that the flooding point is reached when shear stress of the flowing gas is large enough to entrain the entire liquid volume to the top of the column. This results in the velocity gradient of the liquid film becoming zero at the packing interface. Based on this, they derived the equations used for determining the flooding point gas velocity.

To determine the gas flow rate at flooding, a flooding point resistance coefficient is calculated, while the exponent, n_{Fl}, is determined by the flow parameter.

$$u_{G,Fl} = \sqrt{2} \cdot \sqrt{\frac{g}{\psi_{Fl}}} \cdot \frac{(\varepsilon - h_{L,Fl})^{\frac{3}{2}}}{\varepsilon^{\frac{1}{2}}} \cdot \sqrt{\frac{h_{L,Fl}}{a}} \cdot \sqrt{\frac{\rho_L}{\rho_G}} \qquad [2.21]$$

$$\psi_{Fl} = \frac{g}{C_{Fl}^2} \cdot \left[\frac{L}{G} \cdot \sqrt{\frac{\rho_G}{\rho_L}} \cdot \left(\frac{\mu_L}{\mu_G} \right)^{0.2} \right]^{-2 \cdot n_{Fl}} \qquad [2.22]$$

$$u_{L,Fl} = \frac{\rho_G}{\rho_L} \cdot \frac{L}{G} \cdot u_{G,Fl} \qquad [2.23]$$

$$n_{Fl} = -0.194 \text{ and } \quad C_{Fl} = C_{Fl,P} \quad \text{for} \quad \frac{L}{G} \cdot \sqrt{\frac{\rho_G}{\rho_L}} \leq 0.4 \qquad [2.24]$$

$$n_{Fl} = -0.708 \text{ and } \quad C_{Fl} = 0.6244 \cdot C_{Fl,P} \cdot \left(\frac{\mu_L}{\mu_G} \right)^{0.1028} \text{for} \quad \frac{L}{G} \cdot \sqrt{\frac{\rho_G}{\rho_L}} > 0.4 \qquad [2.25]$$

With a number of implicit variables, Billet and Schultes' model requires iterative calculations to solve for the different hydrodynamic parameters.

Table 2.2 summarizes the ranges of the different parameters for which the Billet and Schultes model was verified.

Table 2.2: Ranges of parameters for which the Billet and Schultes model was verified

	Units	Flooding Points	Liquid Hold-up	Pressure Drop
Vapour flow Factor	$(m/s)\cdot(kg/m^3)^{0.5}$	0.47-4.59	0.10-2.78	0.21-5.09
Gas Density	kg/m^3	0.30-1.37	N/A	0.06-28
Gas Viscosity	$m^2/s \times 10^6$	8.15-41.5	N/A	0.14-106
Liquid Load	$m^3/(m^2.h)$	4.88-144	1.33-82.8	0.61-60.1
Liquid Density	kg/m^3	750-1026	800-1810	361-1115
Liquid Viscosity	$m^2/s \times 10^6$	0.4-104	0.74-142	0.14-99.0
Liquid Surface Tension	mN/m	N/A	20.8-86.3	N/A
Column Diameter	M	N/A	N/A	0.15-0.80
Packed Bed Height	M	N/A	N/A	0.76-3.95
Specific Packing Area	m^3/m^2	N/A	N/A	54-380
Packing Void Fraction	m^3/m^3	N/A	N/A	0.66-0.98

Maćkowiak Model

Maćkowiak also developed a hydrodynamic model, based on the channel model, for both random and structured packing. Maćkowiak (1990) incorporated the effect of suspended droplets on the effective void fraction into his modelling approach. Initially Maćkowiak (1990) developed a model that predicted the flooding velocity and liquid hold-up in packed columns up to the flooding point. A later model was published that also predicted the pressure drop, together with the liquid hold-up over the entire operating range (Maćkowiak, 1991). In 2009 the model was extended to predict the dry bed pressure drop for both random and structured packing, without the need for any experimental evaluation for ring- and ball-shaped packings (Maćkowiak, 2009). For more complicated packing shapes a form factor is required that can be determined experimentally.

Maćkowiak (1990) derived an expression for the gas velocity at flooding based on the suspended bed of droplets. When considering a single droplet, there are three forces acting on this droplet: the gravitational force (K_g), the gas thrust force (K_ψ) and the lift force or buoyancy force (K_A) as a result of the difference in density between liquid and gas. This droplet can only be entrained if the thrust force is equal to or larger than the gravitational force minus the lift force.

$$K_\psi = K_g - K_A \quad [2.26]$$

$$\psi_T \cdot \left(\frac{{u_0}^2 \cdot \rho_G}{2}\right) \cdot \frac{\pi \cdot {d_T}^2}{4} = \frac{\pi \cdot {d_T}^3}{6} \cdot (\rho_L - \rho_G) \cdot g \quad [2.27]$$

When solving for the effective falling velocity of the droplet, the following equation is obtained.

$$u_0 = \sqrt{\frac{4}{3} \cdot \frac{d_T \cdot g}{\psi_T}} \cdot \sqrt{\frac{\rho_L - \rho_G}{\rho_G}} \quad [2.28]$$

u_0 represents the gas velocity necessary to keep a single droplet in suspension. The gas velocity required to keep a swarm of droplets in suspension is represented by $u_{G,Fl}$. As the percentage of droplets increases, the column floods at lower values of $u_{G,Fl}$. The ratio of $u_{G,Fl}$ to u_0 is thus influenced by the liquid hold-up and $u_{G,Fl}$ can be expressed as:

$$u_{G,Fl} = u_0 \cdot \left(1 - h_{L,Fl}\right)^n \quad [2.29]$$

Accounting for the effect of packing size and surface properties, Maćkowiak (1990) derived the following expression for the gas velocity at flooding in a packed column.

$$u_{G,Fl} = 0.565 \cdot {\psi^*_{Fl}}^{-\frac{1}{6}} \cdot \varepsilon^{1.2} \cdot \left(\frac{d_h}{d_T}\right)^{\frac{1}{4}} \cdot \left(\frac{d_T \cdot \rho_L \cdot g}{\rho_G}\right)^{\frac{1}{2}} \cdot \left(1 - \frac{h_{L,Fl}}{\varepsilon}\right)^{\frac{7}{2}} \quad [2.30]$$

with

$$d_T = \sqrt{\frac{\sigma_L}{(\rho_L - \rho_G) \cdot g}} \quad [2.31]$$

$$d_h = \frac{4 \cdot \varepsilon}{a} \quad [2.32]$$

Surface tension, which is not accounted for in any of the other semi-theoretical models, is used here in calculating the droplet diameter.

For the liquid hold-up at flooding, Maćkowiak (1990) uses two equations depending on the liquid Reynolds number.

$$\boldsymbol{h_{L,Fl} = \left(\frac{\varepsilon}{0.4 \cdot (1 - \lambda_0)}\right) \cdot \left\{\left[1.44 \cdot {\lambda_0}^2 + 0.8 \cdot \lambda_0 \cdot (1 - \lambda_0)\right]^{\frac{1}{2}} - 1.2 \cdot \lambda_0\right\}} \quad [\ 2.33\ ]$$

For $Re_L \geq 2$, and

$$\boldsymbol{h_{L,Fl} = \left(\frac{\varepsilon}{024 \cdot (1 - \lambda_0)}\right) \cdot \left\{\left[1.254 \cdot {\lambda_0}^2 + 0.48 \cdot \lambda_0 \cdot (1 - \lambda_0)\right]^{\frac{1}{2}} - 1.12 \cdot \lambda_0\right\}} \quad [\ 2.34\ ]$$

For $Re_L < 2$

Where

$$\boldsymbol{\lambda_0 = \frac{u_L}{u_{G,Fl}}} \quad [\ 2.35\ ]$$

For the liquid hold-up below the loading point, Maćkowiak (1991) correlated the liquid hold-up as a function of the dimensionless irrigation density and proposed the following correlation.

$$\boldsymbol{h_{L,S} = 2.2 \cdot \sqrt{B_L}} \quad [\ 2.36\ ]$$

Where

$$\boldsymbol{B_L = \left(\frac{\mu_L}{\rho_L \cdot g^2}\right)^{\frac{1}{3}} \cdot \left(\frac{u_L}{\varepsilon^3}\right) \cdot \left(\frac{1 - \varepsilon}{d_p}\right)} \quad [\ 2.37\ ]$$

For the liquid hold-up in the range above the loading point up to the flooding point, the following equation is provided.

$$h_L = h_{L,Fl} - \left(h_{L,Fl} - h_{L,S}\right) \cdot \left\{1 - \left[\frac{\left(\frac{F_G}{F_{G,Fl}}\right) - 0.65}{0.35}\right]\right\}^{\frac{1}{2}} \quad \text{for} \quad 0.65 < \frac{F_G}{F_{G,Fl}} < 1 \qquad [2.38]$$

Finally, with the liquid hold-up calculated, the irrigated pressure drop can be calculated with the following equations.

$$\frac{\Delta P}{H} = \theta \cdot 5.4 \cdot {Re_L}^{-0.14} \cdot \left(\frac{1-\varepsilon}{\varepsilon^3}\right) \cdot \left(\frac{{F_G}^2}{d_p \cdot K}\right) \cdot \left[1 + \left(\frac{h_L}{1-\varepsilon}\right)\right] \cdot \left(1 - \frac{h_L}{\varepsilon}\right)^{-3} \qquad [2.39]$$

For $0.3 \leq Re_L < 12.3$

$$\frac{\Delta P}{H} = 3.8 \cdot \theta \cdot \left(\frac{1-\varepsilon}{\varepsilon^3}\right) \cdot \left(\frac{{F_G}^2}{d_p \cdot K}\right) \cdot \left[1 + \left(\frac{h_L}{1-\varepsilon}\right)\right] \cdot \left(1 - \frac{h_L}{\varepsilon}\right)^{-3} \qquad [2.40]$$

For $Re_L \geq 12.3$

Where

$$K = \left[1 + \frac{2}{3} \cdot \left(\frac{1}{1-\varepsilon}\right) \cdot \left(\frac{d_p}{D}\right)\right]^{-1} \qquad [2.41]$$

The Maćkowiak model requires relatively simple calculations, although two constants are required: the flood point factor and packing shape factor.

Table 2.3 summarizes the ranges of the different parameters for which the Maćkowiak model was verified.

Table 2.3: Ranges of parameters for which the Maćkowiak model was verified

	Units	Flooding Points	Liquid Hold-up & Pressure Drop
Gas Velocity	m/s	0.4-18	N/A
Gas Density	kg/m^3	0.032-4.8	0.03-3.6
Gas Viscosity	$mPa.s \times 10^3$	7-18.2	6.5-18.2
Liquid Load	-	$B_L < 3 \times 10^{-3}$	$0.3 < Re_L < 200$
Liquid Density	kg/m^3	660-1830	660-1260
Liquid Viscosity	$mPa.s \times 10^3$	0.2-90	0.2-8
Liquid Surface Tension	mN/m	14-72	14-74.6
Column Diameter	m	0.1-1.2	0.1-1.4
Packed Bed Height	m	0.6-5.5	0.6-4
Specific Packing Area	m^2/m^3	54-550	54-500
Packing Void Fraction	m^3/m^3	0.63-0.990	0.63-0.987

2.6.2 Particle Models

Stichlmair Model

In the particle model, the packing elements are modelled as spheres with the gas flowing around these spheres. The dimensions of the spheres are based on the bed voidage and the packing surface area. With liquid flowing down the column, wetting the packing surface this dimension increases. As a result, the void fraction of the packed bed is decreased by the presence of the liquid (Stichlmair *et al*. 1989). The pressure drop across the packed bed is attributed to the friction losses due to the drag on the packing elements or spheres, similar to the Ergun model for single-phase flow in a packed bed (Kister, 1992).

Stichlmair *et al*. (1989) developed a particle based hydrodynamic model for predicting the pressure drop, liquid hold-up and flooding point in counter-current liquid and gas packed columns for both random and structured packing. A pooled set of experimental data from various sources was used in the validation of the model, which mostly included different types of random packing, but also included different structure packings. The set of experimental data also mostly consisted of air/water systems.

Based on the Richardson Zaki relationship, an expression for the dry bed pressure drop is derived by performing a force balance on a single particle in a packed bed:

$$\frac{\Delta P_{dry}}{H} = \frac{3}{4} \cdot f_0 \cdot \left(\frac{1-\varepsilon}{\varepsilon^{4.65}}\right) \cdot \left(\frac{\rho_G \cdot u_G^2}{d_p}\right) \quad [2.42]$$

Where

$$f_0 = \frac{C_1}{Re_G} + \frac{C_2}{\sqrt{Re_G}} + C_3 \quad [2.43]$$

$$d_p = \frac{6 \cdot (1-\varepsilon)}{a} \quad [2.44]$$

and C_1, C_2 and C_3 are packing-specific constants, with Stichlmair *et al*. (1989) providing values for these constants for a number of different types of random packing as well as some structured packings.

To calculate the irrigated pressure drop the decrease in the bed void fraction due to liquid hold-up is taken into account. This is achieved by extending the equation for calculating the dry bed pressure drop by including a modification to the friction factor as well as particle diameter, which effectively increases as a result of the increased liquid hold-up.

$$\frac{\Delta P_{irr}}{H} = \frac{3}{4} \cdot {f_0}' \cdot \left(\frac{1-\varepsilon'}{\varepsilon^{4.65}}\right) \cdot \left(\frac{\rho_G \cdot u_G^2}{{d_p}'}\right) \quad [2.45]$$

Where

$$\varepsilon' = \varepsilon - h_L \quad [2.46]$$

$$\frac{(1-\varepsilon')}{[{d_p}']^3} = \frac{(1-\varepsilon)}{{d_p}^3} \quad \rightarrow \quad d_p' = d_p \cdot \left[\frac{1-\varepsilon\cdot\left(1-\frac{h_L}{\varepsilon}\right)}{1-\varepsilon}\right]^{\frac{1}{3}} \quad [2.47]$$

$$f_0' = f_0 \cdot \left(\frac{d_{p'}}{d_p}\right)^c \quad \rightarrow \quad f_0' = f_0 \cdot \left\{\frac{\left[1-\varepsilon\cdot\left(1-\frac{h_L}{\varepsilon}\right)\right]}{1-\varepsilon}\right\}^{\frac{c}{3}} \qquad [\ 2.48\ ]$$

$$c = \frac{-\frac{C_1}{Re_G} - \frac{C_2}{2\cdot\sqrt{Re_G}}}{f_0} \qquad [\ 2.49\ ]$$

For Equation [2.47], the number of particles in the irrigated and dry bed are considered the same and thus a change in the void fraction should correspond with a change in particle diameter.

The ratio of the irrigated pressure drop in Equation [2.45] to the dry bed pressure drop in Equation [2.42], in combination with Equations [2.46] to [2.49], yields:

$$\frac{\Delta P_{irr}}{\Delta P_{dry}} = \left[\frac{1-\varepsilon\cdot\left(1-\frac{h_L}{\varepsilon}\right)}{1-\varepsilon}\right]^{\frac{2+c}{3}} \cdot \left(1-\frac{h_L}{\varepsilon}\right)^{-4.65} \qquad [\ 2.50\ ]$$

Two correlations for calculating liquid hold-up are provided, one for below the loading point and another for above. The correlation for liquid hold-up below the loading point was derived from experimental data for an air/water system for 9 different types of packing, which included both random and structured packing. However, this correlation does not take any liquid properties into account and is only dependent on the liquid load, packing surface area and void fraction.

$$h_{L,S} = 0.555 \cdot Fr_L^{\frac{1}{3}} \qquad [\ 2.51\ ]$$

Stichlmair and Fair (1998), who also describe the Stichlmair model, provide an additional correlation for calculating the liquid hold-up below the loading point which takes into account liquid density, viscosity and surface tension.

$$h_{L,S} = 0.93 \cdot \left(\frac{u_L^2 \cdot a}{g}\right)^{\frac{1}{6}} \cdot \left(\frac{\mu_L^2 \cdot a^3}{\rho_L^2 \cdot g}\right)^{\frac{1}{10}} \cdot \left(\frac{\sigma \cdot a^2}{\rho_L \cdot g}\right)^{\frac{1}{8}} \qquad [\ 2.52\ ]$$

Stichlmair and Fair (1998) also summarize values for the exponents in Equation [2.52] published by a number of other authors, who included either all, none, or some of the expounded terms in Equation [2.52]. They note that the large variation in the involved parameters and their exponents highlight the poor and ambiguous knowledge in this field.

Also noteworthy is that the first, second and third expounded terms in Equation [2.52] represent the Froude number, inverse Galilei number and the inverse Bond number, respectively.

The liquid hold-up above the loading point is calculated with an expression which takes into account the influence of gas friction as well as the effect of the pressure gradient:

$$\boldsymbol{h_L = h_{L,S} \cdot \left[1 + 20 \cdot \left(\frac{\Delta P_{irr}}{H \cdot \rho_L \cdot g}\right)^2\right]} \qquad [\ 2.53\ ]$$

Since the irrigated pressure drop is an implicit variable in the liquid hold-up expression in Equation [2.53], an iterative approach is required to calculate the irrigated pressure drop.

The flooding point is defined as the point where a small increase in the gas flow rate results in an infinite increase in irrigated pressure drop. Thus, to determine the flooding point, the derivative of the irrigated pressure drop in Equation [2.50] in combination with the above equations are used in an iterative manner to solve for the gas flow rate at flooding.

$$\left(\frac{\Delta P_{irr}}{H \cdot \rho_L \cdot g}\right)_{Fl}^{-2} - \left[\frac{40 \cdot \left(\frac{2+c}{3}\right) \cdot h_{L,S}}{1 - \varepsilon + h_{L,S} \cdot \left[1 + 20 \cdot \left(\frac{\Delta P_{irr}}{H \cdot \rho_L \cdot g}\right)_{Fl}^2\right]}\right] + \left[\frac{186 \cdot h_{L,S}}{\varepsilon - h_{L,S} \cdot \left[1 + 20 \cdot \left(\frac{\Delta P_{irr}}{H \cdot \rho_L \cdot g}\right)_{Fl}^2\right]}\right] = 0 \qquad [\ 2.54\ ]$$

According to Stichlmair *et al*. (1989) the expression for the liquid hold-up below the loading point in Equation [2.51] is only applicable for liquid viscosities up to 5 cP, with the influence of higher viscosities not being accounted for. Since the model was only verified with experimental data on air/water systems, large errors can be obtained when using the model with liquids having substantially different properties compared to that of water.

2.6.3 KG-TOWER

Koch-Glitch, the manufacturer of Intalox Ultra random packing, provides a software package to customers that assist in the specification of mass transfer equipment. The software package is known as KG-TOWER and can be used to predict, among other, the pressure drop over a packed bed of packing material manufactured by Koch-Glitch. Table 2.4 lists the inputs that are required for calculating the pressure drop over a packed bed:

Table 2.4: Required Parameters in KG-Tower

Liquid	Gas	Column specifications
Flow rate	Flow rate	Packing type
Density	Density	Packing size
Viscosity	Viscosity	Column diameter
Surface tension		Packed bed height

The software provides the calculated pressure drop at the specified conditions, which can be adjusted to calculate the pressure drop up to the flooding point. However, the software does not predict the liquid hold-up or entrainment. Furthermore, the liquid viscosity and surface tension is limited to the following ranges:

Liquid viscosity : 0.07 - 5 mPa.s

Surface Tension : 3 - 73 mN/m

2.7 Literature Conclusion

Throughout the years an extensive range of different random packings have been developed in the pursuit of improvements in capacity and separation efficiency. However, to utilise a certain random packing, the hydrodynamic behaviour that can be expected from the packing should be known. In most cases, this requires a model that can predict this behaviour. While the general influence of different physical properties on the hydrodynamic behaviour in packed columns are known and a number of different hydrodynamic models are available for predicting this behaviour, experimental data are still required for verifying the accuracy of the model predictions. The accuracy of the semi-theoretical hydrodynamic models discussed in this section are investigated in a following section with regard to the fourth generation Intalox Ultra random packing.

3. Experimental Design and Methodology

3.1 Existing Experimental Setup

The pilot plant setup that was used throughout this project was designed and constructed during a previous master's project by Sarel Lamprecht in 2010. A brief description of the pilot plant will be given. For a detailed design, refer to Lamprecht (2010).

To investigate the hydrodynamic behaviour throughout the hydrodynamic operating range, a setup is required in which the liquid and gas flow rates can be independently varied. This is not possible in a distillation column operated under total reflux, and deviating from production rates in an industrial column for research purposes would also not be feasible. For this reason, the pilot plant was designed so that liquid and gas flow rates can be varied independently and physical liquid and gas properties can be altered to investigate their respective effects. By careful consideration of the liquid and gas systems studied, mass transfer could be minimized or eliminated. While in an industrial column the physical properties change throughout the column as a result of mass transfer, the pilot plant provides a simplified version, since the fluid properties remain constant throughout the column.

Since the plant was constructed to investigate modern high capacity packings, it was important to be able to achieve liquid flow rates that are higher than what is typically associated with previous generation packings (Billet & Schultes, 1999; Maćkowiak, 2009). The column was designed to operate at liquid flow rates between 0 – 122 $m^3/(m^2.h)$.

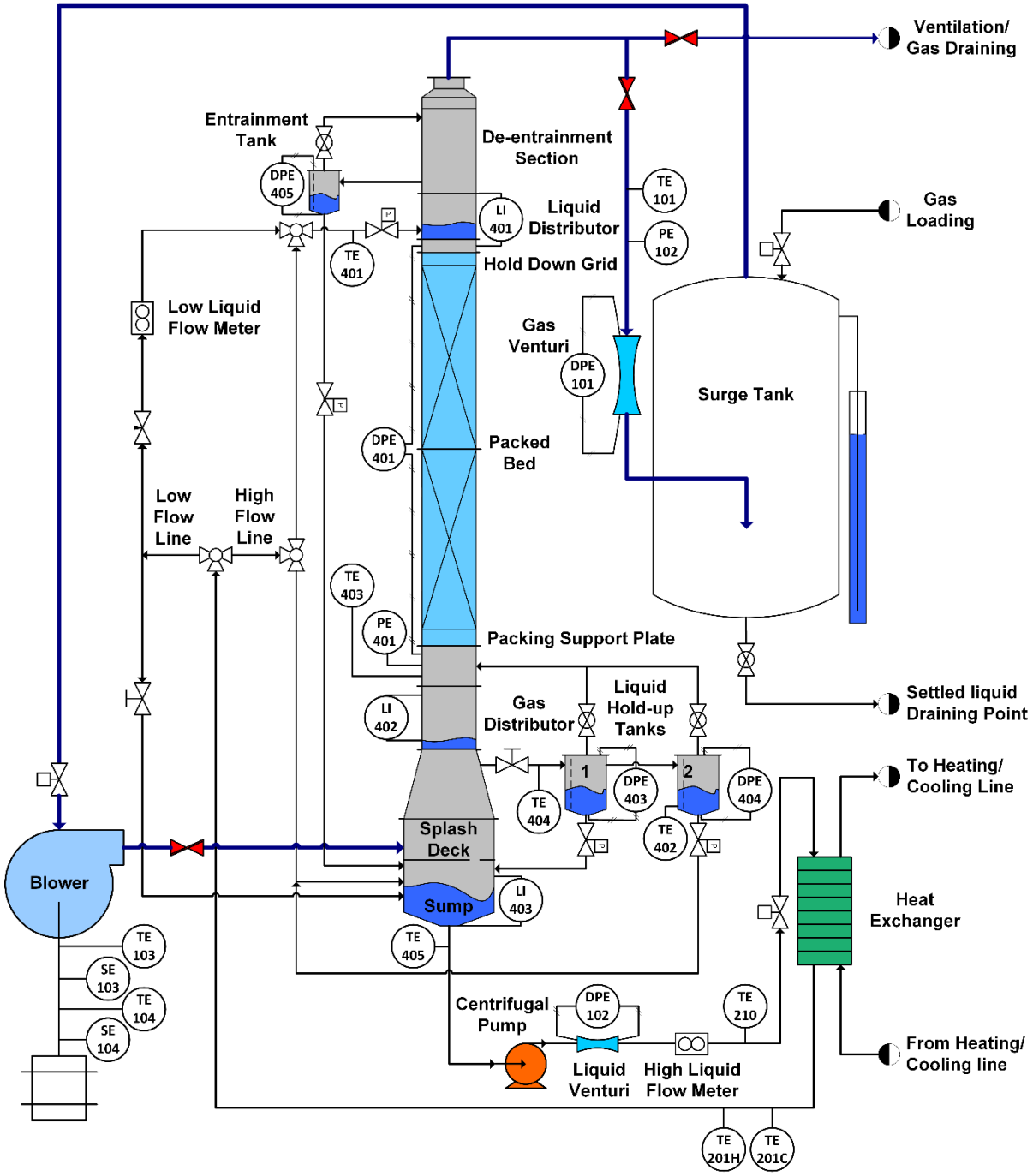

Figure 3.1: Packed Column Pilot Plant Process Flow Diagram [Adapted from Lamprecht (2010)]

3.1.1 Packed Column

The column has an inside diameter of 393 mm with tolerance of ± 3 mm. This diameter was chosen to ensure that the experimental data generated would be of industrial value, since wall-effects become more prominent in smaller diameter columns (Kister, 1992). Another reason was to accommodate the standard size structured packings that are produced by packing manufacturers for future research on

these packings. The column has a packed bed height of 3 meters, which is smaller than the suggested height before redistribution of liquid is required (Kister, 1992; Sinnott & Towler, 2009).

From the bottom, the column consists of a liquid sump with a splash deck above the liquid return line and below the blower inlet. This is to prevent the entrainment of liquid returning to the sump. Situated above the splash deck is a deck type gas distributor on which liquid is collected, which flows to the two cascading liquid hold-up tanks. A random packing support plate is situated above the gas distributor. The packed bed section consists of a borosilicate glass column to provide visual access to the packed bed. Above the packed bed a hold-down grid prevents the packing material from becoming fluidised at high gas velocities. A channel type liquid distributor is used for uniformly distributing the liquid over the packed bed. Situated above the liquid distributor is a de-entrainer which induces a centrifugal force on the gas flow, removing any liquid droplets that are entrained. The entrained liquid is collected and passed to an entrainment tank. A demister pad is also used above the de-entrainer to remove any additional liquid droplets not removed by the de-entrainer.

3.1.2 Liquid Circulation loop

The liquid is pumped by a centrifugal pump through both a venturi flow meter and a positive displacement, high liquid flow meter, after which it passes through a control valve to a heat exchanger. The heat exchanger is used to either heat up or cool down the liquid depending on the current liquid temperature and set point. Via a 3-way valve, the liquid can then be diverted in two directions depending on the liquid flow rate, since the high liquid flow meter is not able to accurately measure the low liquid flow rates investigated here. For a low liquid flow rate (< 2 m^3/h), the liquid is diverted to the low liquid line where it passes through a needle valve and a positive displacement, low liquid flow meter. For a high liquid flow rate (2 – 20 m^3/h), the liquid is diverted to a high liquid line. The high liquid line is split again by a 3-way valve to return the liquid either back to the sump or to a third 3-way valve were the low and high liquid lines join to feed the liquid to the top of the column. The return line to the sump is used to circulate the liquid through the heat exchanger to obtain the operating liquid temperature. Liquid flowing either through the low or high liquid line is pumped to the top of the column entering the liquid distributor. The liquid that flows down the column is brought into contact with the gas and is collected on the gas distributor plate. From here, the liquid flows through the liquid hold-up tank (hold-up tank 1) and back to the liquid sump. A second liquid hold-up tank (hold-up tank 2) is situated next to hold-up tank 1, where liquid can cascade over to hold-up tank 2 when measuring liquid hold-up and the volume of collected liquid is larger than the volume of hold-up tank 1. Any liquid that is entrained is collected in the entrainment tank, which can also be passed back down to the liquid sump.

3.1.3 Gas Circulation Loop

A centrifugal blower is used to circulate gas through the plant. From the blower, the gas flows to the top section of the sump above the splash deck. The gas passes through the gas distributor to enter the packed column where it comes into contact with the liquid. Above the packed bed the gas flows past the liquid distributor and through the de-entrainer and demister to exit at the top of the column. Finally, the gas pass through a venturi gas flow meter after which it enters a surge tank connected to the suction side of the blower.

3.1.4 Sensor Placement

A number of sensors are placed throughout the pilot plant. These include temperature probes, pressure transmitters and flow meters. A summary of the placement of the different sensors are given below.

Temperature Probes

1. Liquid sump outlet line (TE-405)
2. After the high liquid flow meter (TE-210)
3. 2 x Heat exchanger outlet line (processing side) (TE-201C, TE-201H)
4. At the liquid feed point to the packed column (TE-401)
5. In the feed line to liquid hold-up tank 1 (TE-404)
6. Inside liquid hold-up tank 2 (TE402)
7. Above the gas distributor (T-403)
8. Before the gas venturi flow meter (TE-101)
9. 2 x Gas blower shaft (TE-103, TE-104)
10. In the hot water bath (heat transfer fluid) [not shown on Figure 3.1] (TE-301)

Differential Pressure Transmitters

1. Over packed bed (DPE-401)
2. Over liquid venturi flow meter (DPE-102)
3. Over gas venturi flow meter (DPE-101)
4. Over of liquid hold-up tank 1 (DPE-403)
5. Over of liquid hold-up tank 2 (DPE-404)
6. Over of entrainment tank (DPE-405)

Absolute Pressure Transmitter

Two absolute pressure transmitters are used. One of these transmitters (PE-102) is placed at the inlet of the gas venturi flow meter. The other transmitter (PE-401) is placed below the packing support at the bottom of the packed bed.

Flow Meters

The low liquid flow line contains a positive displacement low liquid flow meter (E-402) that is used for measuring liquid flow rates below 2 m^3/h. Although a positive displacement high liquid flow meter (E-207) is installed in the high liquid line, it was found that this flow meter gave inaccurate flow rate measurements. The liquid venturi flow meter (E-206) was originally installed as a backup and verification tool, but was used throughout this project for measuring flow rates between 2 and 20 m^3/h.

A gas venturi flow meter (E-103) is positioned before the gas inlet to the surge tank and is used for measuring the gas flow rate. The venturi flow meter is used since it can cover the entire operating range with a single flow meter.

Level Indicators

Liquid level indicators are installed in the liquid distributor (LI-401), gas distributor (LI-402) and liquid sump (LI-403).

Vibration Sensors

Two vibration sensors are installed on the gas blower shaft (SE-103 and SE-104) for detecting malfunction of the blower with regard to shaft misalignment or any other excessive vibrations.

3.1.5 Equipment Calibration and Verification

To ensure the accurate measurement of pressure drop, liquid hold-up and entrainment, a number of calibration and verification procedures were performed. This includes the calibration of the liquid venturi flow meter, both the liquid hold-up tanks and the entrainment tank. The differential pressure transmitters used for measuring the column pressure drop and the pressure drop over the gas venturi flow meter were verified, as well as the positive displacement low liquid flow meter. The procedures and results are provided in Sections 9.1 to 9.5.

3.2 Liquid Distributor Design

Through Lamprecht's (2010) work on the pilot plant, it was found that the entrainment data that was measured showed very low resolution at the start of the entrainment measurements. As the gas flow rate was increased, the measured entrainment rate would remain zero until a point was reached where the entrainment rate would suddenly jump to over 10 % liquid entrainment. The cause of this phenomenon was reasoned to be the low open area of the pan type liquid distributor that was used. To investigate this phenomenon and to measure entrainment data with a higher resolution, it was decided to design and build a new liquid distributor with a larger open area.

3.2.1 Objectives

In the design of the new liquid distributor, the following objectives were set:

- Maximize open area available for gas flow
- One distributor to cover the entire liquid flow rate range that will be investigated (Turn down ratio of 20:1)
- Does not require the column to be opened for any adjustment or changes to the distributor for different liquid flow rates
- Fit into the column with minimum change to the current setup (height limitation of 624 mm)
- Velocity of liquid distributed onto packing below 1.5 m/s

3.2.2 Designs Considered

A number of different distributor designs were considered during the design of the new liquid distributor. These different designs are listed below together with their respective advantages and disadvantages with regard to the set design objectives.

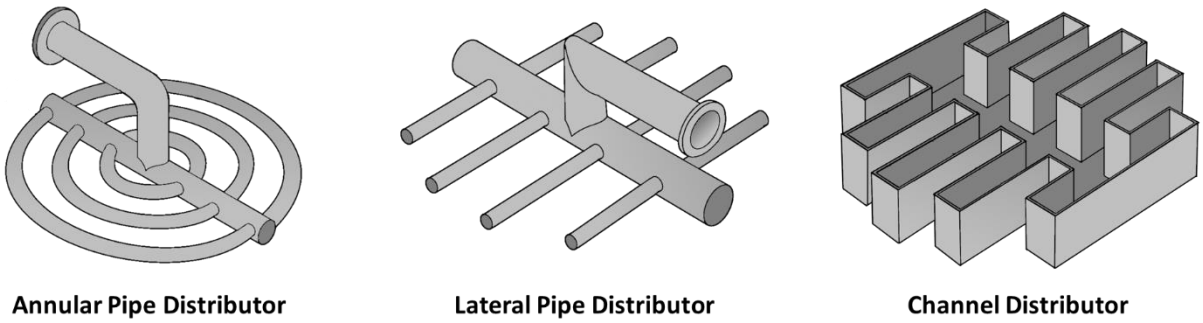

Figure 3.2: Distributor designs considered [Redrawn from BTS Engineering (2015)]

Annular Pipes with Orifices/Drip Tubes

While this design would provide a large open area for gas flow it would not be able to cover the large liquid flow rate range (turn down) with a single liquid distributor. Since the distributor would be operated under pressure, small orifices would ensure even flow as well as low liquid velocity onto the packing for low liquid flow rates, but would result in very high liquid velocity at high liquid flow rates. If the orifices were to be increased to reduce the liquid velocity at high liquid flow rates, it would result in uneven flow from orifices at low liquid flow rates. This design also requires a very large number of orifices/drip tubes to keep a constant distribution of drip point density in the radial direction.

Lateral Pipes with Orifices/Drip Tubes

While also providing a large open area for gas flow, this design presents the same problem as the annular pipe design with regard to orifice size and liquid velocity. However, it does not present the same problem with regard to drip point distribution.

Channel Type Distributor

With a channel type distributor, a larger open area can be attained compared to the deck type distributor used by Lamprecht (2010), but smaller than what can be achieved with an annular or lateral pipe distributor. Since this design would make use of gravity feed, a large flow rate range can be accommodated by using conductor/drip tubes with metering orifices, ensuring a liquid level in the distributor, even at low flow rates.

Considering the mentioned advantages, the channel type distributor was chosen for the design of the new liquid distributor.

3.2.3 Design of Channel Type Distributor

The mechanical design drawings for the channel type distributor are provided in Section 9.6.1 and different stages of assembly illustrated in Figure 3.3.

The distributor channel section was constructed from 2 mm 306 stainless steel to prevent corrosion and to prevent problems with weld distortion and sheet metal bending.

The new design has the same number of drip points (19) as the distributor used by Lamprecht (2010) and thus also has the same drip point density (157 per m^2). Increasing the number of drip points will

either result in a decrease in open area or an uneven distribution of drip points. The new design also has the same arrangement of drip points.

The conductor tubes, manufactured from 306 stainless steel, have an outer diameter of 19.05 mm and a wall thickness of 1.5 mm. The size was chosen to minimize the liquid velocity onto the packing while also minimizing the liquid level in the distributor. Each conductor tube has a total of 8 metering orifices, 4 on each side of the tube, increasing in size from the bottom (3, 6, 9, 9 mm). The 3 mm orifice at the bottom of the conductor tube, flush with the distributor base, is required to completely drain the distributor when changing the test liquid.

The new design has a total open area for gas flow equal to 60 % compared to the 30 % of the distributor used by Lamprecht (2010) (Figure 3.4).

To maximize the open area available for gas flow the distributor is fed from the top. A total of 14 feed points are arranged throughout the distributor to minimize the liquid velocity into the distributor and to ensure an even balance of liquid head throughout the distributor. Each feed pipe, manufactured from 306 stainless steel, has an outer diameter of 19.05 mm with a wall thickness of 1.5 mm and extends to 10 mm above the distributor base. The pre-distributor is fed from three directions and operated under pressure.

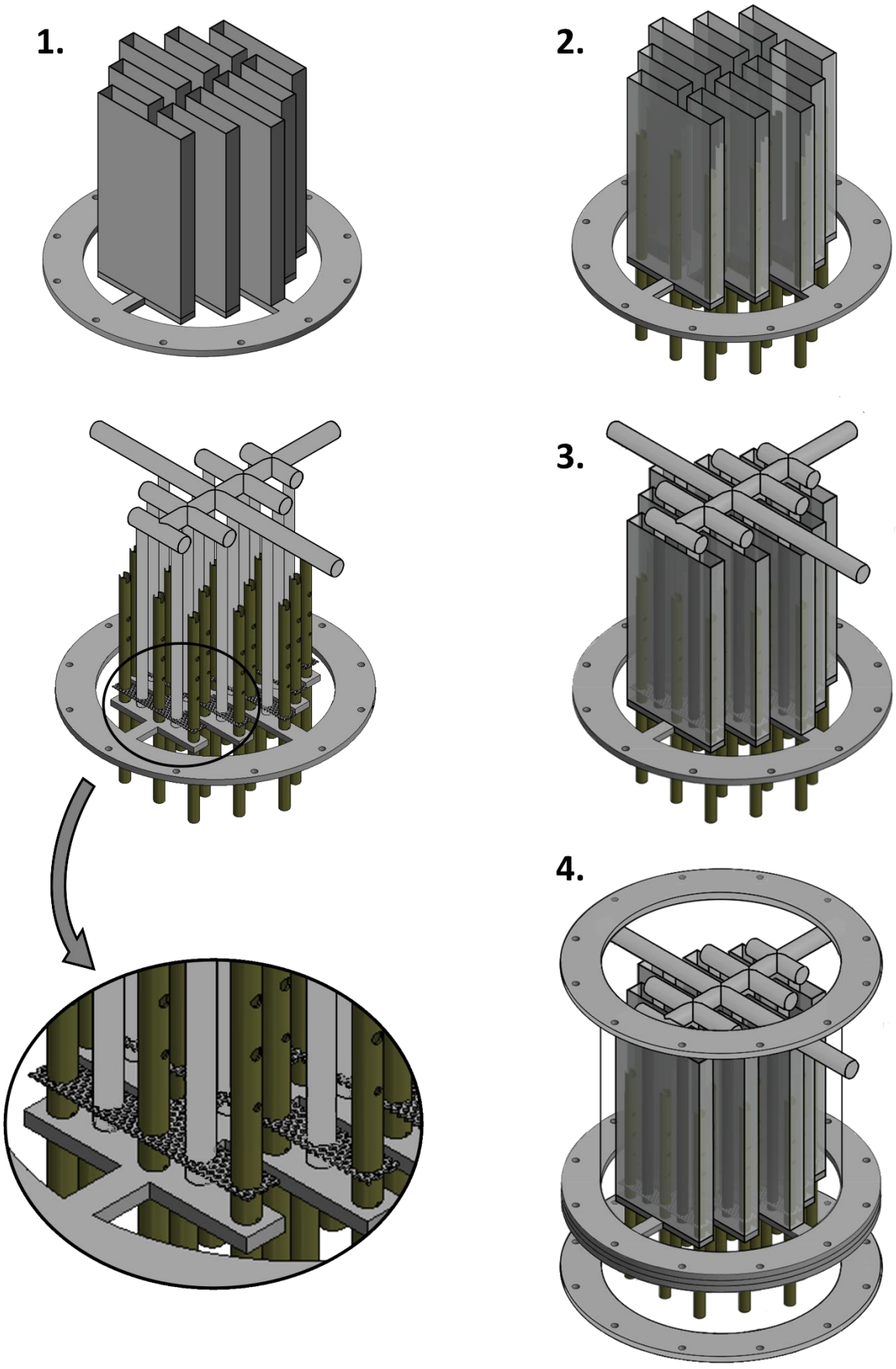

Figure 3.3: Stages of distributor assembly

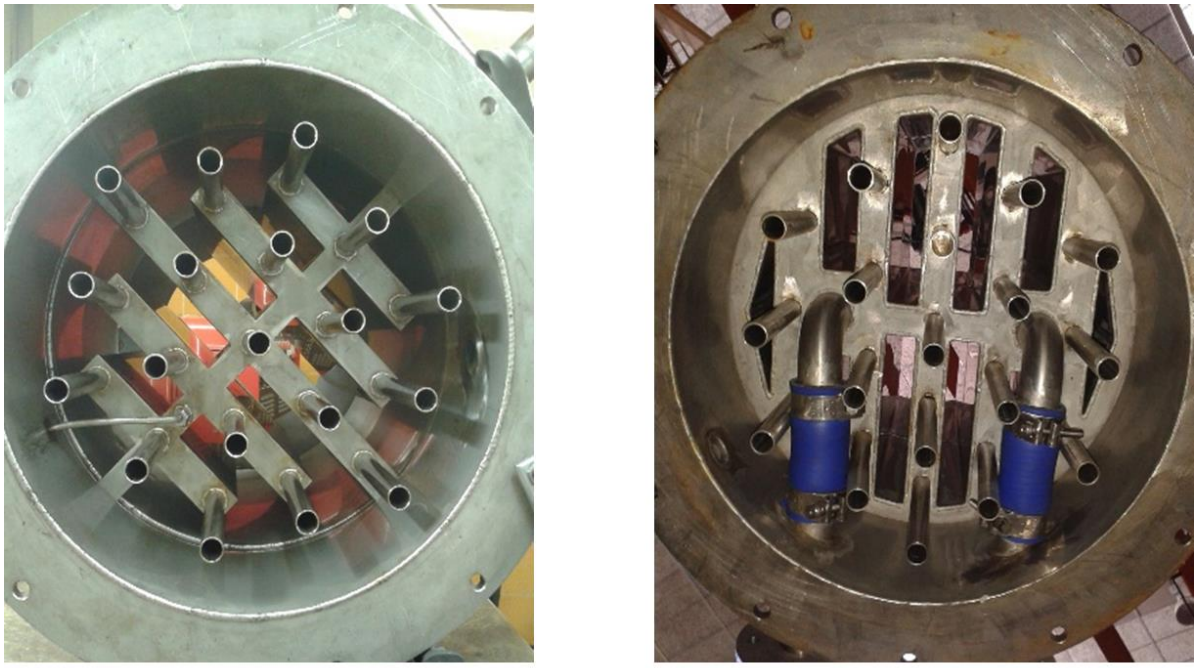

Figure 3.4: Visual comparison of the open area of the new channel type liquid distributor (a) and the old pan type liquid distributor (b) from below

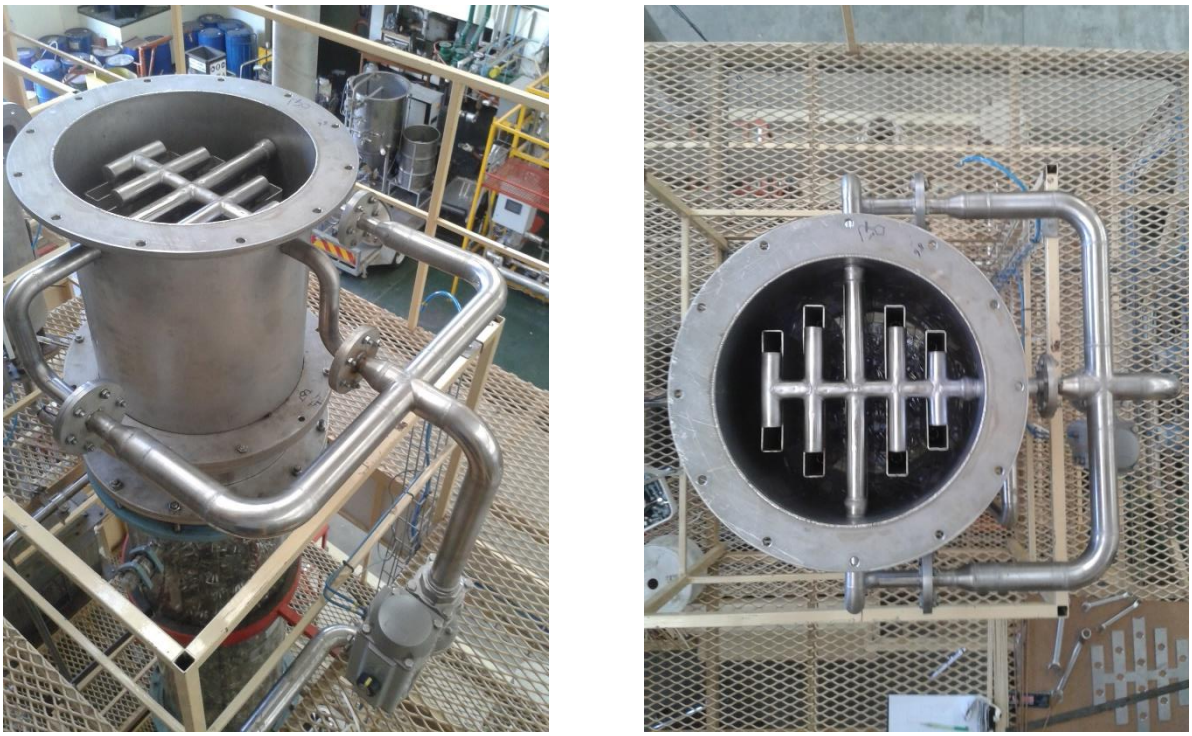

Figure 3.5: Installed liquid distributor assembly

Note in Figure 3.5 that the liquid feed to the top of the column is lower than the liquid feed lines into the liquid distributor. The reason for this is to minimize the volume of liquid that drains out of the pre-distributor when liquid hold-up is measured.

A perforated baffle, manufactured from 306 stainless steel, is inserted 25 mm above the distributor base to minimize turbulence and horizontal velocity higher up in the distributor. The perforated baffle has an op area of 51 %, consisting of 3/16" holes in a staggered pattern with 1/4" hole-centres.

A liquid level indicator tube was installed on the outside of the distribution section. The bottom part of the tube passes through the column wall and connects to the underside of the distributor channel, while the top part is flush with the inside column wall.

Liquid Velocities and Distribution Quality

The liquid velocities through the feed pipes to the pre-distributor, distributor and conductor tubes are summarized in Table 3.1 below (also refer to Figure 3.6). The design objective to keep the distributed liquid velocity onto the packing below 1.5 m/s was met, with the maximum liquid velocity calculated to be 1.1 m/s.

Table 3.1: Liquid velocities to and from liquid distributor

Feed to Pre-distributor (1)		
Max feed velocity	2.1	m/s
Min feed velocity	0.10	m/s

Feed to Distributor (2)		
Max feed velocity	1.5	m/s
Min feed velocity	0.073	m/s

Conductor Tubes (3)		
Max velocity	1.1	m/s
Min velocity	0.053	m/s

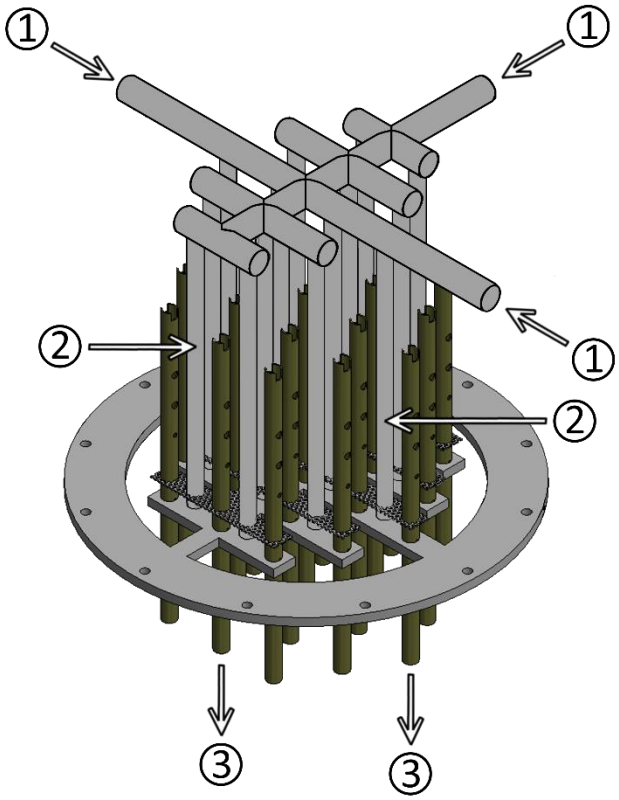

Figure 3.6: Pre-distributor and drip tubes assembly

The liquid distribution quality was indirectly tested by measuring the liquid level at multiple points in the distributor channel with both water and silicone oil at different liquid flow rates. A widely used measure for liquid distribution quality is the coefficient of variance, which, in this case, expresses the standard deviation over the mean liquid level in the liquid distributor (Xu, 2000). The highest coefficient of variance that was obtained was equal to 2 %, which is well within the acceptable criteria of <5 % for good liquid distribution quality (Dhabalia and Pilling, 2006). The testing procedure, as well as the test results, is provided in Section 9.6.2.

3.3 Other Modifications to Pilot Plant

3.3.1 De-entrainment Section

The de-entrainment section above the liquid distributor has a diameter equal to 270 mm, which is smaller than the column diameter. To minimize liquid impingement on the annulus below the de-entrainer and ensure a smooth transition of entrained liquid into the de-entrainment section, a cone with an angle of 35° with respect to the horizontal was installed in the available space below the de-entrainer.

It was also found that the pipe leading from the de-entrainment liquid hold-up section to the entrainment tank was not flush with the de-entrainer base. This created a dead space that had to fill up with liquid before the entrained liquid could pass to the entrainment tank. This was caused by the de-entrainment section's bottom flange being in the way (Figure 3.7). To rectify this, a slanted toroidal shape (3° with respect to the horizontal) was installed to fill up the dead space and ensure that all entrained liquid in the hold-up section can flow to the entrainment tank.

Figure 3.7: Dead space in de-entrainment section and slanted toroidal shape to fill up the volume

3.3.2 Larger Liquid Hold-up Tank

Lamprecht (2010), after finishing his project, installed a secondary liquid hold-up tank (45 L) to accommodate higher liquid hold-up volumes, especially when working with silicone oil. After the primary tank filled up, liquid would cascade over to the second tank. Through this project however, it was found that the combined volume of both tanks was still too small to measure the liquid hold-up at the high liquid flow rates when working with the more viscous liquids. For this reason, the secondary tank was replaced with a larger tank with a volume of 75 litres.

3.4 Experimental Method

This section provides an overview of the experimental procedures for measuring the pressure drop, liquid hold-up and entrainment. Detailed step-by-step procedures are provided in Section 9.10 for

plant start-up, gas loading, pressure drop, liquid hold-up and entrainment measurements, static liquid hold-up measurement and plant shutdown. For these procedures, it is assumed that the procedures for loading the column with packing (the columns is dry-packed and the packing washed to remove any oil or grease still present from production), flushing the system with a suitable solvent, as well as drying the column and loading the system with liquid have already been completed.

3.4.1 Start-up Procedure

The liquid in the sump is circulated through the heat exchanger and back to the sump via the high liquid flow line, allowing the liquid to reach the operating temperature. When the liquid temperature is close to the operating temperature, the liquid flow is diverted to flow through the packed bed. To allow for proper wetting of the packing, the liquid should be allowed to flow through the packed bed for about 30 minutes at a high liquid flow rate. At this point the gas blower is started, allowing the gas to circulate through the plant and reach the operating temperature. When the operating conditions have been reached, the gas blower is switched off. Next, the “Hold-up Sync” sequence is triggered, filling liquid hold-up tank 2 to its minimum liquid level. After the sequence has finished the pump is switched off.

Depending on the desired liquid flow rate (either high or low as described earlier) the liquid circulation loop is set to the desired flow path. The centrifugal pump is started again to allow liquid to circulate through the packed bed. The blower is also switched on. The flow rate is adjusted until the desired liquid flow rate is reached, after which the gas flow rate is also adjusted to the desired flow rate.

3.4.2 Pressure Drop

To measure the pressure drop over the column, the control panel is monitored to ensure that a stable gas and liquid flow rate, as well as a stable pressure drop over the column, has been reached and remains stable for at least 5 minutes. If all parameters are stable at their desired values, including liquid and gas temperature, the pressure drop is sampled once per second for a period of two minutes.

3.4.3 Liquid Hold-up

The total liquid hold-up, as discussed in Section 2.3.2, consists of the static and dynamic liquid hold-up. While the dynamic liquid hold-up is measured in the packed column, the static liquid hold-up is measured in a separate 1:10 scale test section of the column, consisting of a stainless steel cylinder, 400 mm in diameter and 300 mm high, with the bottom covered with a coarse grid. To measure the static liquid hold-up, a procedure is followed where the entire test scale section, both empty and filled with packing, is weighed before and after being completely submerged in the liquid of interest and

allowed to drain from the packing for 10 to 15 minutes. With the measured weights, the static liquid hold-up is calculated.

The dynamic liquid hold-up is measured after the pressure drop measurement, while all the relevant parameters are still stable at their desired values. The process by which the dynamic liquid hold-up is measured consists of the drain valve of hold-up tank 1 closing, allowing the tank to fill with liquid. When the liquid level reaches a pre-set minimum level in hold-up tank 1, the liquid feed to the column is cut and the pump and blower are switched off. This allows the liquid present in the column to drain into hold-up tank 1 and cascade over to hold-up tank 2 once hold-up tank 1 is filled.

Before the liquid hold-up can be measured, minimum liquid levels are set for the liquid hold-up tanks, establishing a reference point at which the liquid feed is cut and from which the liquid hold-up volume is calculated. It is recommended that this liquid level be higher than the viewing port in hold-up tank 1 and well above the dish bottom section of hold-up tank 2. By monitoring the liquid hold-up graph on the control panel, the end of the sampling period is reached when a zero gradient is achieved. This takes approximately 10 to 15 minutes, depending on the viscosity of the liquid.

To determine the dynamic liquid hold-up, the liquid present on the liquid and gas distributors also has to be taken into account, since this liquid also drains into the hold-up tanks when measuring the dynamic liquid hold-up. The volume of liquid present on the liquid and gas distributors is determined by measuring the height of the liquid level through the level indicators on both distributors. The liquid volume is then calculated by multiplying this height by the area that the liquid occupies. In addition, with the new liquid distributor, the liquid volume draining from the pre-distributor should also be accounted for. The liquid volume that drains from the pre-distributor was measured during the commissioning of the new liquid distributor over the range of liquid flow rates investigated for water and silicone oil. More information about these measurements are provided in Section 9.6.3.

By subtracting the volume of liquid in both the liquid and gas distributors, as well as the volume of liquid drained form the pre-distributor, from the liquid hold-up measured through the above process, the dynamic liquid hold-up is obtained. The total liquid hold up is then calculated by adding the static and dynamic liquid hold-up.

3.4.4 Liquid Entrainment

Unlike the liquid hold-up measurement procedure, which requires the liquid and gas flow to be stopped, entrainment is measured while the column is in operation. A similar start-up procedure to that discussed for the pressure drop measurements is followed to achieve the desired stable operating

conditions. To measure liquid entrainment, the entrainment tank draining valve is closed, which allows the tank to fill with entrained liquid. Entrainment is calculated as the rate of liquid volume that is entrained as a function of time. As a result the entrained liquid is either captured for a certain period of time (5 minutes) or until the entrainment tank is filled with liquid.

3.4.5 Analytical Methods

Liquid Density

The liquid density of all liquids was analysed with the SIGMA 702 Tensiometer which is also capable of measuring liquid density with a resolution of 0.1 kg/m^3. The density is measured by submerging a glass ball, connected to a sensitive micro balance, into the liquid and measuring the buoyancy force exerted by the liquid on the glass ball.

Liquid Surface Tension

The surface tension of all liquids was analysed with the SIGMA 702 Du Noüy Ring Tensiometer, which has a resolution of 0.01 mN/m. The tensiometer measures the surface tension by submersing a platinum ring into the liquid and precisely measuring the force required to pull the ring from the liquid.

Liquid Viscosity

The liquid viscosity of all liquids was analysed with a Paar Physica MCR501 Rheometer, which has a resolution of 0.01 mPa.s. The liquid viscosity is measured by submersing a cylinder into a sleeve section with the liquid occupying the space between the cylinder and sleeve. The cylinder is rotated and the force acting on the cylinder as a result of the viscous friction between the cylinder and sleeve is measured. From here, the liquid viscosity is calculated.

Gas Composition

The gas composition in the pilot plant was determined using an HP 5890 gas chromatograph with TCD detector and a Hayesep Q column (6 ft x 2.1 mm), which is supplied by Supelco. The response factor for nitrogen with the TCD detector was determined during the development of the GC method, while the response factor for carbon dioxide used in this project was determined by Uys (2012). The GC method and the procedure by which the response factor was determined are provided in Sections 9.8 and 9.9.

3.5 Design of Experiments

Since the factors that were investigated, which influenced the different response variables, were set to more than two or three levels, a statistical design of experiments was not possible. A complete randomized design was also not used, since both changing the gas and liquid loaded to the system result in losing the gas that was in the system as well as the time associated with changing the system. What creates further complexity is the fact that the physical properties cannot be individually adjusted, but are grouped together as the different chemicals that will be used. However, the interest is in the properties of these chemicals and not the chemicals themselves. The order in which the different liquid and gas flow rate runs were performed was randomized to a certain extent. The number of experiments that were performed can be determined when considering the number of levels for each factor investigated.

Table 3.2: Factors and levels that were investigated

Factor	Number of Levels	Level value
Packing	2	Intalox Ultra A and O
Liquids	4	Water, Ethylene Glycol, Isopar G, Medium silicone oil
Gasses	2	Air, Carbon Dioxide
Liquid flow rates	5	6, 37, 73, 98, and 122 $m^3/(m^2.h)$
Total	**80**	-

The combination of Isopar G and air was however not tested because of the safety concern associated with the flammability of this liquid. Instead air was substituted with nitrogen for these experiments. The centrifugal pump was not able to achieve a liquid flow rate of 122 $m^3/(m^2.h)$ when working with silicone oil. For this reason silicone oil/air and silicone oil/CO_2 was only tested at the four lower liquid flow rates. Thus a total of 76 different combinations of packing, liquids, gasses and liquid flow rates were tested. For each of these, approximately 15 pressure drop and liquid hold-up data points were measured throughout the hydrodynamic range, from the pre-loading region to beyond flooding.

3.6 Measurement Accuracy

A number of factors can influence the accuracy of the experimental data. These include system leakages, incorrect calibration of sensors, hydrodynamic equilibrium and experimental error. The packed column was tested for any leakages and all sensors were calibrated by Lamprecht (2010) during commissioning of the plant. Repeated leakage checks were also performed throughout this project, as well as a number of calibration and verification test as discussed in Section 3.1.5. Table 3.3 provides the maximum error in the different experimental parameters. A more in-depth analysis of the errors in these parameters and the different sensors required for calculating the parameters are provided in Section 9.7.

Table 3.3: Maximum error in experimental parameters

Parameter	Measurement Range	Maximum Error	Units
Gas flow rate	293 – 3292	182	kg/h
Vapour flow factor	0.51 – 6.11	0.32	$(m/s).(kg/m^3)$
Low liquid flow rate	0 – 2	0.018	m^3/h
Venturi Liquid flow rate	4.38 – 14.90	0.43	m^3/h
Packed bed pressure drop	5 – 2266	11	Pa/m
Liquid hold-up	0.0094 – 0.3254	0.0083	m^3/m^3
Entrainment rate	0 – 52	1.76	% of feed

4. Experimental Results & Discussion

In this section the experimental data that were measured are verified and a method to determine the loading and flooding points from the experimental data is described. This is followed by a discussion on the effect of physical liquid and gas properties as well as packing size on the hydrodynamic behaviour with regard to the experimental data.

4.1 Experimental Data Verification

Lamprecht (2010), in commissioning the pilot plant after construction, verified the measured pressure drop and liquid hold-up data for 38 mm Pall Rings with water and air, by comparing the measured data to the pressure drop and liquid hold-up predicted with the Billet and Schultes (1999) hydrodynamic model. Lamprecht (2010) also compared the experimental pressure drop data for 1.5" IMTP with water and air to the pressure drop predicted with the KG-Tower simulation package. Lamprecht (2010) concluded that the measured data followed similar trends as the models, within their reliable limits. According to Lamprecht (2010) the experimental setup can accurately measure pressure drop and liquid hold-up data.

The experimental data measured in this project is verified with the experimental data for 1.5" Intalox Ultra A measured by Lamprecht (2010).

Initial experimental pressure drop measurements were in good agreement with the experimental pressure drop measured by Lamprecht (2010). Figure 4.1 and Figure 4.2 compares the repeated experimental pressure drop measurements for 1.5" Intalox Ultra A with air and water at 37 and 98 $m^3/(m^2.h)$, respectively, to the pressure drop measured by Lamprecht (2010) for the same conditions. The measured pressure drop trends for both flow rates follow the same trends as measured by Lamprecht (2010). For 37 $m^3/(m^2.h)$, all experimental pressure drop measurements are within ± 10 % of the pressure drop measured by Lamprecht (2010). For 98 $m^3/(m^2.h)$, there are slight differences in the loading region between the repeated experimental pressure drop measurements and Lamprecht's data, although the overall comparison is relatively good.

The experimental dry bed pressure drop for the 1.5" Intalox Ultra A with air also agreed very well with what was measured by Lamprecht (2010), with all pressure drop measurements within ± 10 % of Lamprecht's data.

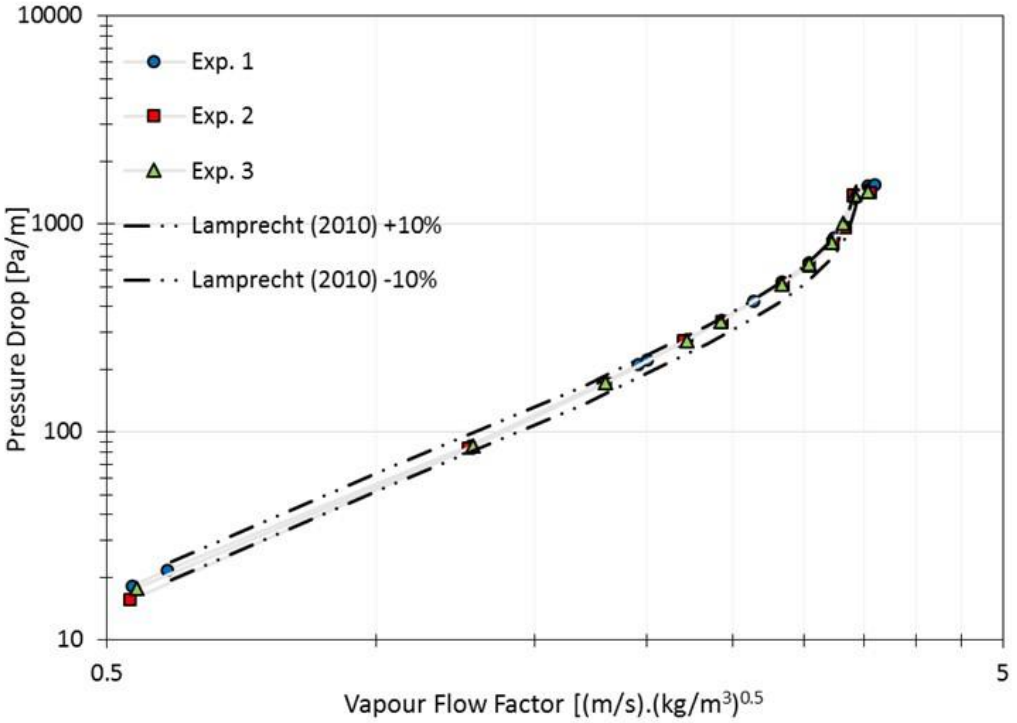

Figure 4.1: Comparison of repeated experimental pressure drop measurements with the pressure drop measured by Lamprecht (2010) for 1.5" Intalox Ultra A, air and water at 37 $m^3/(m^2.h)$

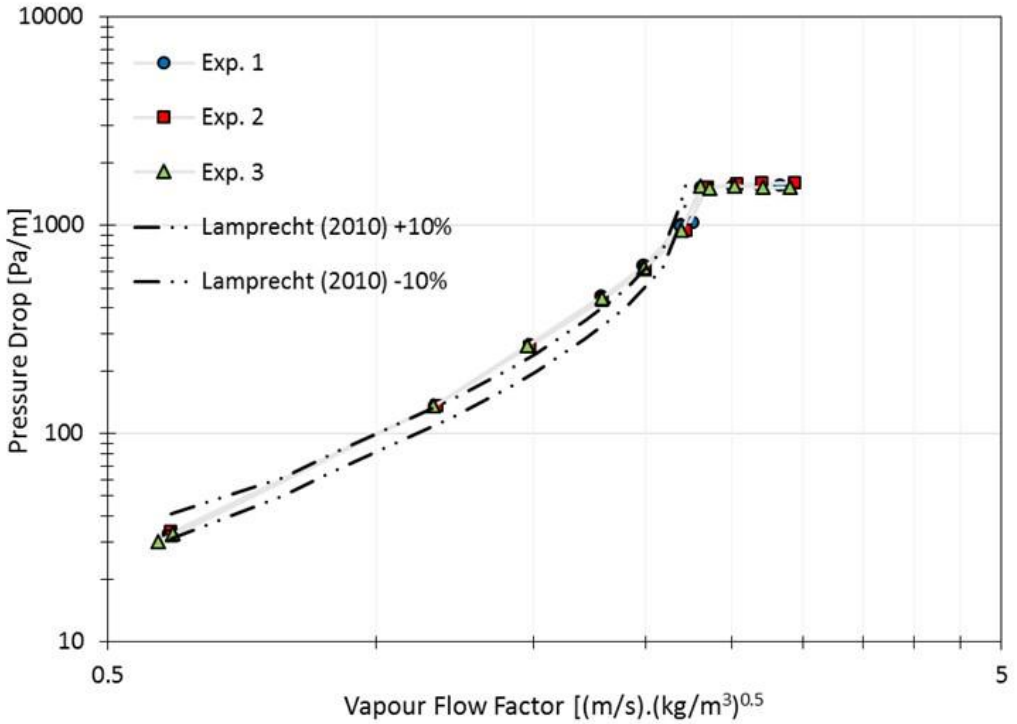

Figure 4.2: Comparison of repeated experimental pressure drop measurements with the pressure drop measured by Lamprecht (2010) for 1.5" Intalox Ultra A, air and water at 98 $m^3/(m^2.h)$

The liquid hold-up data that was measured initially for water/air with 1.5" Intalox Ultra A were significantly higher than what was measured by Lamprecht (2010) and also showed significant amount of variation between repeated measurements. The large difference between the measured liquid hold-up data and that of Lamprecht (2010) was found to be caused by an empty column hold-up volume that Lamprecht (2010) added when calculating the dynamic liquid hold-up. The empty column hold-up volume that Lamprecht (2010) added was is the liquid hold-up that was measured when no packing was present in the column.

The large variation in the measured liquid hold-up data was caused by hold-up tank 1's minimum liquid level set at a value that was too low. This minimum level is the level the liquid must reach to trigger the hold-up sequence and cut the liquid feed to the column. If the level is set too low, an oscillating liquid level, caused by liquid splashing, can result in premature trigger of the hold-up sequence at a level different from the set minimum level, resulting in an inaccurate reference point from which the liquid hold-up volume is measured.

When accounting for the empty column hold-up in Lamprecht's data and setting the minimum liquid level to an appropriate value, the measured liquid hold-up in the pre-loading region was in good agreement with what was measured by Lamprecht (2010).

When water/air experiments, with 1.5" Intalox Ultra A, were repeated at a later stage in the project, variations in the flooding point were observed, with all of these at higher gas flow rates than what was measured by Lamprecht (2010) (Figure 4.3 and Figure 4.4). The variation in the data was initially observed after a water/CO_2 system was tested.

The measured dry bed pressure drop was however still in good agreement with what was measured by Lamprecht (2010) and with what was measured before. The phenomenon thus had to be related to the liquid phase.

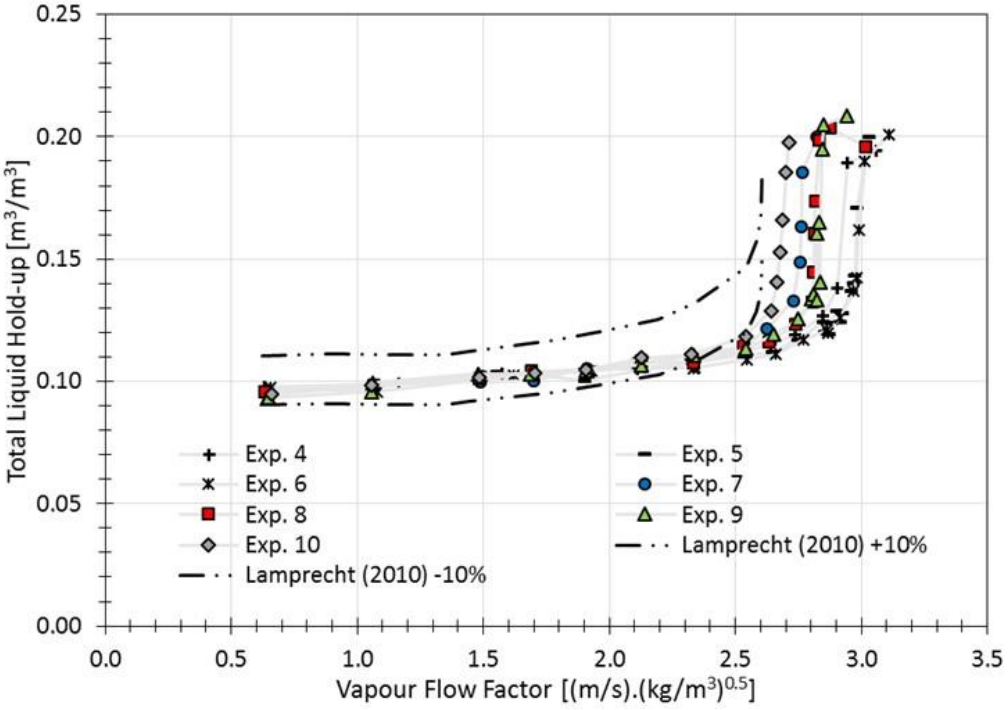

Figure 4.3: Comparison of repeated liquid hold-up measurements with the liquid hold-up measured by Lamprecht (2010)* [accounted for empty column hold-up] for 1.5" Intalox Ultra A, air and water at 73 $m^3/(m^2.h)$

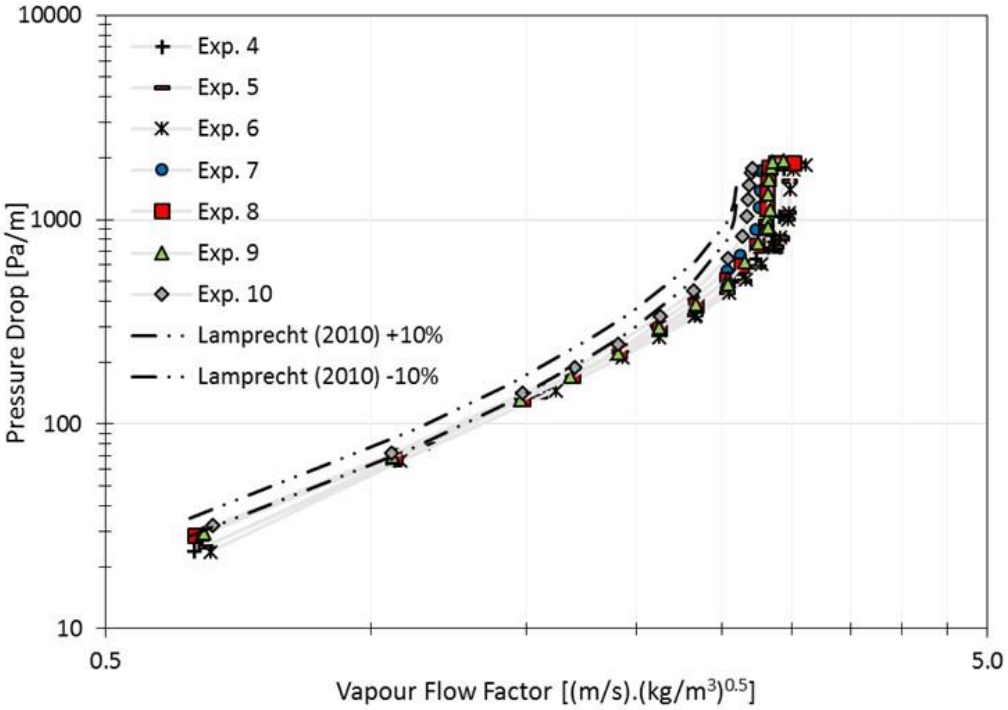

Figure 4.4: Comparison of repeated experimental pressure drop measurements with the pressure drop measured by Lamprecht (2010) for 1.5" Intalox Ultra A, air and water at 73 $m^3/(m^2.h)$

When repeated experiments were performed with an ethylene glycol/air system with 1.5" Intalox Ultra A, very good repeatability was achieved, with all experimental measurements within ± 10 % of the initial measurements (Figure 4.5 and Figure 4.6). The ethylene glycol/air system was thus not affected by the phenomenon experienced with the water/air system.

This was also true when a water/CO_2 system was repeated, with all repeated measurements within ± 10 % of the initial measurements.

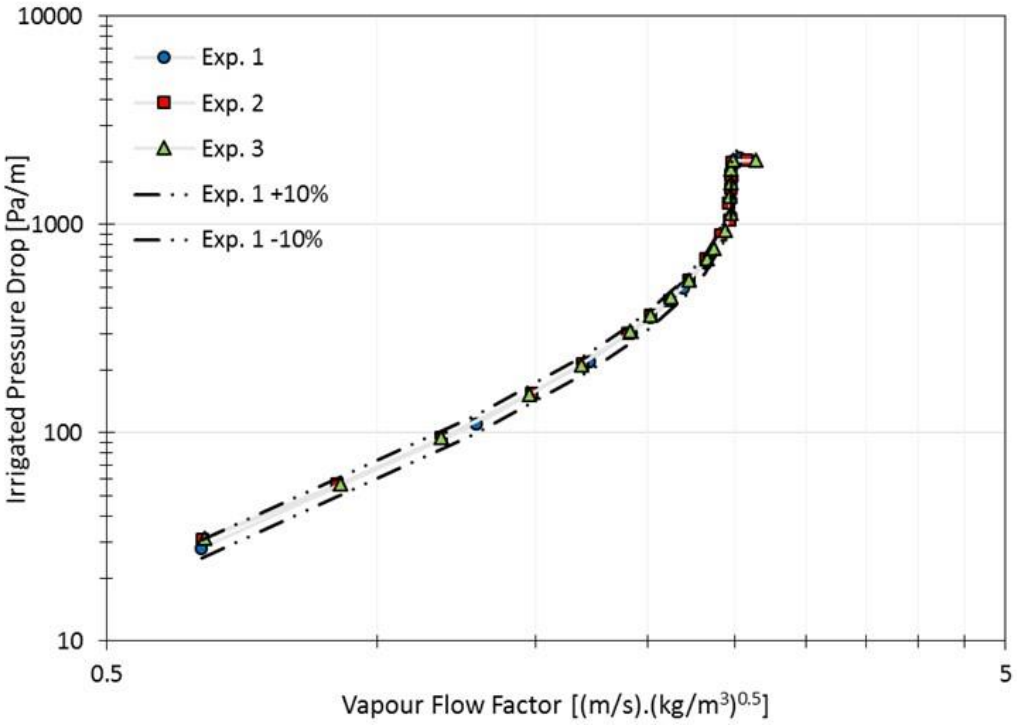

Figure 4.5: Comparison of repeated experimental pressure drop measurements for 1.5" Intalox Ultra A, air and ethylene glycol at 73 $m^3/(m^2.h)$

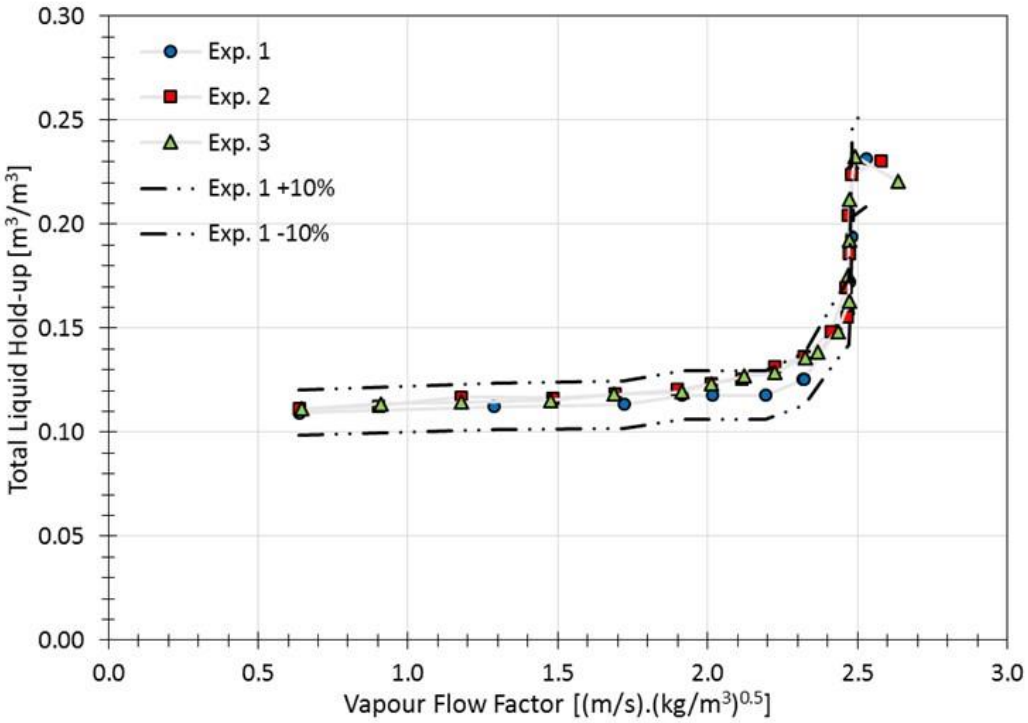

Figure 4.6: Comparison of repeated experimental liquid hold-up measurements for 1.5" Intalox Ultra A, air and ethylene glycol at 73 $m^3/(m^2.h)$

A possible explanation for this phenomenon was speculated to be caused by a brown residue that was noticed on the packing material after the water/CO_2 system was tested (during which the water turned a yellow/brown colour), affecting the wettability of the packing when working with high surface tension water. The effect is believed to be reduced for lower surface tension liquids such as ethylene glycol, Isopar G and silicone oil.

An extensive cleaning process was performed to remove the residue as far as possible. This included flushing the system multiple times with an alcohol mixture, as well as with a low concentration citric acid solution, which offered some improvement on the deviation from initial measurements. It was however possible to produce a proportionate data set over all liquid flow rates, where experimental measurements showed good repeatability, when no changes to the system were made (e.g. flushing of the system, testing a different system).

4.2 Intalox Ultra Capacity Quantification

To quantify the capacity for all experimentally measured conditions, a reliable and repeatable method for determining the loading and flooding points is necessary. The required human input should be

minimal and the method should rely solely on the experimental data that it is provided to determine the loading and flooding points.

4.2.1 Experimental Loading and Flooding Point Determination

The position of the loading and flooding points with respect to the vapour flow factor relies on the definition of loading and flooding. The definitions used in developing the method that is applied here are discussed in Section 2.3.4. As a result, the loading and flooding points determined with this method represent the onset of the loading and flooding regions.

Since the experimental measurement of the total liquid hold-up consists of the addition and subtraction of a number of different liquid volumes, each of which adds a certain degree of uncertainty, the liquid hold-up data has much larger variance compared to the pressure drop data, which was determined by averaging the measured pressure drop over a two minute sampling period. For this reason, the pressure drop data was used rather than the liquid hold-up data, to determine the loading and flooding points. The general method can however, also be applied to the liquid hold-up data.

The method is a modification to the method proposed by Lamprecht (2010) and also makes use of the prediction intervals of regressed curves to determine the loading and flooding points. The statistical theory is described by Ostle (1966).

Prediction Interval Calculation

While a confidence interval provides upper and lower bands along the regressed curve in which the true best fit line for the population lie with a specified probability, the prediction interval provides upper and lower bands around an individual predicted value, in which the real value lies for a specified probability. In other words, the prediction interval highlights the distribution of values, while the confidence interval highlights the uncertainty in determining the population mean. The prediction interval is always wider than the confidence interval, since the prediction interval accounts for both the uncertainty of the population mean and the scatter of data.

To calculate the $100 \cdot \gamma$ percent prediction interval for a predicted value, the following equation is used:

$$\boldsymbol{L', U' = \hat{y} \pm t_{\left(\frac{1+\gamma}{2}\right),(n-2)} \cdot S_{\hat{Y}}} \qquad [\ 4.1\ ]$$

$$\boldsymbol{S_{\hat{Y}}{}^2 = S_E{}^2 \cdot \left[1 + \frac{1}{n} + \frac{(x_0 - \bar{x})^2}{\sum (x - \bar{x})^2}\right]} \qquad [\ 4.2\ ]$$

$$\boldsymbol{S_E{}^2 = \frac{\sum (y - \hat{y})^2}{n - 2}} \qquad [\ 4.3\ ]$$

Where

L' : Predicted interval lower value

U' : Predicted interval upper value

$\hat{y}$: Predicted value for a given independent variable x_0

n : Number of data points in the sample used in the regression

$S_{\hat{Y}}{}^2$: Estimated variance of the predicted individual $\hat{y}$ for a given x_0

$S_E{}^2$: Residual mean square

$t_{\left(\frac{1+\gamma}{2}\right),(n-2)}$: T-value from the t-distribution for a $100 \cdot \gamma$ percent probability with $n - 2$ degrees of freedom

$\bar{x}$: Mean value of the sample's independent variable used in the regression

x : Independent variable of sample used in the regression

y : Dependent variable of the sample used in the regression

In the application of the method to the pressure drop data, the independent variable is the vapour flow factor and the dependent variable the pressure drop when applied to the determination of the loading point. For the determination of the flooding point these are reversed, for reasons explained in Section 0.

Loading Point Determination

The loading point has been described earlier as the point where the experimental pressure drop trend starts to deviate from the linear dry bed pressure drop trend on a log-log plot of pressure drop versus vapour flow factor. To determine this point, a power law curve is initially fitted to the first three data points in the sample. An upper prediction bound is then calculated for this curve at the vapour flow factor of the 4th data point (Figure 4.7). If the pressure drop for this data point is above the upper

prediction bound, the previous data point is flagged as the data point around which the loading point lies. If the pressure drop of the 4th data point is below the upper prediction bound, the 4th data point is included in the regression of the fitted curve and the procedure is repeated for the 5th. This process is continued until a data point with a pressure drop above the upper prediction bound is found.

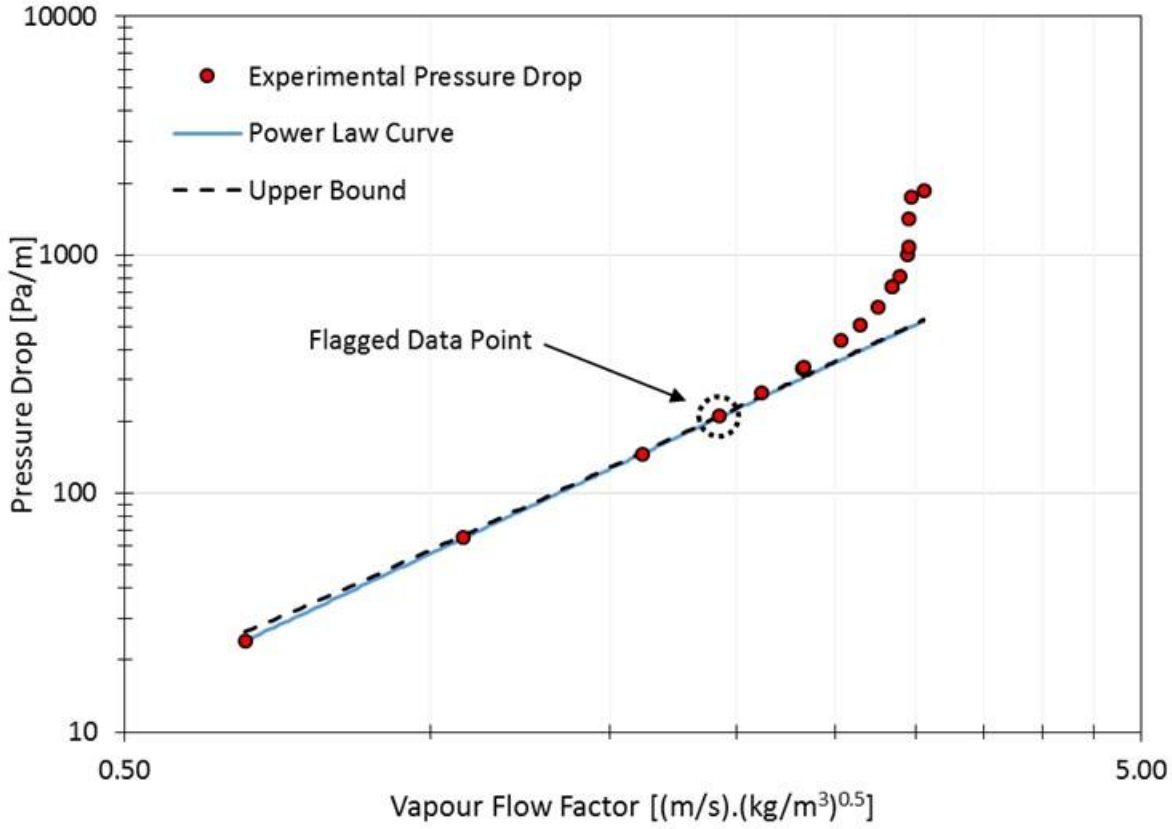

Figure 4.7: Loading point flagged data point for Water/Air, 1.5" Intalox Ultra A at 73 $m^3/(m^2.h)$

To determine the loading point with a higher resolution than just the flagged data point, artificial data are required for both the pressure drop and the vapour flow factor around the flagged point. For this reason a second order polynomial curve is fitted to the flagged data point plus two data points above and below the flagged data point (Figure 4.8). The incremental step size at which data can be generated over the five data points is dependent on the standard deviation of the experimental data, where the step size should be larger than one standard deviation of the experimental data (Lamprecht, 2010). Each experimental pressure drop data point consists of the average of the measured pressure drop and gas flow rate over a two minute sampling period, with a sampling rate of one sample per second. Thus, every pressure drop data point consists of at least 120 individual pressure drop and gas flow rate measurements. To determine the minimum incremental step size at which data can be

generated, the standard deviation of the vapour flow factor for each of the five data points is calculated. The largest of these then determines the minimum step size.

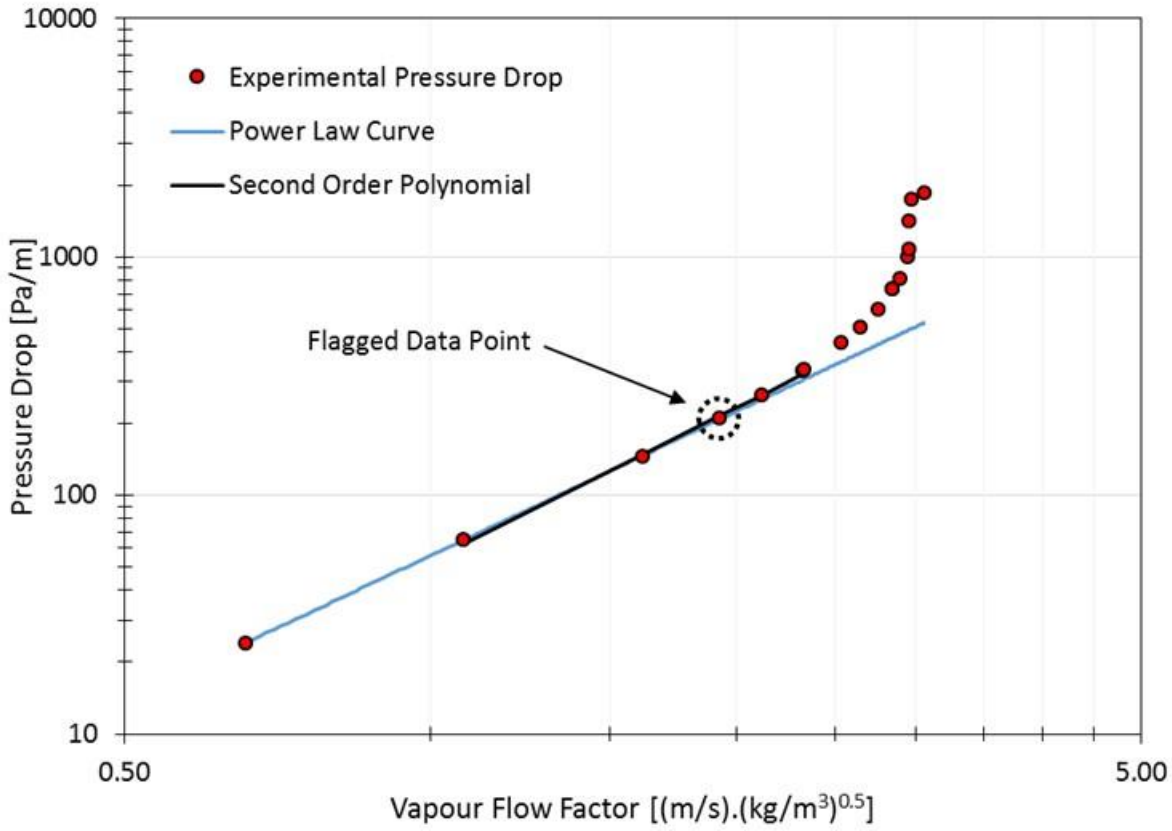

Figure 4.8: Second order polynomial fitted around the loading point region for Water/Air, 1.5" Intalox Ultra A at 73 $m^3/(m^2.h)$

With the minimum incremental step size determined, upper and lower prediction bounds are calculated for the power law curve initially fitted and the polynomial curve, respectively. The loading point is then identified by the point at which the upper bound of the power law curve crosses the lower bound of the polynomial curve (Figure 4.9). If these curves cross twice because of the second order polynomial, the second point at which they cross is identified as the loading point.

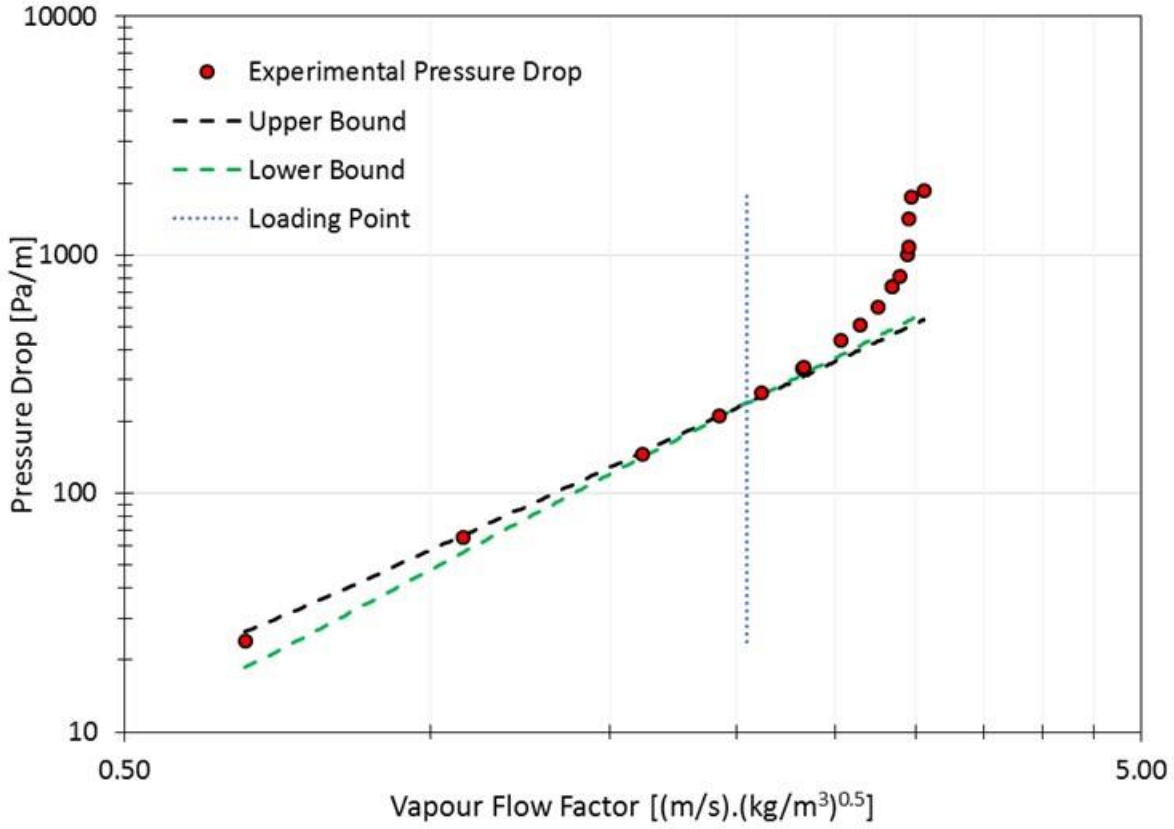

Figure 4.9: Loading point determination with upper and lower prediction bounds for Water/Air, 1.5" Intalox Ultra A at 73 $m^3/(m^2.h)$

Flooding Point Determination

The onset of flooding is determined through a similar approach to the way the loading point was determined. While the loading point was determined by approaching the potential loading point from the lower pressure drop and vapour flow rate side of the curve, the flooding point is determined by approaching the potential flooding point from the highest pressure drop and vapour flow factor and moving down. To apply this approach, the pressure drop/vapour flow factor graph is inverted, with the pressure drop now as the abscissa and the vapour flow factor as the ordinate.

The flooding point has been described earlier as the point at which the pressure drop starts to drastically increase, tending towards infinity as the gas flow rate increases. Starting at the highest pressure drop measured, a straight line is initially fitted on the first three data points, ignoring any data points before the superflood breakpoint. A lower prediction band is then calculated for this line at the 4^{th} data point (Figure 4.10). If the vapour flow factor for this data point is below the prediction band, this data point is flagged as the data point around which the flooding point lies. If the pressure

drop of the 4th data point is above the lower prediction bound, the 4th data point is included in the regression of the straight line and the procedure is repeated for the 5th. This process is continued until a data point with a pressure drop below the lower prediction bound is found.

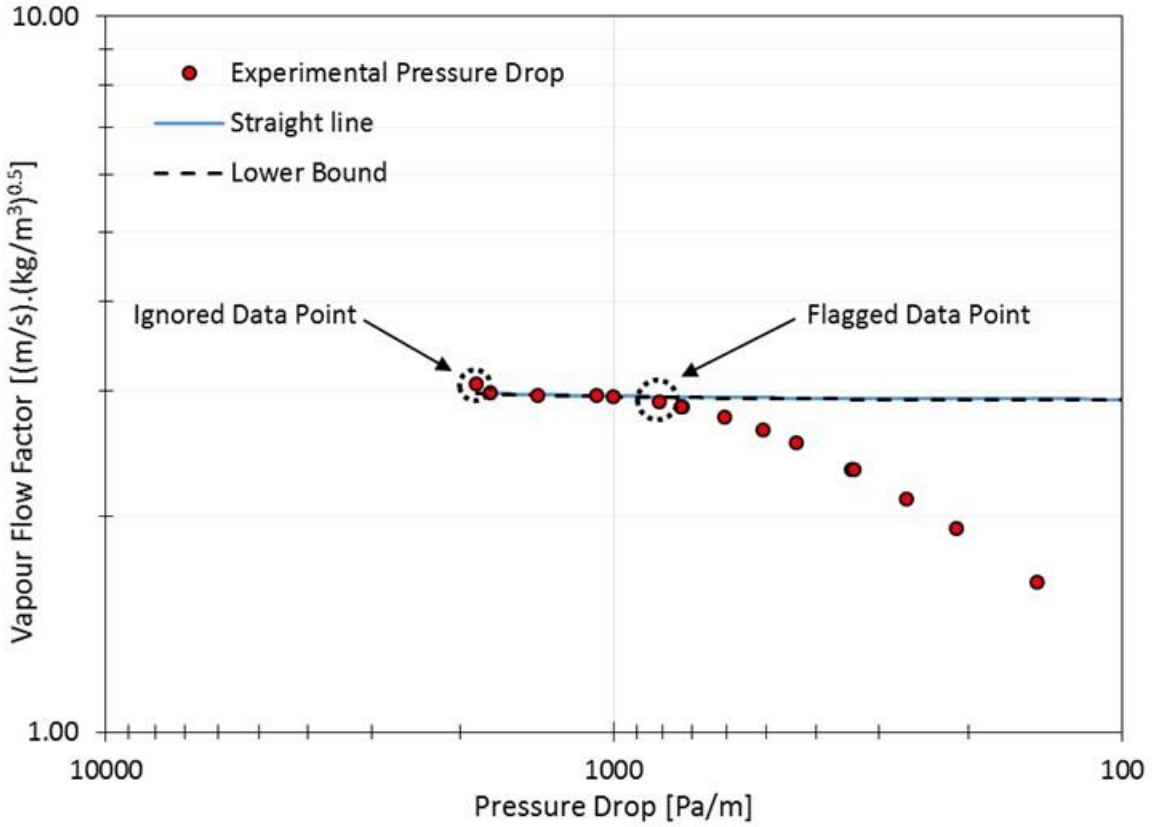

Figure 4.10: Flooding point flagged data point for Water/Air, 1.5" Intalox Ultra A at 73 $m^3/(m^2.h)$

A second order polynomial curve is fitted on the flagged data point plus two data points above and below the flagged data point (Figure 4.11). Similar to the determination of the loading point, the standard deviation for the relevant pressure drop data points are calculated and used to determine the minimum incremental step size.

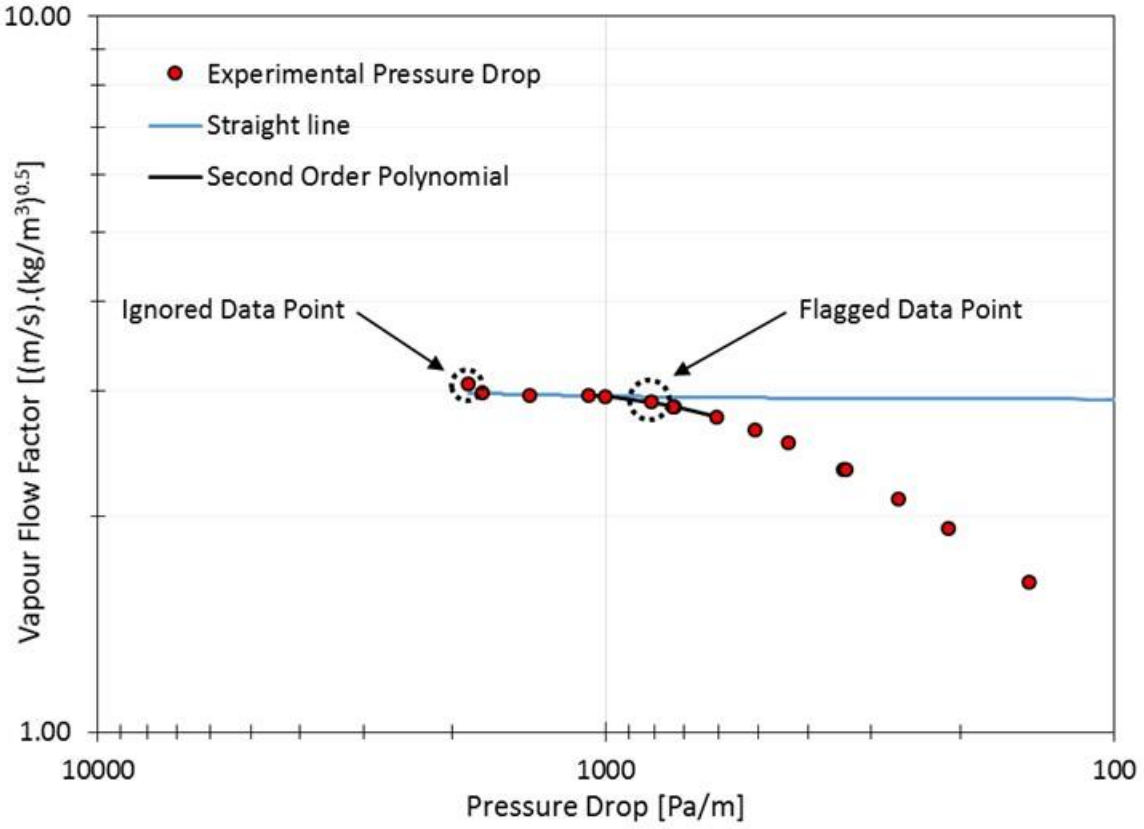

Figure 4.11: Second order polynomial fitted around the flooding point region for Water/Air, 1.5" Intalox Ultra A at 73 $m^3/(m^2.h)$

Finally, upper and lower prediction bounds are calculated for the straight line initially fitted and the polynomial curve, respectively. The flooding point is then identified by the point at which the lower bound of the straight line crosses the upper bound of the polynomial curve (Figure 4.12). If these curves cross twice because of the second order polynomial, the second point at which they cross is identified as the flooding point.

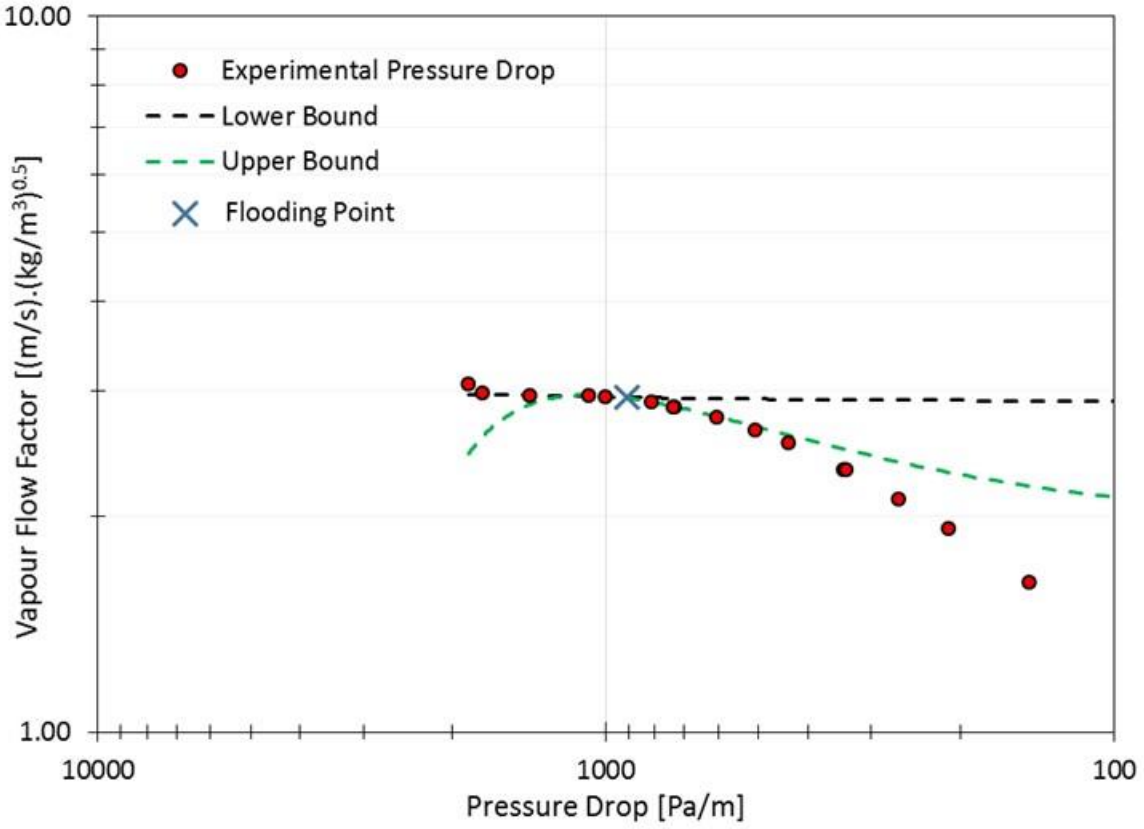

Figure 4.12: Flooding point determination with upper and lower prediction bounds for Water/Air, 1.5" Intalox Ultra A at 73 $m^3/(m^2.h)$

Confidence level

In calculating the prediction interval, a confidence level is specified in the t-value used in Equation [**4.1**]. The higher the confidence level, the wider the prediction interval is (Figure 4.13). This is because to confine a certain spread of data within the calculated prediction interval, the level of confidence should be high enough to be certain that all the data will lie inside the prediction interval. Another parameter required for determining the t-value is the number of data points; and as a result, the width of the prediction interval is also very dependent on the number of data points used in the regression.

Since for most of the systems investigated in this project, only three to four data points were measured in the loading region and a similar amount in the flooding region, using a very high confidence level results in very broad prediction intervals, especially when the residuals from the fitted curve are relatively high. As a result, a very high confidence level leads to over-prediction of the loading point and under-prediction of the flooding point. After considering multiple confidence levels, a

compromise between prediction accuracy (with regard to visual identification) and prediction confidence, a confidence level of 70 % was chosen and used throughout.

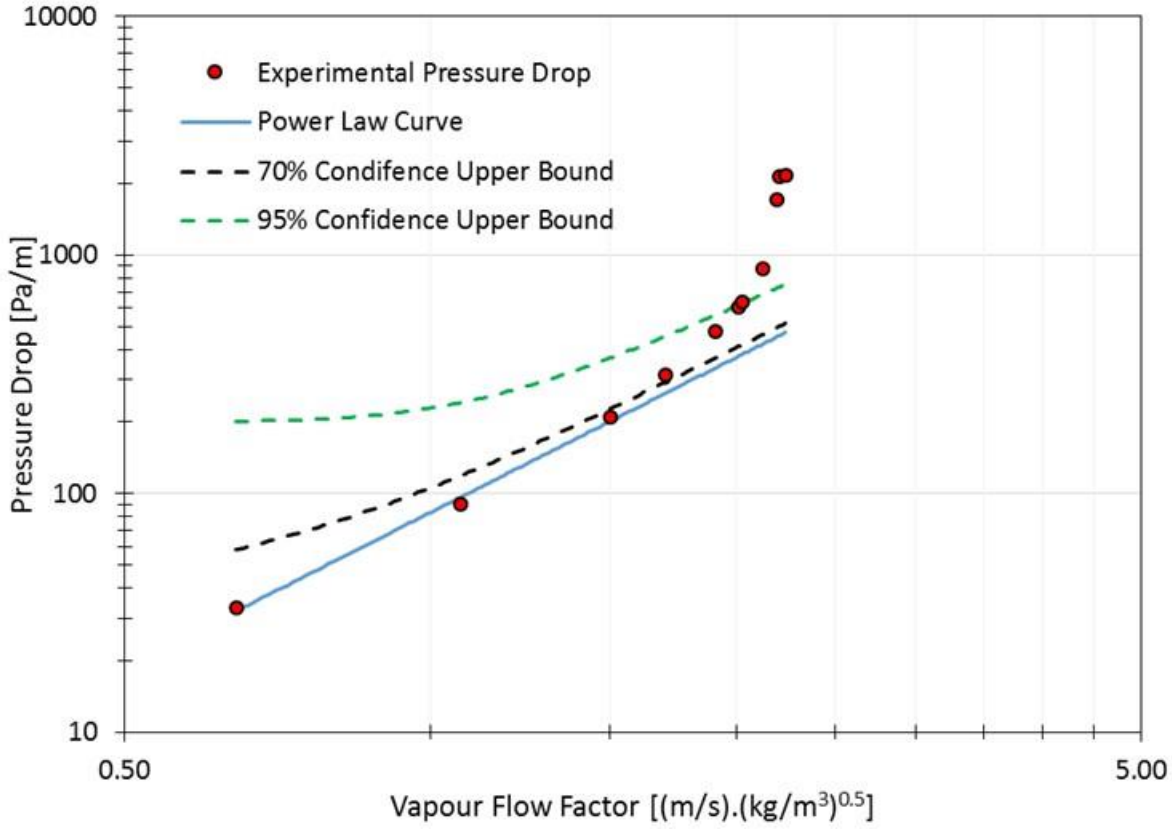

Figure 4.13: Comparison of 70 % and 90 % confidence upper bounds for Ethylene Glycol/Air, 1.5" Intalox Ultra A at 73 $m^3/(m^2.h)$

Evaluation of Capacity Quantification Method

Accurate quantification of the loading and flooding points with the described method rely heavily on the quality of the data. If there are a large number of data points describing a region and most of these data points show little deviation from the general pressure drop trend, a small deviation near the loading or flooding point can lead to the false flagging of this data point. This is a result of the prediction interval being relatively small because of the quality of the data up to that point. Accurate quantification is also reliant on the number of data points, where a small number of data points in the relevant region can lead to an over-prediction of the loading point, or an under-prediction of the flooding point, due to a wide prediction interval. Since the transition from the pre-loading region to the loading region is much more gradual than the transition from loading to flooding, identification of

the loading point is generally much more susceptible to these factors. Generally, the method gives more accurate identification of the flooding point.

At high liquid flow rates, the flooding region can be identified by the characteristic sharp increase in both pressure drop and liquid hold-up. At lower liquid flow rates, and especially at 6 $m^3/(m^2.h)$, the increase in pressure drop and liquid hold-up in the flooding region is not as drastic. With the method based on the sharp increase in pressure drop for identification of the flooding point, identification at low liquid flow rates might not be as accurate. In addition, the transition from the pre-loading to the loading region is also much more gradual for lower liquid flow rates.

Overall, the method provides relatively accurate identification of the loading and flooding points at high liquid flow rates. At low liquid flow rates, and especially at 6 $m^3/(m^2.h)$, some uncertainty arises due to the more gradual pressure drop and liquid hold-up trends.

4.2.2 Flooding Point Determination with Entrainment Data

According to Nieuwoudt (2016), the flooding point can also be identified by making use of liquid entrainment data. More specifically, by using the percentage of liquid entrainment with regard to the liquid feed rate (liquid entrainment rate over the liquid feed rate). The flooding point can be identified as the gas flow rate resulting in approximately 15 % liquid entrainment (Nieuwoudt, 2016).

It is well known that liquid will be entrained from the top of packed column, operated counter currently, when the gas flow rate is sufficiently increased (Maćkowiak, 2010; Elgin and Weiss, 1939). Elgin and Weiss (1939) however, describe the violent entrainment of liquid from a packed column at low liquid flow rates at the identified flooding point, while at high liquid flow rates a phase inversion, from liquid continuous to gas continuous occurs, with no pronounced entrainment. The stated 15 % liquid entrainment for flooding identified by Nieuwoudt (2016) is most likely based on experience rather than a theoretical basis, applicable to a range of liquid flow rates.

When considering the general trend of the entrainment data for all system investigated at different liquid flow rates, the following is evident: at low liquid flow rates the percentage entrainment displays an exponential type relationship with respect to the gas flow rate; at high liquid flow rates the trend displays an abrupt start which then increases, almost vertically, as the gas flow rate increases (Figure 4.14).

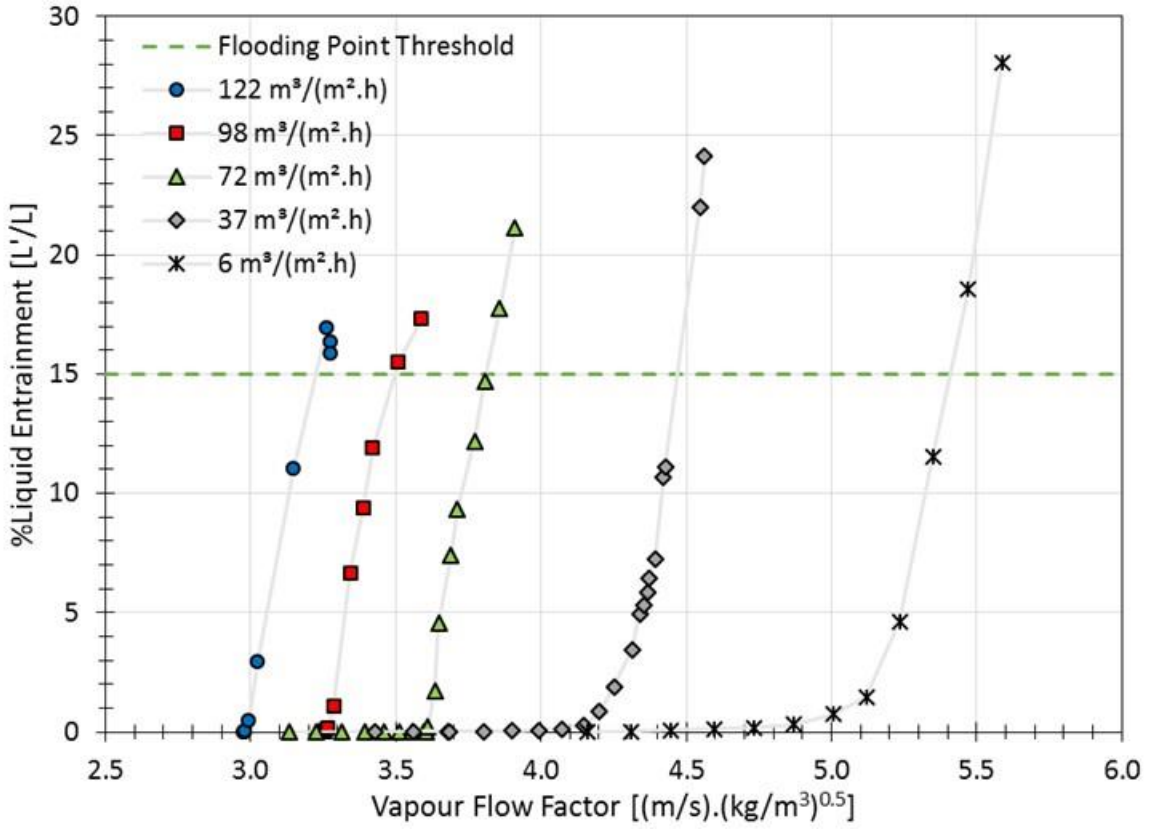

Figure 4.14: Liquid entrainment trends for 2.5" Intalox Ultra O, air and water

At low liquid flow rates and close to the flooding point, most of the liquid held up in the packing is in the form of droplets. As the gas flow rate increases, more of these droplets are entrained, resulting in the exponential increase in entrainment. At high liquid flow rates and close to the flooding point the liquid flows down the column as a stream of liquid, filling up the packing voids. As the gas flow rate is increased, a point is reached where the gas starts to vigorously bubble through the liquid, resulting in the formation of droplets, which are then entrained from the top of the column.

For most of the systems investigated, the abrupt start of entrainment at high liquid flow rates is closer to the superflood breakpoint than the flooding point, with the 15 % entrainment threshold at even higher gas flow rates. Identifying the flooding point with entrainment data at high liquid flow rates largely over-predicts the flooding point (Figure 4.15).

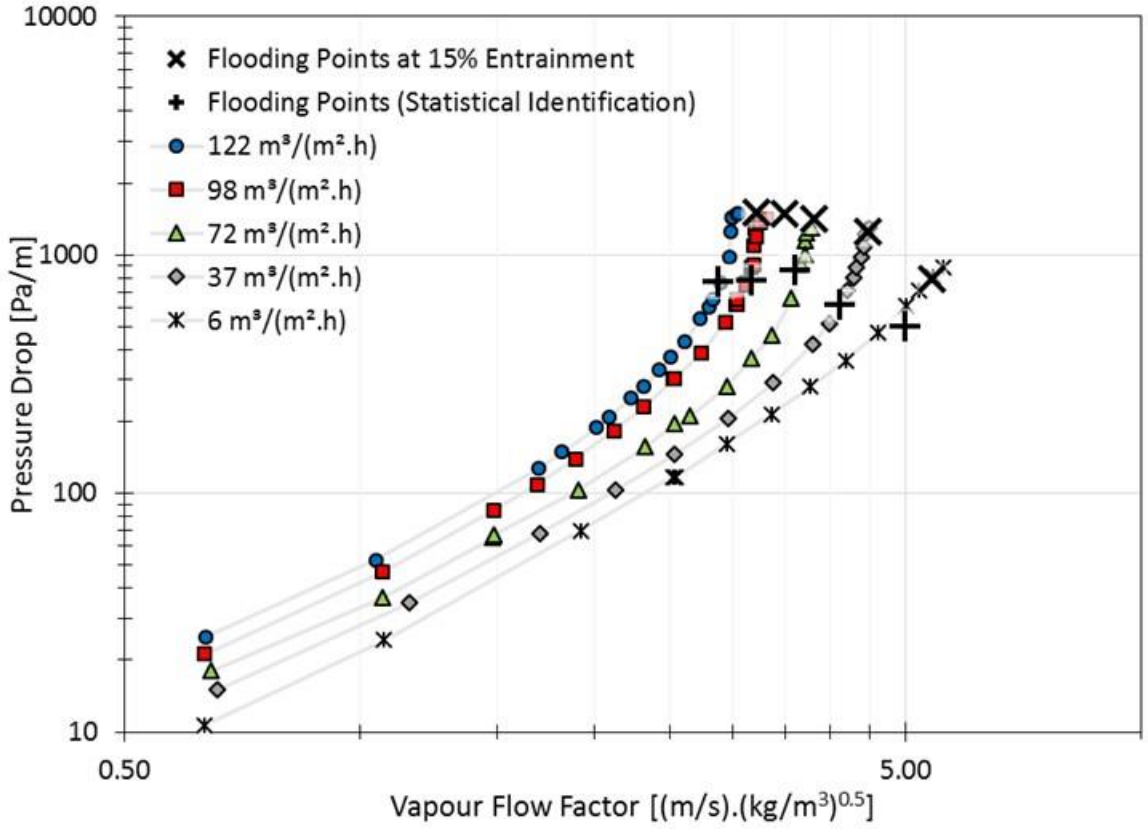

Figure 4.15: Comparison of flooding points determined with the statistical method and the entrainment data for 2.5" Intalox Ultra O, air and water

For a liquid flow rate of 6 $m^3/(m^2/h)$, the flooding point, identified with entrainment data, lies below the superflood break point, while for the liquid flow rates of 37 and 73 $m^3/(m^2/h)$, the flooding point, identified with entrainment data, coincide with the superflood break point. Commenting on the accuracy of the identified flooding point with the entrainment data at low liquid flow rates is restricted by the difficulty of identifying the flooding point at these liquid flow rates with the method described in the previous section. However, for liquid flow rates of 6 and 37 $m^3/(m^2/h)$, the true flooding point is most likely located between the two identified flooding points.

At the high liquid flow rates of 98 and 122 $m^3/(m^2/h)$, the entrainment data fail to predict the flooding point. As described by Elgin and Weiss (1939), the column is flooded before any significant entrainment occurs. For the liquid flow rates of 37 and 73 $m^3/(m^2/h)$, the entrainment data provide a more accurate identification of the flooding point compared to the higher liquid flow rates, although most likely still over-predicted. The statistical method is therefore still recommended. For 6 $m^3/(m^2/h)$, either method is recommended, although a value of 10 % liquid entrainment may be used for a more conservative flooding point identification.

4.3 Foaming of Isopar G

When working with Isopar G with both 1.5" Intalox Ultra A and 2.5" Intalox Ultra O and with both nitrogen and carbon dioxide, the Isopar G had a tendency to foam. However, for a liquid flow rate of 6 $m^3/(m^2.h)$, the foam collapsed as soon as a gas load was applied, while for a liquid flow rate of a 37 $m^3/(m^2.h)$, a decrease in foaming was observed as the gas flow rate was increased, with the foam disappearing at higher gas flow rates (Figure 4.16).

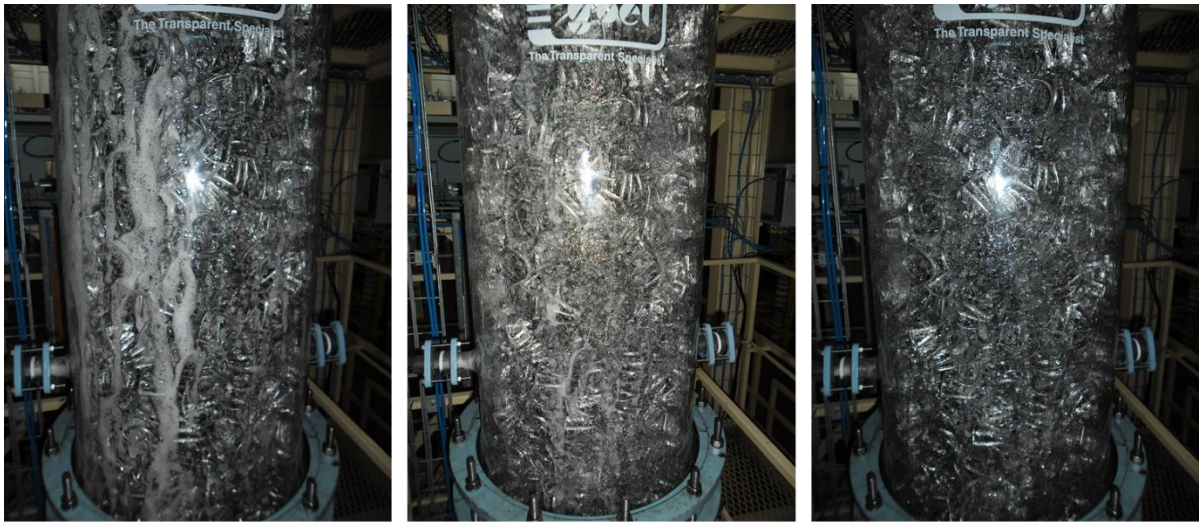

Figure 4.16: Foaming of Isopar G, CO_2 with 2.5" Intalox Ultra O at a liquid flow rate of 37 $m^3/(m^2.h)$ for gas flow rates of: (a) 300 kg/h, (b) 800 kg/h and (c) 1350 kg/h

For higher liquid flow rates, the foaming persisted when the gas flow rate was increased, but did show a change in the foaming, with the bubbles being much smaller and less foam streaking down the column wall (Figure 4.17). The foaming increased in severity as the liquid flow rate increased (Figure 4.18). Overall the foaming was more severe for 2.5" Intalox Ultra O compared to the 1.5" Intalox Ultra A. The cause of the foaming is believed to be the result of contamination of the Isopar G liquid with water. Since the 2.5" Intalox Ultra O was tested after the 1.5" Intalox Ultra A, the increase in the severity of foaming for the 2.5" Intalox Ultra O is a result of more contamination of the liquid.

Figure 4.17: Foaming of Isopar G, CO_2 with 2.5" Intalox Ultra O at a liquid flow rate of 73 $m^3/(m^2.h)$ for gas flow rates of: (a) 300 kg/h, (b) 800 kg/h and (c) 1163 kg/h

Figure 4.18: Foaming of Isopar G, CO_2 with 2.5" Intalox Ultra O at a gas flow rate of 300 kg/h for: (a) 73 $m^3/(m^2.h)$, (b) 98 $m^3/(m^2.h)$ and (c) 122 $m^3/(m^2.h)$

A layer of foam was also present on the liquid held up on the gas distributor. The stability of the foam was checked by observing how long it took for the foam to collapse after liquid feed was cut. The foam collapsed in less than 10 seconds.

The foaming had a noticeable effect on the liquid hold-up trends for liquid flow rates above 37 $m^3/(m^2.h)$ in the form of an increase in liquid hold-up in the pre-loading region as the gas flow rate

increased for 2.5" Intalox Ultra O with both nitrogen and carbon dioxide (Figure 4.19). This trend is not present in the liquid hold-up data for 1.5" Intalox Ultra A. According to Bartelmus and Janecki (2003), the liquid hold-up of a foaming system is lower than the liquid hold-up of a non-foaming system with similar physico-chemical properties at the same liquid and gas flow rates. The increase in liquid hold-up in the pre-loading region is a result of the decrease in foaming as the gas flow rate increases. For higher gas flow rates the liquid hold-up follows the general liquid hold-up trend as expected in the loading and flooding regions, although the total liquid hold-up should be lower than what would be expected if the liquid was non-foaming.

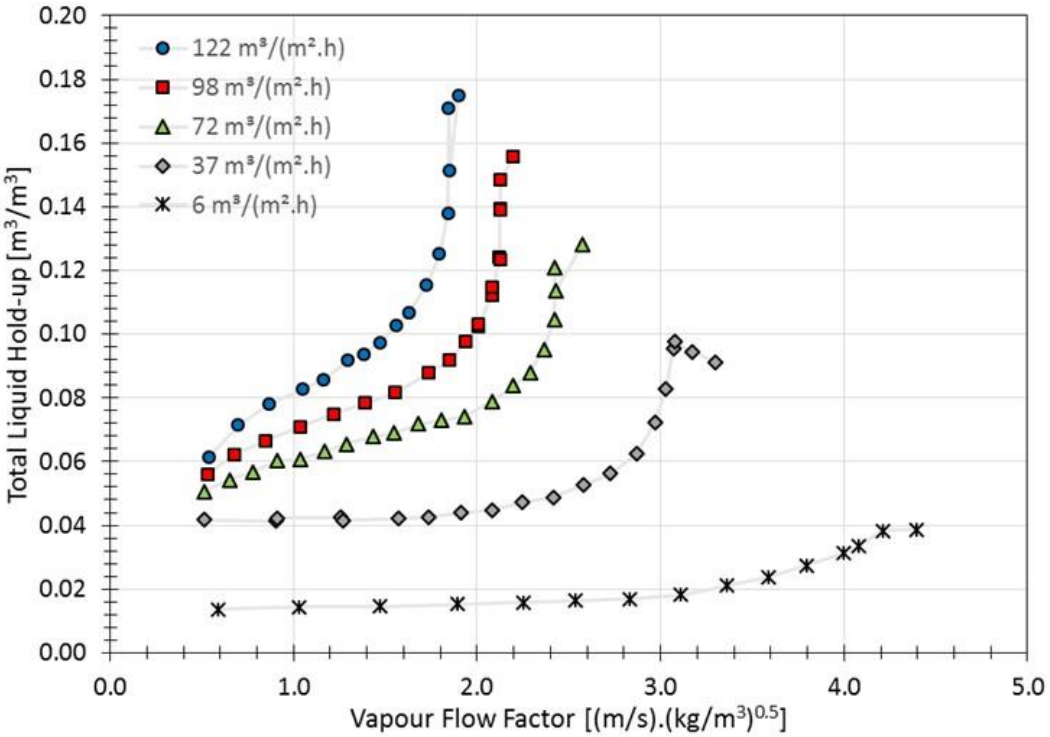

Figure 4.19: Experimental liquid hold-up for Isopar G with CO_2 and 2.5" Intalox Ultra O

It is well known that foaming in packed columns results in higher pressure drop and lower capacity compared to similar non-foaming systems (Górak and Olujić, 2014; Kister, 1992; Strigle, 1994). Senger and Wozny (2012) investigated the effect of foaming in a packed column with a diameter of 300 mm and a packed bed height of 2000 mm. The packings that were investigated included, amongst others, different sizes of the Raschig Super-Ring. Water and air was used as a non-foaming reference system, while the foaming systems consisted of different aqueous mixtures, which included 2 wt% butanol mixture as well as 10 mg/L and 30 mg/L Triton X-100 surfactant mixtures. While the density and viscosity of all mixtures were very similar to that of water, all mixtures had lower surface tension. They

found that for the low liquid flow rate of 10 $m^3/(m^2.h)$, the foaming and non-foaming systems had nearly identical pressure drops for all systems investigated. Furthermore, an increase in liquid flow rate resulted in an increase in foaming, leading to larger differences between the pressure drop of the foaming and non-foaming systems.

Thiele *et al.* (2004) also investigated the effect of foaming in a packed column with water/butanol mixtures. They too found that pressure drop increased as a result of foaming and that the effect is larger at higher liquid flow rates. Foaming also resulted in significant decrease in capacity. Thiele *et al.* (2004) compared the experimental flooding points of the foaming systems that were investigated to the flooding points predicted with the Maćkowiak (1991) model. They found that the experimental flooding points were much lower than what was predicted by the model. Although the model takes into account the geometric parameters of the packing and physical properties of the fluids, these properties alone do not provide information about the foaming behaviour. The model can therefore not predict the higher pressure drop and lower flooding points caused by the foaming.

The experimental pressure drop for Isopar G measured in this project should thus be higher than what would have been measured if the liquid was not foaming, while the flooding points and liquid hold-up should be lower. Figure 4.20 and Figure 4.21 show the experimental pressure drop for Isopar G compared to the pressure drop predicted with KG-Tower (V5.3) for a liquid with the same physical properties as Isopar G with nitrogen and 1.5" Intalox Ultra A and 2.5" Intalox Ultra O, respectively. For the 1.5" Intalox Ultra A, KG-tower gives a very good prediction of the pressure drop for liquid flow rates of 6 and 37 $m^3/(m^2.h)$. At higher liquid flow rates, the predicted pressure drop in the pre-loading region is lower than the experimental pressure drop. The difference between predicted and experimental pressure drop in the pre-loading region also increases as the liquid flow rate increases. At higher gas flow rates in the loading region, the difference between the predicted and experimental pressure drop decreases and the predicted pressure drop trend follows the experimental data much better. However, the predicted pressure drop trend does not follow the same sharp increase as the experimental pressure drop at the flooding point, resulting in a slightly higher flooding point. For 2.5" Intalox Ultra O, the overall difference between the predicted and experimental pressure drop is higher than for 1.5" Intalox Ultra A, although the change in the difference of the predicted and experimental pressure drop as the gas flow rate increases follows a similar trend as for the 1.5" Intalox Ultra A.

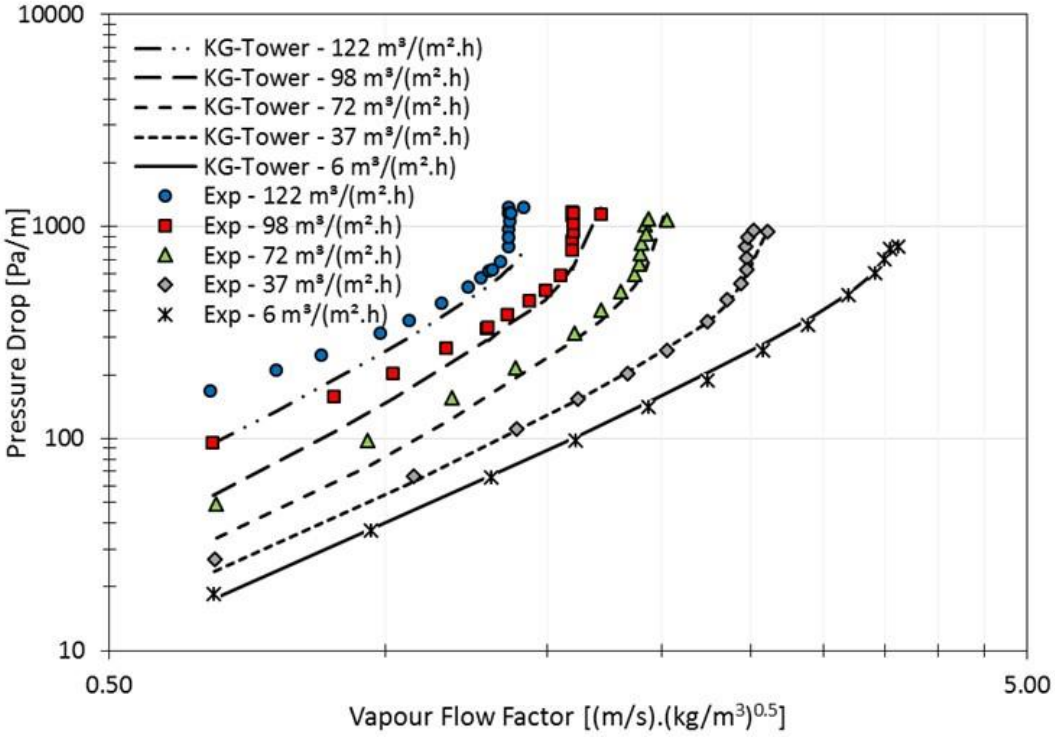

Figure 4.20: Experimental pressure drop vs. KG-Tower for Isopar G with N_2 and 1.5" Intalox Ultra A

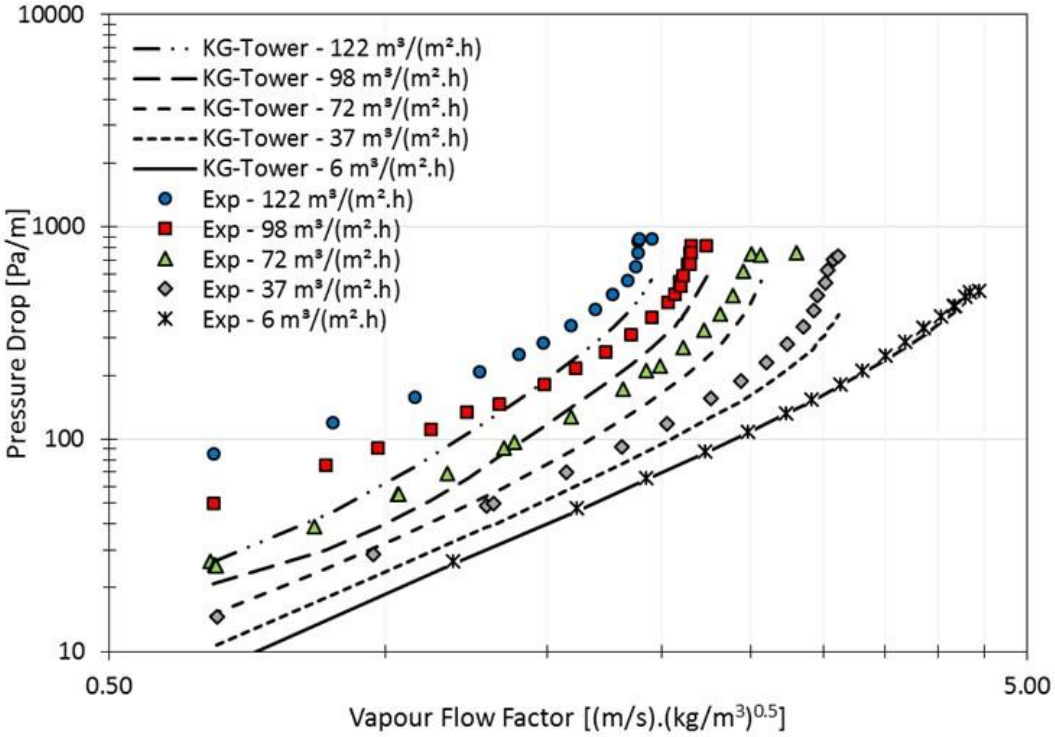

Figure 4.21: Experimental pressure drop vs. KG-Tower for Isopar G with N_2 and 2.5" Intalox Ultra O

All of the noted differences between the predicted and experimental pressure drop can be explained by the foaming of Isopar G:

- The absence of foaming at the lower liquid flow rates results in better prediction of the pressure drop at these liquid flow rates
- The increase in foaming, as the liquid flow rate increases, results in larger differences between the predicted and experimental pressure drop as the liquid flow rate increases
- The decrease in foaming, as the gas flow rate increases, results in the difference between the predicted and experimental pressure drop decreasing as the gas flow rate increases
- The increase in foaming for the 2.5" Intalox Ultra O compared to the 1.5" Intalox Ultra A results in larger differences between the predicted and experimental pressure drop of 2.5" Intalox Ultra O compared to 1.5" Intalox Ultra A

To compare the extent to which the foaming influenced the capacity of Isopar G with regard to the other liquids, Figure 4.22 shows the experimental pressure drop for the different liquids investigated in this project with 2.5" Intalox Ultra O at a liquid flow rate of 98 $m^3/(m^2.h)$ (the packing and liquid flow rate combination that had the most foaming and for which pressure drop data for silicone oil was also measured). The extent to which the foaming affects the capacity of Isopar G is relatively small compared to the difference between the flooding points of the other liquids. An interpretation of the flooding behaviour of the different liquids with regard to their physical properties should still hold true.

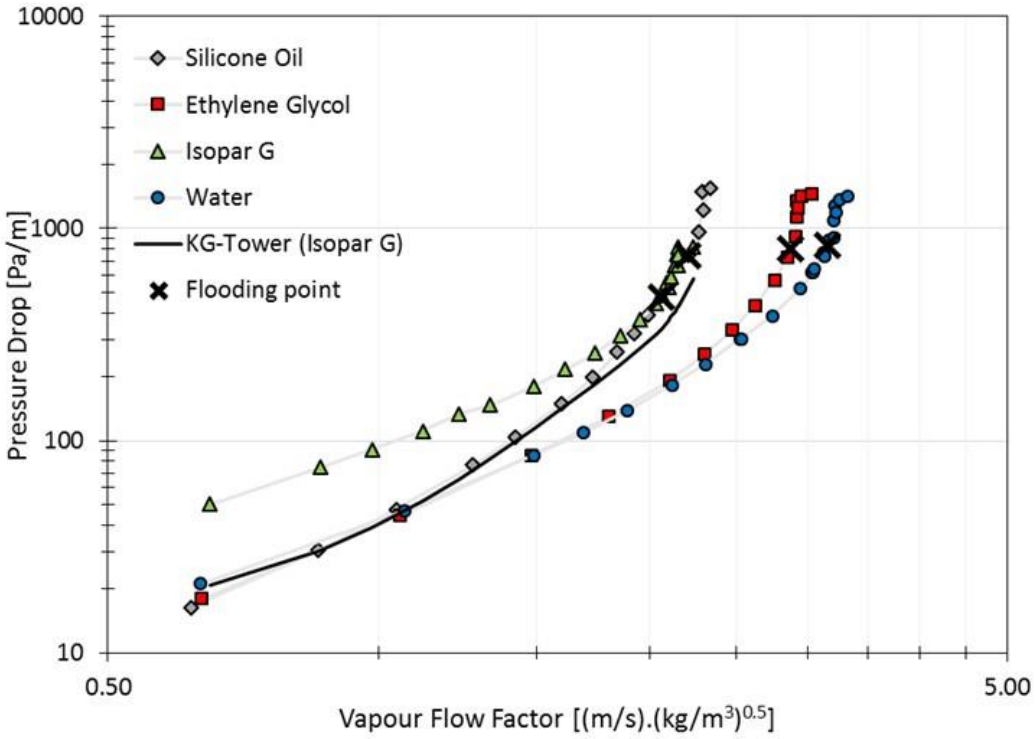

Figure 4.22: Comparison of measured pressure drop for the different liquids with air/N_2, 2.5" Intalox Ultra O at 98 $m^3/(m^2.h)$ and predicted pressure drop of Isopar G with KG-Tower

4.4 Effect of Physical Liquid Properties

For all four of the liquids investigated in this project, the three physical liquid properties that are examined are all different. For this reason it is not possible to comment on the effect of a single liquid property. Rather the combined effect of all properties on the hydrodynamic behaviour can be investigated with regard to different liquids.

Although the conclusions that are drawn here on the effect of liquid physical properties on the hydrodynamic behaviour are discussed with regard to 2.5" Intalox Ultra O with CO_2 at a liquid flow rate of 73 m3/(m2.h), these conclusions also apply to 2.5" Intalox Ultra O with air as well as 1.5" Intalox Ultra A with both air and CO_2 for all liquid flow rates investigated, since all of these show similar trends with regard to pressure drop and liquid hold-up trends. Graphs of all the experimental data are provided in Section 9.11.

4.4.1 Liquid Hold-up

When examining the liquid hold-up of the different liquids in the pre-loading region shown in Figure 4.23, silicone oil has by far the highest liquid hold-up, followed by ethylene glycol. These two liquids also have the highest liquid viscosities, with silicone oil's viscosity about 5.5 times that of ethylene glycol. Isopar G has a liquid hold-up much lower than silicone oil and ethylene glycol. Even though the foaming of Isopar G would have caused a decrease in the liquid hold-up, the liquid hold-up of Isopar G is also much lower than that of silicone oil and ethylene glycol for the liquid flow rates where foaming did not occur [6 and 37 $m^3/(m^2.h)$]. It can therefore be concluded that foaming is not the primary cause of the difference in liquid hold-up between Isopar G and silicone oil/ethylene glycol. From literature, it was concluded that lower liquid density results in higher liquid hold-up. Even though Isopar G has a much lower density than ethylene glycol and silicone oil, the lower liquid hold-up of Isopar G compared to silicone oil/ethylene glycol is a result of the large difference in viscosity between these liquids and Isopar G. For silicone oil and ethylene glycol, the ratio of viscous forces over the gravitational forces is much larger than for Isopar G. The same argument can be made for water and ethylene glycol, with water having a lower liquid density than ethylene glycol, but still lower liquid hold-up as a result of the higher viscosity of ethylene glycol compared to that of water.

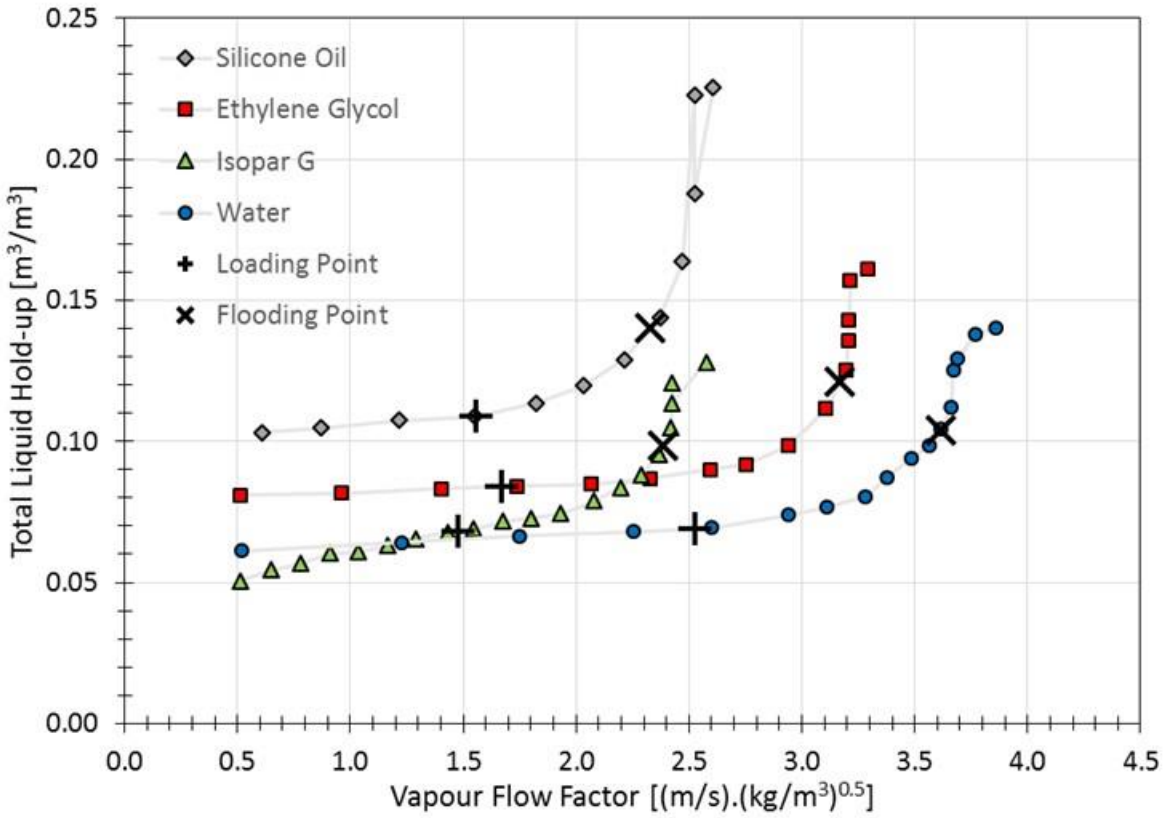

Figure 4.23: Comparison of measured liquid hold-up for the different liquids with CO_2, 2.5" Intalox Ultra O at 73 $m^3/(m^2.h)$

Recognising the effect of surface tension on the pre-loading liquid hold-up is not possible with the combination of physical liquid properties investigated here. However, according to Strigle (1994) the low surface tension of silicone oil and Isopar G should have a decreasing effect in the overall contribution of physical properties on liquid hold-up when compared to that of water. However, this is only the case for the lowest liquid flow rate of 6 $m^3/(m^2.h)$ investigated here, since according to Strigle (1994), the effect of surface tension on liquid hold-up becomes negligible at liquid flow rates above 17 $m^3/(m^2.h)$.

4.4.2 Flooding Point

When considering the liquid hold-up and pressure drop trends in Figure 4.23 and Figure 4.24, it is evident that the different liquids investigated here illustrate different behaviour with regard to the occurrence of flooding. Isopar G and silicone oil, with very different physical liquid properties, have very low flooding points close to each other, while water floods at a much higher gas flow rate. Ethylene glycol has a flooding point at a lower gas flow rate than that of water, but higher than Isopar G and silicone oil.

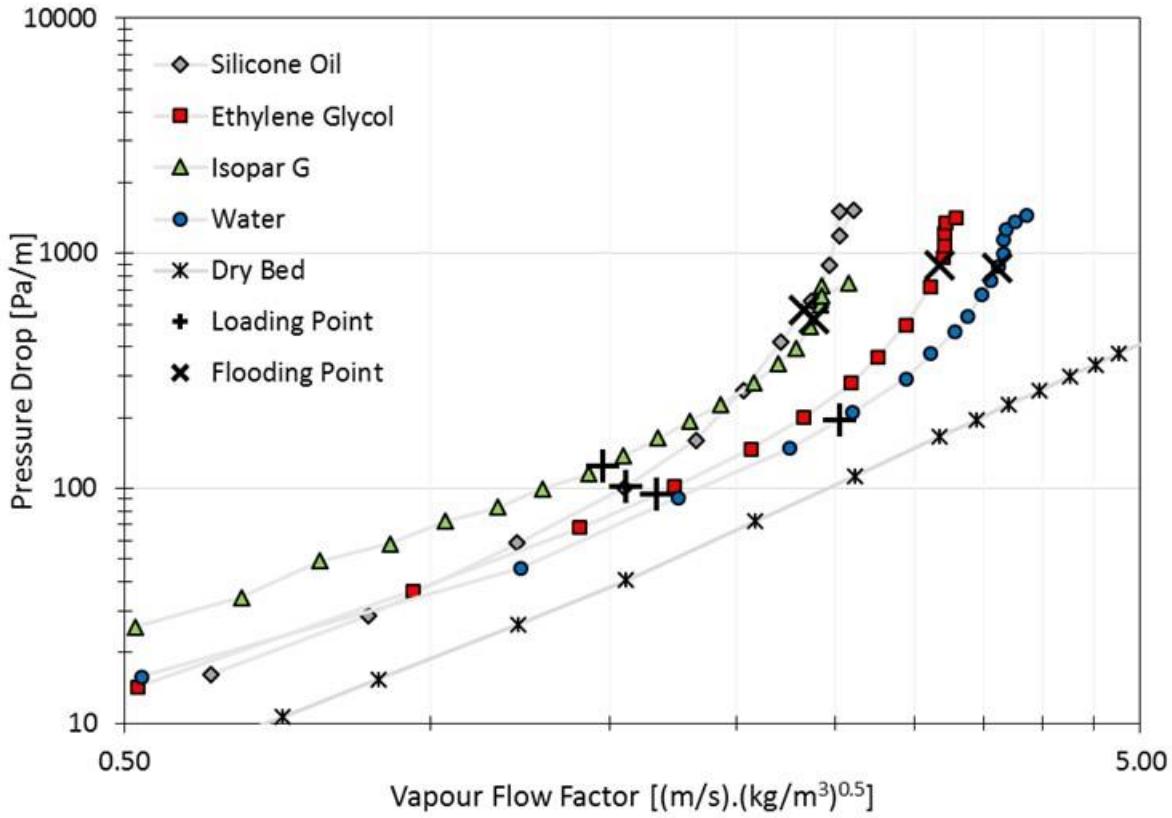

Figure 4.24: Comparison of measured pressure drop for the different liquids with CO_2, 2.5" Intalox Ultra O at 73 $m^3/(m^2.h)$

For Isopar G, with a very low liquid density compared to the other liquids investigated here, the frictional force of the gas counteracts the gravitational force on the liquid at a much lower gas flow rate, resulting in the low flooding point of Isopar G. While silicone oil has a flooding point close to that of Isopar G, silicone oil has a liquid density much higher than Isopar G and more comparable to that of water and ethylene glycol. The low flooding point of silicone oil, compared to that of water and ethylene glycol, is a result of the high viscosity of silicone oil resisting the flow of liquid down the column. Ethylene glycol has the highest liquid density of the four liquids and a liquid viscosity higher than water and Isopar G, but smaller than silicone oil. While the high viscosity of ethylene glycol compared to water has the same effect on the flooding point as described for silicone oil (i.e. a larger resistance to the flow of liquid down the column), the high liquid density has the opposite effect as described for Isopar G, where the gravitational force that has to be countered by the gas frictional forces is much larger than for the other liquids. Ethylene glycol's lower viscosity and higher density compared to silicone oil result in ethylene glycol having a higher flooding point than silicone oil. While the higher density of ethylene glycol, compared to water, has an increasing contribution on the

flooding point, the higher viscosity of ethylene glycol ultimately results in ethylene glycol having a lower flooding point than water.

According to Strigle (1994) the effect of surface tension on packed column capacity is small to none. However, the studies that came to these conclusions used Raschig rings as packing material, which are less prone to droplet formation and thus flooding as a result of droplet entrainment. For modern lattice-type packings, the contribution of droplet entrainment to flooding is larger. For these types of packings, the influence of surface tension on capacity would depend on the effect of surface tension on droplet formation. According to Maćkowiak (2010), the formation of droplets depends on the Weber number, with droplet formation from films and runlets only occurring if the Weber number is larger than a critical value. With surface tension appearing in the denominator of the Weber number, lower surface tension would result in a larger Weber number and thus earlier droplet formation. Through this argument, a decrease in surface tension should have a decreasing effect on capacity, regardless of foaming. Uys *et al*. (2017) investigated the influence of liquid physical properties on entrainment in a tray column and found that an increase in surface tension and viscosity resulted in a decrease in the number of droplets produced. While Isopar G and silicone oil both have much lower surface tension than water and ethylene glycol (which should promote the formation of droplets), the high viscosity of silicone oil would hinder droplet formation if the effect of viscosity on droplet formation applicable to tray columns is also true for packed columns. The low surface tension of Isopar G should thus have a contributing effect on the low flood point of Isopar G, while for silicone oil the effect would be hindered as a result of its high viscosity.

4.4.3 Pressure Drop

When considering the pre-loading pressure drop for the different liquids in Figure 4.24, Isopar G has a much higher pressure drop than the other liquids. It was already established in Section 4.3 that the cause of such higher pressure drop was a result of the foaming of Isopar G. As the gas passes upwards through the column, rather than flowing past the liquid films and rivulets, the gas is encapsulated in the liquid, resulting in the formation of the foam. This has a significant effect on the resistance to the flow of gas through the column, resulting in a much higher pressure drop compared to a non-foaming system.

In Figure 4.24 all four liquids have pressure drops higher than the dry bed pressure drop. The difference between dry bed pressure drop and the pressure drop of the different liquids is a result of the presence of the liquid on the packing. The liquid flowing over the packing reduces the open area available for gas to pass through the column, resulting in a higher pressure drop. Although water,

ethylene glycol and silicone oil produce very different liquid hold-ups in the pre-loading region, the respective pressure drops were rather similar.

As the gas flow rate increases, a point is reached where the gas starts to influence the flow of liquid down the column. At this point, known as the loading point, the upwards flow of gas starts to hinder the downwards flow of liquid, causing liquid to start accumulating in the packed bed. The point at which this occurs for the different liquids can be explained by the same argument made with regard to the difference in the flooding points of the different liquids. At the loading point, the pressure drop trend starts to move away from the parallel dry bed pressure drop trend, as illustrated in Figure 4.24 for the different liquids. Up until this point the rate at which the pressure drop increased as the gas flow rate increased, increased linearly. Consider the difference between the pressure drop at a gas flow rate above the loading point and the pressure drop that would have resulted at this gas flow rate if the rate at which the pressure drop increased continued increasing linearly. This difference in pressure drop is a result of the energy lost by suspending the liquid. As the liquid hold-up increases with an increase in the gas flow rate, this difference in pressure drop also increases.

4.5 Effect of Physical Gas Properties on Hydrodynamic Behaviour

To investigate the effect of physical gas properties on the hydrodynamic behaviour, the pressure drop, liquid hold-up and liquid entrainment were experimentally evaluated while using two different gases, namely air and carbon dioxide. However, when Isopar G was evaluated, air was substituted with nitrogen for safety concerns. The substitution of air with nitrogen is believed to be acceptable with negligible effect, since the difference in their physical properties is insignificant compared to that of carbon dioxide. Although the gasses differ in both gas density and viscosity, from literature it follows that gas viscosity generally has a very small influence on hydrodynamic behaviour, especially with the small viscosity difference of the gasses investigated here. For this reason all the effects of gas properties identified are attributed to the difference in gas density.

For all four liquids and at all liquid flow rates, the difference in gas density had no effect on the pre-loading liquid hold-up. This is expected, since the gas has no effect on the liquid hold-up in the pre-loading region. For each of the four liquids at all liquid flow rates, a plot of the measured liquid hold-up against the vapour flow factor for air and carbon dioxide shows that the liquid hold-up trends with air and carbon dioxide coincide. The same is true for the measured pressure drop. This is illustrated in Figure 4.25 for all liquids at a liquid flow rate of 98 $m^3/(m^2.h)$ with 2.5” Intalox Ultra O.

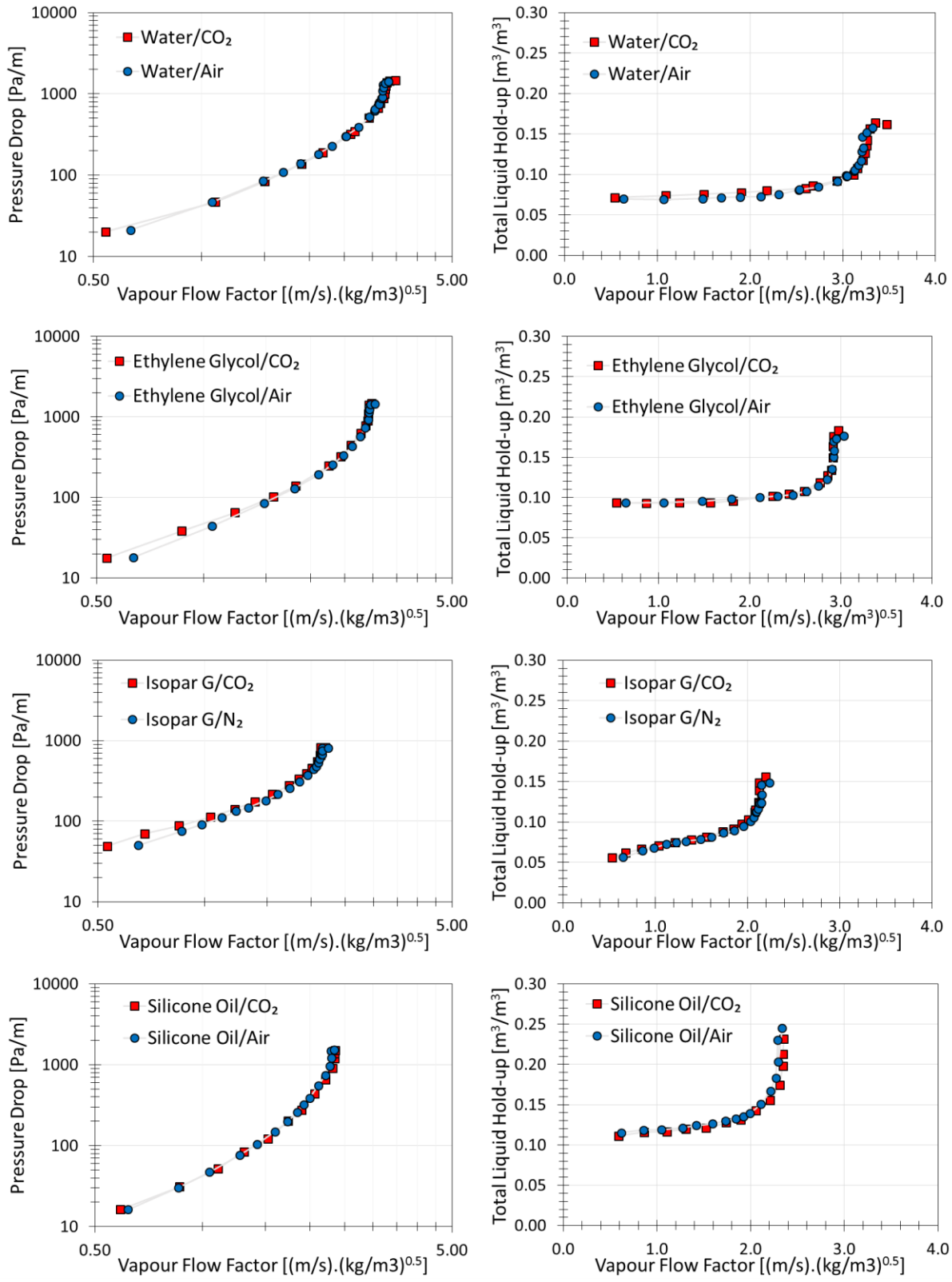

Figure 4.25: Comparison of measured pressure drop and liquid hold-up vs. vapour flow factor for water, ethylene glycol, Isopar G and silicone oil with air and CO_2, 2.5" Intalox Ultra O at 98 $m^3/(m^2.h)$

The vapour flow factor is the square root of the gas kinetic energy, calculated as the superficial gas velocity times the square root of the gas density. Figure 4.25 illustrates that to induce a certain liquid hold-up above the loading point for a specific liquid, the gas requires a certain kinetic energy. Since carbon dioxide has a higher density than air, carbon dioxide would induce this liquid hold-up at a lower superficial gas velocity (Figure 4.26). The same argument applies to the flooding point, where a certain gas kinetic energy is required to flood the column, resulting in a flooding point at a lower superficial gas velocity for carbon dioxide compared to air.

Considering the pre-loading pressure drop of carbon dioxide and air in Figure 4.26, carbon dioxide has a higher pressure drop than air at the same superficial gas velocity for all liquids. When considering the pressure drop in the pre-loading region as a measure of the energy that is required to pass the gas through the column at a certain superficial gas velocity, air requires less energy than carbon dioxide, since air would have lower kinetic energy at this superficial gas velocity. At higher superficial gas velocities, the difference in the pressure drop between carbon dioxide and air also includes the pressure drop of carbon dioxide as a result of the increase in liquid hold-up.

The above discussion was with regard to carbon dioxide and air. Initially it was assumed that the effect of the difference in gas viscosity of these two gasses will have an insignificant effect on the hydrodynamic behaviour. This assumption was based on both the small difference in viscosity between the two gasses as well as the conclusion from literature that gas viscosity generally has a very small effect on hydrodynamic behaviour. If the difference in gas viscosity of carbon dioxide and air had a significant effect, this would have resulted in a significant difference in the liquid hold-up above the loading point and an overall difference in pressure drop for the two gasses in Figure 4.25 at the same vapour flow factor. The gas with the higher viscosity would have had a higher liquid hold-up and pressure drop. It can therefore be concluded that the difference in viscosity between air and carbon dioxide has no significant effect on the hydrodynamic behaviour.

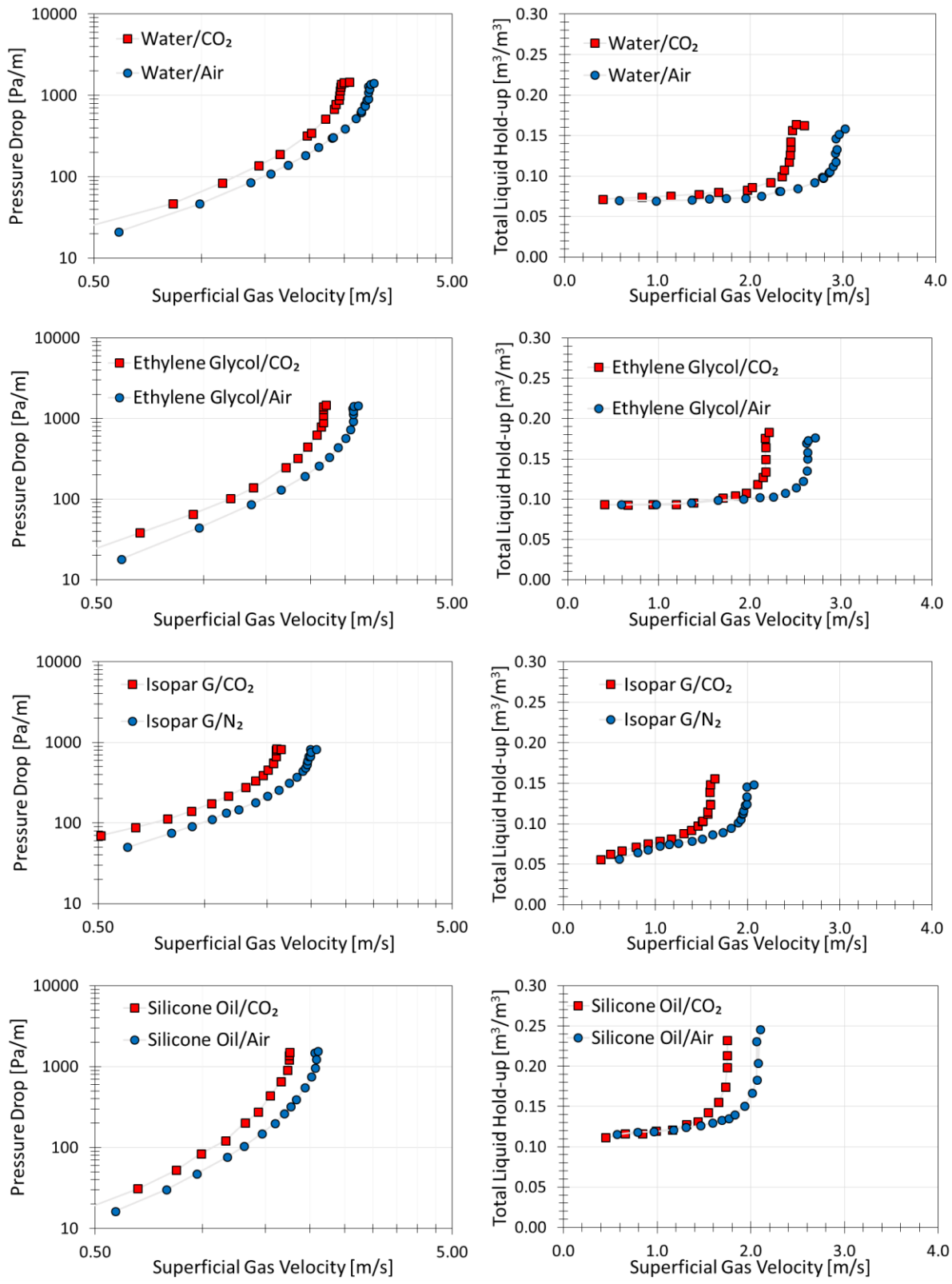

Figure 4.26: Comparison of measured pressure drop and liquid hold-up vs. superficial gas velocity for water, ethylene glycol, Isopar G and silicone oil with air and CO_2, 2.5" Intalox Ultra O at 98 $m^3/(m^2.h)$

4.6 Effect of Packing Size on Hydrodynamic Behaviour

The specific packing surface areas and void fractions of 1.5" Intalox Ultra A and 2.5" Intalox Ultra O were determined from the packing geometry. While the 1.5" Intalox Ultra A and 2.5" Intalox Ultra O have very similar packing void fractions, 1.5" Intalox Ultra A has a higher specific surface area than the 2.5" Intalox Ultra O. The experimental liquid hold-up and pressure drop data measured in this project showed that the 1.5" Intalox Ultra A produced a higher liquid hold-up and pressure drop than the 2.5" Intalox Ultra O when compared at the same vapour flow factor for the same liquid/gas system and at the same liquid flow rate. In addition, the capacity of 1.5" Intalox Ultra A was found to be lower than for 2.5" Intalox Ultra O. This is true for all liquids and gasses investigated here and is illustrated for all liquids with air at a liquid flow rate of 98 $m^3/(m^2.h)$ in Figure 4.27.

The higher pre-loading liquid hold-up of 1.5" Intalox Ultra A compared to 2.5" Intalox Ultra O is a result of the higher specific surface area of 1.5" Intalox Ultra A. Since the pre-loading liquid hold-up is primarily a result of the liquid coating the packing in the form of films and rivulets, higher specific surface area results in higher liquid hold-up. The pre-loading liquid hold-up is approximately 43 % lower for water with 2.5" Intalox Ultra O relative to the liquid hold-up of 1.5" Intalox Ultra A and approximately 28 % and 23 % for ethylene glycol and silicone oil, respectively. As a result of the foaming of Isopar G and related effects on the pre-loading liquid hold-up, the percentage at which the pre-loading hold-up decreases could not be determined accurately for Isopar G.

With the lower pre-loading liquid hold-up of the 2.5" Intalox Ultra O, the open area available for gas to pass through the column is higher compared to the 1.5" Intalox Ultra A, resulting in a lower pre-loading pressure drop, as illustrated for all liquids in Figure 4.27. The pre-loading pressure drop for all liquids at all liquid flow rates investigated here is approximately 50 % lower for 2.5" Intalox Ultra O relative to the pressure drop of 1.5" Intalox Ultra A.

With a larger open area for gas to pass through the column for the 2.5" Intalox Ultra O, the gas flow rate at which the gas starts to influence the flow of liquid, and thus increase the liquid hold-up, is higher for 2.5" Intalox Ultra O compared to the 1.5" Intalox Ultra A. This also results in a higher flooding point for 2.5" Intalox Ultra O compared to 1.5" Intalox Ultra A. Table 4.1 shows the percentage increase in the identified flooding points (vapour flow factor) for 2.5" Intalox Ultra O relative to the flooding point of 1.5" Intalox Ultra A for all liquids and at all liquid flow rates investigated here. The percentage increases in the identified flooding points were calculated with the average of the identified flooding points (vapour flow factor) of carbon dioxide and air/nitrogen.

Table 4.1: Percentage increase in flooding point for 2.5" Intalox Ultra O relative to 1.5" Intalox Ultra A

Liquid Flow Rate [$m^3/(m^2.h)$]	Water [%]	Ethylene Glycol [%]	Isopar G [%]	Silicone Oil [%]	Average for all liquids [%]
6	8	15	10	11	11
37	21	24	23	22	22
73	31	31	26	31	30
98	34	37	32	40	36
122	37	40	35	-	37

While the increase in capacity for the different liquids is relatively similar at each liquid flow rate, the relative increase in capacity is smaller at lower liquid flow rates. At higher liquid flow rates however, the relative increase in capacity tends towards a maximum increase of approximately 37 %.

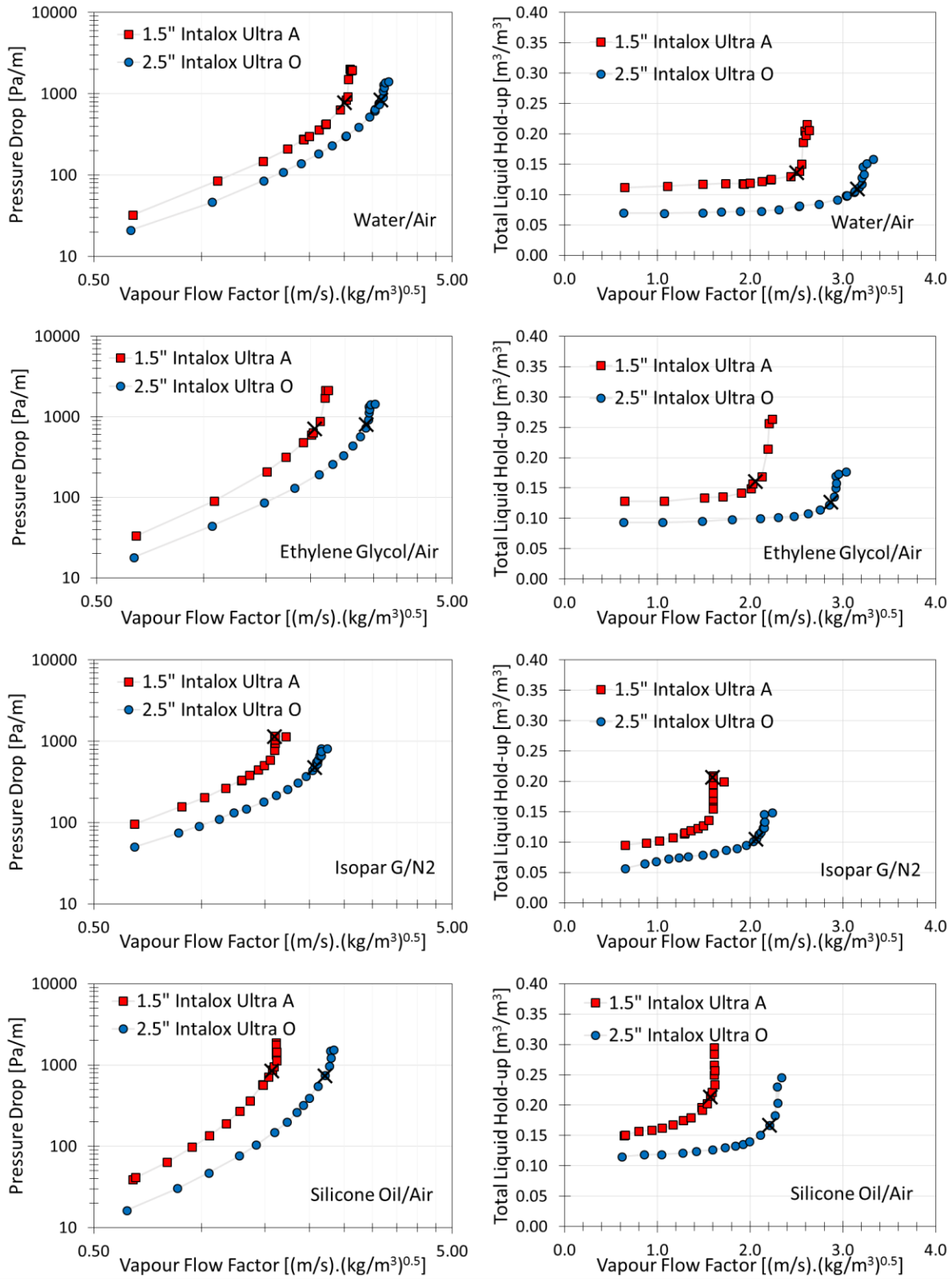

Figure 4.27: Comparison of measured pressure drop and liquid hold-up for water, ethylene glycol, Isopar G and silicone oil with 1.5" Intalox Ultra A and 2.5" Intalox Ultra O at 98 $m^3/(m^2.h)$ with air

5. Hydrodynamic Modelling

The experimental pressure drop and liquid hold-up data for 1.5" Intalox Ultra A and 2.5" Intalox Ultra O were compared to the predictions with the three semi-theoretical models discussed in Section 2.6, namely the Billet and Schultes, Maćkowiak and Stichlmair models. As mentioned, none of the packing-specific constants required for these models are available for Intalox Ultra random packing. The required constants were therefore calculated through a minimization procedure from the experimental data with physical liquid and gas properties and operating conditions within the ranges for which the models were validated. Since none of the models account for foaming, the experimental data for Isopar G were excluded in all calculations of the packing-specific constants.

5.1 Calculation of the Packing-specific Constants

The Billet and Schultes model requires three packing-specific constants for calculating the pre-loading liquid hold-up, the pressure drop and the flooding gas velocity, respectively. The liquid hold-up calculated with the Billet and Schultes model was validated for liquid flow rates ranging from 1.33-82.8 $m^3/(m^2.h)$. Therefore, the experimental data for liquid flow rates of 98 and 120 $m^3/(m^2.h)$ were excluded from the calculation of pre-loading liquid hold-up constant. This is the only limiting factor in the liquid hold-up validation range with regard to the physical properties and operating conditions of the experimental data measured for this project. The pre-loading liquid hold-up constant, used in Equations [2.13] and [2.14], was calculated by minimizing the AARE between the experimental and calculated pre-loading liquid hold-up. The constant required in Equation [2.7] for calculating the irrigated pressure drop is also required in Equation [2.4] for calculating the dry bed pressure drop. This constant was calculated by minimizing the AARE between the experimental and calculated dry bed pressure drop. The constant required in Equation [2.24] and [2.25] for calculating the flooding gas velocity was calculated by minimizing the AARE between the experimental flooding gas velocity, determined with the method described in Section 4.2, and the calculated flooding gas velocity. Since the flooding point calculation in the Billet and Schultes model was only validated for a liquid and gas density range of 750-1026 kg/m^3 and 0.30-1.37 kg/m^3 respectively, only the water/air and silicone oil/air experimental flooding gas velocities were used in the calculation of the flooding gas velocity constant.

The Maćkowiak model requires two packing-specific constants for calculating the flooding gas velocity and pressure drop, respectively. According to Maćkowiak (1990) the suspended bed of droplets modelling approach with regard to the flooding gas velocity is only valid for dimensionless liquids $B_L < 3 \times 10^{-3}$ in Equation [2.37]. For the calculation of the flooding gas velocity constant required in

Equation [2.30], experimental data with liquid loads that exceeded this value were not included (silicone oil at liquid flow rates of 98 and 120 $m^3/(m^2.h)$ with 1.5" Intalox Ultra). The flooding gas velocity constant was calculated by minimizing the AARE between the experimental flooding gas velocity, determined with the method described in Section 4.2, and the calculated flooding gas velocity. The constant required for calculating the pressure drop in Equation [2.39] and [2.40], which Maćkowiak (1991) calls a packing shape factor, was calculated by minimizing the AARE between the experimental and calculated pressure drop. Since the pressure drop in the Maćkowiak model was only validated for liquid Reynolds numbers below 200, experimental data with liquid Reynolds numbers higher than this were excluded from the calculation of the packing shape factor.

The calculation of the flooding gas velocity in the Billet and Schultes and Maćkowiak models are solved iteratively. To calculate the flooding gas velocity constant thus required these models to be solved iteratively for each value of the constant in a range of values until a value is obtained for which the AARE is a minimum.

The Stichlmair model requires three packing-specific constants which are required for calculating the dry bed pressure drop friction factor in Equation [2.43]. The dry bed pressure drop friction factor, together with two of the constants, is required for calculating the irrigated pressure drop friction factor in Equations [2.48] and [2.49]. The dry bed pressure drop friction factor is a function of the gas Reynolds number as shown in Equation [2.43]. At very high gas Reynolds numbers (turbulent gas flow), the value of the dry bed pressure drop friction factor approaches the value of C_3. At lower gas Reynolds numbers, the friction factor is higher and a function of all three constants. The dry bed pressure drop friction factor, calculated from the experimental dry bed pressure drop data, also followed this trend. To calculate the values of the three constants, the data was divided at the point at which the friction factor approached a constant value at higher Reynolds numbers. The value for C_3 was calculated by minimizing the AARE between the experimental and calculated friction factor beyond the point at which the data was divided, while the values for C_1 and C_2 were calculated by minimizing the AARE at lower Reynolds numbers.

The calculated values of the required packing-specific constants for the three models are provided in Table 5.1 together with a reference to the equations for which they are required.

Table 5.1: Calculated packing-specific constants for Billet and Schultes, Maćkowiak and Stichlmair Models for 1.5" Intalox Ultra A and 2.5" Intalox Ultra O

		Equations in which constants are required	1.5" Intalox Ultra A	2.5" Intalox Ultra O
Billet and Schultes Model	C_p	[**2.4**], [**2.7**]	0.704	0.590
	C_h	[**2.13**], [**2.14**]	0.835	0.823
	$C_{Fl,P}$	[**2.24**], [**2.25**]	1.773	1.462
Maćkowiak Model	θ	[**2.39**], [**2.40**]	0.203	0.129
	ψ_{Fl}^{*}	[**2.30**]	1.067	1.060
Stichlmair Model	C_1	[**2.43**], [**2.49**]	13.67	13.68
	C_2	[**2.43**], [**2.49**]	0	0
	C_3	[**2.43**]	2.48	2.15

The calculated values for the packing-specific constants for all three models are within the relative range of published values for other packings.

5.2 Experimental Data vs. Model Predictions

5.2.1 Pre-loading Liquid Hold-up

Table 5.2 summarizes the ARE between the predicted and experimental pre-loading liquid hold-up of the four liquids, at the different liquid flow rates investigated here for 1.5" Intalox Ultra A and 2.5" Intalox Ultra O. The ARE for each liquid/packing/liquid flow rate combination includes both air/nitrogen and carbon dioxide. The AARE for each liquid/packing combination is also provided.

As a result of the effect the foaming of Isopar G had on the pre-loading liquid hold-up with 2.5" Intalox Ultra O at liquid flow rates of 73 $m^3(m^2.h)$ and higher, the ARE between the experimental and predicted pre-loading liquid hold-up at these conditions are not included in Table 5.2.

The Stichlmair model under-predicts the pre-loading liquid hold-up for most liquid/packing/liquid flow rate combinations with the under-prediction increasing as the liquid flow rate increases. For the Billet and Schultes and Maćkowiak models, where the pre-loading liquid hold-up is under-predicted at low liquid flow rates, an increase in liquid flow rate decreases the under-prediction. Where these models over-predict the pre-loading liquid hold-up, an increase in liquid flow rate increases the over-prediction. The pre-loading liquid hold-up predicted with the Billet and Schultes and Maćkowiak models thus increases relative to the experimental pre-loading liquid hold-up as the liquid flow rate

increases, while the opposite occurs for the Stichlmair model. The difference in behaviour of the models is a result of the difference in the dependence of the pre-loading liquid hold-up on liquid flow rate. The dependence of the pre-loading liquid hold-up for the three models is as follows:

Billet and Schultes model: $h_{L,S} \infty u_L^{0.8}$

Maćkowiak Model: $h_{L,S} \infty u_L^{0.5}$

Stichlmair Model: $h_{L,S} \infty u_L^{0.333}$

This suggests that the true dependence of the pre-loading liquid hold-up on the liquid flow rate lies between that of the Stichlmair and Maćkowiak Models:

$h_{L,S} \infty u_L^x$ with $0.333 < x < 0.5$

Overall, the Stichlmair model gives the poorest prediction of the pre-loading liquid hold-up when considering the AARE. The Billet and Schultes model gives the best prediction of the pre-loading liquid hold-up of water, while the Maćkowiak model gives the best prediction of the pre-loading liquid hold-up of ethylene glycol. For Isopar G the Billet and Schultes model gives the best prediction of the pre-loading liquid hold-up for the 1.5" Intalox Ultra A, while the Maćkowiak model gives a better prediction for 2.5" Intalox Ultra O. For silicone oil, the Billet and Schultes model gives the poorest prediction for the 1.5" Intalox Ultra A, while for the 2.5" Intalox Ultra O the Stichlmair model gives the poorest prediction.

Table 5.2: Comparison of the average relative error between the experimental and calculated pre-loading liquid hold-up for the Billet and Schultes & Schultes, Maćkowiak and Stichlmair models

	1.5" Intalox Ultra A			2.5" Intalox Ultra O		
	Water					
Liquid Flow Rate [m³/(m².h)]	ARE [%]			ARE [%]		
	Billet & Schultes	Maćkowiak	Stichlmair	Billet & Schultes	Maćkowiak	Stichlmair
6	-39	-38	-18	17	24	42
37	-21	-30	-39	-2	-14	-31
73	-16	-29	-47	-3	-17	-44
98	-8	-24	-47	0	-16	-47
122	-9	-25	-51	5	-14	-49
AARE [%]	19	29	41	5	17	43
	Ethylene Glycol					
Liquid Flow Rate [m³/(m².h)]	ARE [%]			ARE [%]		
	Billet & Schultes	Maćkowiak	Stichlmair	Billet & Schultes	Maćkowiak	Stichlmair
6	-27	-31	-11	-30	-27	-16
37	1	-6	-23	-6	-12	-33
73	10	-1	-31	6	-5	-39
98	16	2	-34	10	-3	-42
122	21	5	-35	19	3	-41
AARE [%]	15	9	27	14	10	34
	Isopar G					
Liquid Flow Rate [m³/(m².h)]	ARE [%]			ARE [%]		
	Billet & Schultes	Maćkowiak	Stichlmair	Billet & Schultes	Maćkowiak	Stichlmair
6	-22	-21	-5	-10	-4	2
37	-2	-13	-30	-5	-16	-38
73	4	-12	-40	-	-	-
98	8	-10	-43	-	-	-
122	1	-17	-50	-	-	-
AARE [%]	7	15	34	17	7	31
	Silicone Oil					
Liquid Flow Rate [m³/(m².h)]	ARE [%]			ARE [%]		
	Billet & Schultes	Maćkowiak	Stichlmair	Billet & Schultes	Maćkowiak	Stichlmair
6	-11	-21	-3	-20	-27	-16
37	21	9	-14	3	-2	-29
73	27	15	-23	13	6	-34
98	32	20	-24	22	13	-35
AARE [%]	23	16	16	15	12	28

5.2.2 Pre-loading Pressure Drop

Table 5.3 summarizes the ARE between the predicted and experimental pressure drop up to the experimental loading point, for the different liquids with air/nitrogen at the different liquid flow rates for 1.5” Intalox Ultra A and 2.5” Intalox Ultra O. The AARE for each liquid/packing combination is also provided.

Similar to the pre-loading liquid hold-up, an increase in the liquid flow rate results in the pre-loading pressure drop predicted with the Billet and Schultes and Maćkowiak models for water, ethylene glycol and silicone to increase relative to the experimental pressure drop. For the Stichlmair model the opposite occurs. This is expected since the pressure drop is dependent on the pre-loading liquid hold-up.

In general all three models predict the pre-loading pressure drop for both packings with all four liquids poorly. In particular, the prediction error of the Billet and Schultes model for 2.5” Intalox Ultra O at higher liquid flow rates is significantly higher than that of the other two models. At lower liquid flow rates, however, the Billet and Schultes model performs better than the other two models for most liquids with both packings.

Table 5.3: Comparison of the average relative error between the experimental and calculated pressure drop up to the experimental loading point for the Billet and Schultes, Maćkowiak and Stichlmair models

	1.5" Intalox Ultra A			2.5" Intalox Ultra O		
	Water					
Liquid Flow Rate [m³/(m².h)]	ARE [%]			ARE [%]		
	Billet & Schultes	Maćkowiak	Stichlmair	Billet & Schultes	Maćkowiak	Stichlmair
6	15	-21	74	-	-50	32
37	39	26	98	75	-31	66
73	82	47	88	218	-24	23
98	108	45	66	327	-33	0
122	145	47	51	521	-34	-10
AARE [%]	78	37	75	285	34	26
	Ethylene Glycol					
Liquid Flow Rate [m³/(m².h)]	ARE [%]			ARE [%]		
	Billet & Schultes	Maćkowiak	Stichlmair	Billet & Schultes	Maćkowiak	Stichlmair
6	15	34	118	-	-20	103
37	36	89	146	85	2	108
73	50	91	103	218	10	80
98	72	92	79	346	5	53
122	-	93	62	547	1	34
AARE [%]	43	80	102	299	8	76
	Isopar G					
Liquid Flow Rate [m³/(m².h)]	ARE [%]			ARE [%]		
	Billet & Schultes	Maćkowiak	Stichlmair	Billet & Schultes	Maćkowiak	Stichlmair
6	11	-22	66	17	-47	59
37	13	4	53	47	-41	30
73	-5	-21	-7	85	-56	-20
98	-25	-48	-44	89	-70	-50
122	-41	-66	-66	104	-79	-68
AARE [%]	19	32	47	68	58	45
	Silicone Oil					
Liquid Flow Rate [m³/(m².h)]	ARE [%]			ARE [%]		
	Billet & Schultes	Maćkowiak	Stichlmair	Billet & Schultes	Maćkowiak	Stichlmair
6	8	100	138	18	19	124
37	30	206	180	90	66	147
73	54	224	147	227	70	115
98	-	224	123	364	59	84
AARE [%]	30	188	147	175	53	118

5.2.3 Flooding Gas velocity

Table 5.4 shows percentage error between the experimental flooding gas velocity, determined with the method described in Section 4.2, and the flooding gas velocity calculated with the three models for both 1.5" Intalox Ultra A and 2.5" Intalox Ultra O for the four liquids with air/nitrogen.

The observations with regard to the error in the prediction of the flooding gas velocity with the different models can also be observed in Figure 5.1, with the different models displaying different trends for the flooding gas velocity versus liquid flow rate.

The Stichlmair model generally shows a consistent over-prediction of the flooding gas velocity, with the over-prediction increasing as the liquid flow rate increases. For water and ethylene glycol the Billet and Schultes model significantly under-predicts the flooding gas velocity at the liquid flow rate of 6 $m^3/(m^2.h)$, with the prediction improving at higher liquid flow rates. For ethylene glycol however, the Billet and Schultes model significantly under-predicts the flooding gas velocity at a liquid flow rate of 122 $m^3/(m^2.h)$ for 1.5" Intalox Ultra A. For Isopar G, the Billet and Schultes model also under-predicts the flooding gas velocity at 6 $m^3/(m^2.h)$, with the prediction improving as the liquid flow rate initially increases. At the high liquid flow rates however, the Billet and Schultes model over-predicts the flooding gas velocity. For silicone oil, the Billet and Schultes model gives relatively good predictions at the lower liquid flow rates, but significantly under-predicts the flooding gas velocity at the liquid flow rate of 98 $m^3/(m^2.h)$ for 1.5" Intalox Ultra A. The prediction error with the Maćkowiak model is more consistent with regard to liquid flow rate and, to a certain extent, the different packings, compared to the other two models. Overall, the Maćkowiak model predicts the flooding gas velocity for water and Isopar G better than the other two models. For ethylene glycol the error in the prediction of the flooding gas velocity with the Maćkowiak model is comparable to that of the other two models. For silicone oil the Maćkowiak model over-predicts the flooding gas velocity more than for the other liquids. Except for the significant under-prediction of the Billet and Schultes model at 98 $m^3/(m^2.h)$ for 1.5" Intalox Ultra A, the Billet and Schultes model gives the best flooding gas velocity predictions for silicone oil.

Table 5.4: Comparison of the average relative error between the experimental and calculated flooding gas velocity for the Billet & Schultes, Maćkowiak and Stichlmair models at a liquid flow rate of 73 $m^3/(m^2.h)$ with air/nitrogen

	1.5" Intalox Ultra A			2.5" Intalox Ultra O		
	Water					
Liquid Flow Rate $[m^3/(m^2.h)]$	Percentage Error [%]			Percentage Error [%]		
	Billet & Schultes	Maćkowiak	Stichlmair	Billet & Schultes	Maćkowiak	Stichlmair
6	-49	-3	-2	-54	4	33
37	-17	6	9	-32	3	28
73	-4	0	16	-20	-4	32
98	7	-2	28	-9	-6	45
122	4	-10	36	-5	-14	48
AARE [%]	16	4	18	24	6	37
	Ethylene Glycol					
Liquid Flow Rate $[m^3/(m^2.h)]$	Percentage Error [%]			Percentage Error [%]		
	Billet & Schultes	Maćkowiak	Stichlmair	Billet & Schultes	Maćkowiak	Stichlmair
6	-23	9	2	-38	10	29
37	10	26	14	-11	14	26
73	8	14	16	-4	5	27
98	10	11	27	0	0	32
122	-45	0	32	-7	-8	36
AARE [%]	19	12	18	12	8	30
	Isopar G					
Liquid Flow Rate $[m^3/(m^2.h)]$	Percentage Error [%]			Percentage Error [%]		
	Billet & Schultes	Maćkowiak	Stichlmair	Billet & Schultes	Maćkowiak	Stichlmair
6	-35	7	22	-44	11	62
37	4	12	36	-12	12	65
73	30	8	59	9	6	81
98	47	2	79	21	-2	94
122	49	-10	101	33	-11	109
AARE [%]	33	8	59	24	8	82
	Silicone Oil					
Liquid Flow Rate $[m^3/(m^2.h)]$	Percentage Error [%]			Percentage Error [%]		
	Billet & Schultes	Maćkowiak	Stichlmair	Billet & Schultes	Maćkowiak	Stichlmair
6	5	22	4	-10	24	34
37	13	31	7	7	24	24
73	-1	29	20	7	15	27
98	-64	19	26	1	5	29
AARE [%]	21	25	14	6	17	28

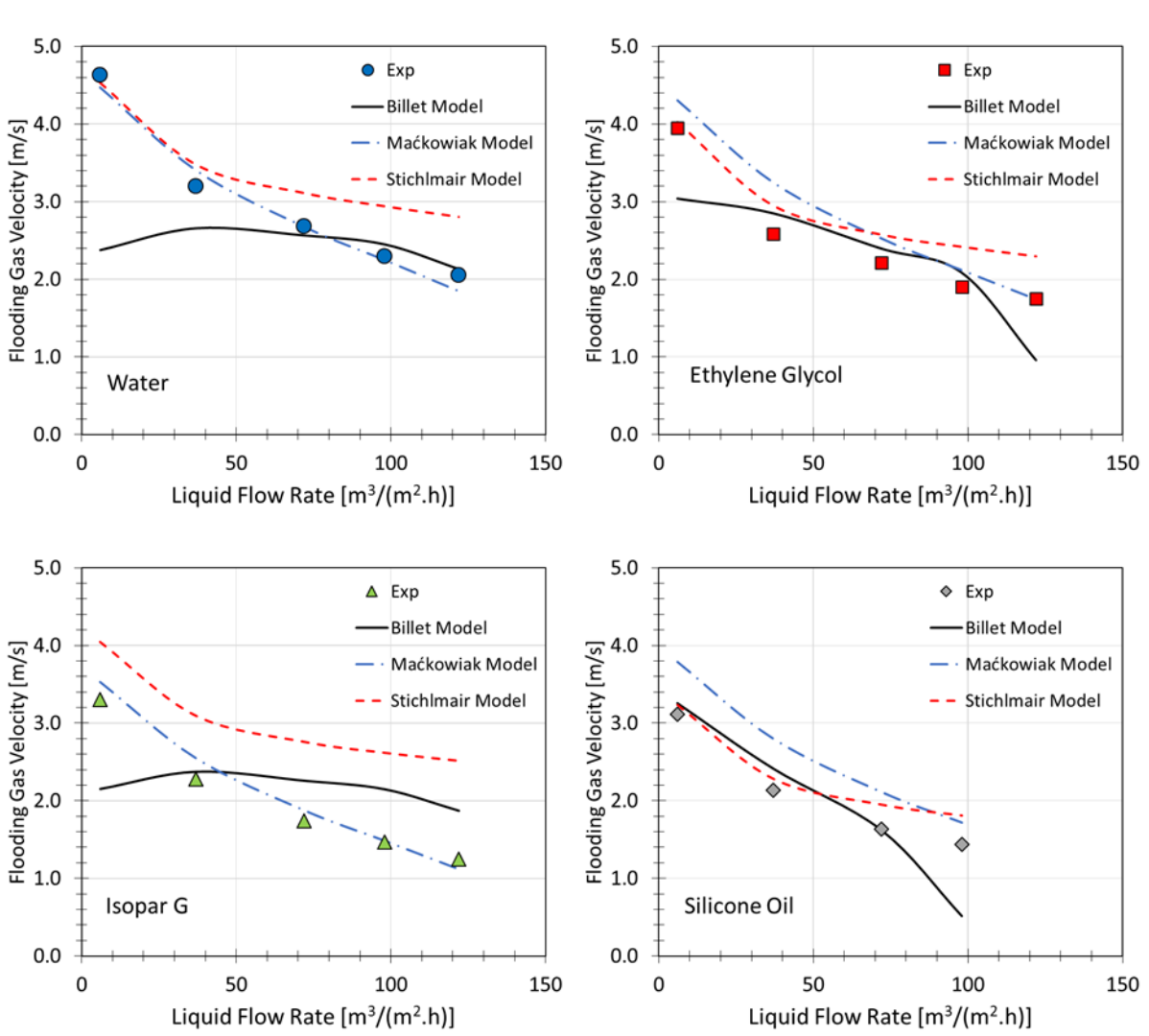

Figure 5.1: Comparison of the experimental and calculated superficial flooding gas velocity vs. liquid flow rate for Billet & Schultes, Maćkowiak and Stichlmair models with 1.5" Intalox Ultra A with air/nitrogen

Overall, the Maćkowiak model performs better in predicting the flooding point than the other two models. The Maćkowiak model is the only model based on the droplet entrainment modelling approach, whereas the Billet Schultes and Stichlmair models are based on the film modelling approach. The Maćkowiak model is also the only model that takes into account the surface tension of the liquid.

While the Billet and Schultes and Stichlmair models have similar flooding gas velocity prediction errors for carbon dioxide compared to air/nitrogen, the Maćkowiak model prediction errors differ. For an under-prediction of the flooding gas velocity with air/nitrogen, carbon dioxide will have a larger under-prediction, and for an over-prediction with air/nitrogen, carbon dioxide will either have a lower over-prediction or an under-prediction.

Figure 5.2, Figure 5.3, Figure 5.4 and Figure 5.5 show the predicted pressure drop and liquid hold-up trends for the Billet and Schultes, Maćkowiak and Stichlmair models compared to the experimental data for water, ethylene glycol, Isopar G and silicone oil with air/nitrogen and the 1.5" Intalox Ultra A at a liquid flow rate of 73 $m^3(m^2.h)$.

The Stichlmair model fails to predict the sharp increase in both pressure drop and liquid hold-up in the flooding region for all four liquids investigated here. Both the Billet and Schultes and Maćkowiak models predicts the sharp increase in pressure drop and liquid hold-up in the flooding region for water, although the Billet and Schultes model slightly under-predicts the flooding point. While the Billet and Schultes model predicts the sharp increase in liquid hold-up and pressure drop for ethylene glycol, the Maćkowiak model shows an increase in the loading region but over-predicts the flooding point. For Isopar G, only the Maćkowiak predicts the sharp increase in the flooding region, with the Billet and Schultes model over-predicting the flooding point. While the Maćkowiak and Stichlmair models fail to predict the sharp increase in the flooding region for silicone oil, the Billet and Schultes model does predict this but under-predicts the flooding point.

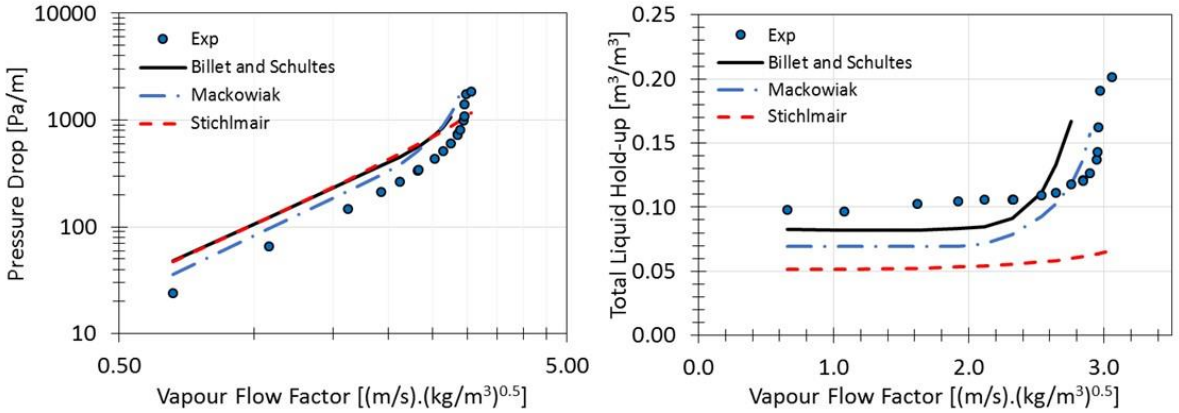

Figure 5.2: Comparison of the experimental pressure drop and liquid hold-up vs. the model prediction with the Billet & Schultes, Maćkowiak and Stichlmair models for water with 1.5" Intalox Ultra A and air at a liquid flow rate of 73 $m^3/(m^2.h)$

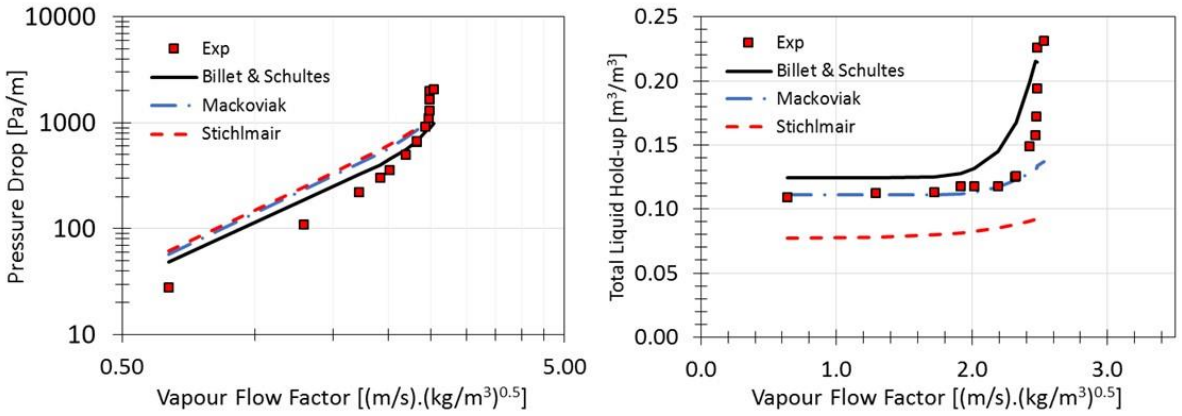

Figure 5.3: Comparison of the experimental pressure drop and liquid hold-up vs. the model prediction with the Billet & Schultes, Maćkowiak and Stichlmair models for ethylene glycol with 1.5" Intalox Ultra A and air at a liquid flow rate of 73 $m^3/(m^2.h)$

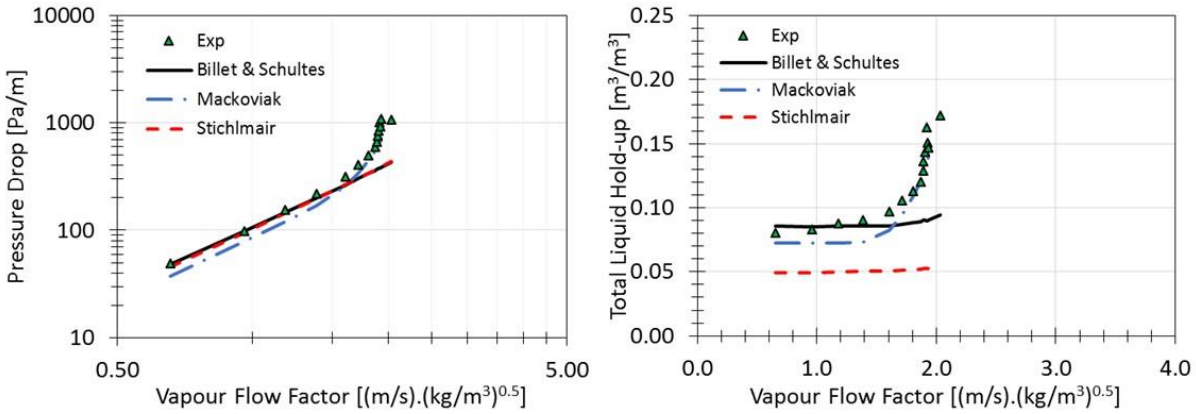

Figure 5.4: Comparison of the experimental pressure drop and liquid hold-up vs. the model prediction with the Billet & Schultes, Maćkowiak and Stichlmair models for Isopar G with 1.5" Intalox Ultra A and nitrogen at a liquid flow rate of 73 $m^3/(m^2.h)$

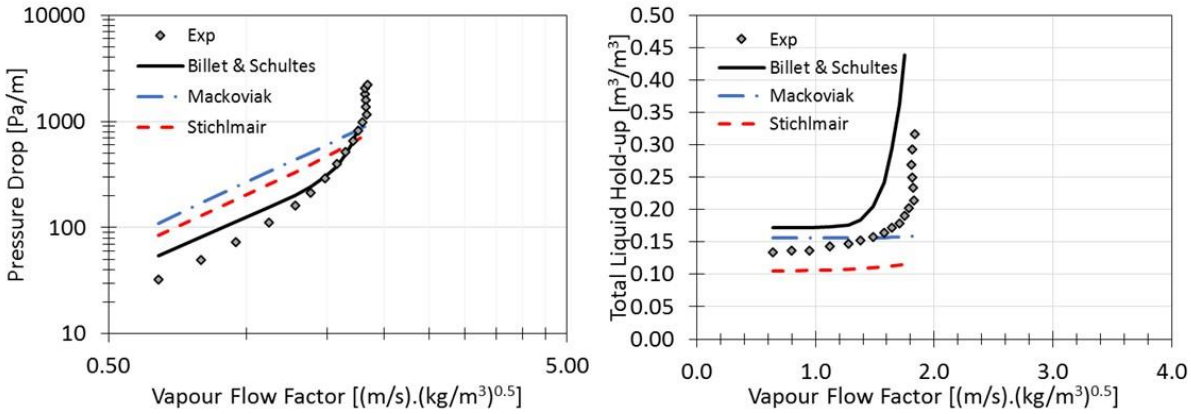

Figure 5.5: Comparison of the experimental pressure drop and liquid hold-up vs. the model prediction with the Billet & Schultes, Maćkowiak and Stichlmair models for silicone oil with 1.5" Intalox Ultra and air at a liquid flow rate of 73 $m^3/(m^2.h)$

5.2.4 KG-Tower

The experimental pressure drop data for both 1.5" Intalox Ultra A and 2.5" Intalox Ultra O with water, ethylene glycol, Isopar G and silicone oil, with air/nitrogen at a liquid flow rate of 73 $m^3/(m^2.h)$ were compared to the pressure drop predicted with KG-Tower (V5.3) (Figure 5.6 and Figure 5.7).

For 1.5" Intalox Ultra A, the experimental pressure drop for water is significantly lower than the pressure drop predicted with KG-tower. In Section 4.1, the variation in the experimental measurements with the water/air system with 1.5" Intalox Ultra A was discussed, where a lower pressure drop was measured after a brown residue was noticed on the packing material. For 2.5" Intalox Ultra O, the experimental data agrees well with the pressure drop predicted with KG-Tower in the pre-loading region, but deviates at higher gas flow rates, with a higher flooding point.

Despite the foaming that was experienced with Isopar G, the pressure drop predicted with KG-Tower compares relatively well with the experimental pressure drop in the flooding region for both packings, where the foaming consisted of smaller bubbles. In the pre-loading and loading regions, KG-Tower under-predicts the pressure drop as a result of the foaming of Isopar G. Overall, the predicted and experimental pressure drop compares better for 1.5" Intalox Ultra A, which experienced less foaming than the 2.5" Intalox Ultra O.

For ethylene glycol and silicone oil, the high viscosity of these liquids was beyond the range of viscosities the KG-Tower model was developed with (< 5 mPa.s). Despite this, KG-Tower still provides a prediction for the pressure drop. For ethylene glycol with 1.5" Intalox Ultra A, KG-Tower over-predicts the experimental pressure drop, although not as significant as for water. For the 2.5" Intalox

Ultra O, the experimental and predicted pressure drop for ethylene glycol are in relatively good agreement. For silicone oil with 1.5" Intalox Ultra A, the experimental and predicted pressure drop agrees very well in the pre-loading region, but deviates at higher gas flow rates with a lower predicted pressure drop. KG-Tower fails to predict the increase in pressure drop in the loading and flooding regions. For 2.5" Intalox Ultra O, the experimental and predicted pressure drop for silicone oil also agrees very well in the pre-loading region and predicts the increase in pressure drop in the loading and flooding regions better than for the 1.5" Intalox Ultra A.

Overall, KG-Tower predicted the pressure drop better than the Billet and Schultes, Maćkowiak and Stichlmair models.

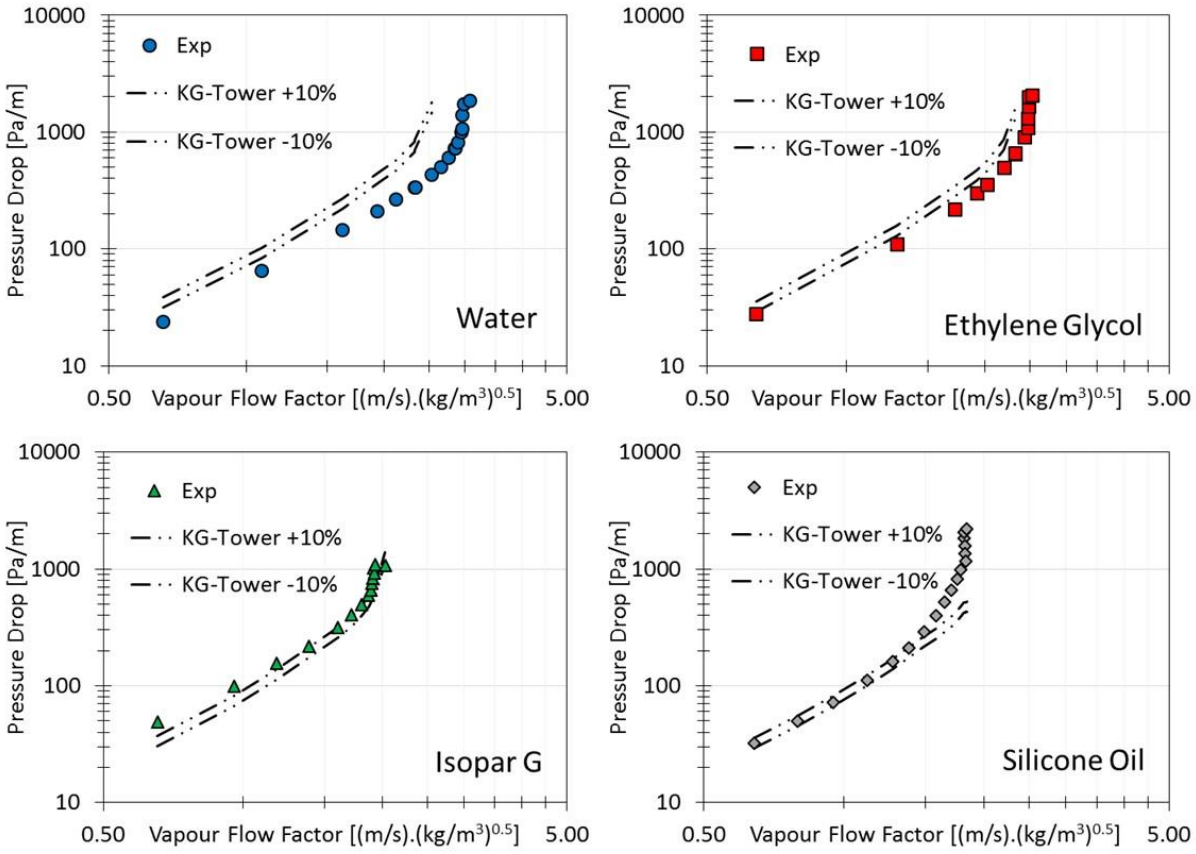

Figure 5.6: Experimental pressure drop vs. KG-Tower for water, ethylene glycol, Isopar G and silicone oil with air/nitrogen at a liquid flow rate of 73 $m^3/(m^2.h)$ with 1.5" Intalox Ultra A

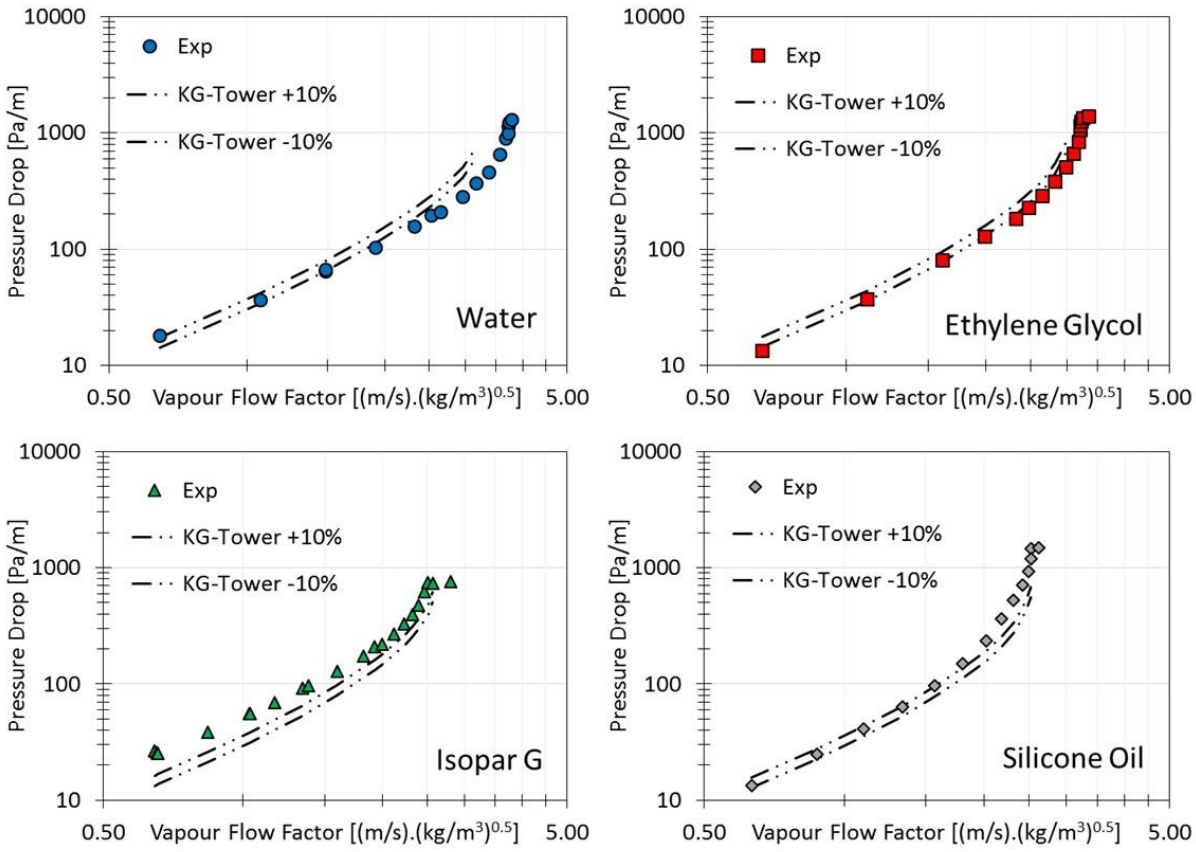

Figure 5.7: Experimental pressure drop vs. KG-Tower for water, ethylene glycol, Isopar G and silicone oil with air/nitrogen at a liquid flow rate of 73 $m^3/(m^2.h)$ with 2.5" Intalox Ultra O

6. Conclusions

In recent years modern random packings have been developed with improved capacity and separation efficiency. However, to utilise these modern random packings, and to take full advantage of the improved performance, experimental data is still required for developing and verifying the necessary hydrodynamic models.

The aim of this project was to investigate the effect of physical liquid and gas properties on the hydrodynamic behaviour of a modern fourth generation random packing. This aim was pursued by setting a number of objectives.

6.1 Liquid Distributor Design and Experimental Data Validation

With the goal of measuring liquid entrainment more accurately, a new liquid distributor was designed and built, with an open area equal to 60%; doubling the open area of the old distributor that was available. Furthermore, the distribution quality was found to be very good, with a CV value equal to 2 %. This is well within the acceptable criteria of < 5 % for good liquid distribution quality.

The experimental pressure drop and liquid hold-up data was verified by comparing the measured data for 1.5" Intalox Ultra A with an air/water system with the data measured by Lamprecht (2010). Initial pressure drop and liquid hold-up measurements were in good agreement with Lamprecht (2010). Although variations in the flooding point were observed when air/water experiments with 1.5" Intalox Ultra A were repeated at a later stage, repeated experiments with ethylene glycol/air and water/CO_2 showed good repeatability. The dry bed pressure drop compared very well with Lamprecht's data and showed good repeatability, isolating the cause of observed variations in water/air data to the liquid phase. A brown residue present on the packing material, after the water/CO_2 system was tested, is speculated to be a possible cause of the variation in experimental data, affecting the wettability of the packing when working with high surface tension water. An extensive cleaning procedure offered some improvement in the deviation from initial measurements. Overall it was possible to produce a proportionate data set with regard to the different liquid flow rates, with good repeatability within the specific system being tested.

6.2 Experimental Measurements and Data Interpretation

The pressure drop, liquid hold-up and entrainment data were measured as described in the stated objective, except for silicone oil, for which the centrifugal pump was not able to achieve the liquid flow rate of 122 $m^3/(m^2.h)$. Furthermore, Isopar G had a tendency to foam with both

1.5" Intalox Ultra A and 2.5" Intalox Ultra O for liquid flow rates of 73 $m^3/(m^2.h)$ and higher. The foaming had an identifiable effect on the pre-loading liquid hold-up of 2.5" Intalox Ultra O for liquid flow rates of 73 $m^3/(m^2.h)$ and higher, in the form of an increase in liquid hold-up in the pre-loading region as the gas flow rate increased. For both packings, the foaming resulted in an increase in pressure drop relative to the severity of the foaming.

A **method was developed to identify the loading and flooding points** when presented with the experimental pressure drop data, by making use of the prediction intervals of regressed curves fitted to the data. Overall, the method provides relatively accurate identification of the loading and flooding points at high liquid flow rates. At low liquid flow rates, and especially at 6 $m^3/(m^2.h)$, some uncertainty arises due to the more gradual pressure drop trend at such a low flow rate. The identification of the flooding point with entrainment data was found to be inaccurate at high liquid flow rates, over-predicting the flooding point. At low liquid flow rates, it is concluded that the true flooding point is between the points identified with the two methods.

With regard to the effect of **physical liquid properties** on the hydrodynamic behaviour, the following conclusions are made. Liquid viscosity has a significant effect on liquid hold-up, where an increase in viscosity results in an increase in liquid hold-up. Silicone oil and ethylene glycol, having much higher liquid viscosities than water and Isopar G, have much higher liquid hold-up in the pre-loading region. From literature, it is concluded that a decrease in liquid density results in an increase in liquid hold-up. Despite the low liquid density of Isopar G, it still has a liquid hold-up lower than that of ethylene glycol and silicone oil. This is because for silicone oil and ethylene glycol, the ratio of viscous forces over the gravitational forces is much larger than for Isopar G. The same argument applies to water and ethylene glycol, where water has a lower liquid density than ethylene glycol, but still has a pre-loading liquid hold-up lower than ethylene glycol, which is a result of the higher liquid viscosity of ethylene glycol.

With very different physical liquid properties, silicone oil and Isopar G flood at about the same gas flow rate, much lower than water and ethylene glycol. This is explained by the low liquid density of Isopar G, resulting in the upward drag force of the gas counteracting the gravitational force on the liquid at a much lower gas flow rate. The low flooding gas velocity of silicone oil is explained by the high viscosity of silicone oil resisting the flow of liquid down the column.

While Isopar G has a much higher pre-loading pressure drop as a result of the foaming, water, ethylene glycol and silicone oil have very similar pre-loading pressure drop, despite the large difference in their pre-loading liquid hold-up.

Regarding **gas physical properties**, gas density had no effect on the pre-loading liquid hold-up for all four liquids when comparing carbon dioxide and air/nitrogen. The pressure drop and liquid hold-up trends versus the vapour flow factor for the same liquid, packing and liquid flow rate for air/nitrogen and carbon dioxide were found to coincide. This illustrates that a certain gas kinetic energy is required to induce a certain liquid hold-up and pressure drop. At the same superficial gas velocity, carbon dioxide with a higher gas kinetic energy results in higher pressure drop and higher liquid hold-up above the loading point.

The general effect of the increase in **packing size** from 1.5" Intalox Ultra A to 2.5" Intalox Ultra O is a reduction in both pressure drop and liquid hold-up, and an increase in capacity. The pre-loading liquid hold-up of water is approximately 43 % lower with 2.5" Intalox Ultra O relative to the liquid hold-up of 1.5" Intalox Ultra A, and approximately 28 % and 23 % for ethylene glycol and silicone oil, respectively. The pre-loading pressure drop of all liquids at all liquid flow rates is approximately 50 % lower with 2.5" Intalox Ultra O relative to the pressure drop of 1.5" Intalox Ultra A. All liquids experienced an increase in capacity of approximately 11 % at a liquid flow rate of 6 $m^3/(m^2.h)$, with this percentage increasing to approximately 37 % at a liquid flow rate of 122 $m^3/(m^2.h)$.

6.3 Hydrodynamic Modelling

The packing-specific constants for the Billet and Schultes, Maćkowiak and Stichlmair models, for both 1.5" Intalox Ultra A and 2.5" Intalox Ultra O, were calculated from the experimental data by a minimization procedure, taking into account only the experimental data that fell in the range of properties and parameters for which the models were verified.

Overall, the Stichlmair model gave the poorest prediction of the pre-loading liquid hold-up. While the Billet and Schultes model gave the best prediction of the pre-loading liquid hold-up of water, the Maćkowiak model gave the best prediction of the pre-loading liquid hold-up of ethylene glycol and, to a certain extent, for silicone oil.

In general all three models predict the pre-loading pressure drop for both packings with all four liquids poorly. In particular, the prediction error of especially the Billet and Schultes model for 2.5" Intalox Ultra O at higher liquid flow rates is significantly higher than that of the other two models. At lower liquid flow rates however, the Billet and Schultes model performs better than the other two models for most liquids with both packings.

The Stichlmair model generally shows a consistent over-prediction of the flooding gas velocity, increasing at higher liquid flow rates. Overall, the Maćkowiak model performs better with regard to

the prediction of flooding points than the other two models. The Maćkowiak model is the only model based on the droplet entrainment modelling approach, whereas the Billet and Schultes and Stichlmair models are based on the film modelling approach. The Maćkowiak model is also the only model that takes liquid surface tension into account.

The experimental pressure drop data was compared to the pressure drop predicted with KG-Tower with air/nitrogen at a liquid flow rate of 73 $m^3/(m^2.h)$. In general KG-Tower gives a relatively good prediction of the pre-loading pressure drop for all four liquids, with both packings, although the predictions for the 2.5" Intalox Ultra O is slightly better. At higher gas flow rates however, some deviation occurs, where the flooding point is under-predicted for water and ethylene glycol and over-predicted for Isopar G and silicone oil. Overall, KG-Tower predicted the pressure drop better than the Billet and Schultes, Maćkowiak and Stichlmair models.

Overall the project achieved all of the set objectives and also created an extensive data set of experimental hydrodynamic data, for a range of physical fluid properties, which can be used in both the verification of existing hydrodynamic models and the development of new models.

7. Recommendations

The following recommendations are made with regard to future work:

1. Although varied physical liquid properties were investigated, the change in almost all properties from one liquid to another limits the identification of the effect of these properties on the hydrodynamic behaviour. These types of data are however, much better suited for the verification of hydrodynamic models. It is therefore recommended that the data set be used for this purpose.

2. Hydrodynamic studies with varied liquid and gas properties should be performed on different packing types, especially other 4^{th} generation packings to investigate the effect of different packing shapes.

3. The generation of mass transfer data together with hydrodynamic data would ensure a much more accurate identification of the loading and flooding points when these sets are compared.

8. References

Alekseenko, S.V., Markovich, D.M., Evseev, A.R., Bobylev, A.V., Tarasov, B.V., Karsten, V.M. (2008), "Experimental investigation of liquid distribution over structured packing", *AIChE Journal*, 54(6):1424-1430.

Bartelmus, G., Janecki, D. (2003) "Hydrodynamics of a cocurrent downflow of gas and foaming liquid through the packed bed. Part II. Liquid holdup and gas pressure drop", *Chemical Engineering and Processing*, 42(5):993-1005.

Bessou, V., Rouzineau, D., Prévost, M., Abbé, F., Dumont, C., Maumusb, J., Meyer, M. (2010) "Performance Characteristics of a New Structured Packing", *Chemical Engineering Science,* 65(16):4855-4865.

Billet, R., Schultes, M. (1993) "A Physical Model for the Prediction of Liquid Holdup in Two-phase Countercurrent Columns", *Chemical Engineering Technology*, 16(6):370-375.

Billet, R., Schultes, M. (1991) "Modelling of Pressure Drop in Packed Columns", *Chemical Engineering Technology*, 14(2):89-95.

Billet, R., Schultes, M. (1995) "Fluid Dynamics and Mass Transfer in the Total Capacity Range of Packed Columns up to the Flood Point", *Chemical Engineering Technology*, 18(6):371-379.

Billet, R., Schultes, M. (1999) "Prediction of mass transfer columns with dumped and arranged packings: Updated summary of the calculation method of Billet and Schultes." *Chemical Engineering Research and Design*, 77(6):498-504.

Böcker, S., Ronge, G. (2005) "Distillation of Viscous Systems", *Chemical Engineering Technology*, 28(1):25-28.

Brunazzi, E., Paglianti, A., Spiegel, L., Tolaini, F. (2002) "Hydrodynamics of a Gas-Liquid Column Equipment with MellapakPlus Packing", Presented at Distillation and Absorption Conference, 30 September – 2 October, Baden-Baden.

BTS Engineering (2015) *Liquid Distributor / Redistributor (LDT)*, accessed 7 May 2017, from <www.bts.net.ua/eng/column/column_internals/liquid_distributor>

Dhabalia, D., Pilling M. (2006) *Distributor Design and Testing*, Digital Refining, accessed 25 November 2014, <http://www.digitalrefining.com/article/1000441,Distributor_design_and_testing_.html>

Dutta, B.K. (2007) "*Principles of Mass Transfer and Separation Processes*", Learning Private Limited, New Delhi.

Elgin, J.C., Weiss, F.B. (1939) "Liquid Hold-up and Flooding in Packed Towers", *Industrial and Engineering Chemistry*, 41(4):435-445.

Ergun, S., Orning, A.A. (1949) "Fluid Flow through Randomly Packed Columns and Fluidized Beds", *Industrial & Engineering Chemistry*, 41(6):1179-1184.

Fourati, M., Roig, V., Raynal, L. (2012) "Experimental study of liquid spreading in structured packings", *Chemical Engineering Science*, 80:1-15.

Górak, A., Olujić, Z. (2014) *Distillation: Equipment and Processes*, Elsevier Inc.

Henley, E.J., Seader, J.D., Roper, D.K. (2011) *Separation Process Principles*, Third Edition, John Wiley & Sons, Inc., Hoboken, NJ.

Ishii, M., Mishima, K. (1989) "Droplet entrainment correlation in annular two-phase flow", *International Journal of Heat and Mass Transfer*, 32(10):1835-1846.

Kister, H.Z. (1992) *Distillation Design*, McGraw-Hill. New York.

Kister, H.Z., Scherffius, J., Afshar, K., Abkar, E. (2007) "Realistically Predict Capacity and Pressure Drop for Packed Columns", *Chemical Engineering Progress*, 103(7):28-38.

Koch-Glitch LP. (2010) *Intalox Packed Tower Systems: Packing Tower Internals*, accessed 19 February 2014, from <www.koch-glitsch.com/Document%20Library/KGMTIG.pdf >

Kuźniewska-lach, I. (1999), "Estimation of phase velocities at flooding point in packed columns for any gas/liquid system", *The Canadian Journal of Chemical Engineering*, 77(3): 439-446.

Lamprecht, S. M. (2010) "Establishing a facility to measure packed column hydrodynamics." Master's Thesis, Department of Process Engineering, Stellenbosch University, Stellenbosch.

Lerner, B.J., Grove, C.S. (1951) "Critical Conditions of Two-Phase Flow in Packed Columns", *Industrial & Engineering Chemistry*, 43(1):216-225.

Ludwig, E.E. (1997) *Applied Process Design for Chemical and Petrochemical Plants: Volume 2*, Third Edition, Gulf Publishing Company, Houston, TX.

Maćkowiak, J. (1990) “Determination of Flooding Gas Velocity and Liquid Hold-up at Flooding in Packed Columns for Gas/Liquid Systems”, *Chemical Engineering Technology*, 13(1):184-196.

Maćkowiak, J. (1991) “Pressure Drop in Irrigated Packed Columns”, *Chemical Engineering & Processing: Process Intensification*, 29(2):93-105.

Maćkowiak, J. (2009) “Extended Channel Model for Prediction of Pressure Drop in Single-Phase Flow in Packed Columns”, *Chemical Engineering Research & Design*, 89(2):123-134.

Maćkowiak, J. (2010) *Fluid dynamics of packed columns: Principles of the fluid dynamic design of columns for gas/liquid and liquid/liquid systems,* Springer, Heidelberg.

Mersmann A. (1965) “Zur Berechnung des Flutpunktes in Füllkörperschüttungen”, *Chemie Ingenieur Technik*, 37(3):218-226.

Nakov, S., Dzhonova-Atanasova, D.B., Kolev, N.N. (2012) “Pressure drop of high performance random Intalox Metal Tower Packing”, *Bulgarian Chemical Communications*, 44(4):283-288.

Nakov, S., Kolev, N., Ljutzkanov, L., Kolev, D. (2007) “Comparison of the effective area of some highly effective packings”, *Chemical Engineering and Processing: Process Intensification*, 46(12):1385-1390.

Nieuwoudt, I. (2016) R&D Director at Koch-Glitsch, Personal communication.

Nieuwoudt, I., Corio, C., Degarmo, J. (2010) “Improvements in Random Packing Performance”, *PTQ*, Q4:67-75.

Niewoudt, I. (2010) “Intalox Ultra Random Packing – Pushing the Envelope”, Distillation & Absorption Conference, Eindhoven, 12 – 15 September.

Olujić, Z., Ali, A.M., Jansens, P.J. (2004) "Effect of the initial gas maldistribution on the pressure drop of structured packings", *Chemical Engineering & Processing*, 43(3):465-476.

Olujić, Ž., Jödecke, M., Shilkin, A., Schuch, G., Kaibel, B. (2009) “Equipment Improvement Trends in Distillation”, *Chemical Engineering and Processing: Process Intensification,* 48(6):1089-104.

Olujić, Z., Stoter, F., de Graauw, J. (1991) “Gas Distribution in Large-Diameter packed Columns”, *Gas Separation & Purification*, 5(2):59-66.

Ostle, B., (1966) *Statistics in Research*, Second Edition, The Iowa State University Press., Iowa.

Perry, R.H., Green, D.W. (2008) *Perry's Chemical Engineer's Handbook*, Eight Edition, McGraw-Hill

Piché, S., Larachi, F., Grandjean, B.P.A. (2001-A) "Flooding Capacity in Packed Towers: Database, Correlations, and Analysis", *Industrial & Engineering Chemistry Research*, 40(1):476-487.

Piché, S.R., Larachi, F., Grandjean, B.P.A. (2001-B) "Improving the prediction of irrigated pressure drop in packed absorption towers", *The Canadian Journal of Chemical Engineering*, 79(4):584-594.

Raschig-USA (n.d.) *Raschig Super Ring*, accessed 6 May 2017, from <www.raschig-usa.com/portals/0/140417_Raschig_Super_Ring_02bw_small.jpg>

Senger, G., and Wozny, G. (2012) "Impact of Foam to Column Operation", *Technical Transactions: Mechanics*, 109(1-M):209-222.

Schultes, M. (2003) "Raschig Super-Ring: A new fourth generation packing offers new advantages", *Chemical Engineering Research & Design*, 81(1):48-57.

Schultes, M., Chambers, S., Fleming, B. (2010) "Commercial Scale Test Validation of Modern High Performance Random and Structured Packings for CO2 Capture Ranking", Presented at Distillation and Absorption Conference, Eindhoven, 12 – 15 September.

Sherwood, T.K., Shipley, G.H., Holloway, F.A.L. (1938) "Flooding Velocity in Packed Columns", *Industrial & Engineering Chemistry*, 30(7):765-769.

Sinnott, R., Towler, G. (2009) *Chemical Engineering Design*, Fifth Edition, Elsivier Ltd.

Spekuljak, Z. (1985) "Liquid Entrainment in Regular Packings", *International Communications in Heat and Mass Transfer*, 12(6):719-735.

Stichlmair, J., Bravo, J.L., Fair, J.R. (1989) "General Model for Prediction of Pressure Drop and Capacity of Countercurrent Gas/Liquid Packed Columns", *Gas Separation & Purification*, 3(1):19-28.

Stichlmair, J., Fair, J.R. (1998). *Distillation: principles and practices*. New York, Wiley.

Strigle, R.F., (1994) *Packed tower design and applications: Random and Structured Packings*. Second Edition, Gulf Publishing Company, Houston.

Sun, C.G., Yin, F.H., Afacan, A., Nandakumar, K., Chuang, K.T. (2000) "Modelling and Simulation of Flow Maldistribution in Random Packed Columns with Gas-Liquid Countercurrent Flow", *Chemical Engineering Research & Design*, 78(3):378-388.

Thiele, R., Wiehler, H., Repke, J.U., Thielert, H., Wozny, G. (2004) “Hydrodynamics of Foaming Systems in Packed Towers”, Conference Proceedings at AIChE Annual 2004, Austin, Texas.

Uys, E.C. (2010) “Entrainment in an Air/water System Inside a Sieve Tray Column”, Master’s thesis at the University of Stellenbosch, Stellenbosch.

Uys, E.C. (2012) “The influence of gas and liquid physical properties on entrainment inside a sieve tray column”, PhD dissertation, Department of Process Engineering, Stellenbosch University. Stellenbosch.

Uys, E.C., Burger, A.J., Du Preez, L.J., Knoetze, J.H. (2017) “The influence of liquid physical properties on entrainment inside a sieve tray column”, *Chemical Engineering Research and Design*, 117:205-217.

Woerlee, G.F., Berends, J. (2001) “A Capacity Model for Vertical Pipes and Packed Columns based on Entrainment”, *Chemical Engineering Journal*, 84(3):355-366.

Xu, S.X. (2000) “Quantitatively Measure and Assess Maldistribution in Industrial Packed Towers”, Paper Prepared for CE Expo 2000, Houston, Texas.

Yin, F., Afacan, A., Nandakumar, K., Chuang, K.T. (2002) “Liquid Hold-up Distribution in Packed Columns: Gamma Ray Tomography and CFD Simulation”, *Chemical Engineering & Processing*, 41(5):473-483.

Yin, F., Wang, Z., Afcan, A., Nandakumar, K., Chuang, T. (2000) “Experimental Studies of Liquid Flow Maldistribution in a Random Packed Column”, *Canadian Journal of Chemical Engineering*, 78(3):449-457.

Zakeri, A., Einbu, A., Wiig, P.O., Øi, L.E., Svendsen, H.F. (2011) “Experimental investigation of pressure drop, liquid hold-up and mass transfer parameters in a 0.5 m diameter absorber column”, *Energy Procedia*, 4:606-613.

9. Appendix

9.1 Liquid Venturi Calibration

The liquid venturi was designed and constructed by Lamprecht (2010), to which the reader is referred for the design drawings. Lamprecht (2010) used following equation for calculating the volumetric flow rate for incompressible flow under isothermal conditions.

$$\boldsymbol{Q = C_D \cdot A_0 \cdot \sqrt{2 \cdot \left(\frac{\Delta P}{\rho_L}\right)} \cdot 3600} \qquad [\ 9.1\ ]$$

To calibrate the liquid venturi, and thus determined the discharge coefficient for the different liquids used in this project, the time it took to drain a certain volume of liquid from the sump was measured, while simultaneously recording the pressure drop over the liquid venturi. The liquid flow rate was determined by dividing the volume of liquid drained by the time it took to drain this volume. This process was repeated at multiple liquid flow rates for each liquid, while at each liquid flow rate three repeated measurement were performed. For water, ethylene glycol and Isopar G the discharge coefficient was determined by minimizing the difference between the measured liquid flow rate and the liquid flow rate calculated with Equation [9.1] for all liquid flow rates by changing the discharge coefficient (Table 9.1, Table 9.2 and Table 9.3). Even though the discharge coefficient is dependent on the liquid flow rate, the use of an average discharge coefficient for all liquid flow rates resulted in an error less than 1.5 % for all three liquids.

For silicone oil the use of a single discharge coefficient for all liquid flow rates resulted in too large an error (4.3 %). Instead a discharge coefficient was calculated for each liquid flow rate (Table 9.4) and a straight line was fitted on the calculated discharge coefficients versus the liquid flow rate (Figure 9.1).

Table 9.1: Results of liquid venturi calibration for water

Water									
	Liquid Draining			Liquid Venturi					
	Liquid Volume [L]	Time [s]	Liquid Flow Rate [m^3/h]	Venturi Pressure Drop [Pa]	Venturi Contraction Area [m^2]	Liquid Density [kg/m^3]	Discharge Coefficient	Liquid Flow Rate [m^3/h]	% Difference
Low	106	67.7	5.64	6349	0.000452	998	0.981	5.69	0.89
	106	67.7	5.64	6218	0.000452	998	0.981	5.63	-0.14
	106	67.4	5.67	6130	0.000452	998	0.981	5.60	-1.24
Med	106	44.1	8.66	14963	0.000452	998	0.981	8.74	0.96
	106	39.0	9.80	18573	0.000452	998	0.981	9.74	-0.65
	106	39.3	9.73	18573	0.000452	998	0.981	9.74	0.14
High	106	28.9	13.21	34201	0.000452	998	0.981	13.22	0.01
	106	26.8	14.24	39953	0.000452	998	0.981	14.28	0.31
	106	26.6	14.34	40113	0.000452	998	0.981	14.31	-0.20

Table 9.2: Results of liquid venturi calibration for ethylene glycol

Ethylene Glycol									
	Liquid Draining			Liquid Venturi					
	Liquid Volume [L]	Time [s]	Liquid Flow Rate [m^3/h]	Venturi Pressure Drop [Pa]	Venturi Contraction Area [m^2]	Liquid Density [kg/m^3]	Discharge Coefficient	Liquid Flow Rate [m^3/h]	% Difference
Low	106	66.6	5.73	7356	0.000452	1097	0.964	5.75	0.21
	106	67.1	5.70	7275	0.000452	1097	0.964	5.71	0.34
	106	66.2	5.77	7409	0.000452	1097	0.964	5.77	-0.03
High	106	28.3	13.49	40428	0.000452	1097	0.964	13.47	-0.14
	106	26.7	14.31	45570	0.000452	1097	0.964	14.30	-0.04
	106	28.4	13.45	40403	0.000452	1097	0.964	13.47	0.11

Table 9.3: Results of liquid venturi calibration for Isopar G

Isopar G									
	Liquid Draining			Liquid Venturi					
	Liquid Volume [L]	Time [s]	Liquid Flow Rate [m^3/h]	Venturi Pressure Drop [Pa]	Venturi Contraction Area [m^2]	Liquid Density [kg/m^3]	Discharge Coefficient	Liquid Flow Rate [m^3/h]	% Difference
Low	71	43.5	5.85	4974	0.000452	736	0.981	5.87	0.33
	71	43.2	5.89	5153	0.000452	736	0.981	5.98	1.43
	71	43.1	5.91	5153	0.000452	736	0.981	5.98	1.09
High	106	26.7	14.28	29260	0.000452	736	0.981	14.24	-0.30
	106	26.5	14.40	29105	0.000452	736	0.981	14.20	-1.35
	106	27.1	14.08	29232	0.000452	736	0.981	14.23	1.07

Table 9.4: Results of liquid venturi calibration for silicone oil

Silicone Oil										
	Liquid Draining			Liquid Venturi						
	Liquid Volume [L]	Time [s]	Liquid Flow Rate [m^3/h]	Venturi Pressure Drop [Pa]	Venturi Contraction Area [m^2]	Liquid Density [kg/m^3]	Discharge Coefficient	Liquid Flow Rate [m^3/h]	Discharge Coefficient Calc	% Difference
Low	106	92.7	4.12	3856	0.000452	950	0.890	4.12	0.894	0.54
	106	92.3	4.14	3767	0.000452	950	0.904	4.14	0.895	-1.02
	106	94.3	4.05	3729	0.000452	950	0.888	4.05	0.894	0.66
High	106	33.0	11.56	27793	0.000452	950	0.929	11.56	0.926	-0.29
	106	30.8	12.42	31558	0.000452	950	0.936	12.42	0.930	-0.66
	106	28.5	13.39	37498	0.000452	950	0.926	13.39	0.934	0.89

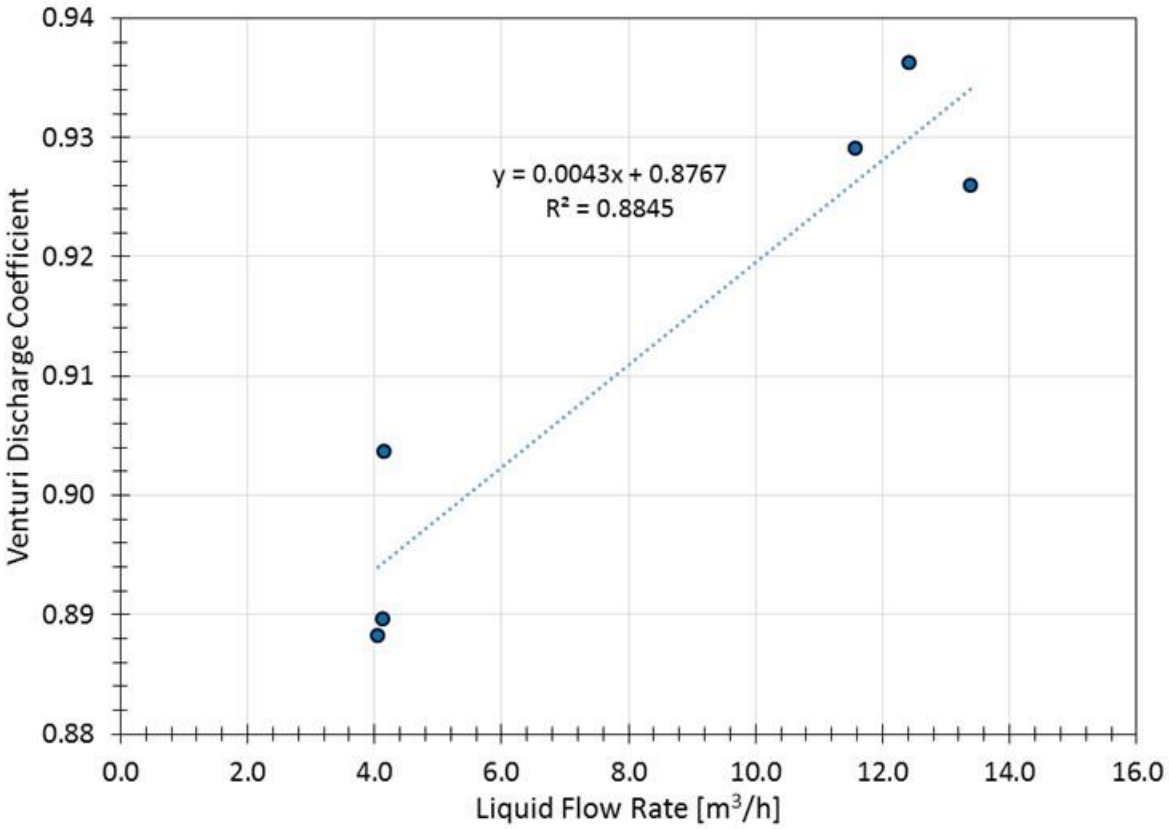

Figure 9.1: Liquid venturi discharge coefficient calculation for silicone oil

9.2 Positive Displacement Low Liquid Flow Meter Verification

The positive displacement low liquid flow meter, that was used for measuring liquid flow rates of 6 $m^3/(m^2.h)$, was verified by draining a certain volume of liquid from the sump and measuring the time to drain this volume of liquid. The liquid flow rate determined through this process was compared to the liquid flow rate measured with the flow meter. The results are presented below in Table 9.5.

Table 9.5: Positive displacement low liquid flow meter verification

Liquid	Liquid Draining			Liquid Flow Meter	
	Liquid Volume [L]	Time [s]	Liquid Flow Rate [m^3/h]	Liquid Flow Rate [m^3/h]	% Difference
Water	106	519.8	0.73	0.72	-1.72
Ethylene Glycol	106	525.8	0.73	0.72	-0.70
Isopar G	106	530.3	0.72	0.72	-0.53
Silicone Oil	88	431.2	0.74	0.73	-1.36

The verification of the positive displacement low liquid flow meter was found to be in satisfactory limits of accuracy.

9.3 Differential Pressure Transmitter Verification

The differential pressure transmitters used for measuring the pressure drop over the gas venturi and the pressure drop over the packed bed were verified with a water manometer. The pressure drop with the manometer was determined as follows:

$$\Delta \boldsymbol{P} = \boldsymbol{\rho_{Water}} \cdot \boldsymbol{g} \cdot \Delta \boldsymbol{H} \qquad [\,9.2\,]$$

The results of these verifications are presented in Table 9.6 and Table 9.7. Both the gas venturi pressure drop measurements and the packed bed pressure drop measurements were found to be in satisfactory limits of accuracy.

Table 9.6: Gas Venturi Pressure Drop Verification

Manometer				Transmitter Displayed Value	
Height Diff [mm]	Water Density [kg/m^3]	Gravitational Constant [m/s^2]	Pressure Drop [Pa]	Pressure Drop [Pa]	% Difference
31	998	9.81	304	311	2.49
55	998	9.81	534	530	-0.72
67	998	9.81	651	652	0.12
85	998	9.81	832	843	1.30
120	998	9.81	1175	1174	-0.04
160	998	9.81	1566	1572	0.35
190	998	9.81	1860	1857	-0.17
222	998	9.81	2173	2177	0.14
279	998	9.81	2732	2731	-0.02
330	998	9.81	3231	3227	-0.13
384	998	9.81	3755	3755	0.02
398	998	9.81	3897	3897	0.02

Table 9.7: Packed Bed Pressure Drop Verification

Manometer				Transmitter Displayed Value	
Height Diff [mm]	Water Density [kg/m^3]	Gravitational Constant [m/s^2]	Pressure Drop [Pa]	Pressure Drop [Pa]	% Difference
6	998	9.81	59	60	2.11
17	998	9.81	166	171	2.80
31	998	9.81	304	311	2.59
16	998	9.81	157	159	1.34
51	998	9.81	499	506	1.31
56	998	9.81	548	554	1.06
64	998	9.81	627	633	0.97
81	998	9.81	793	806	1.58
101	998	9.81	989	997	0.80
128	998	9.81	1248	1259	0.87
158	998	9.81	1542	1553	0.70
191	998	9.81	1865	1876	0.57
209	998	9.81	2041	2050	0.43
244	998	9.81	2384	2398	0.59
312	998	9.81	3055	3071	0.55
395	998	9.81	3867	3887	0.52
453	998	9.81	4430	4477	1.06

9.4 Liquid Hold-up & Entrainment Tank Calibration

The volume of liquid hold-up and liquid entrainment was determined by measuring the static pressure head in the respective tanks as a result of the volume of liquid present in the tanks. With all tanks having a constant cross-sectional area the volume of liquid was determined as follows:

$$\boldsymbol{Volume\ of\ liquid} = \frac{\boldsymbol{\Delta P \cdot A_{cross-sectional}}}{\boldsymbol{g \cdot \rho_L}} \qquad [\ 9.3\ ]$$

The mass of liquid could also be calculated with:

$$\boldsymbol{Mass\ of\ liquid} = \frac{\boldsymbol{\Delta P \cdot A_{cross-sectional}}}{\boldsymbol{g}} \qquad [\ 9.4\ ]$$

The procedure for calibrating each tank was as follows. The tank was filled with water up to the minimum liquid level used as the zero reference when measuring liquid hold-up. A known mass of water was then added to the tank. With the static pressure head from the differential pressure transmitter and the geometrical cross-sectional area the mass of water that was added was calculated. This process was repeated, incrementally increasing the liquid level in the tank. The percentage difference between the added mass and the calculated mass of water for each mass of water added was minimized by adjusting the cross-sectional area. The results for the calibration of liquid hold-up tank 1, hold-up tank 2 and the entrainment tank are presented in Table 9.8, Table 9.9 and Table 9.10, respectively. The accuracy of liquid hold-up and entrainment volume measurements were found to be in satisfactory limits of accuracy.

Table 9.8: Liquid Hold-up Tank 1 Calibration

Mass Added [kg]	Pressure Difference [Pa]	Gravitational Constant [m/s²]	Cross-sectional Area [m²]	Mass Calculated [kg]	% Difference
23.23	1461	9.81	0.157	23.37	0.61
39.07	2458	9.81	0.157	39.31	0.63
55.49	3426	9.81	0.157	54.80	-1.24

Table 9.9: Liquid Hold-up Tank 2 Calibration

Mass Added [kg]	Pressure Difference [Pa]	Gravitational Constant [m/s^2]	Cross-sectional Area [m^2]	Mass Calculated [kg]	% Difference
10.55	824	9.81	0.126	10.56	0.10
22.19	1730	9.81	0.126	22.17	-0.08
34.73	2706	9.81	0.126	34.68	-0.14
44.48	3475	9.81	0.126	44.54	0.13
57.11	4455	9.81	0.126	57.10	-0.03

Table 9.10: Entrainment Tank Calibration

Volume Added [mL]	Density [kg/m^3]	Mass Added [kg]	Pressure Difference [Pa]	Gravitational Constant [m/s^2]	Cross-sectional Area [m^2]	Mass Calculated [kg]	% Difference
50	998	0.05	16	9.81	0.031	0.05	2.06
25	998	0.07	24	9.81	0.031	0.08	2.06
25	998	0.10	32	9.81	0.031	0.10	2.06
25	998	0.12	39	9.81	0.031	0.12	-0.49
25	998	0.15	47	9.81	0.031	0.15	-0.06
25	998	0.17	55	9.81	0.031	0.18	0.24
25	998	0.20	63	9.81	0.031	0.20	0.47
50	998	0.25	79	9.81	0.031	0.25	0.79
50	998	0.30	95	9.81	0.031	0.30	1.00
100	998	0.40	124	9.81	0.031	0.39	-1.13
50	998	0.45	140	9.81	0.031	0.45	-0.77
100	998	0.55	172	9.81	0.031	0.55	-0.26
150	998	0.70	219	9.81	0.031	0.70	-0.21
200	998	0.90	282	9.81	0.031	0.90	-0.06
250	998	1.15	360	9.81	0.031	1.15	-0.16
300	998	1.45	452	9.81	0.031	1.44	-0.58
350	998	1.80	561	9.81	0.031	1.79	-0.59
400	998	2.20	686	9.81	0.031	2.18	-0.55
450	998	2.64	826	9.81	0.031	2.63	-0.58
500	998	3.14	982	9.81	0.031	3.13	-0.57
550	998	3.69	1154	9.81	0.031	3.67	-0.52
600	998	4.29	1341	9.81	0.031	4.27	-0.53
650	998	4.94	1544	9.81	0.031	4.91	-0.51
700	998	5.64	1762	9.81	0.031	5.61	-0.53
750	998	6.39	1995	9.81	0.031	6.35	-0.58

9.5 Gas Venturi Verification

The gas venturi used in this project for measuring the gas flow rate was designed and constructed by Uys (2010). The venturi was designed to have a discharge coefficient close to one in the Reynolds number range of $2x10^5$ to $1x10^6$, where the discharge coefficient will range between 1 and 1.02. Uys (2010) derived an equation for measuring the gas flow rate from the Euler equation for compressible flow under isothermal conditions.

$$\boldsymbol{G = C_D \cdot A_0 \cdot P_2 \cdot \sqrt{\frac{2 \cdot ln\left(\frac{P_1}{P_2}\right)}{R \cdot T}} \cdot 3600} \qquad [9.5]$$

$$\boldsymbol{G = C_D \cdot A_0 \cdot (P_{abs} - \Delta P) \cdot \sqrt{\frac{2 \cdot ln\left(\frac{P_{abs}}{P_{abs} - \Delta P}\right)}{R \cdot T}} \cdot 3600} \qquad [9.6]$$

Where:

G	: is the gas mass flow rate	[kg/h]
C_D	: is the discharge coefficient	[-]
A_0	: is the venturi contraction area	[m^2]
P_1	: is the pressure before the venturi	[Pa]
P_2	: is the pressure at the venturi contraction	[Pa]
$P_{abs} = P_1$	: is the absolute pressure before the venturi	[Pa]
$\Delta P = P_1 - P_2$	: is the pressure drop over the gas venturi	[Pa]
R	: is the specific gas constant	[J/(kg.K)]
T	: is the gas temperature in kelvin	[K]

To measure the gas flow rate of different gasses the specific gas constant is adjusted with respect to the composition of the gas.

The gas venturi was verified by comparing the gas flow rate measured with the gas venturi, with a discharge coefficient of one, to the gas flow rate determined with a Pitot tube. Using the pressure drop over the Pitot tube, velocity profiles for seven air flow rates were constructed with Equation [9.7], by moving the Pitot tube in 13 increments from the pipe centre to the pipe wall. The air density was determined from the absolute pressure, measured 1 meter behind the Pitot tube, by conversion with the ideal gas law.

$P_1 \cdot \rho + \frac{V_1^2}{2} + \rho \cdot g \cdot h_1 = P_2 \cdot \rho + \frac{V_2^2}{2} + \rho \cdot g \cdot h_2$: Bernoulli equation for incompressible flow

$P_1 \cdot \rho = P_2 \cdot \rho + \frac{V_2^2}{2}$: $h_1 = h_2$ and $V_1 = 0$ at stagnation point

$$\boldsymbol{V = \sqrt{\frac{2 \cdot \Delta P}{\rho}}} \qquad [\ 9.7\ ]$$

Where:

V	: is the gas velocity	[m/s]
ΔP	: is the Pitot pressure drop	[Pa]
ρ	: is the gas density	[kg/m^3]

The velocity profiles developed for the seven gas flow rates were used to construct graphs similar to Figure 9.2 for all gas flow rates. The average gas mass flow rate was calculated from the area under the graph:

$$\boldsymbol{G = \int \rho_G \cdot V(r) \cdot dA_C = \int \rho_G \cdot V(r) \cdot 2 \cdot \pi \cdot r \cdot dr} \qquad [\ 9.8\ ]$$

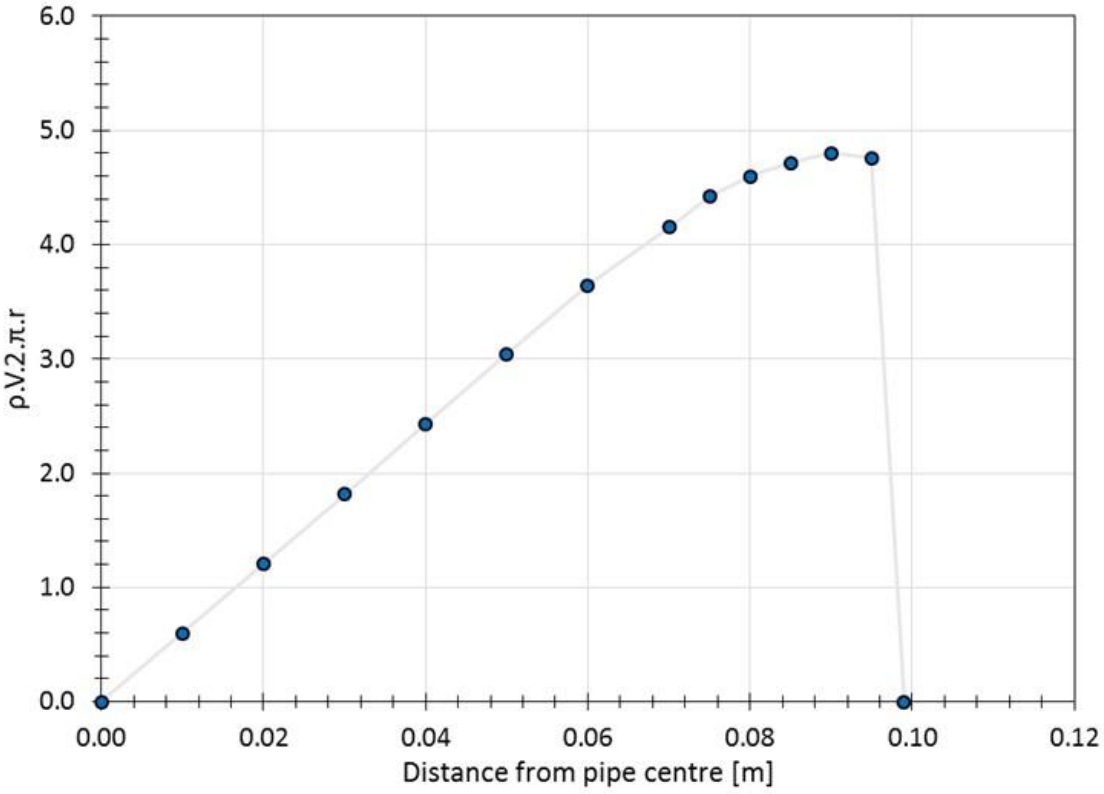

Figure 9.2: Area under the graph method for determining the average gas mass flow rate with the Pitot tube

A comparison of the gas flow rates determined with the gas venturi and the Pitot tube are presented in Table 9.11. The accuracy of the gas flow rate measurements with the gas venturi was found to be acceptable when compared to the measurements with the Pitot tube.

Table 9.11: Gas Venturi Verification

Venturi Gas Flow Rate [kg/h]	Pitot Tube Gas Flow Rate [kg/h]	% Difference
300	293	2.40
603	592	1.98
955	981	-2.63
1237	1282	-3.48
1510	1558	-3.09
2014	2084	-3.33
2478	2562	-3.29

9.6 Liquid Distributor Design & Testing

9.6.1 Mechanical Design Drawings

The mechanical design drawings of the liquid distributor base and channel, drip tubes and orifice arrangement and pre-distributor are presented in Figure 9.3, Figure 9.4 and Figure 9.5, respectively. The material of construction for all sheet metal and pipe sections are 306 stainless steel.

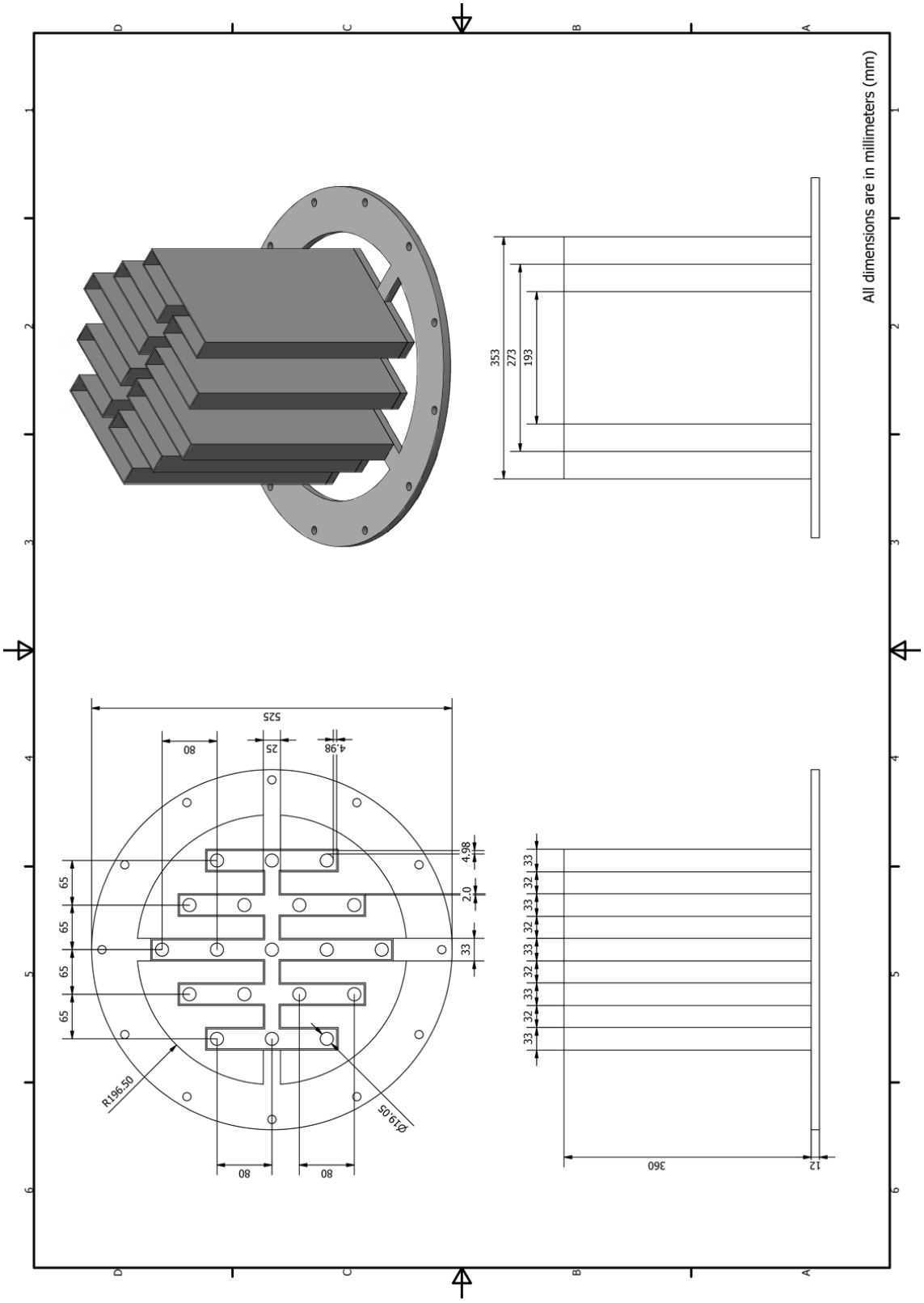

Figure 9.3: Distributor base and channel

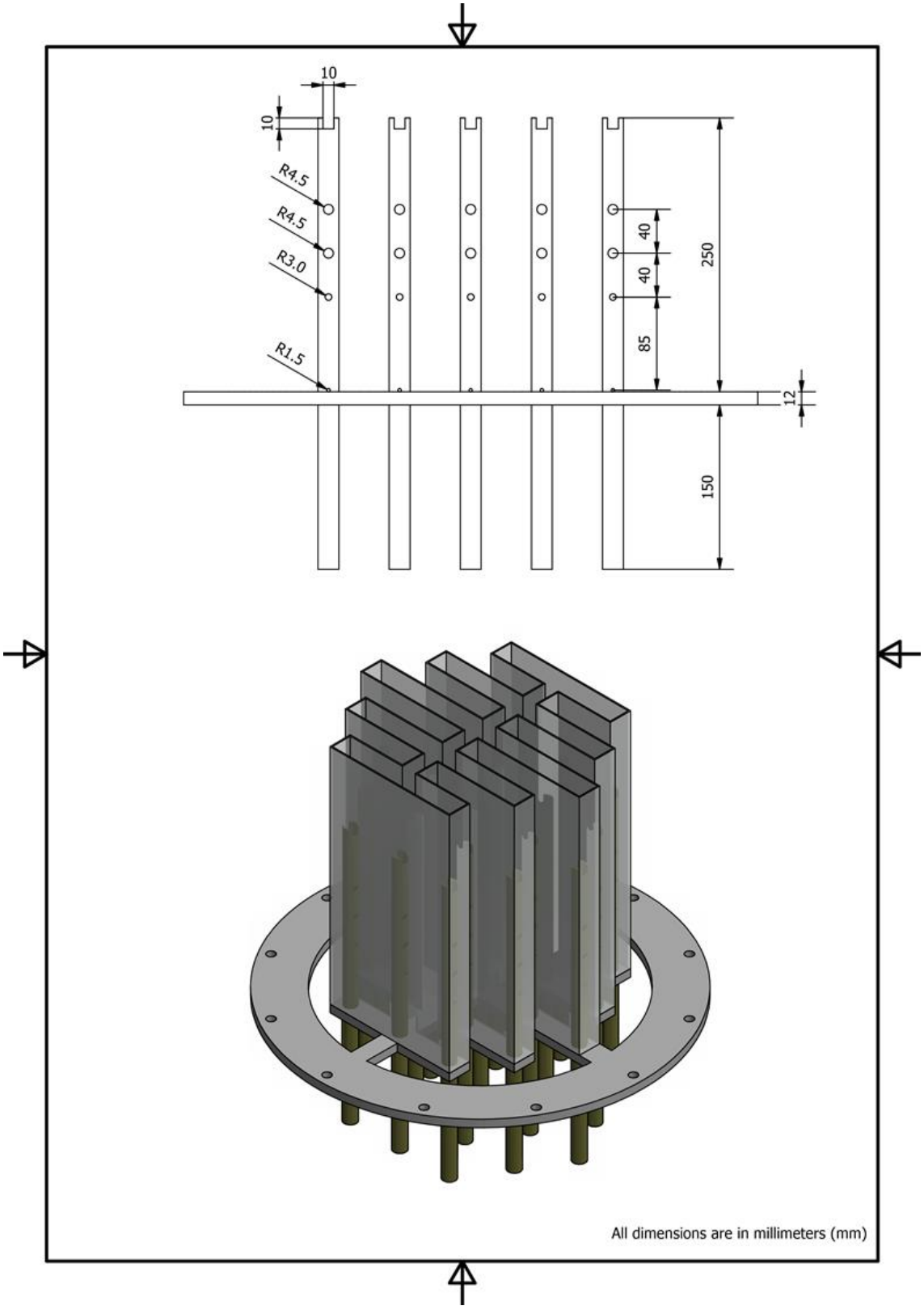

Figure 9.4: Distributor drip tubes and orifice arrangement

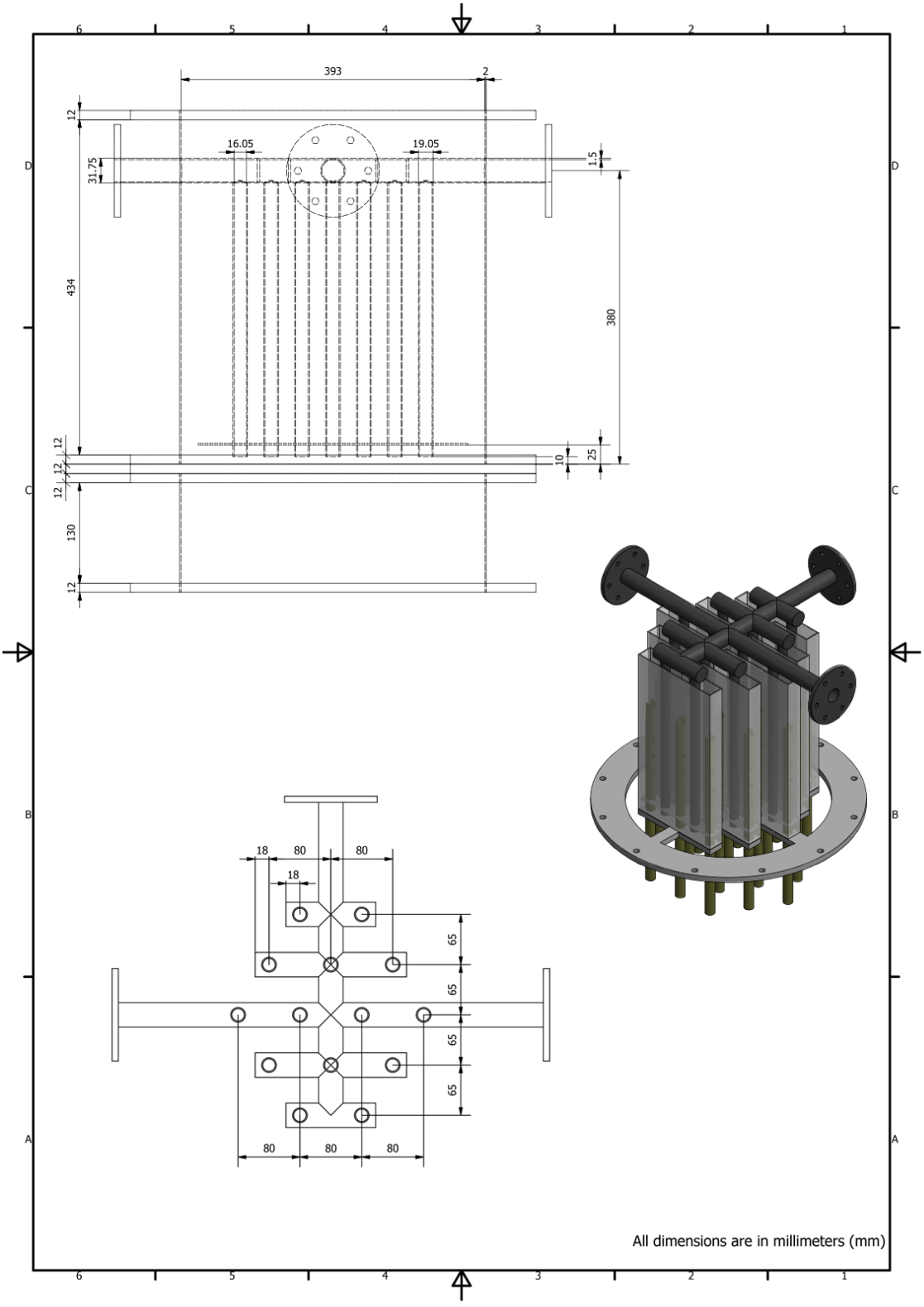

Figure 9.5: Pre-distributor

9.6.2 Distribution Quality Testing

The distribution quality was determined by measuring the liquid level at multiple point in the distributor channel (Figure 9.6) with dowel rods as dipsticks for water and silicone oil at multiple liquid flow rates. The liquid level that was measured was thus the maximum liquid level, although the liquid level remained relatively constant for all liquid flow rates. The results of the liquid distribution quality tests for water and silicone oil are presented in Table 9.12.

A widely used measure for liquid distribution quality is the coefficient of variance, which is expressed as the standard deviation over the mean liquid level in the liquid distributor. The highest coefficient of variance that was obtained was equal to 2.03 % for silicone oil at 4.49 m^3/h, which is well within the acceptable criteria of <5 % for good liquid distribution quality.

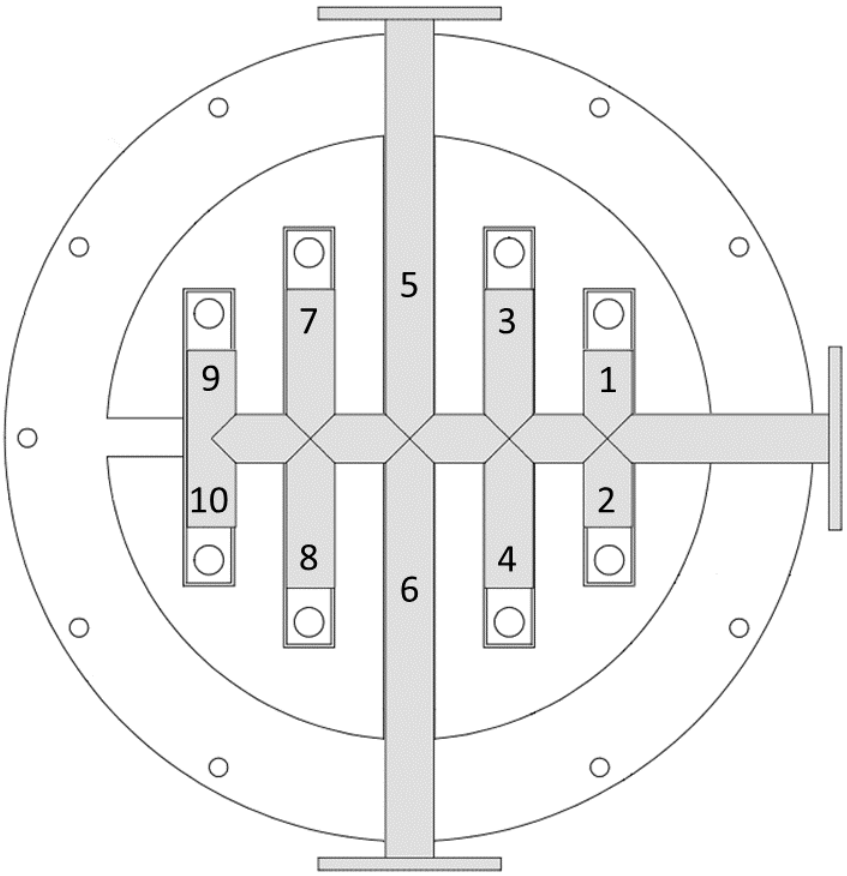

Figure 9.6: Points at which the liquid level were measured to determine the distribution quality

Table 9.12: Results of the liquid distribution quality tests for water and silicone oil

Water					
	Liquid Level [mm]				
Position	0.73 [m3/h]	4.49 [m3/h]	8.86 [m3/h]	11.89 [m3/h]	14.80 [m3/h]
1	45	129	141	164	170
2	45	129	140	164	170
3	45	129	141	164	170
4	45	129	141	163	170
5	45	130	142	166	170
6	43	128	142	166	170
7	44	130	145	168	173
8	43	129	144	168	173
9	43	129	141	166	170
10	43	128	141	163	170
Standard Deviation	0.88	0.67	1.55	1.87	1.26
Mean	43.9	129.0	141.8	165.2	170.6
CV	2.01	0.52	1.09	1.13	0.74

Silicone Oil					
	Liquid Level [mm]				
Position	0.73 [m3/h]	4.49 [m3/h]	8.86 [m3/h]	11.89 [m3/h]	12.70 [m3/h]
1	91	136	158	214	232
2	91	136	158	214	231
3	91	135	158	213	232
4	90	136	158	213	232
5	89	131	157	210	232
6	89	130	157	210	231
7	88	130	157	210	231
8	88	130	157	210	231
9	89	133	160	212	232
10	89	135	160	212	231
Standard Deviation	1.18	2.70	1.15	1.69	0.53
Mean	89.5	133.2	158.0	211.8	231.5
CV	1.32	2.03	0.73	0.80	0.23

9.6.3 Pre-distributor Liquid Drain Volume

With the new channel type liquid distributor, the volume of liquid that drains out of the pre-distributor during liquid hold-up measurements need to be subtracted from the volume of liquid collected in the hold-up tanks to determine the dynamic liquid hold-up.

Before the pre-distributor was installed in the liquid distributor section, the pre-distributor was connected to the liquid feed at the top of the column and liquid was allowed to pass through the pre-distributor down the column. Drain volume measurements were performed with water and silicone oil at different liquid flow rates by cutting the feed to the pre-distributor, similar to how liquid hold-up measurements are performed. A bucket was placed below the pre-distributor as soon as the liquid hold-up measurements were triggered, allowing the volume of liquid that drained from the pre-distributor to be measured. There was found that the drain volume for water and silicone oil were very similar at all liquid flow rates (Figure 9.7). The variation in data that is observed at different liquid flow rates is a result of the variation in response time associated with placing the bucket underneath the pre-distributor as soon as the hold-up measurement was triggered. A second order polynomial curve was fitted on both the water and silicone data to calculate the liquid drain volume at different liquid flow rates. There was assumed that ethylene glycol and Isopar G will have similar liquid drain volumes and was also estimated from the fitted curve.

$$\boldsymbol{Pre-distributor\ drain\ volume}\ [\boldsymbol{L}] = -\mathbf{0.0032}\cdot\boldsymbol{Q}^{\mathbf{2}} + \mathbf{0.3091}\cdot\boldsymbol{Q} + \mathbf{0.3771} \qquad [9.9]$$

Also captured in the drain volumes is the volume of liquid that still passes through the liquid feed cut-off valve during the time it takes for this valve to close. The drain volume thus also incorporates this volume of liquid that is not part of the total liquid hold-up.

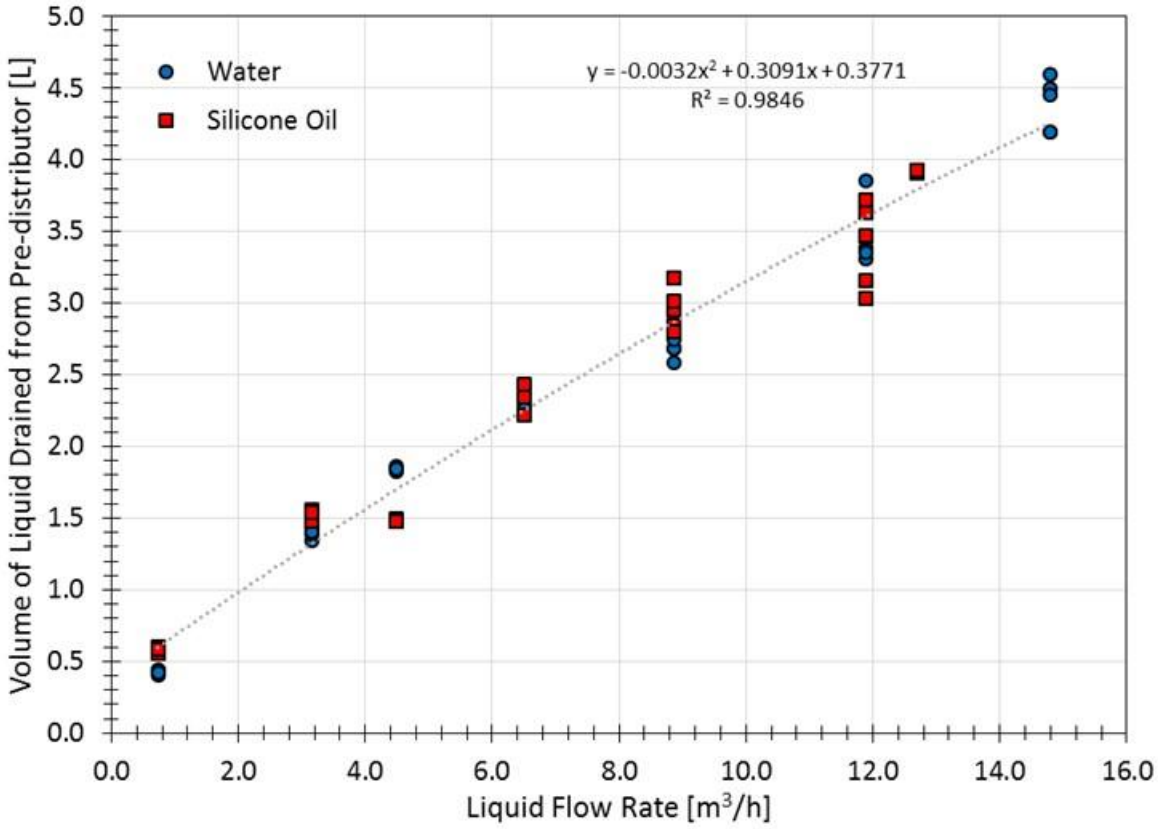

Figure 9.7: Liquid volume that drains from the pre-distributor at different liquid flow rates

9.7 Measurement Accuracy

9.7.1 Temperature Sensors

Lamprecht (2010) verified all temperature sensor measurements (PT-100) over a range of 20-80°C and found that the measurements were ± 1°C accurate. The temperature sensors were not verified again in this project and assumed to still have the same accuracy.

9.7.2 Pressure Transmitters

The accuracy of the pressure transmitters are affected by a number of factors, which include the reference accuracy determined by the manufacturer through the design and testing of the device, the turn-down ratio and set span, the ambient and process temperature, static pressure as well as the time in operation. The error in the measurements of the different pressure transmitters, for their respective measuring parameters, were calculated as described in their technical manuals and summarized in the following tables. Table 9.13, Table 9.15 and Table 9.17 provides the equations to calculate the different parameters affecting the accuracy, while Table 9.14, Table 9.16 and Table 9.18 summarizes the calculated parameters and errors.

Table 9.13: Accuracy calculation parameters for the differential pressure transmitters DPE-101, DPE-403, DPE-404, DPE-405 and DPE-401

Endress + Hauser DeltaBar S PMD75			
Reference Accuracy	E_1	0.05	% of span
Temperature Effect	E_2	$0.07 \cdot TD + 0.07 + 0.05$	% of span
Static Pressure Effect	E_3	$(0.203 \cdot TD + 0.15) \cdot \left(\frac{101.325}{700}\right)$	% of span
Total Performance	E_P	$\sqrt{E_1^2 + E_2^2 + E_3^2}$	% of span
Long-term Stability	E_S	0.14 (5 years)	% of URL
Error	E	$\frac{E_P}{100} \cdot Span + \frac{E_S}{100} \cdot URL$	kPa
PLC Conversion Error	E_{PLC}	0.5	% of error
Total Error	E_T	$E \cdot \left(1 + \frac{E_{PLC}}{100}\right)$	kPa

Table 9.14: Calculated errors for differential pressure transmitters DPE-101, DPE-403, DPE-404, DPE-405 and DPE-401

Parameters	DPE-401	DPE-403, DPE-404, DPE-405	DPE-101	Units
URL	10	10	10	kPa
LRV	0	0	0	kPa
URV	10	5	4	kPa
TD	1	2	2.5	
Span	10	5	4	kPa
Reference Accuracy	0.05	0.05	0.05	% of Span
Temperature Effect	0.19	0.26	0.30	% of Span
Static Pressure Effect	0.05	0.08	0.10	% of Span
Total Performance	0.20	0.28	0.31	% of Span
Error	34	28	27	Pa
Total Error	34	28	27	Pa

Table 9.15: Accuracy calculation parameters for the differential pressure transmitter DPE-102

Fuji Electric FKC			
Reference Accuracy	E_1	0.065	% of span
Temperature Effect	E_2	$\left(0.095 + 0.125 \cdot \left[\frac{URL}{Span}\right]\right) \cdot \left(\frac{25°C}{28°C}\right)$	% of span
Static Pressure Effect	E_3	$0.035 \cdot \left(\frac{0.101325}{6.9}\right)$	% of URL
Over-range Effect	E_4	$0.1 \cdot \left(\frac{0.101325}{16}\right)$	% of URL
Supply Voltage Effect	E_5	$0.005 \cdot Voltage = 0.005 \cdot 24$	% of span
Long-term Stability	E_S	$0.1 \cdot \left(\frac{5}{10}\right)$	% of URL
Error	E	$\sqrt{\frac{Span}{100}(E_1 + E_2 + E_5) + \frac{URL}{100}(E_3 + E_4 + E_S)}$	kPa
PLC Conversion Error	β_{PLC}	0.5	% of error
Total Error	E_T	$E \cdot \left(1 + \frac{E_{PLC}}{100}\right)$	kPa

Table 9.16: Calculated error for differential pressure transmitter DPE-102

Parameters	DPE-102	Units
URL	130	kPa
LRV	0	kPa
URV	130	kPa
TD	1	
Span	130	kPa
Reference Accuracy	0.085	kPa
Temperature Effect	0.196	kPa
Static Pressure Effect	0.001	kPa
Over-range Effect	0.001	kPa
Supply Voltage Effect	0.156	kPa
Long-term Stability	0.065	kPa
Error	273	Pa
Total Error	274	Pa

Table 9.17: Accuracy calculation parameters for the absolute pressure transmitters PE-102 and PE-401

Endress + Hauser CeraBar S PMP71			
Reference Accuracy	E_1	0.05	% of span
Temperature Effect	E_2	$0.07 \cdot TD + 0.07 + 0.05$	% of span
Total Performance	E_P	$\sqrt{E_1^2 + E_2^2}$	% of span
Long-term Stability	E_S	0.12 (5 years)	% of URL
Error	E	$\frac{E_P}{100} \cdot Span + \frac{E_S}{100} \cdot URL$	kPa
PLC Conversion Error	E_{PLC}	0.5	% of error
Total Error	E_T	$E \cdot \left(1 + \frac{E_{PLC}}{100}\right)$	kPa

Table 9.18 Calculated errors for absolute pressure transmitters PE-102 and PE-401

Parameters	PE-102, PE-401	Units
URL	200	kPa
LRV	80	kPa
URV	120	kPa
TD	1.7	
Span	40	kPa
Reference Accuracy	0.05	% of Span
Temperature Effect	0.197	% of Span
Total Performance	0.20	% of Span
Error	321	Pa
Total Error	323	Pa

9.7.3 Flow Meters

Positive Displacement Low Liquid flow Meter

The positive displacement low liquid flow meter (FLOMEC OMO15) has a measuring range of 0 – 2.4 m^3/h and a stated accuracy of ± 0.25 % of full scale. Taking into account the PLC conversion error (0.5 %), the maximum deviation is thus 0.018 m^3/h.

Liquid Venturi

Considering Equation [9.1], the liquid flow rate measured with the liquid venturi is a function of four parameters (discharge coefficient, contraction area, liquid density and pressure drop), each of which has its own associated error, summarized in Table 9.19. As a result, the liquid flow rate measured with the liquid venturi has an error influenced by the error in these parameters.

Table 9.19: Error in liquid venturi flow rate parameters

Parameter	Error	
C_D [-]:	E_{C_D}	
- Water		1.24 %
- Ethylene Glycol		0.34 %
- Isopar G		1.43 %
- Silicone Oil		1.02 %
A_0 [m^2]	E_{A_0}	1 %
ΔP [Pa]	$E_{\Delta P}$	274
ρ_L [kg/m^3]	E_{ρ_L}	0.1

Since the error in the liquid venturi flow rate is influenced by multiple errors, the error in the liquid flow rate is not constant, but a function of the liquid flow rate itself and can be calculated with the following equations:

$$\textbf{Positive error in liquid venturi flow rate } \left[\frac{m^3}{h}\right]: E_Q{}^+ = C_D \cdot \left(1 + \frac{E_{C_D}}{100}\right) \cdot A_0 \cdot \left(1 + \frac{E_{A_0}}{100}\right) \cdot \sqrt{\frac{\rho_L \cdot \left(\frac{Q}{3600 \cdot C_D \cdot A}\right)^2 + 2 \cdot E_{\Delta P}}{\rho_L - E_{\rho_L}}} \cdot 3600 - Q \quad [9.10]$$

$$\textbf{Negative error in liquid venturi flow rate } \left[\frac{m^3}{h}\right]: E_Q{}^- = C_D \cdot \left(1 - \frac{E_{C_D}}{100}\right) \cdot A_0 \cdot \left(1 - \frac{E_{A_0}}{100}\right) \cdot \sqrt{\frac{\rho_L \cdot \left(\frac{Q}{3600 \cdot C_D \cdot A}\right)^2 - 2 \cdot E_{\Delta P}}{\rho_L + E_{\rho_L}}} \cdot 3600 - Q \quad [9.11]$$

The minimum, maximum and average errors in the venturi liquid flow rate are summarized in Table 9.20. The reason for Isopar G having the highest errors is a result of its low liquid density, while for ethylene glycol, having the highest liquid density results in it having the lowest errors.

Table 9.20: Minimum, maximum and average error in the venturi liquid flow rate

		Q [m^3/h]
Minimum Error (@ Flow Rate, Liquid)	-	0.19 (8.86, Ethylene Glycol)
	+	0.19 (8.86, Ethylene Glycol)
Maximum Error (@ Flow Rate, Liquid)	-	0.42 (14.80, Isopar G)
	+	0.43 (14.80, Isopar G)
Average Error (Standard Deviation)	-	0.29 (0.07)
	+	0.29 (0.07)

Gas Venturi

The gas flow rate measured with the gas venturi is a function of six parameters (discharge coefficient, contraction area, gas temperature, specific gas constant, absolute pressure and pressure drop) as can be seen in Equation [9.6]. When calculating the vapour flow factor from the gas flow rate, the error associated with the column diameter should also be taken into account. The errors associated with the different parameters affecting the gas flow rate error are summarized in Table 9.21.

Table 9.21: Error in gas venturi flow rate parameters

Parameter	Error	
C_D [-]	E_{C_D}	2 %
P_{abs} [Pa]	$E_{P_{abs}}$	323
$P_{\Delta P}$ [Pa]	$E_{\Delta P}$	27
T [K]	E_T	1
D [mm]	E_D	3

As with the liquid venturi, the error in the gas flow rate is influenced by multiple errors and also not constant. The error in the gas flow rate and vapour flow factor can be calculated with the following equations.

$$\textbf{Positive error in gas flow rate } \left[\frac{kg}{h}\right]: E_G{}^{+}$$
$$= C_D \cdot \left(1 + \frac{E_{C_D}}{100}\right) \cdot A_0 \cdot \left[\left(P_{abs} + E_{P_{abs}}\right) - \left(\Delta P + E_{\Delta P}\right)\right]$$
$$\cdot \sqrt{\frac{2 \cdot ln\left[\frac{P_{abs} + E_{P_{abs}}}{\left[\left(P_{abs} + E_{P_{abs}}\right) - \left(\Delta P + E_{\Delta P}\right)\right]}\right]}{R \cdot (T - E_T)}} \cdot 3600 - G \qquad [9.12]$$

$$\textbf{Negative error in gas flow rate } \left[\frac{kg}{h}\right]: E_G{}^{-}$$
$$= C_D \cdot A_0 \cdot \left[\left(P_{abs} - E_{P_{abs}}\right) - \left(\Delta P - E_{\Delta P}\right)\right]$$
$$\cdot \sqrt{\frac{2 \cdot ln\left[\frac{P_{abs} - E_{P_{abs}}}{\left[\left(P_{abs} - E_{P_{abs}}\right) - \left(\Delta P - E_{\Delta P}\right)\right]}\right]}{R \cdot (T + E_T)}} \cdot 3600 - G \qquad [9.13]$$

$$\textbf{Positive error in vapour flow factor } \left[\left(\frac{m}{s}\right) \cdot \left(\frac{kg}{m^3}\right)^{0.5}\right]: E_{F_G}{}^{+}$$
$$= \frac{G + E_G{}^{+}}{\sqrt{\frac{P - E_P}{R \cdot (T + E_T)}} \cdot \frac{\pi \cdot (D - E_D)^2}{4}} - F_G \qquad [9.14]$$

$$\textbf{Negative error in vapour flow factor } \left[\left(\frac{m}{s}\right) \cdot \left(\frac{kg}{m^3}\right)^{0.5}\right]: E_{F_G}{}^{-}$$
$$= \frac{G + E_G{}^{-}}{\sqrt{\frac{P + E_P}{R \cdot (T - E_T)}} \cdot \frac{\pi \cdot (D + E_D)^2}{4}} - F_G \qquad [9.15]$$

The minimum, maximum and average errors in the gas flow rate and vapour flow factor are summarized in Table 9.22.

Table 9.22: Minimum, maximum and average error in the gas flow rate and vapour flow factor

		G [kg/h]	F_G [(m/s)·(kg/m^3)$^{0.5}$]
Minimum Error (@ Flow Rate, Gas)	-	17 (2686, Air)	0.09 (2.08, CO_2)
	+	47 (967, Air)	0.14 (1.61, Air)
Maximum Error (@ Flow Rate, Gas)	-	182 (294, CO_2)	0.32 (0.51, CO_2)
	+	116 (294, CO_2)	0.28 (6.11, CO_2)
Average Error (Standard Deviation)	-	40 (29)	0.12 (0.04)
	+	61 (13)	0.16 (0.02)

9.7.4 Pressure Drop

The error in the pressure drop over the packed bed is equal to 34 Pa or 11.33 Pa/m, as calculated in Table 9.14 (DPE-401).

9.7.5 Liquid Hold-up

Liquid/Gas Distributor & Pre-distributor

As described in Section 3.4.3, to determine the dynamic liquid hold-up the volume of liquid on both the liquid and gas distributors as well as the volume of liquid that drain from the pre-distributor should be taken into account. All three of these liquid volumes has an associated error. The error in the volume of liquid on both the distributors is dependent on the accuracy of the liquid level measurement, while the error in the volume of liquid that drains from the pre-distributor is dependent on the accuracy of Equation [9.9].

The accuracy of the liquid level measurement in both the distributors are ± 1 mm:

$$\boldsymbol{Error\ in\ liquid\ distributor\ volume}\ [\boldsymbol{m^3}]: \boldsymbol{E_{LD}} = \boldsymbol{A_{LD}} \cdot \left[\left(\boldsymbol{H_{LD}} + \frac{\mathbf{1}}{\mathbf{1000}}\right) - \boldsymbol{H_{LD}}\right] \quad [\ 9.16\ ]$$

$$\boldsymbol{Error\ in\ gas\ distributor\ volume}\ [\boldsymbol{m^3}]: \boldsymbol{E_{GD}} = \boldsymbol{A_{GD}} \cdot \left[\left(\boldsymbol{H_{GD}} + \frac{\mathbf{1}}{\mathbf{1000}}\right) - \boldsymbol{H_{GD}}\right] \quad [\ 9.17\ ]$$

Where:

A_{LD} : is the liquid distributor area [m^3]

A_{GD} : is the gas distributor area [m^3]

H_{LD} : liquid level height in the liquid distributor [m]

H_{GD} : liquid level height in the gas distributor [m]

The maximum error in the pre-distributor drain volume at any liquid flow rate estimated with Equation [9.9] is equal to 18.7 %. However, since the pre-distributor drain volume is also dependent on the liquid flow rate, the total error in the pre-distributor drain volume can be expressed as:

$$\begin{aligned}&\boldsymbol{Positive\ error\ in\ pre-distributor\ drain\ volume}\ [\boldsymbol{L}]: \boldsymbol{E_{PD}}^{+}\\ &= [\mathbf{-0.0032} \cdot (\boldsymbol{Q} + \boldsymbol{E_{LV}}^{+})^2 + \mathbf{0.3091} \cdot (\boldsymbol{Q} + \boldsymbol{E_{LV}}^{+}) + \mathbf{0.3771}]\\ &\cdot \left(\mathbf{1} + \frac{\mathbf{18.7}}{\mathbf{100}}\right) - [\mathbf{-0.0032} \cdot \boldsymbol{Q}^2 + \mathbf{0.3091} \cdot \boldsymbol{Q} + \mathbf{0.3771}]\end{aligned} \quad [\ 9.18\ ]$$

$$\begin{aligned}&\boldsymbol{Negative\ error\ in\ pre-distributor\ drain\ volume}\ [\boldsymbol{L}]: \boldsymbol{E_{PD}}^{-}\\ &= [\mathbf{-0.0032} \cdot (\boldsymbol{Q} + \boldsymbol{E_{LV}}^{-})^2 + \mathbf{0.3091} \cdot (\boldsymbol{Q} + \boldsymbol{E_{LV}}^{-}) + \mathbf{0.3771}]\\ &\cdot \left(\mathbf{1} - \frac{\mathbf{18.7}}{\mathbf{100}}\right) - [\mathbf{-0.0032} \cdot \boldsymbol{Q}^2 + \mathbf{0.3091} \cdot \boldsymbol{Q} + \mathbf{0.3771}]\end{aligned} \quad [\ 9.19\ ]$$

Hold-up Tanks

The error in the liquid volume measurement in both liquid hold-up tanks is influenced by three parameters (tank cross-sectional area, differential pressure and liquid density). The errors associated with these parameters provided in Table 9.23.

Table 9.23: Error liquid hold-up tank volume parameters

Parameter	Error	
$A_{cross\ sectional}$ [m²]:	E_{A_c}	
Hold-up Tank 1		1.24 %
Hold-up Tank 2		0.14 %
ΔP [Pa]	$E_{\Delta P}$	28
ρ_L [kg/m³]	E_{ρ_L}	0.1

Since the error in the liquid volume in the liquid hold-up tanks is influenced by multiple errors, the errors in the liquid hold-up tank volumes are not constant, but a function of the liquid volumes itself and can be calculated with the following equations:

$$\boldsymbol{Positive\ error\ in\ liquid\ hold-up\ tank\ volume\ [m^3]: E_{HT}{}^{+}}$$

$$= \frac{\left(V_{HT} \cdot \rho_L + \frac{A_c \cdot E_{\Delta P}}{g}\right) \cdot \left(1 + \frac{E_{A_C}}{100}\right)}{\rho_L - E_{\rho_L}} - V_{HT} \qquad [\ 9.20\ ]$$

$$\boldsymbol{Negative\ error\ in\ liquid\ hold-up\ tank\ volume\ [m^3]: E_{HT}{}^{-}}$$

$$= \frac{\left(V_{HT} \cdot \rho_L - \frac{A_c \cdot E_{\Delta P}}{g}\right) \cdot \left(1 - \frac{E_{A_C}}{100}\right)}{\rho_L + E_{\rho_L}} - V_{HT} \qquad [\ 9.21\ ]$$

Where:

V_{HT} : is the volume of liquid in the hold-up tank [m³]

Equations [9.20] and [9.21] apply to both liquid hold-up tanks. The error in the liquid volume for hold-up tank 2 should however only be accounted for if hold-up tank 1 is entirely filled and liquid cascaded over to hold-up tank 2[1].

[1] The use of two hold-up tanks increases the error in the liquid hold-up measurement. However, as a result of space limitation, primarily with regard to height, the use of two hold-up tanks was necessary. Increasing the diameter of the tank would also result in an increase in the liquid volume measurement error.

Total liquid hold-up

The error in the total liquid hold-up volume is a function of all the errors described in this section and calculated as follows:

$$\boldsymbol{Positive\ total\ error\ in\ liquid\ hold-up\ volume\ [m^3]: E_{Hold-up\ volume}{}^{+}} = -\boldsymbol{E_{LD} - E_{GD} - E_{PD}{}^{+} + E_{HT}{}^{+}{}_{1} + E_{HT}{}^{+}{}_{2}} \quad [9.22]$$

$$\boldsymbol{Negative\ total\ error\ in\ liquid\ hold-up\ volume\ [m^3]: E_{Hold-up\ volume}{}^{-}} = -\boldsymbol{E_{LD} - E_{GD} + E_{PD}{}^{-} + E_{HT}{}^{-}{}_{1} + E_{HT}{}^{-}{}_{2}} \quad [9.23]$$

To calculate the error in the total liquid hold-up $\left(h_L\ \left[\frac{m^3}{m^3}\right]\right)$, the error in the column diameter should also be accounted for.

$$\boldsymbol{Positive\ error\ in\ total\ liquid\ hold-up\ \left[\frac{m^3}{m^3}\right]: E_{h_L}{}^{+}} = \frac{\boldsymbol{\frac{h_L}{\frac{\pi \cdot D^2}{2}} + E_{Hold-up\ volume}{}^{+}}}{\boldsymbol{\frac{\pi \cdot \left(D - \frac{E_D}{1000}\right)^2}{4}}} - \boldsymbol{h_L} \quad [9.24]$$

$$\boldsymbol{Negative\ error\ in\ total\ liquid\ hold-up\ \left[\frac{m^3}{m^3}\right]: E_{h_L}{}^{-}} = \frac{\boldsymbol{\frac{h_L}{\frac{\pi \cdot D^2}{2}} + E_{Hold-up\ volume}{}^{-}}}{\boldsymbol{\frac{\pi \cdot \left(D + \frac{E_D}{1000}\right)^2}{4}}} - \boldsymbol{h_L} \quad [9.25]$$

The minimum, maximum and average errors in the total liquid hold-up are summarized in Table 9.24.

Table 9.24: Minimum, maximum and average error in the total liquid hold-up

		h_L [m^3/m^3]
Minimum Error (@ Flow Rate, Gas)	-	0.0016 (0.0115, Water)
	+	0.0011 (0.0115, Water)
Maximum Error (@ Flow Rate, Gas)	-	0.0083 (0.2639, Water)
	+	0.0079 (0.2639, Water)
Average Error (Standard Deviation)	-	0.0039 (0.0015)
	+	0.0033 (0.0015)

9.8 GC Methods

The GC methods that were used for analysing for nitrogen/oxygen and carbon dioxide/air are summarized in Table 9.25.

Table 9.25: GC Method used for Analysis of Nitrogen and Carbon Dioxide

	Nitrogen/Oxygen	Carbon Dioxide/Air
Detector Temperature	220°C	250°C
Injector Temperature	80°C	120°C
Oven Temperature	35°C	35°C
Initial Temperature	35°C	35°C
Initial Time	4 min	5 min
Rate	20°C/min	20°C/min
Final Temperature	150°C	150°C
Final Time	2 min	2 min

9.9 TCD Relative Response Factors

While the relative response factor of carbon dioxide and air for the GC's TCD detector used in this project has already been determined through a previous project by Uys (2012), the relative response factor for nitrogen and oxygen had to be determined. Since the interest is only on the ratio of the quantity of oxygen to nitrogen an internal standard was not necessary. However, the ratio of the peak areas obtained from the GC analysis does not necessarily represent the quantitative ratio of the two gasses, since the detector response is different for different gasses.

The relative response factor for oxygen and nitrogen was determined by injecting different volumes of air, which was assumed to consist of 78.09 %(v/v) nitrogen and 20.95 %(v/v) oxygen, into the GC and recording the response peak areas. The relative response factor was calculated for all volumes of air injected as follows, with the results presented in Table 9.26:

$$\boldsymbol{RRF} = \frac{\frac{\boldsymbol{A_{N_2}}}{\boldsymbol{x_{N_2}}}}{\frac{\boldsymbol{A_{O_2}}}{\boldsymbol{x_{O_2}}}} \qquad [\ 9.26\ ]$$

Where:

RRF : is the relative response factor

A_{N_2} : is the peak area fraction of nitrogen

A_{O_2} : is the peak area fraction of oxygen

$x_{N_2} = \frac{78.09}{79.09+20.95} = 0.7809$: is the mole fraction of nitrogen with respect to only nitrogen and oxygen

$x_{O_2} = \frac{20.95}{79.09+20.95} = 0.2115$: is the mole fraction of oxygen with respect to only nitrogen and oxygen

Even though some other gasses are present when the column is filled with nitrogen, the quantity of these gasses are relatively small compared to that of nitrogen and oxygen and could be neglected with no significant loss of accuracy.

To calculate the mole fraction of oxygen and nitrogen from the peak area fractions obtained from the GC analysis the following equations were used.

$$\boldsymbol{x_{O_2}} = \frac{\boldsymbol{A_{O_2} \cdot RRF}}{\boldsymbol{1 - A_{O_2} + A_{O_2} \cdot RRF}} \qquad [\ 9.27\ ]$$

$$\boldsymbol{x_{N_2}} = \boldsymbol{1 - x_{O_2}} \qquad [\ 9.28\ ]$$

The average relative response factor for nitrogen and oxygen was found to be equal to 1.049, while Uys (2012) calculated a relative response factor for carbon dioxide and air equal to 1.311. When working with carbon dioxide, the mole fraction of air and carbon dioxide were calculated as follows:

$$x_{Air} = \frac{A_{Air} \cdot RRF}{1 - A_{Air} + A_{Air} \cdot RRF} \quad [9.29]$$

$$x_{CO_2} = 1 - x_{Air} \quad [9.30]$$

Table 9.26: Relative response factor calculation for nitrogen and oxygen

Volume Air Injected [uL]	Peak Area		Peak Area Fraction		Mole Fraction		RRF
	O2	N2	O2	N2	O2	N2	
20	578792	2238390	0.205	0.795	0.2115	0.7885	1.038
30	978972	3830597	0.204	0.796	0.2115	0.7885	1.050
40	1399581	5457956	0.204	0.796	0.2115	0.7885	1.046
40	1385798	5419868	0.204	0.796	0.2115	0.7885	1.049
40	1416926	5535671	0.204	0.796	0.2115	0.7885	1.048
50	1917194	7470866	0.204	0.796	0.2115	0.7885	1.045
50	1899113	7452888	0.203	0.797	0.2115	0.7885	1.053
50	1877366	7336802	0.204	0.796	0.2115	0.7885	1.048
60	2329328	9106260	0.204	0.796	0.2115	0.7885	1.049
60	2393896	9421044	0.203	0.797	0.2115	0.7885	1.056
60	2404356	9448500	0.203	0.797	0.2115	0.7885	1.054
70	2914443	11393643	0.204	0.796	0.2115	0.7885	1.049
Average							1.049

9.10 Experimental Procedures

All procedures are discussed with regard to the PFD presented in Figure 9.8.

9.10.1 Gas Loading

The following procedure was followed to fill the column with either nitrogen or carbon dioxide gas after the packed column sump has been filled with liquid.

1. Switch on the pilot plant control panel and select the packed column configuration.
2. Close V-102 and V-104 disconnecting the tray column from the gas blower (E-102) and surge tank (E-101).
3. Open V-105, V-106 and V-107, connecting the packed column (E-401) to the gas blower (E-102) and surge tank (E-101) and allowing gas to vent through line 57.
4. Ensure that the surge tank (E-101) access port is completely closed and close V-108, which closes the surge tank (E-101) drain port.
5. Connect the absolute pressure transmitter, connected to the gas venturi (E-103), to the pressure port available in line 33.
6. Plug both the gas venturi pressure ports (E-103).
7. Connect a water hose to the port available at the top of the surge tank (E-101).
8. Fill the surge tank (E-101) with water to the level of the lower pressure port on the gas venturi (E-103).
9. Close V-105, V-106 and V-107, disconnecting the packed column (E-401) from the gas blower (E-102) and the surge tank (E-101).
10. Set the set point for the column pressure on the plant control panel to 103 kPa.
11. Open the valve on the connected gas cylinder to allow gas to enter the surge tank (E-101).
12. Partially open V-108 to allow the water in the surge tank (E-101) to drain and be replaced by the gas entering the surge tank (E-101).
13. V-108 can be adjusted to increase the flow rate of the draining water, although the pressure in the surge tank (E-101) should not be allowed to decrease below atmospheric pressure.
14. When all the water has been drained from the surge tank (E-101), close V-108.
15. Connect the absolute pressure transmitter, connected to the pressure port in line 33, back to the gas venturi (E-103) and replace the connected plugs with the differential pressure meter lines on the gas venturi (E-103) removed in step 5.
16. Open V-106 and V-107 to allow gas to pass from the surge tank (E-101) through the gas blower (E-102) and packed column (E-401) out the vent in line 57, purging out the remaining air in the gas blower (E-102) and packed column (E-401).

17. Allow purging for approximately 30 minutes, after which V-107 should be closed.
18. Open V-105.
19. Start the gas blower (E-102) at a frequency of 15 Hz.
20. Adjust the radial vane control to 30 % after the blower has finished its start-up cycle, allowing gas to circulate through the packed column.
21. Allow the gas to circulate for about 10 minutes, after which the gas blower (E-102) should be stopped.
22. Take a sample of gas from the sample port available in line 37 and analyse the gas sample with GC analysis to determine the gas composition.
23. If the mole fraction of air in the gas sample is still above 0.05, repeat steps 16-22.

9.10.2 Start-up Procedure for Experimental Measurements

After the column has been filled with the appropriate gas the following procedure was followed to prepare for experimental measurements. If air was used the gas loading procedure was skipped.

1. Switch on the pilot plant control panel and select the packed column configuration.
2. Adjust the liquid density and liquid venturi discharge coefficient to the appropriate values, as well as the specific gas constant based on the gas composition.
3. Set the set point for the column pressure on the plant control panel to about 1 kPa above atmospheric pressure.
4. Start-up the PC connected to the control panel and start the data logging program.
5. Ensure that V-102 and V-104 are closed, disconnecting the tray column from the gas blower (E-102) and surge tank (E-101).
6. Ensure that V-105 and V-106 are open, connecting the packed column (E-401) to the gas blower (E-102) and surge tank (E-101).
7. Ensure that V-107 is closed disconnecting the packed column (E-401) from the atmosphere.
8. Ensure that the surge tank (E-101) access port is completely closed, as well as V-108, which closes the surge tank (E-101) drain port.
9. Ensure that MV-403, MV-405 and MV-415 are open, allowing gas to vent when the two liquid hold-up tanks (TK-402 and TK-403) and the entrainment tank (TK-401) are filled with liquid during liquid hold-up and entrainment measurements.
10. Completely open MV-407.
11. Although the default setting when switching on the control panel and selecting the packed column is for the high liquid flow configuration, MV-411 still has to be manually adjusted to the high liquid flow configuration.

12. Even though PCV-205 was not used in this project, since it receives input from the faulty E-207 (positive displacement high liquid flow meter), the control valve was completely opened by setting a set point of 20 m^3/h on the control panel and opening MV-204 and MV-206.
13. Open MV-207.
14. The default setting when switching on the control panel and selecting the packed column is the circulation configuration, with PV-401 set to allow liquid to pass from line 6 to line 47.
15. Start the liquid pump (E-204) with a frequency of 15 Hz, allowing the liquid to circulate through the heat exchanger and back to the sump.
16. Set the set point for the liquid temperature to 25°C and switch on the cooling/heating system.
17. Allow the liquid to circulate until the liquid temperature reaches the set point.
18. Switch off the liquid pump (E-204) and on the control panel select the configuration to switch PV-401 to allow liquid to be diverted through the column.
19. Start the liquid pump (E-204) at a frequency of 20 Hz and allow the liquid to circulate through the column for about 15 minutes to ensure proper wetting of the packing material.
20. Start the gas blower (E-102) at a frequency of 15 Hz.
21. Adjust the radial vane control to 30 % after the blower has finished its start-up cycle, allowing gas to circulate through the packed column.
22. Run the gas/liquid circulation cycle through the column until the gas temperature is close to the operating temperature of 25°C for minimum of 30 minutes.
23. Switch of the gas blower (E-102).
24. Set the minimum liquid level (in pascal) in TK-402 and TK-403 to a value that corresponds to a liquid level above the sight glasses in TK-402 and above the dished end in TK-403. The minimum level will depend on the liquid density, although a value of 1300 Pa and 600 Pa, for TK-402 and TK-403 respectively, will be sufficient for all liquid used in this project.
25. Trigger the “Hold-up Sync” sequence on the control panel, which closes PV-406 and PV-416, allowing TK-402 to fill with liquid and cascade over to TK-403. When the minimum level in TK-403 is reached PV-406 will open draining the liquid from TK-402. At this point switch of the liquid pump (E-204).
26. Flush all differential and absolute pressure meter lines to remove any condensate build-up that might result in inaccurate pressure measurements.

The following steps are for measuring a single pressure drop, liquid hold-up and liquid entrainment data point. These steps were repeated for all liquid and gas flow rates, packing size and liquid and gas combinations.

9.10.3 Pressure Drop Measurements

1. Start the liquid pump (E-204) at a frequency of 20 Hz and allow the liquid to circulate through the column.
2. Start the gas blower (E-102) at a frequency of 15 Hz.
3. Adjust the radial vane control to 30 % after the blower has finished its start-up cycle, allowing gas to circulate through the packed column.
4. With the liquid pump (E-204) frequency set to 20 Hz, either increase the pump frequency for higher liquid flow rates or adjust MV-207 to decrease the liquid flow rate to the required liquid flow rate.
5. With the gas blower (E-102) frequency set to 15 Hz, either increase the blower frequency for higher gas flow rates or adjust V-106 to decrease the gas flow rate to the required gas flow rate.
6. Ensure that the liquid and gas temperatures are still at the set point of 25°C. If not, switch on the cooling/heating system to allow the liquid and gas temperatures to reach 25°C.
7. Ensure that the pressure drop over the column, as well as the liquid and gas flow rates have stabilised and hydrodynamic equilibrium has been reached by monitoring the respective graphs on the control panel.
8. Allow the system to run for at least 5 minutes after hydrodynamic equilibrium has been reached.
9. To measure the pressure drop, trigger the “Pressure Drop Sampling” sequence on the control panel, logging the pressure drop over the column for 2 minutes.

The steps described above is applicable for measuring the pressure drop at liquid flow rates of 37 $m^3/(m^2.h)$ and higher. To measure the pressure drop for a liquid flow rate of 6 $m^3/(m^2.h)$ the following steps were followed:

1. Select the low liquid flow rate configuration on the control panel.
2. Adjust MV-411 to allow liquid to flow from line 51 to line 49.
3. Repeat steps 1-9 for Experimental Pressure Drop Measurements, with the only difference being in step 4 were MV-412 is adjusted instead of MV-207 to control the liquid flow rate.

9.10.4 Liquid Hold-up Measurements

After the pressure drop over the column has been measured the following steps were followed for measuring the liquid hold-up.

1. Measure the liquid level on the liquid and gas distributors.
2. Trigger the "Liquid Hold-up Sampling" sequence on the control panel. This closes PV-406, allowing TK-402 to fill with liquid. When the minimum level in TK-402 has been reached, PV-402 closes automatically.
3. When PV-402 has closed completely immediately trigger the "Stop" sequence on the control panel, which switches off the liquid pump (E-204) and gas blower (E-102) and also closes the gas blower vane control valve (RVCV-101).
4. Allow the liquid to drain from the column into the liquid hold-up tanks (TK-402 and TK-403) for approximately 10 to 15 minutes. The liquid level in TK-402 and TK-403 can be monitored on the available graphs of liquid level versus time on the control panel.

9.10.5 Liquid Entrainment Measurements

Liquid entrainment was measured separate from the pressure drop and liquid hold-up measurements. The reason for this was because the liquid entrainment data was measured over a different range of gas flow rates compared to the pressure drop and liquid hold-up measurements. Liquid entrainment was measured primarily in the flooding region. The following procedure was followed for measuring liquid entrainment.

1. Repeat all steps in "Start-up Procedure for Experimental Measurements".
2. Repeat steps 1-8 for "Pressure Drop Measurements".
3. Manually close PV-404 by switching the solenoid valve controlling the compressed air to the pneumatic valve (PV-404).
4. Once a liquid level is detected in TK-401 by monitoring the static head pressure, start a timer of five minutes and record the static head pressure at which the timer was started.
5. Depending on the liquid entrainment rate either record the static head pressure after the five minutes have passed or record the amount of time that has passed when the tank reaches its maximum liquid level.

9.10.6 Shut-down Procedure

1. Switch off the cooling/heating system.
2. Stop the gas blower (E-102) and liquid pump (E-204) by triggering the "Stop" sequence on the control panel.
3. Close V-105 and V-106 to disconnect the packed column from the surge tank (E-101) and gas blower (E-102) and minimize gas loss from the system.
4. Stop the data logging program on the PC connected to the control panel.
5. Switch off the pilot plant control panel.

9.10.7 Static Liquid Hold-up

The static liquid hold-up was measured in a 1:10 scale test section of the column, which consists of a stainless steel cylinder, 400 mm in diameter and 300 mm high, with the bottom covered with a coarse grid. The follow steps were followed to measure the static liquid hold-up for both 1.5" Intalox Ultra A and 2.5" Intalox Ultra O with all four liquids used in this project. The results are presented in Table 9.27.

1. Measure and record the dry weight of the empty 1:10 scale test section ($W_{scale\ section,dry}$).
2. Completely fill the test section with packing as randomly as possible.
3. Measure and record the dry weight of the test section filled with dry packing ($W_{scale\ section+packing,dry}$).
4. Completely submerge the dry test section filled with dry packing in a container filled with the liquid being measured.
5. Carefully remove the wet test section containing the wet packing from the liquid and allow the liquid to drain from the packing for 10 to 15 minutes.
6. Measure and record the weight of the wet test section containing the wet packing ($W_{scale\ section+packing,wet}$).
7. Remove the wet packing from the test section and completely submerge the empty test section in a container filled with the liquid being measured.
8. Carefully remove the empty wet test section from the liquid and allow the liquid to drain from the test section for 10 to 15 minutes.
9. Measure and record the weight of the empty wet test section ($W_{scale\ section,wet}$).

The weight of liquid held up on the packing was calculated as follows:

$$W_{static\ liquid\ hold-up} = \left(W_{scale\ section+packing,wet} - W_{scale\ section,wet}\right) - \left(W_{scale\ section+packing,dry} - W_{scale\ section,dry}\right)$$

The static liquid hold-up presented in Table 9.27 was calculated by dividing the volume of static liquid hold-up by the volume of the scale test section:

$$h_{L,static} = \frac{W_{static\ liquid\ hold-up} \cdot \rho_L}{V_{scale\ section}} \qquad \text{Where:} \qquad V_{scale\ section} = \frac{\pi \cdot 0.4^2}{4} \cdot 0.3 = 0.0377\ m^3$$

Table 9.27: Static liquid hold-up for 1.5" Intalox Ultra A and 2.5" Intalox Ultra O for all liquids investigated

Liquid	Static Liquid Hold-up [m^3/m^3]	
	1.5" Intalox Ultra A	2.5" Intalox Ultra O
Water	0.00815	0.00417
Ethylene Glycol	0.00927	0.00492
Isopar G	0.00360	0.00156
Silicone Oil	0.00528	0.00222

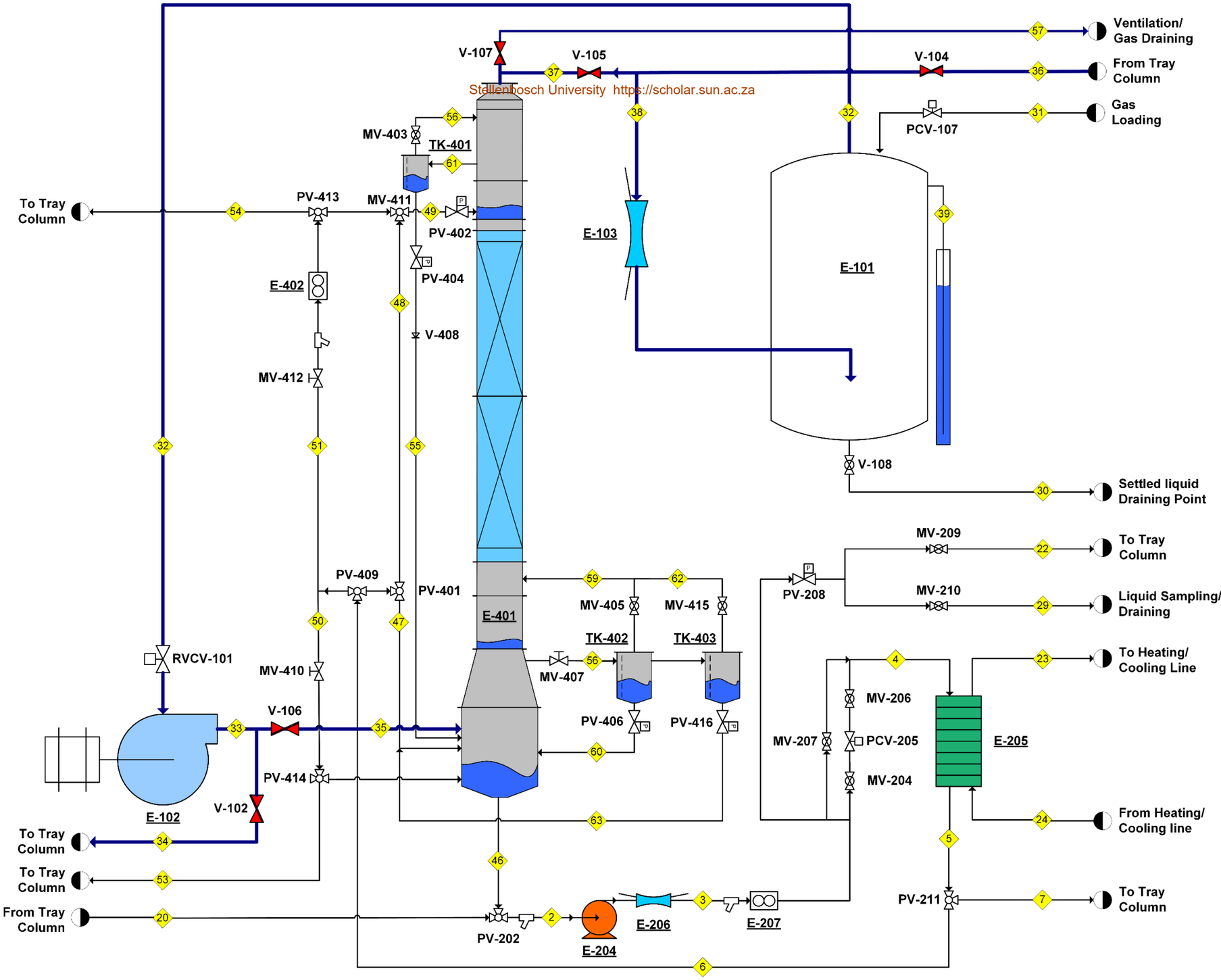

Figure 9.8: Packed Column Pilot Plant PFD [Adapted from Lamprecht (2010)]

9.11 Experimental Data Graphs

9.11.1 1.5” Intalox Ultra A Pressure Drop & Liquid Hold-up

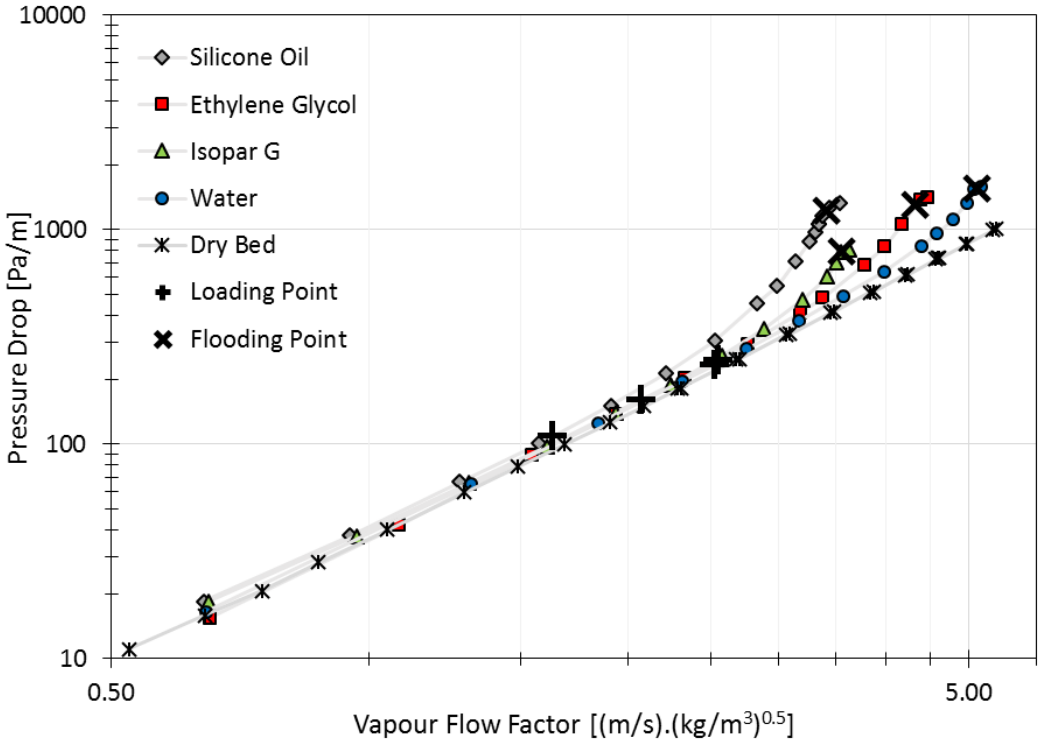

Figure 9.9: Pressure drop, air, 1.5" Intalox Ultra A at 6 $m^3/(m^2.h)$

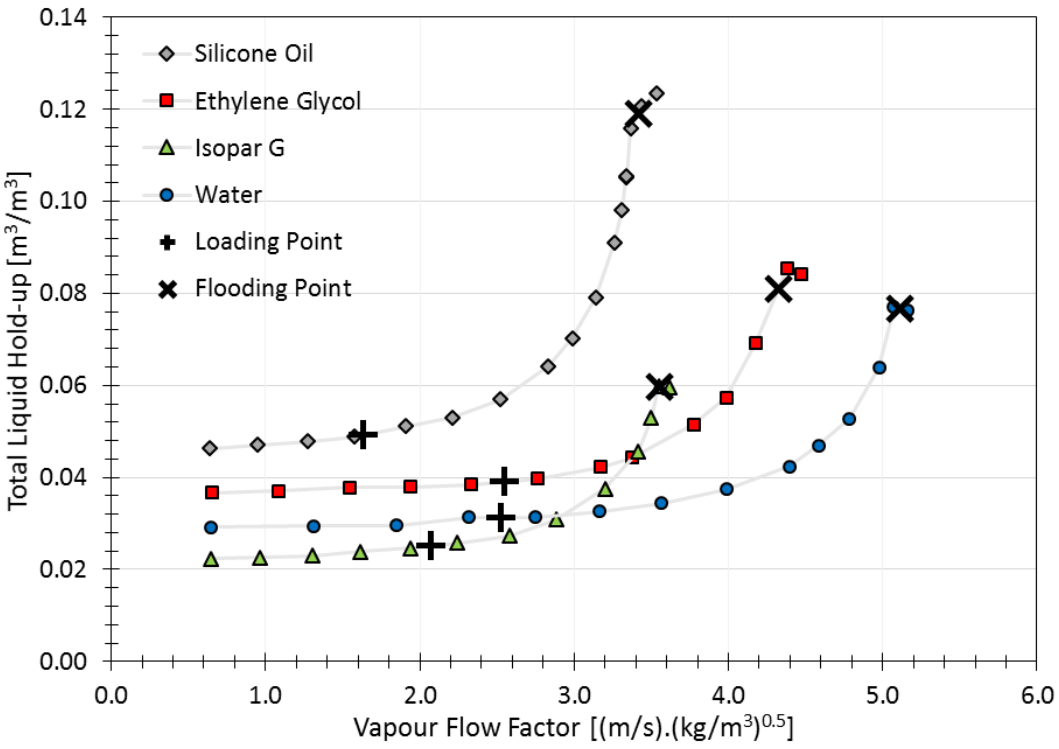

Figure 9.10: Liquid hold-up, air, 1.5" Intalox Ultra A at 6 $m^3/(m^2.h)$

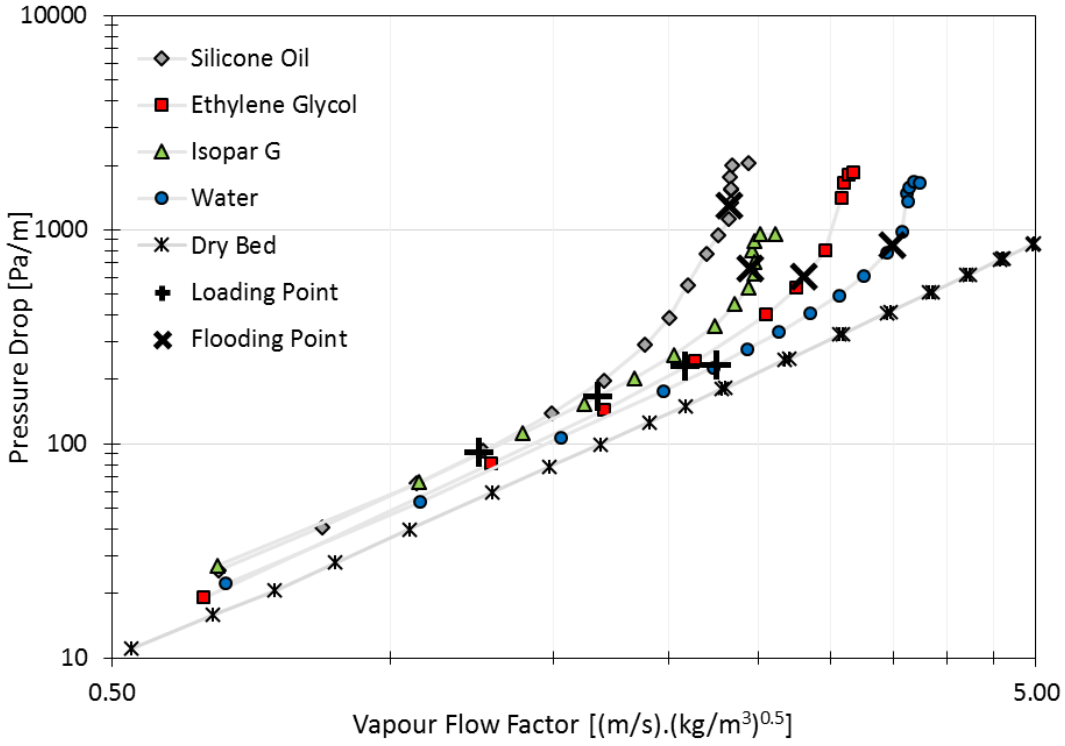

Figure 9.11: Pressure drop, air, 1.5" Intalox Ultra A at 37 $m^3/(m^2.h)$

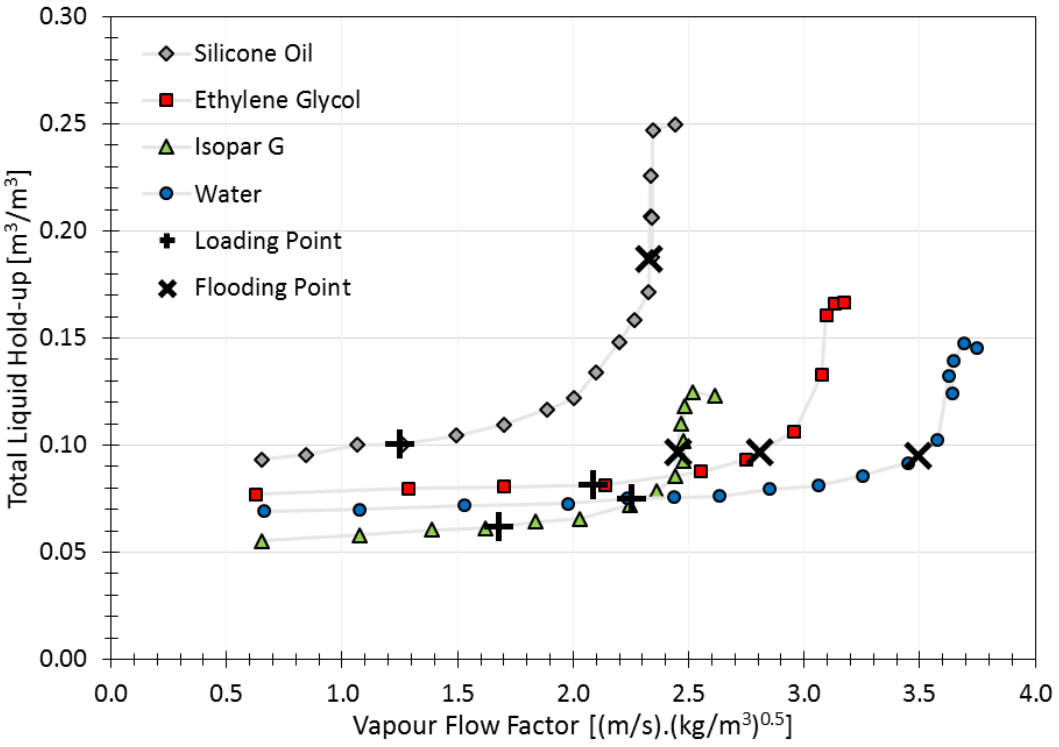

Figure 9.12: Liquid hold-up, air, 1.5" Intalox Ultra A at 37 $m^3/(m^2.h)$

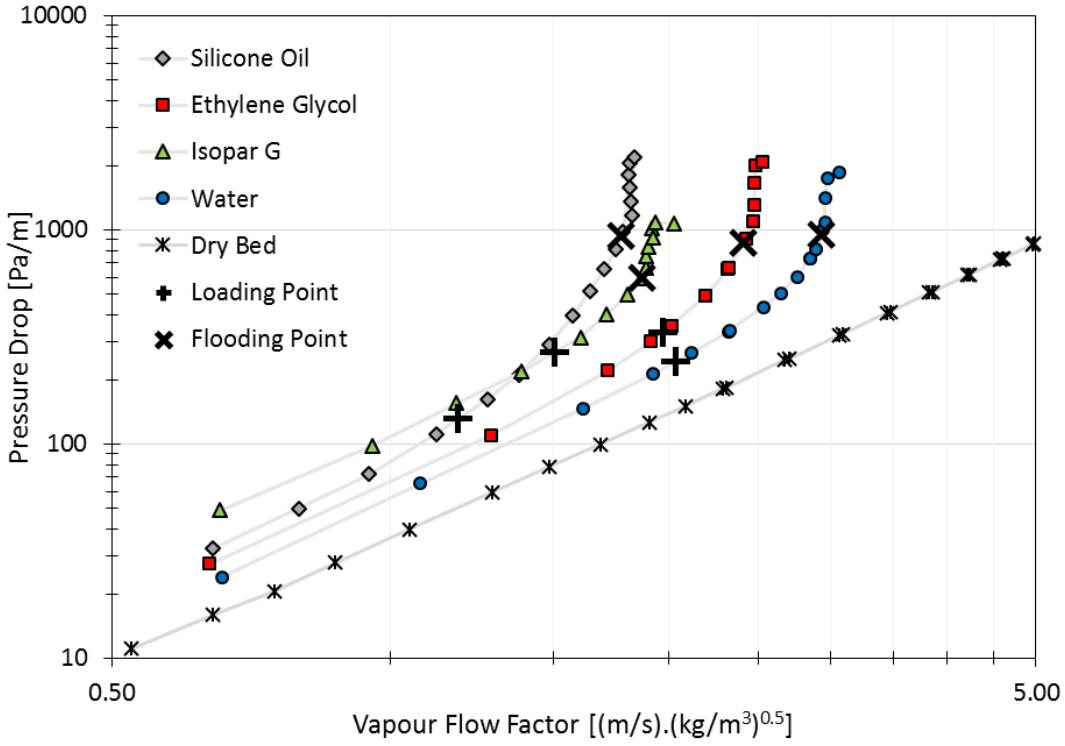

Figure 9.13: Pressure drop, air, 1.5" Intalox Ultra A at 73 $m^3/(m^2.h)$

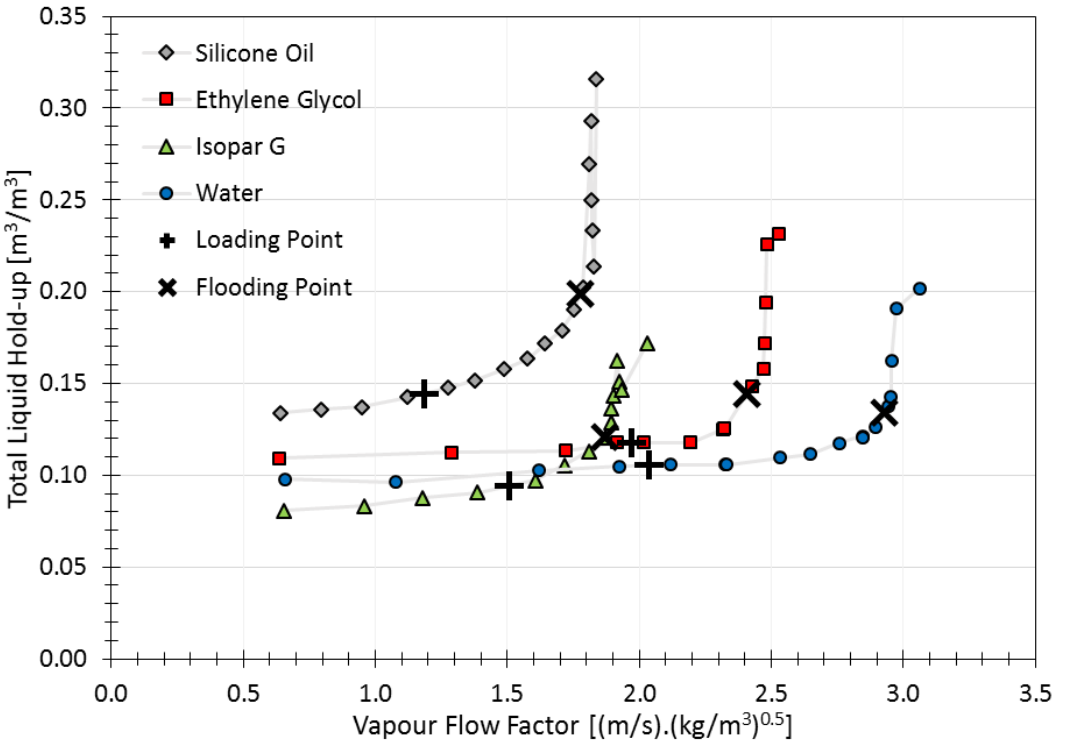

Figure 9.14: Liquid hold-up, air, 1.5" Intalox Ultra A at 73 $m^3/(m^2.h)$

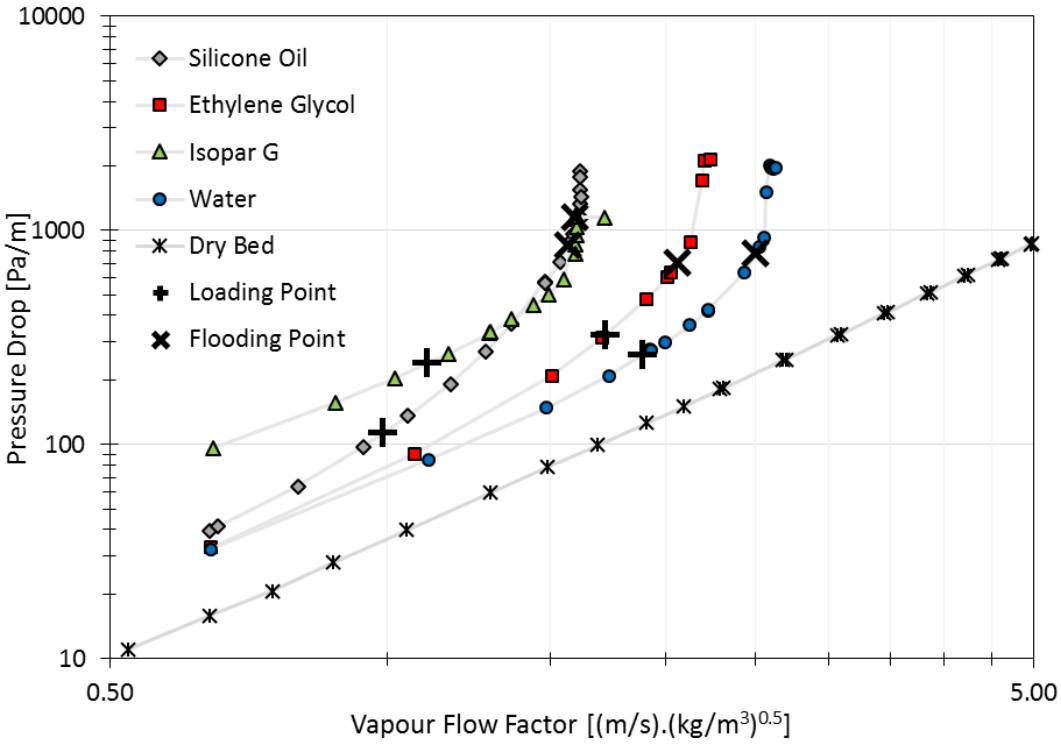

Figure 9.15: Pressure drop, air, 1.5" Intalox Ultra A at 98 $m^3/(m^2.h)$

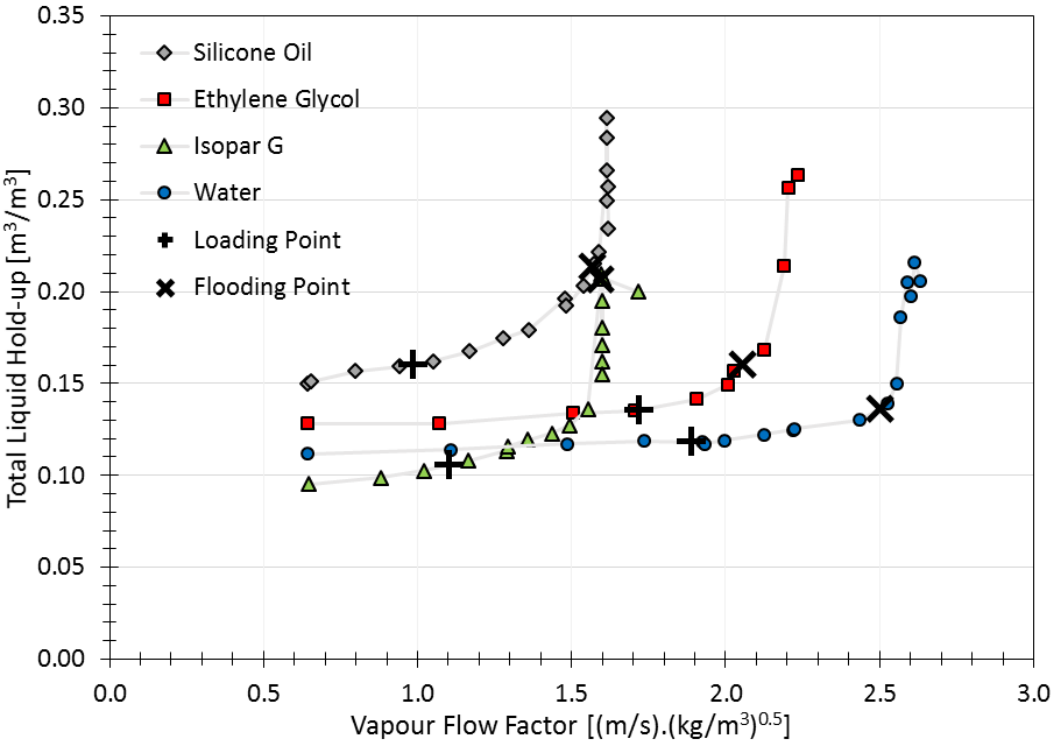

Figure 9.16: Liquid hold-up, air, 1.5" Intalox Ultra A at 98 $m^3/(m^2.h)$

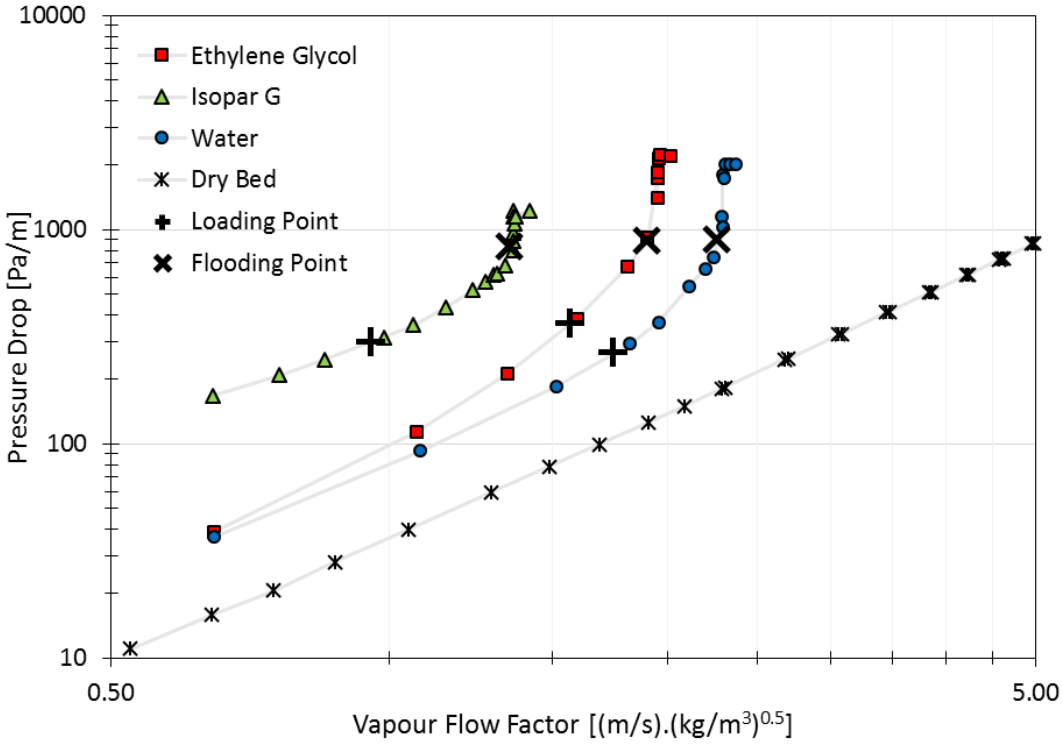

Figure 9.17: Pressure drop, air, 1.5" Intalox Ultra A at 122 $m^3/(m^2.h)$

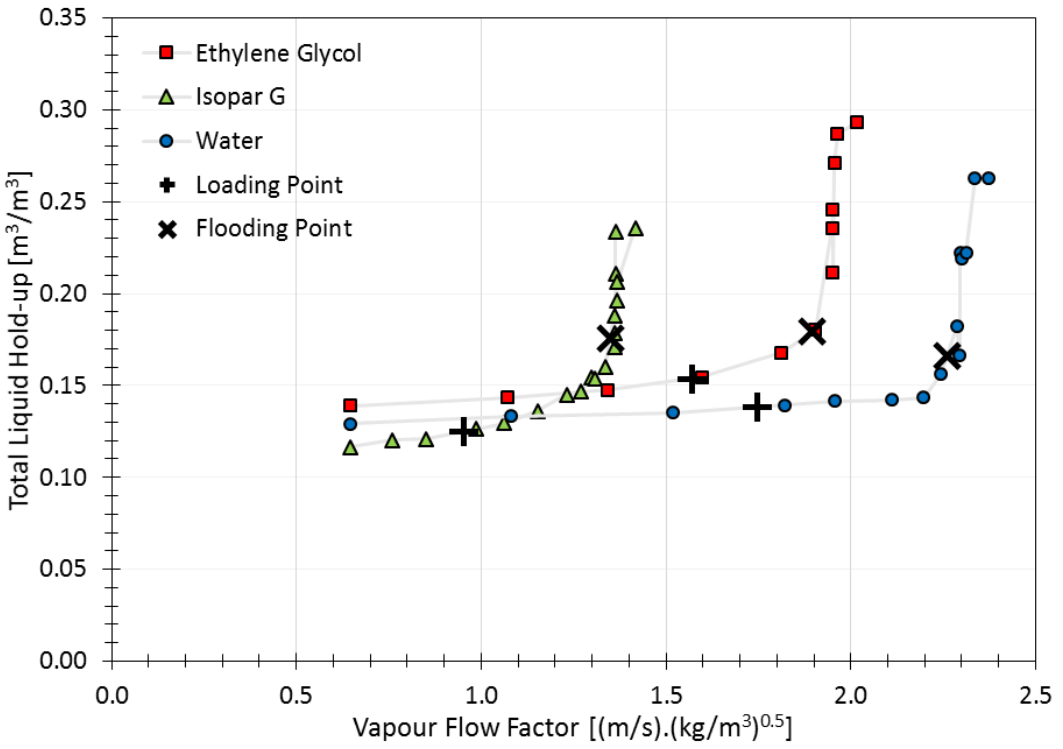

Figure 9.18: Liquid hold-up, air, 1.5" Intalox Ultra A at 122 $m^3/(m^2.h)$

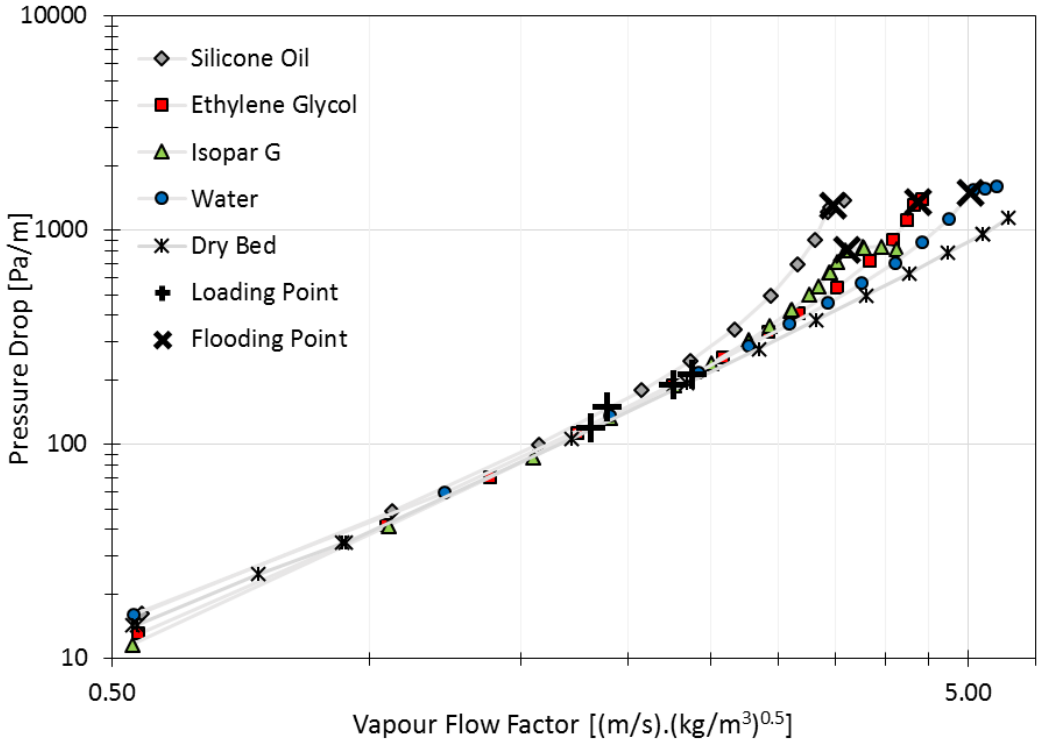

Figure 9.19: Pressure drop, CO_2, 1.5" Intalox Ultra A at 6 $m^3/(m^2.h)$

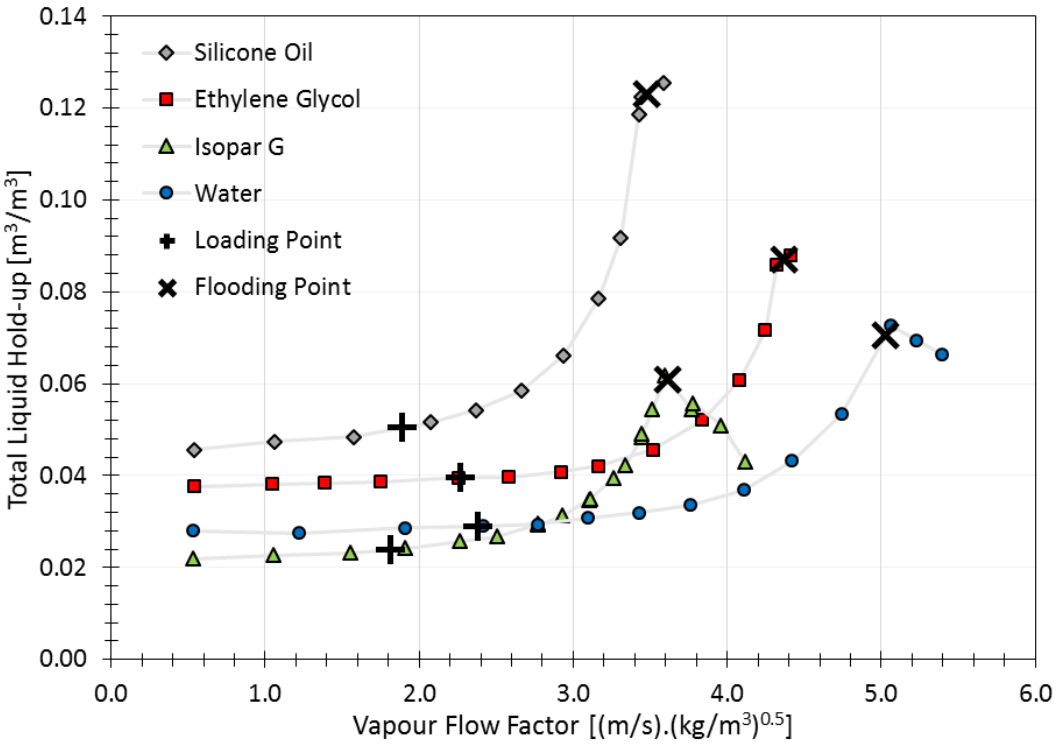

Figure 9.20: Liquid hold-up, CO_2, 1.5" Intalox Ultra A at 6 $m^3/(m^2.h)$

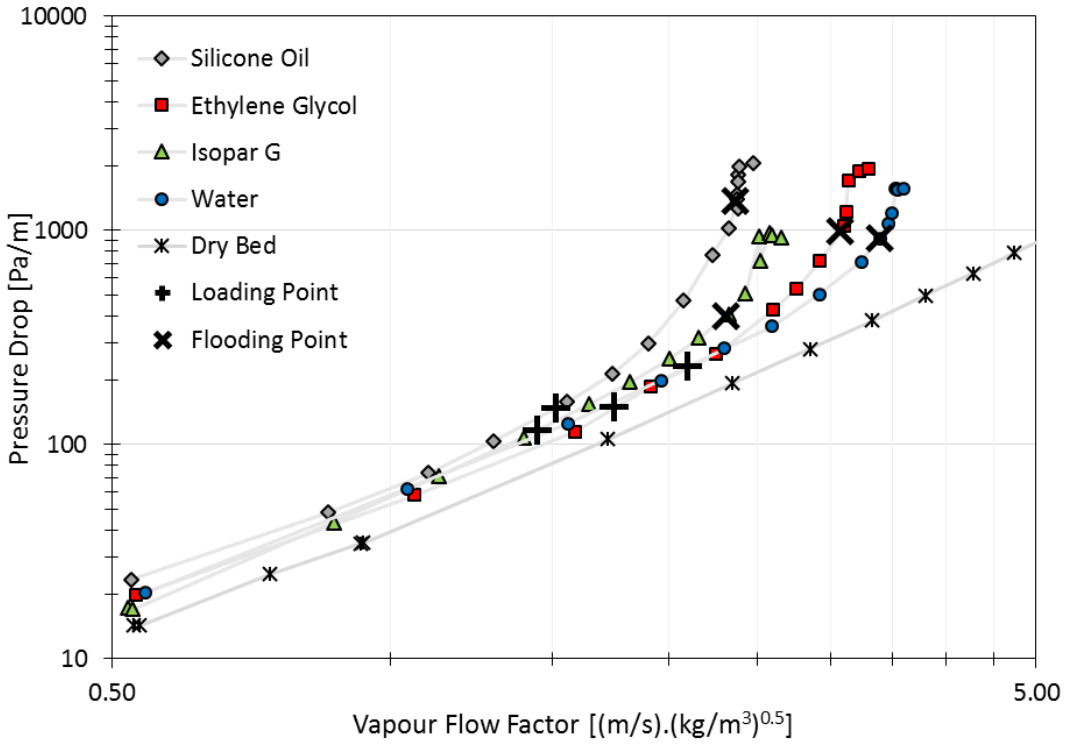

Figure 9.21: Pressure drop, CO_2, 1.5" Intalox Ultra A at 37 $m^3/(m^2.h)$

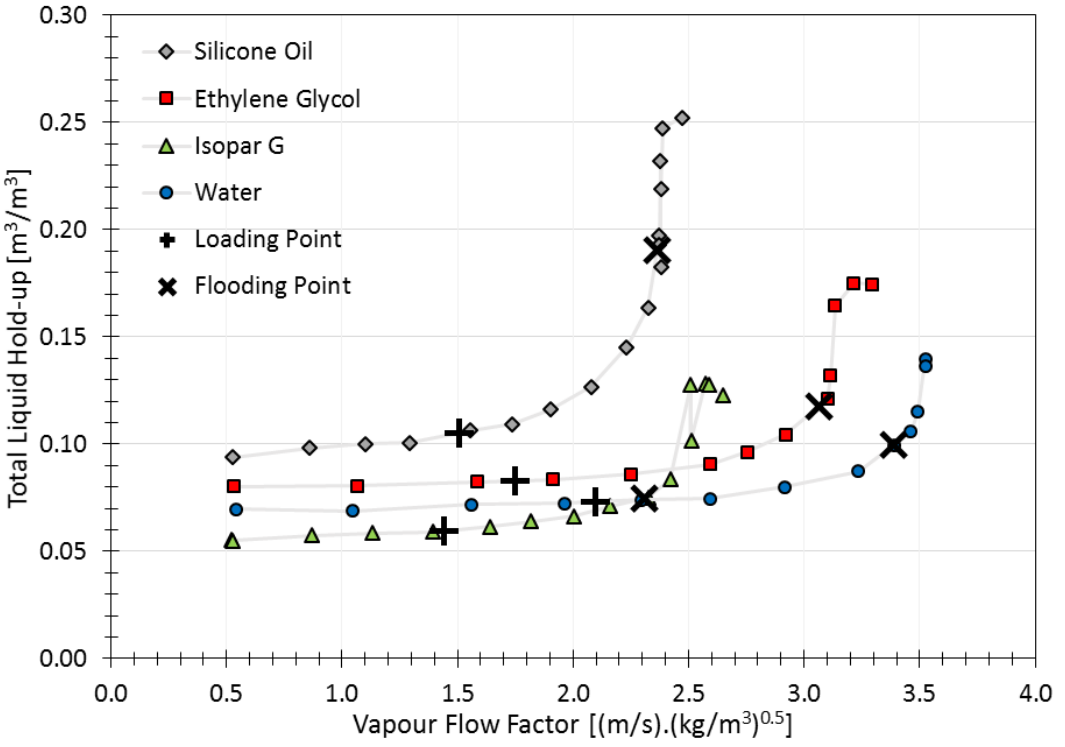

Figure 9.22: Liquid hold-up, CO_2, 1.5" Intalox Ultra A at 37 $m^3/(m^2.h)$

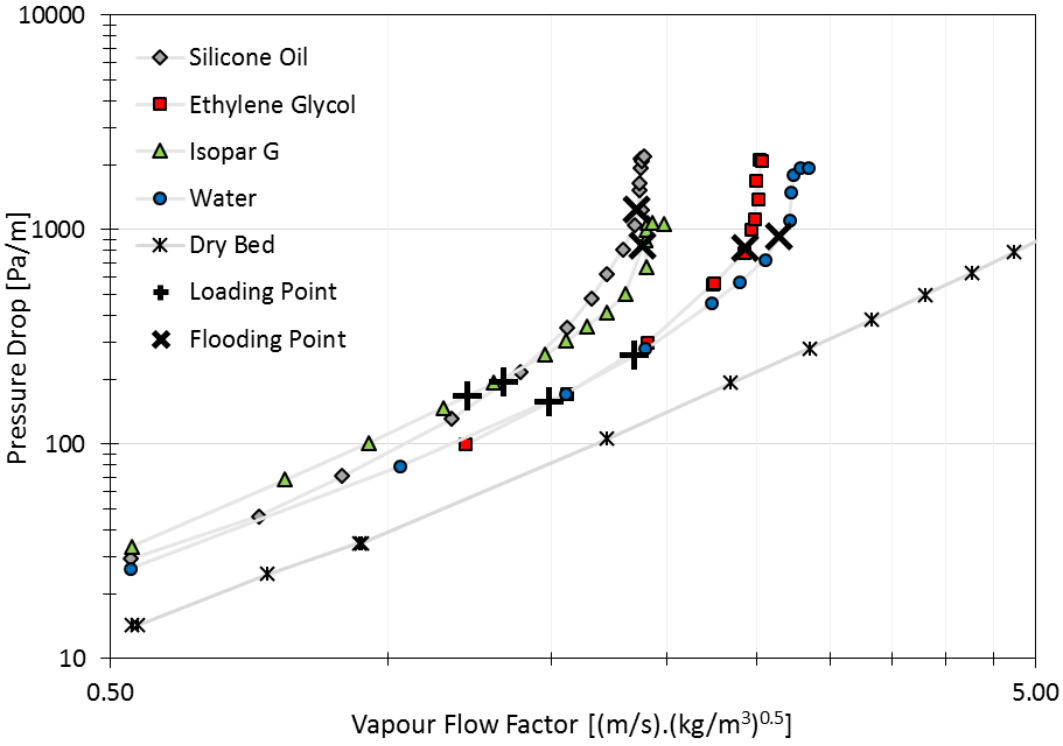

Figure 9.23: Pressure drop, CO_2, 1.5" Intalox Ultra A at 73 $m^3/(m^2.h)$

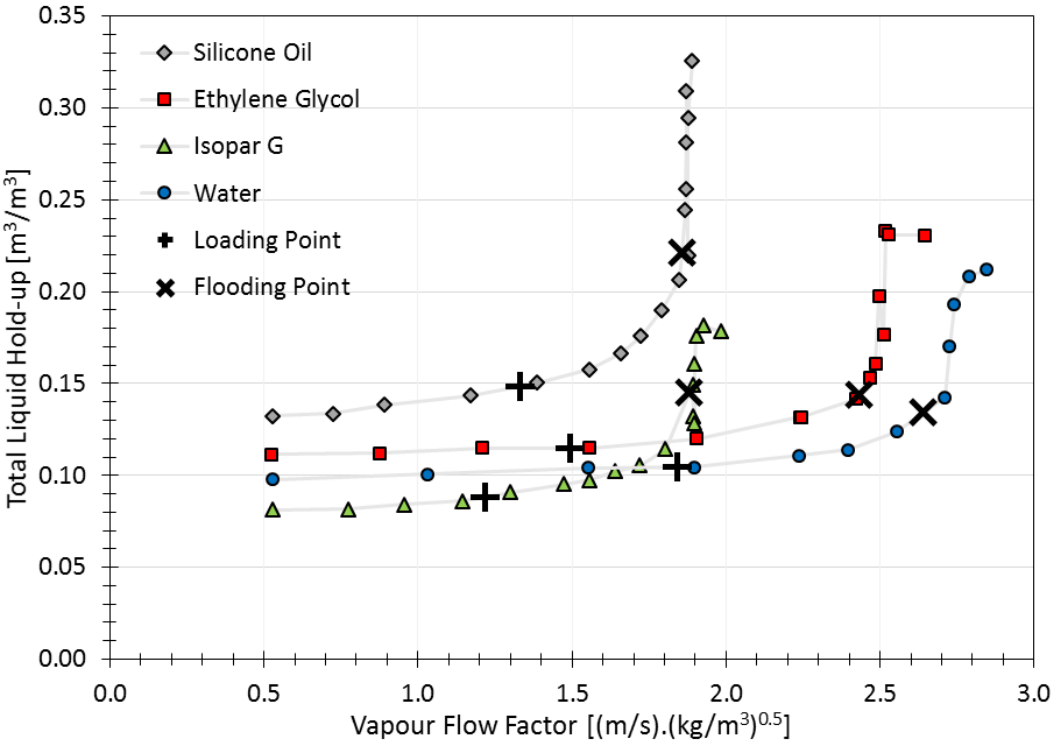

Figure 9.24: Liquid hold-up, CO_2, 1.5" Intalox Ultra A at 73 $m^3/(m^2.h)$

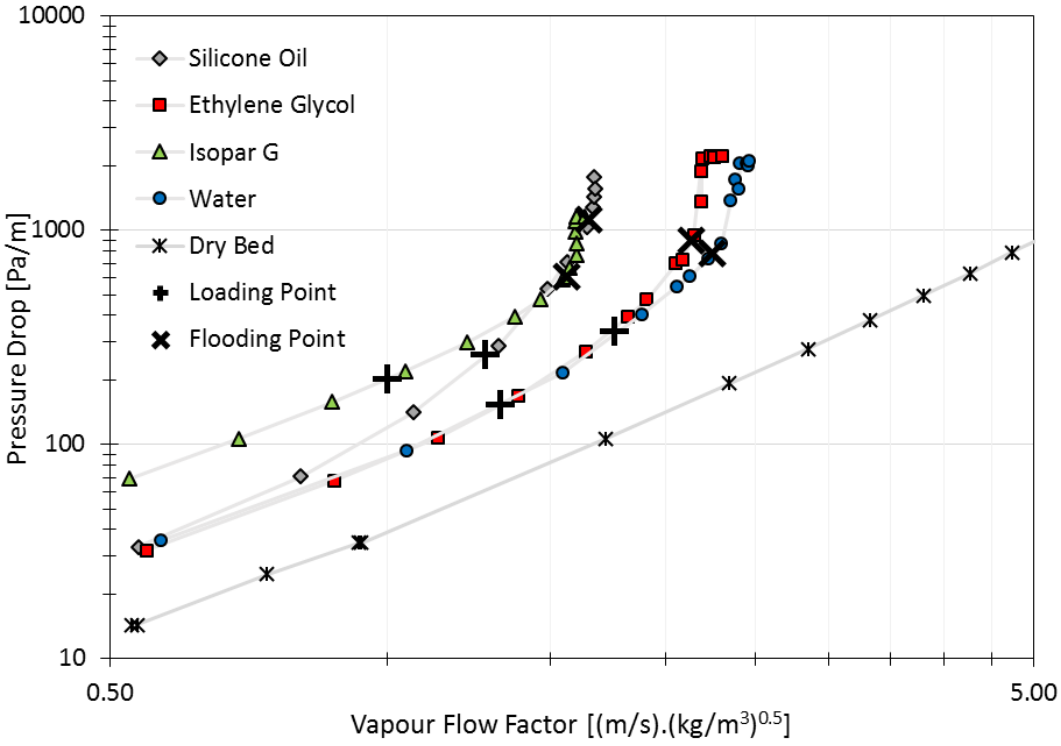

Figure 9.25: Pressure drop, CO_2, 1.5" Intalox Ultra A at 98 $m^3/(m^2.h)$

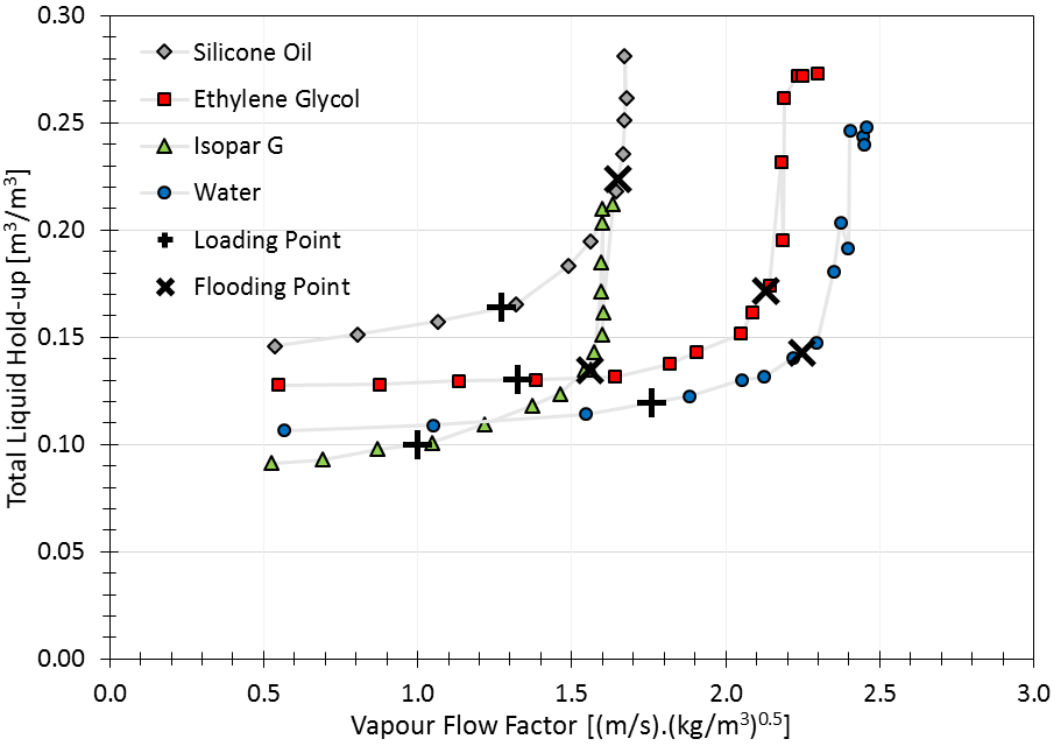

Figure 9.26: Liquid hold-up, CO_2, 1.5" Intalox Ultra A at 98 $m^3/(m^2.h)$

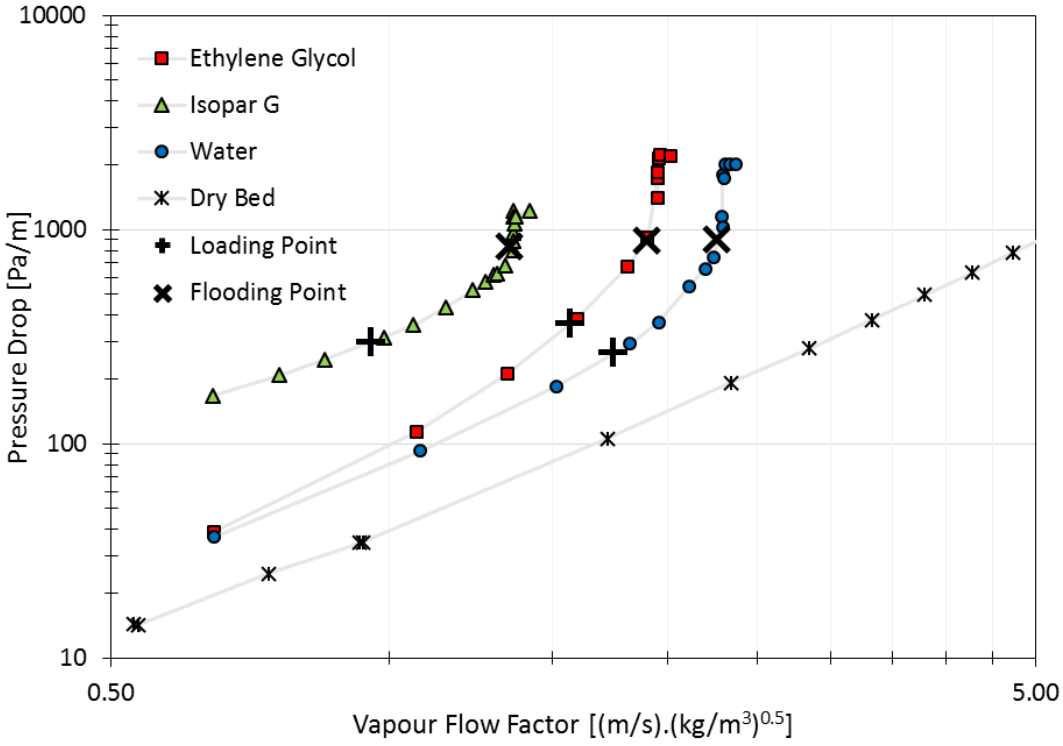

Figure 9.27: Pressure drop, CO_2, 1.5" Intalox Ultra A at 122 $m^3/(m^2.h)$

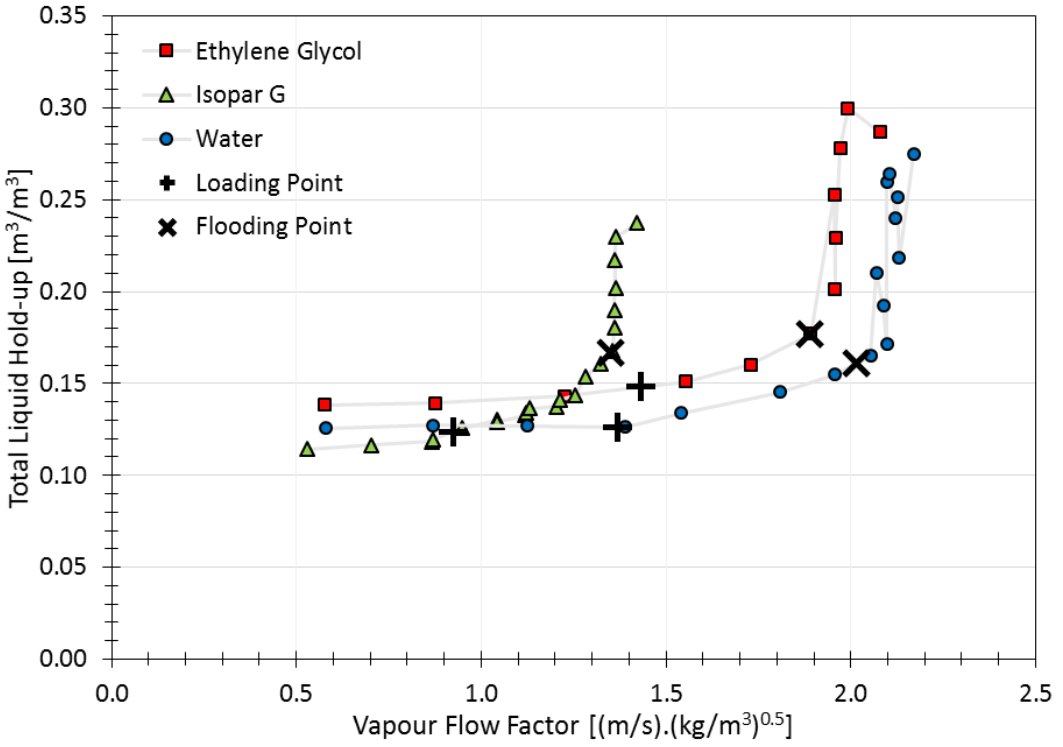

Figure 9.28: Liquid hold-up, CO_2, 1.5" Intalox Ultra A at 122 $m^3/(m^2.h)$

9.11.2 1.5” Intalox Ultra A Entrainment

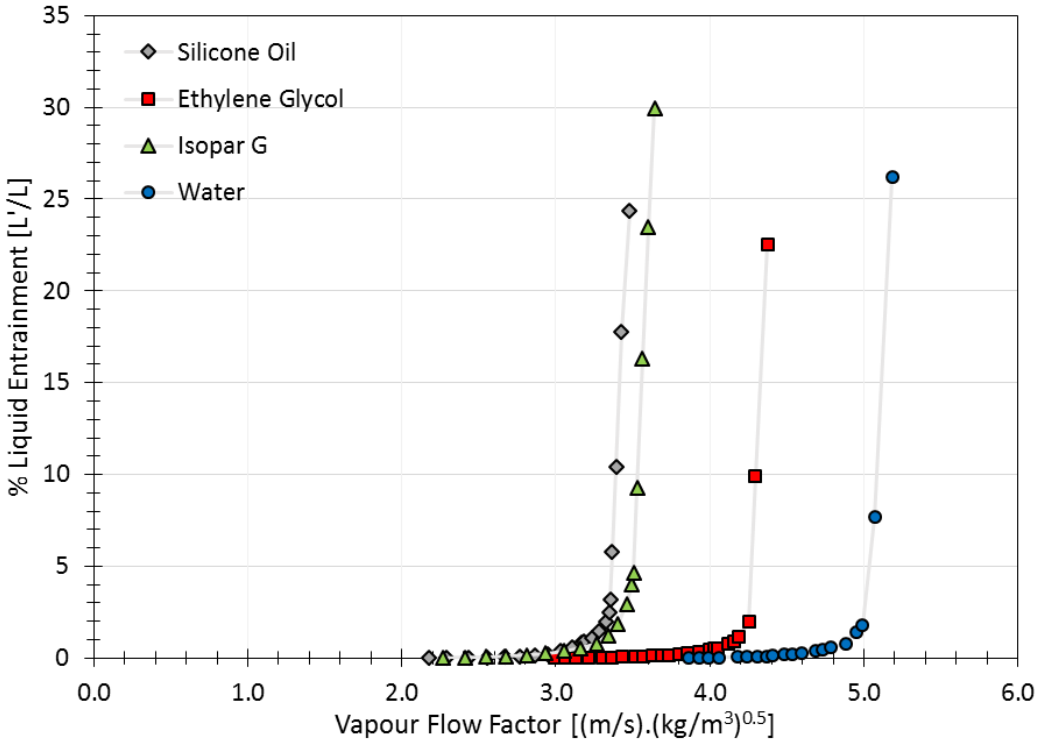

Figure 9.29: Entrainment, air, 1.5" Intalox Ultra A at 6 $m^3/(m^2.h)$

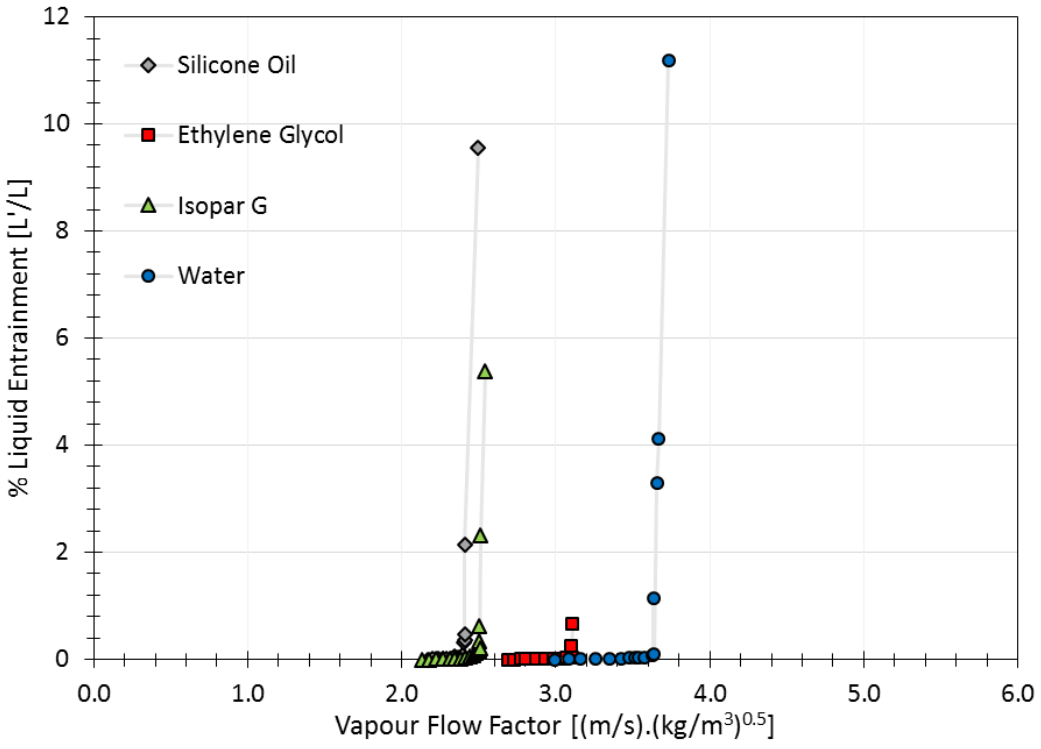

Figure 9.30: Entrainment, air, 1.5" Intalox Ultra A at 37 $m^3/(m^2.h)$

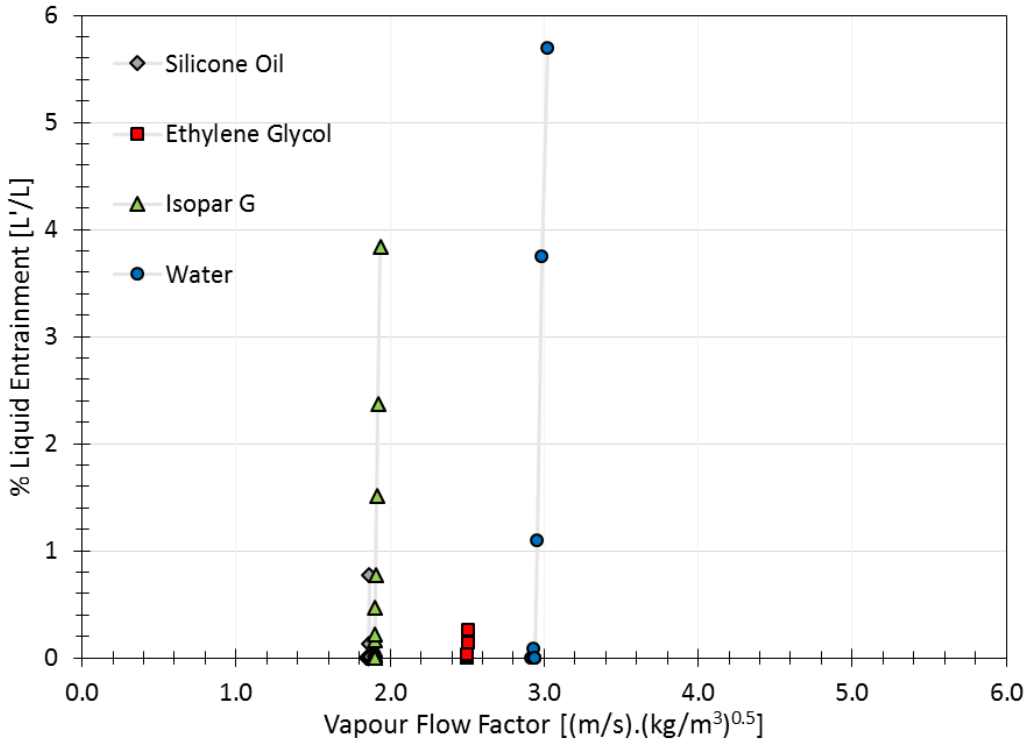

Figure 9.31: Entrainment, air, 1.5" Intalox Ultra A at 78 $m^3/(m^2.h)$

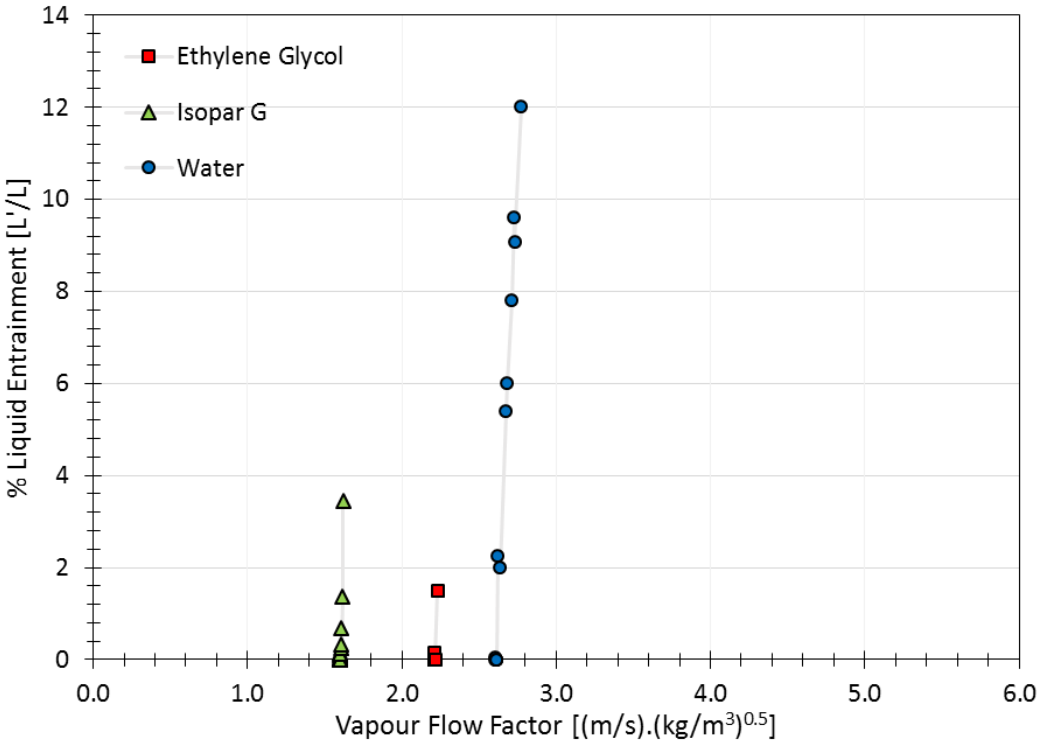

Figure 9.32: Entrainment, air, 1.5" Intalox Ultra A at 98 $m^3/(m^2.h)$

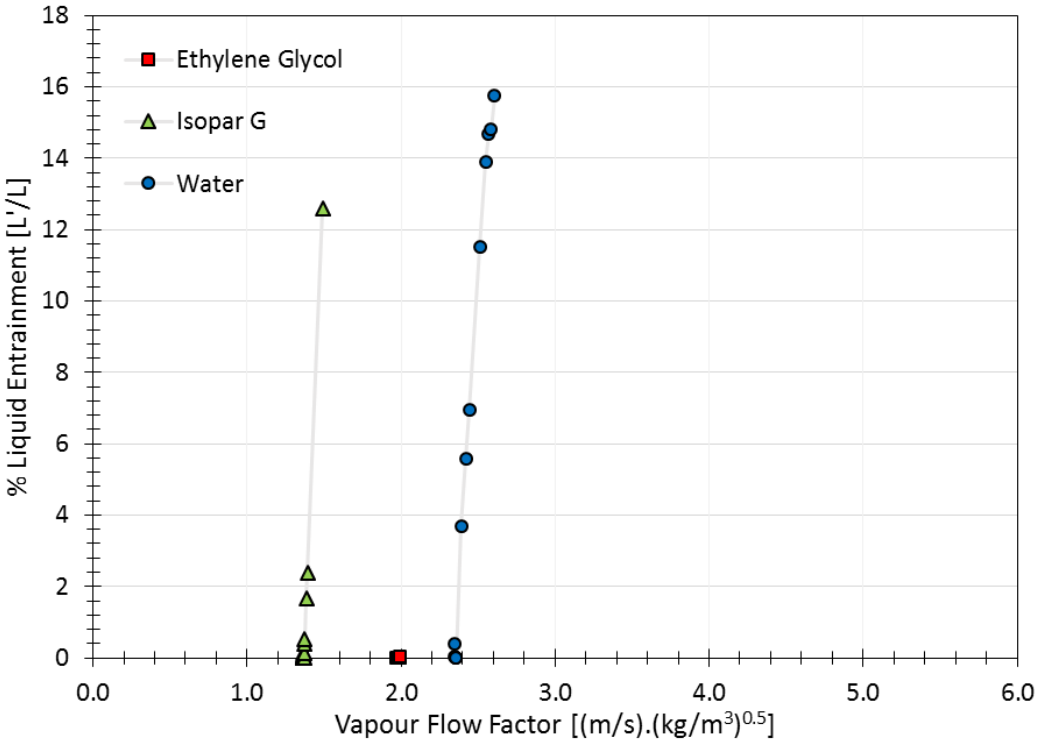

Figure 9.33: Entrainment, air, 1.5" Intalox Ultra A at 122 $m^3/(m^2.h)$

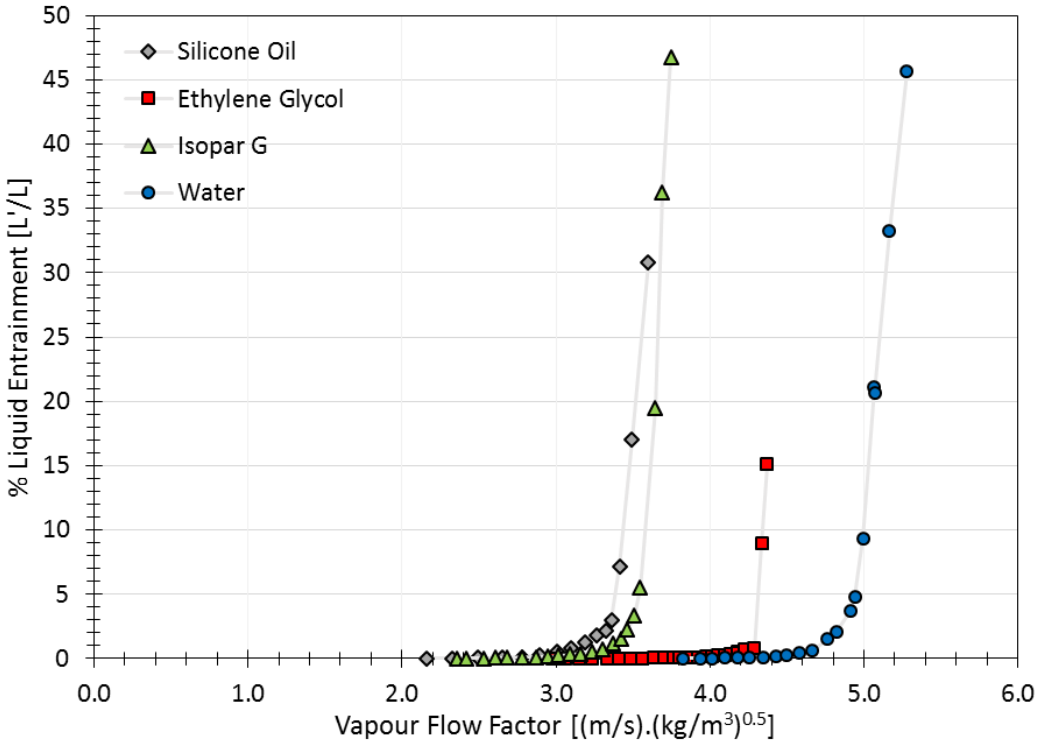

Figure 9.34: Entrainment, CO_2, 1.5" Intalox Ultra A at 6 $m^3/(m^2.h)$

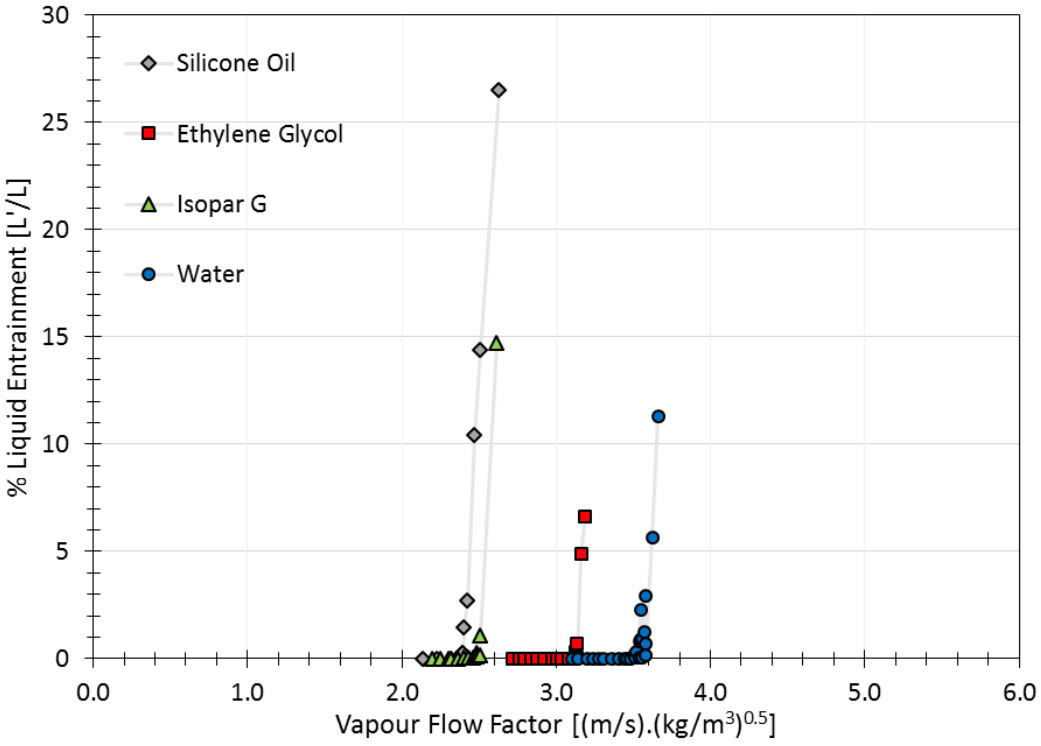

Figure 9.35: Entrainment, CO_2, 1.5" Intalox Ultra A at 37 $m^3/(m^2.h)$

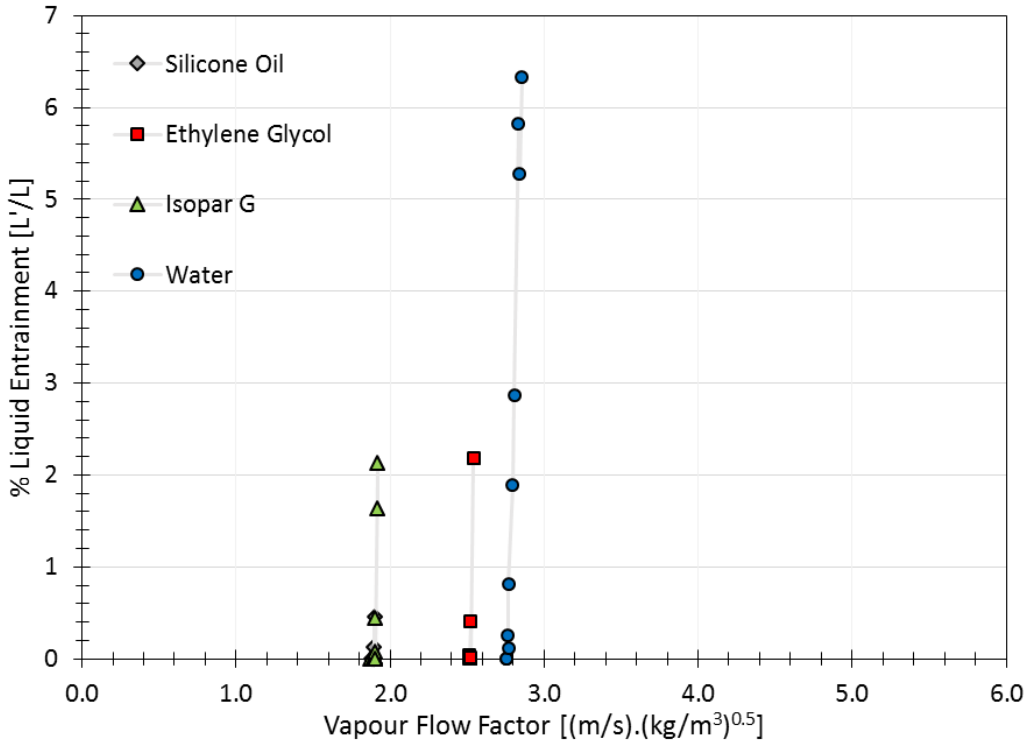

Figure 9.36: Entrainment, CO_2, 1.5" Intalox Ultra A at 73 $m^3/(m^2.h)$

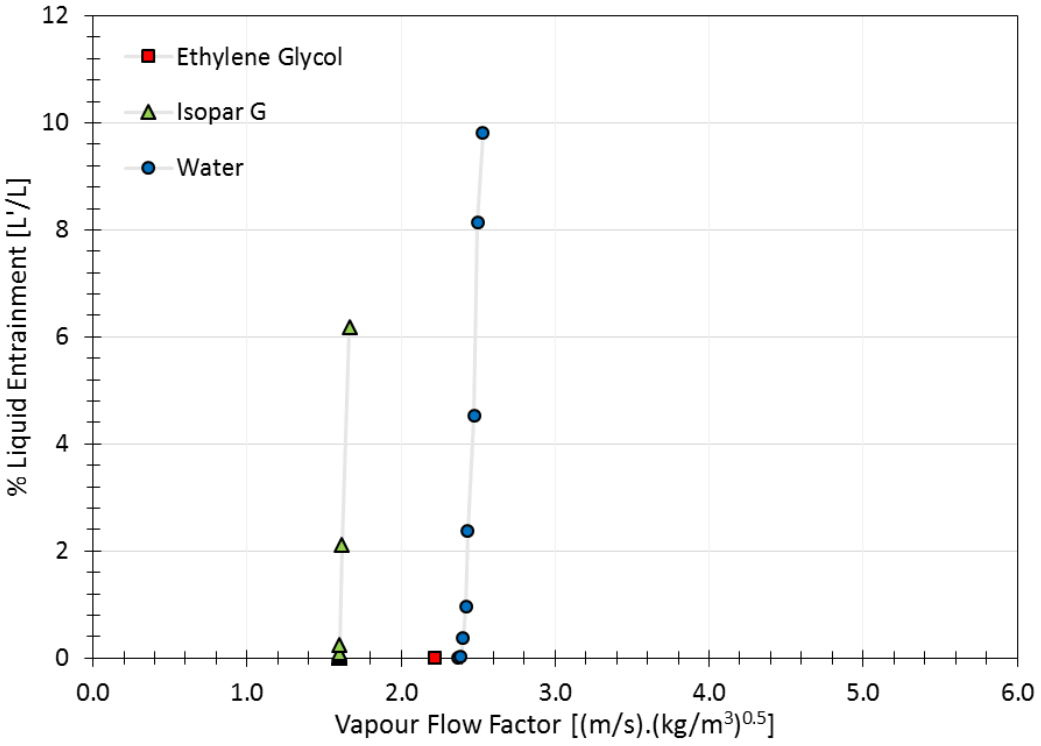

Figure 9.37: Entrainment, CO_2, 1.5" Intalox Ultra A at 93 $m^3/(m^2.h)$

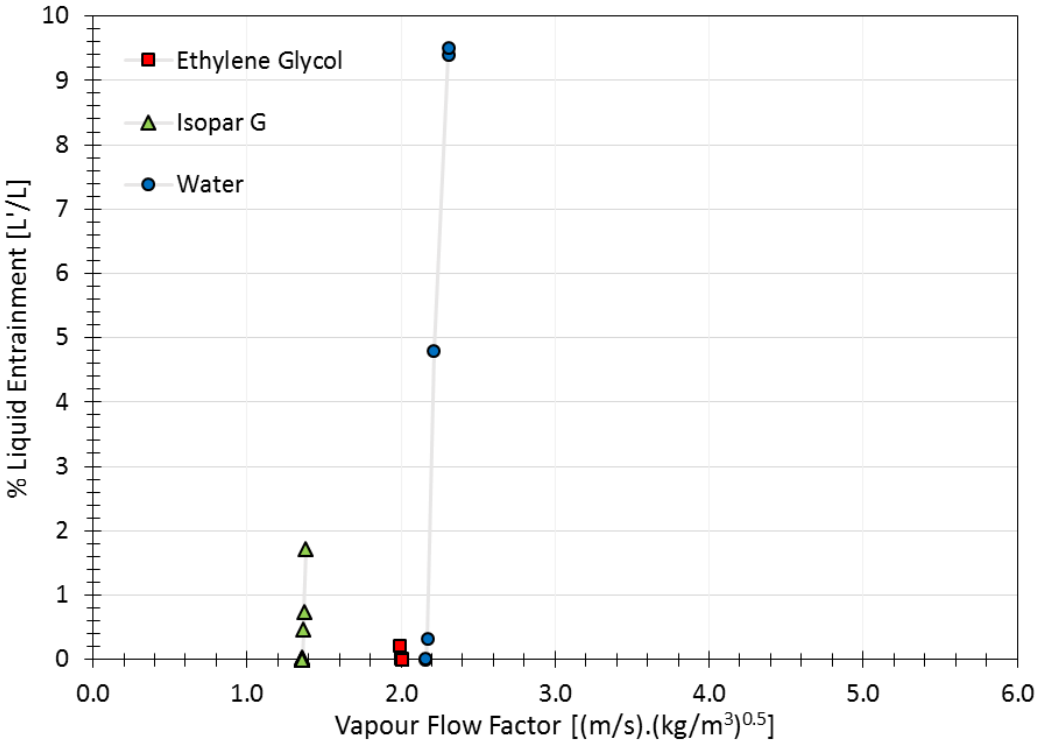

Figure 9.38: Entrainment, CO_2, 1.5" Intalox Ultra A at 122 $m^3/(m^2.h)$

9.11.3 2.5" Intalox Ultra O Pressure Drop & Liquid Hold-up

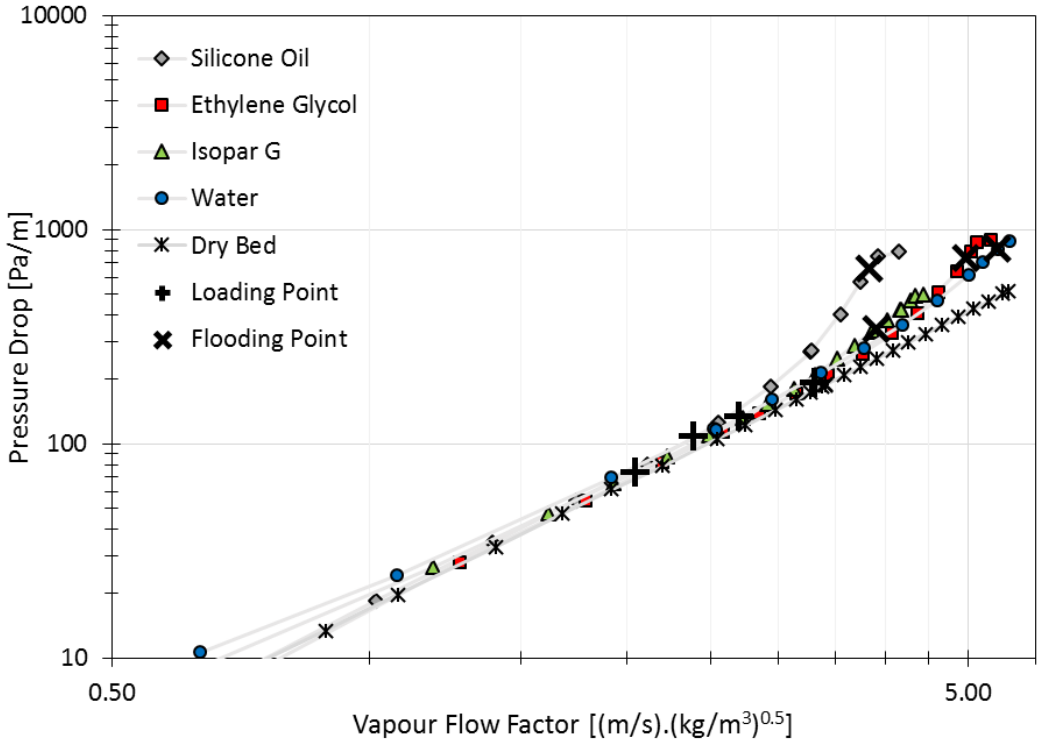

Figure 9.39: Pressure drop, air, 2.5" Intalox Ultra A at 6 $m^3/(m^2.h)$

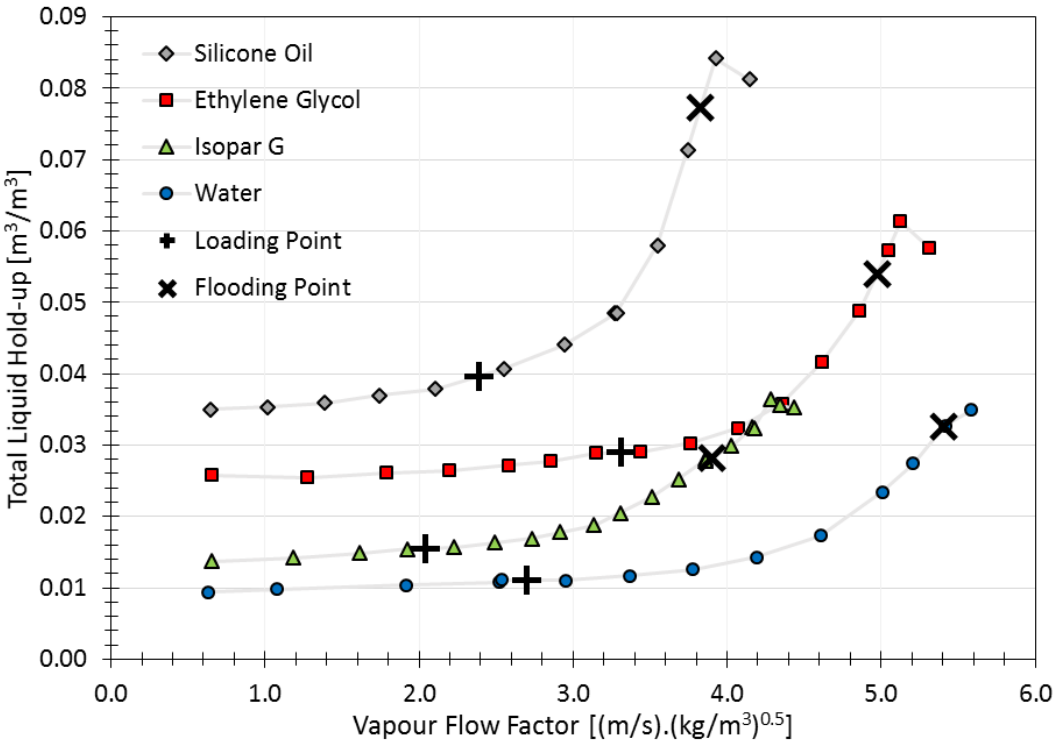

Figure 9.40: Liquid hold-up, air, 2.5" Intalox Ultra A at 6 $m^3/(m^2.h)$

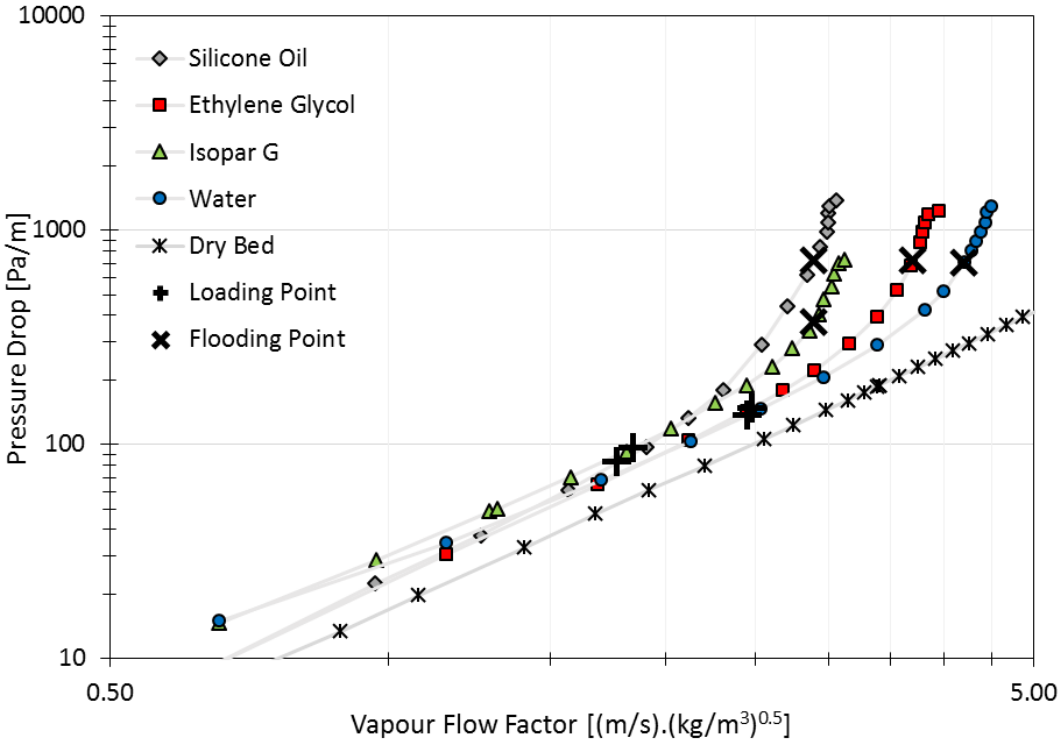

Figure 9.41: Pressure drop, air, 2.5" Intalox Ultra A at 37 $m^3/(m^2.h)$

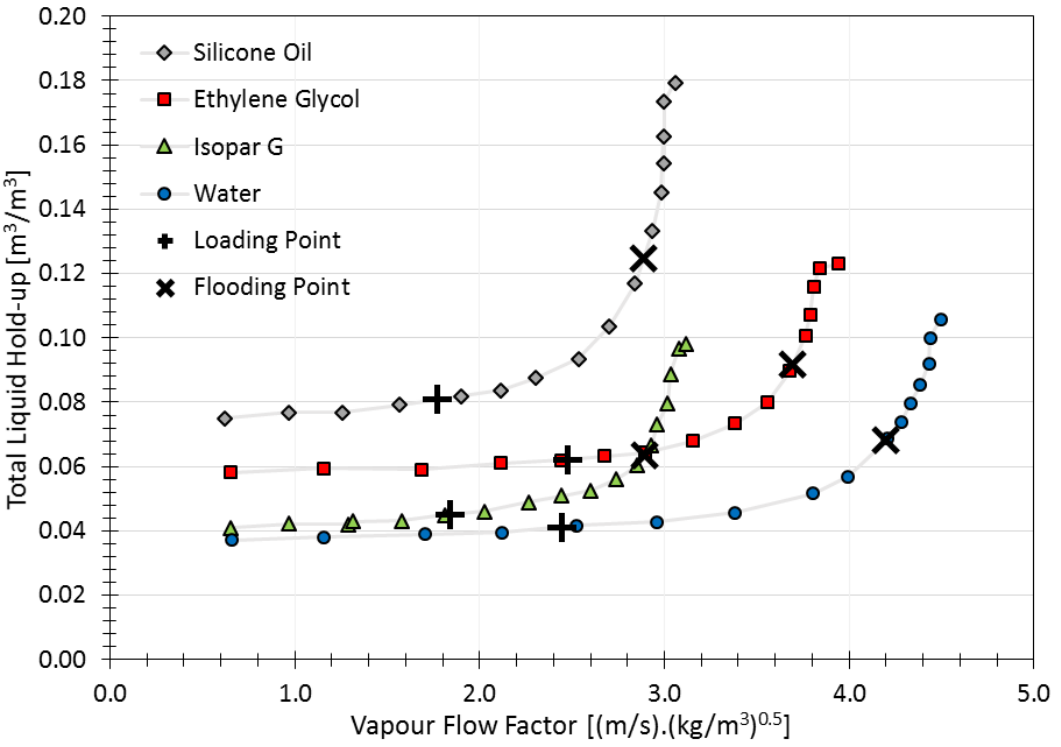

Figure 9.42: Liquid hold-up, air, 2.5" Intalox Ultra A at 37 $m^3/(m^2.h)$

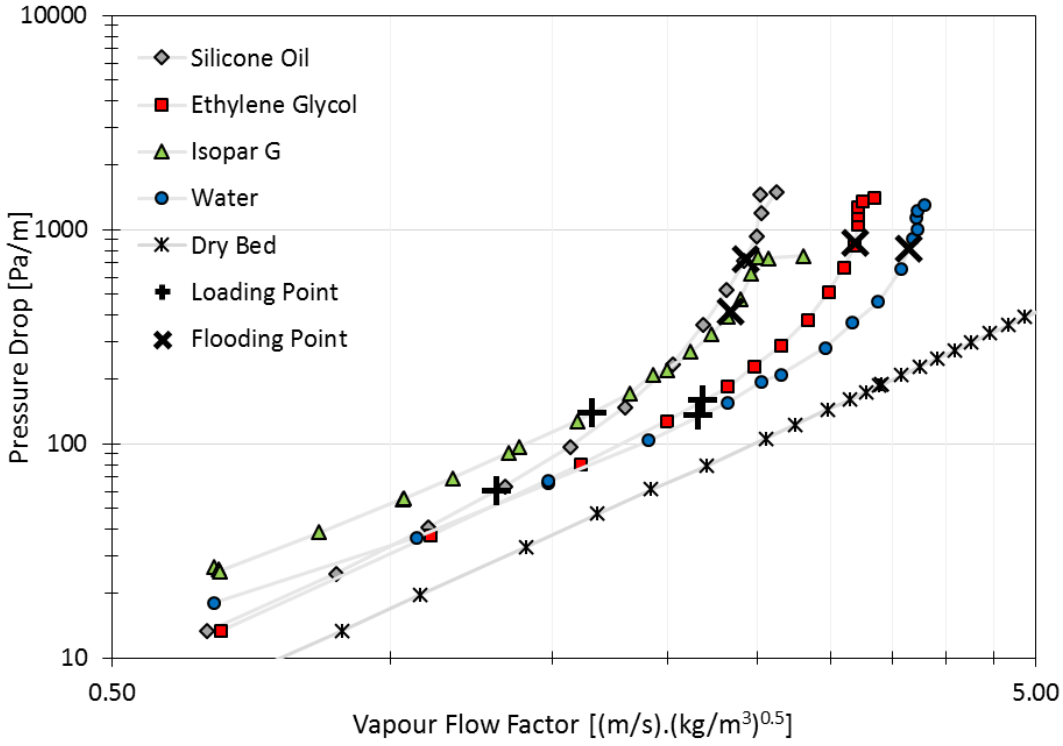

Figure 9.43: Pressure drop, air, 2.5" Intalox Ultra A at 73 $m^3/(m^2.h)$

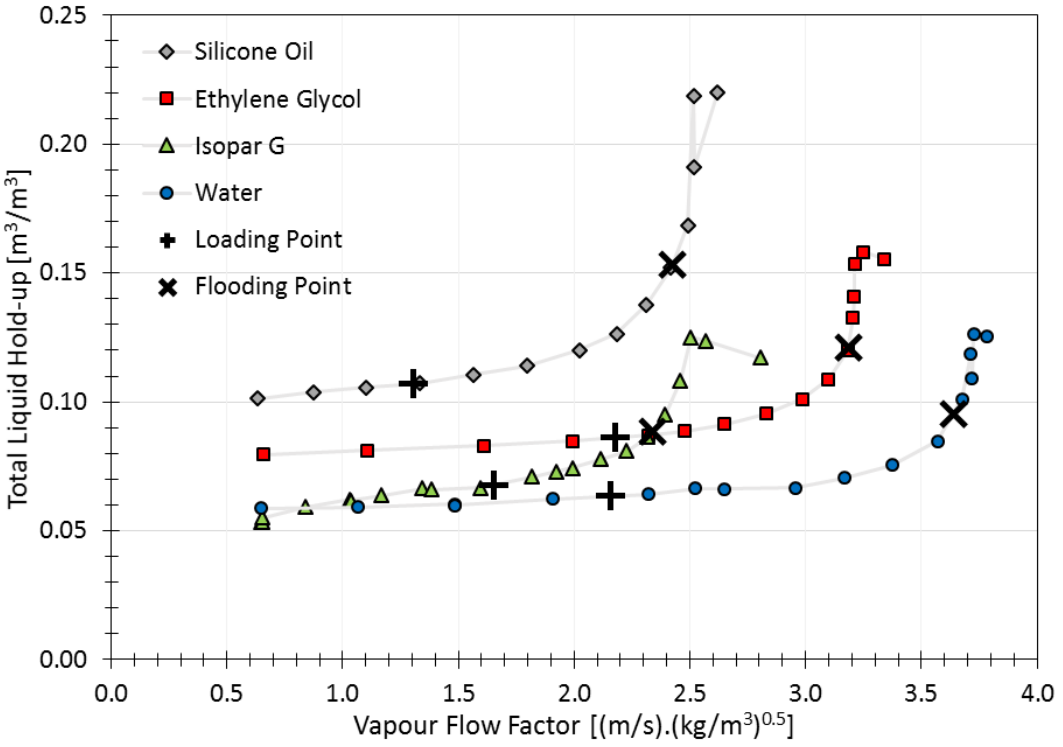

Figure 9.44: Liquid hold-up, air, 2.5" Intalox Ultra A at 73 $m^3/(m^2.h)$

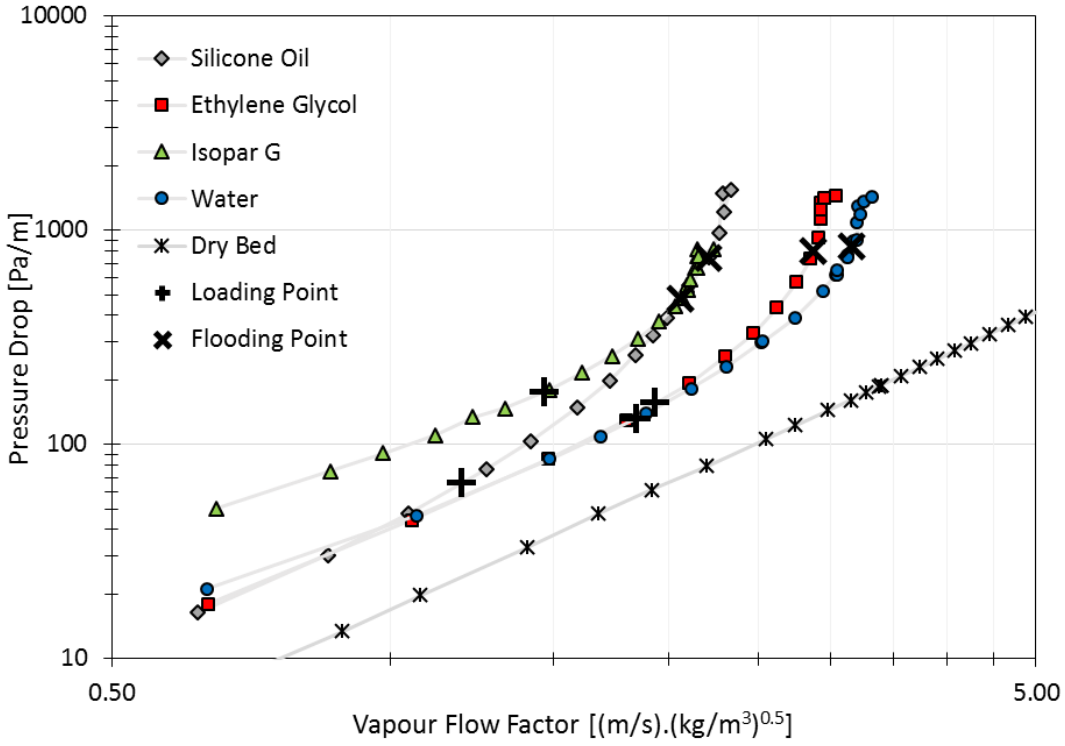

Figure 9.45: Pressure drop, air, 2.5" Intalox Ultra A at 98 $m^3/(m^2.h)$

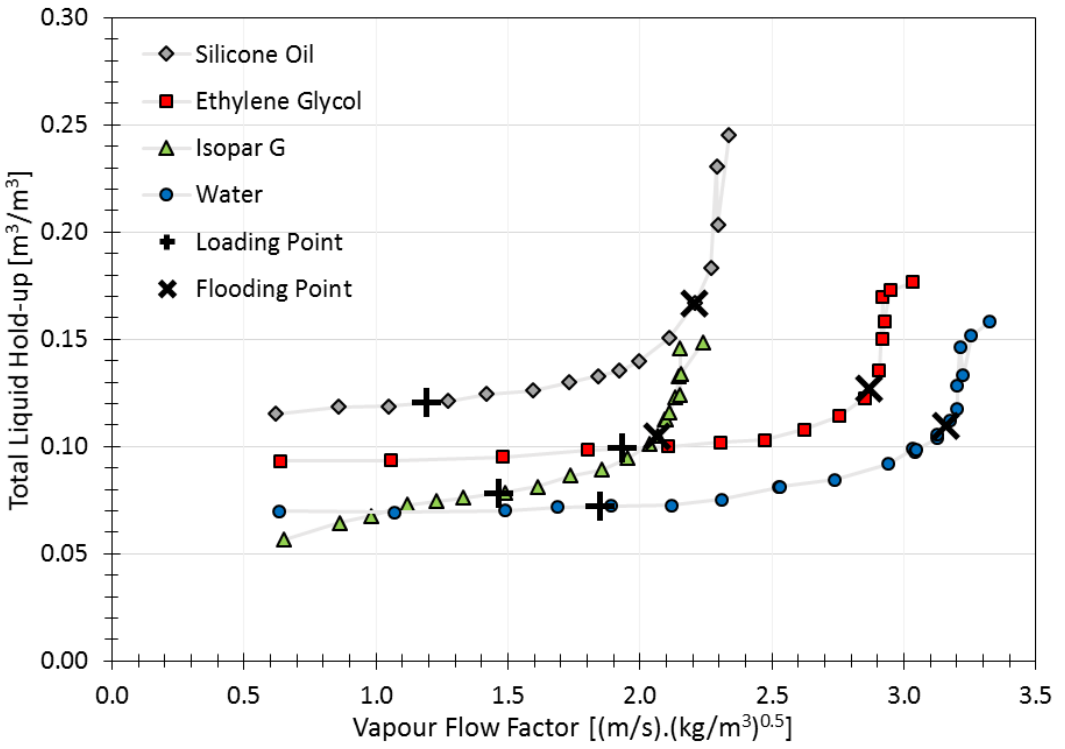

Figure 9.46: Liquid hold-up, air, 2.5" Intalox Ultra A at 98 $m^3/(m^2.h)$

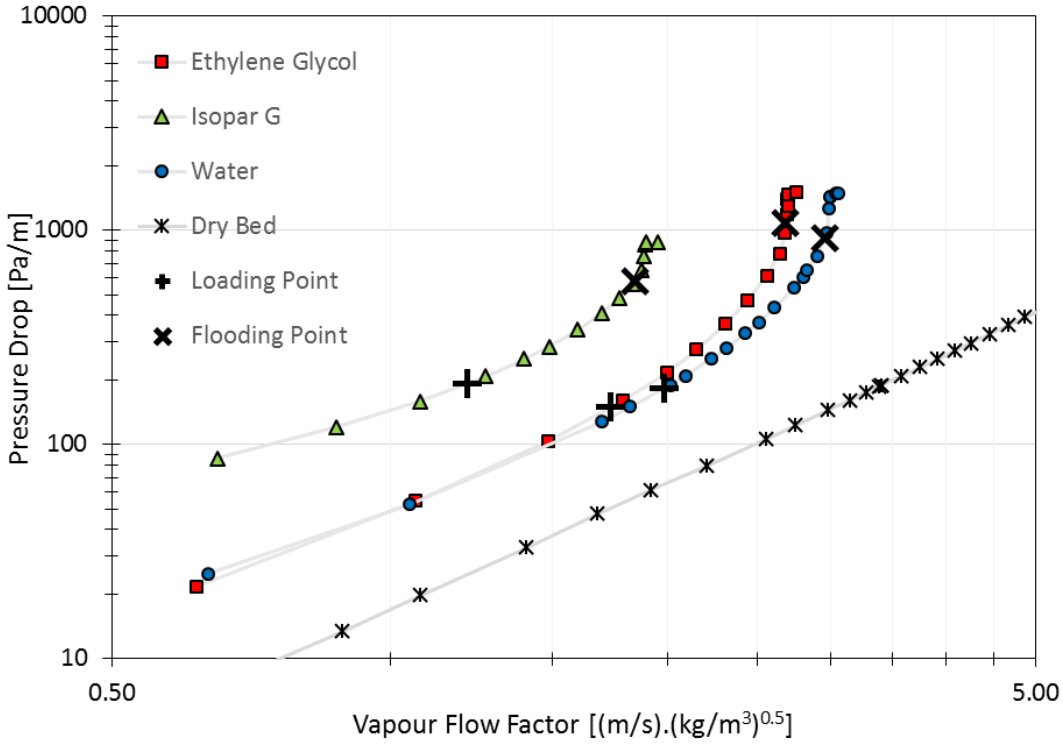

Figure 9.47: Pressure drop, air, 2.5" Intalox Ultra A at 122 $m^3/(m^2.h)$

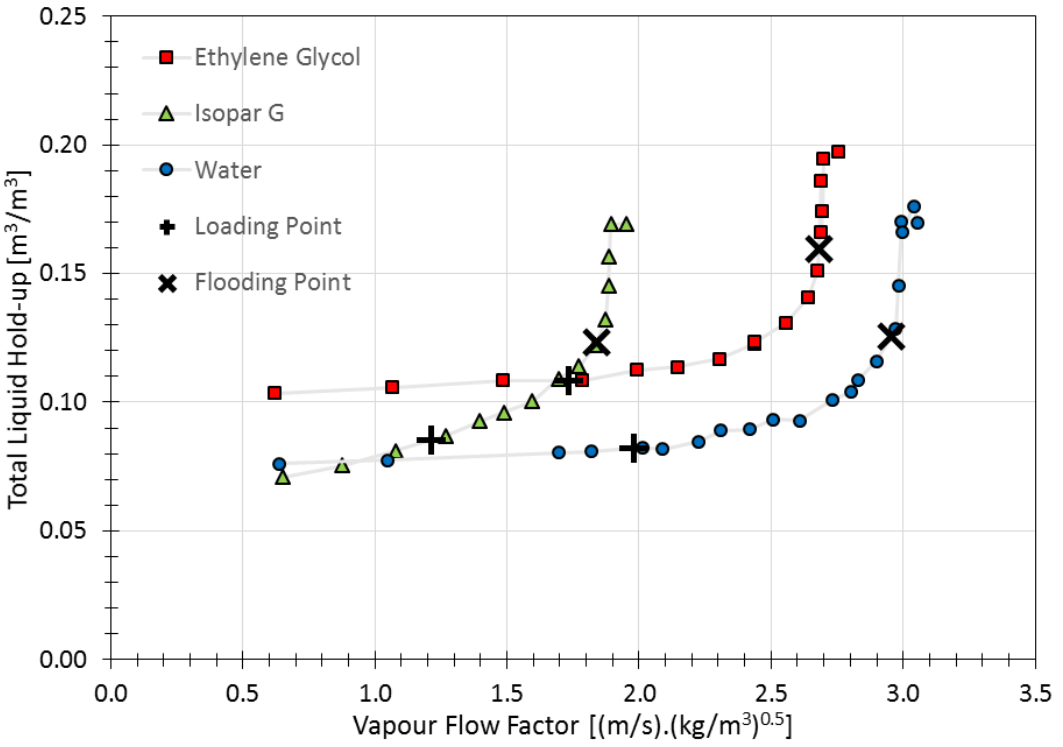

Figure 9.48: Liquid hold-up, air, 2.5" Intalox Ultra A at 122 $m^3/(m^2.h)$

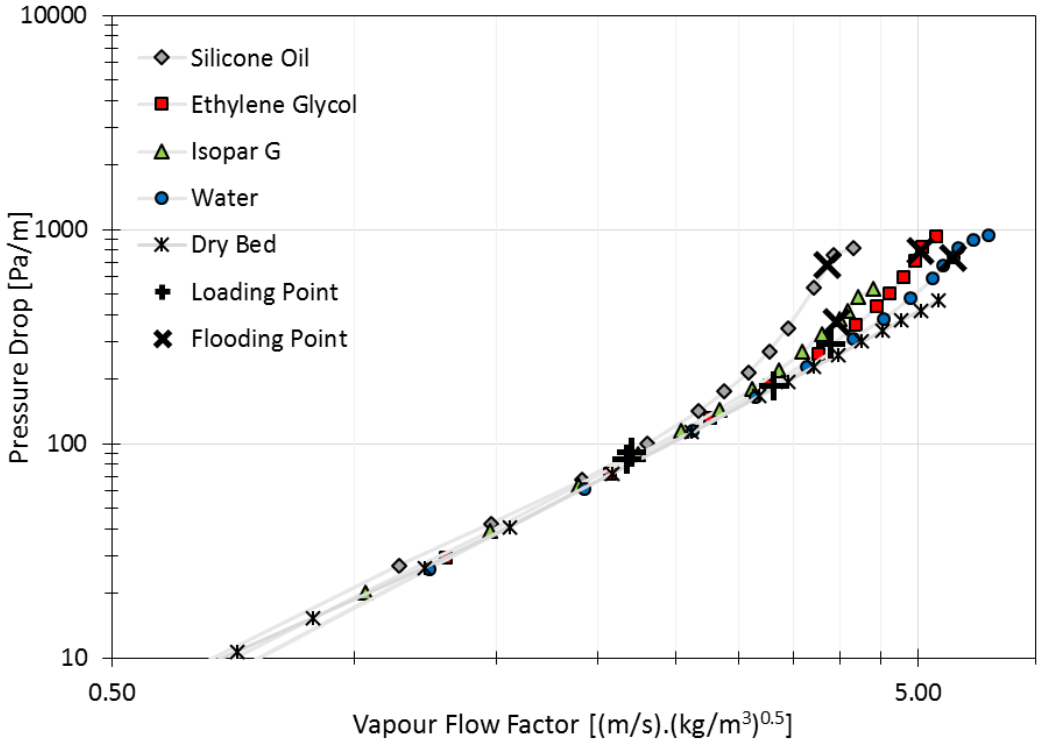

Figure 9.49: Pressure drop, CO_2, 2.5" Intalox Ultra A at 6 $m^3/(m^2.h)$

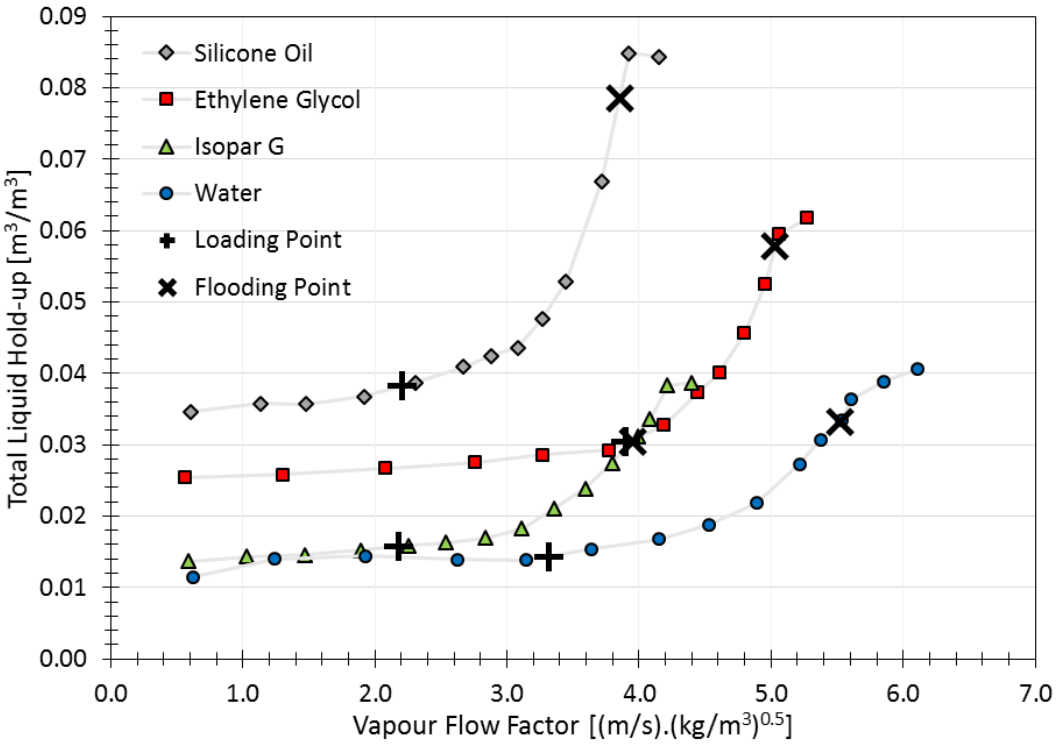

Figure 9.50: Liquid hold-up, CO_2, 2.5" Intalox Ultra A at 6 $m^3/(m^2.h)$

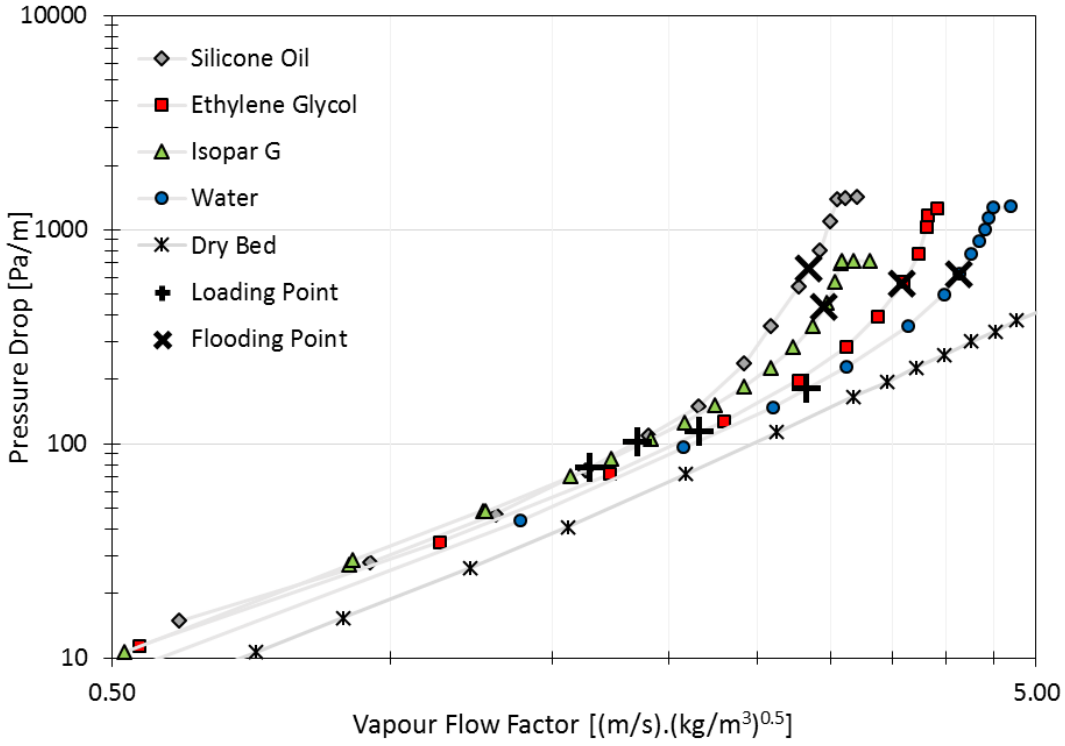

Figure 9.51: Pressure drop, CO_2, 2.5" Intalox Ultra A at 37 $m^3/(m^2.h)$

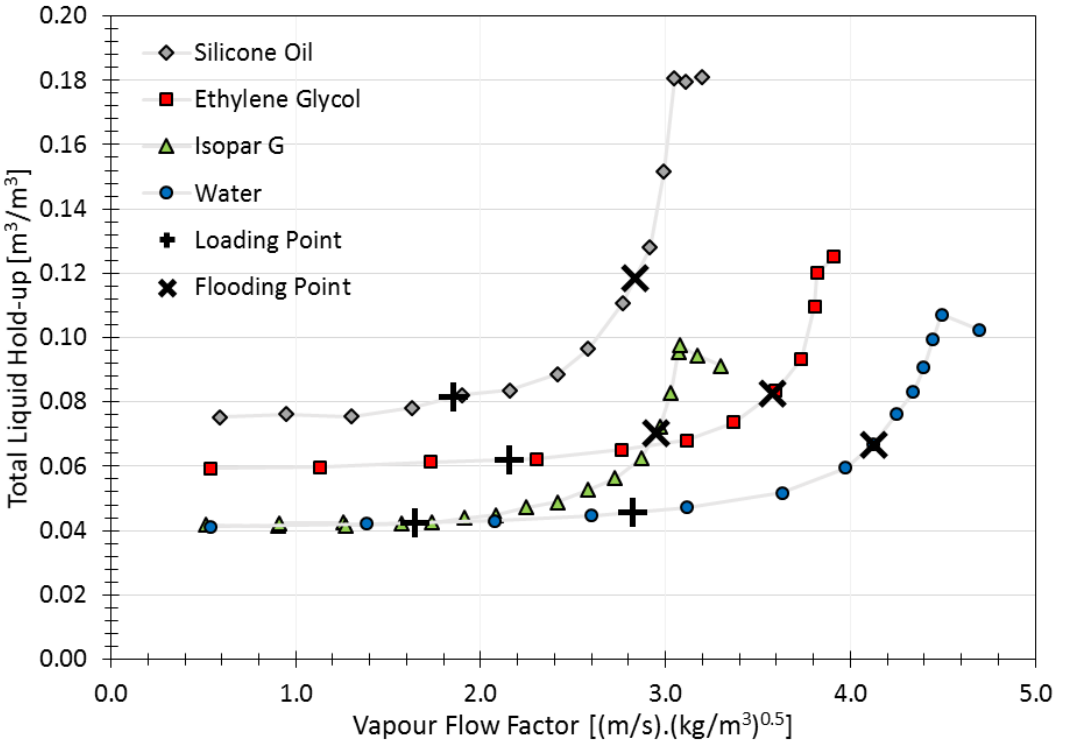

Figure 9.52: Liquid hold-up, CO_2, 2.5" Intalox Ultra A at 37 $m^3/(m^2.h)$

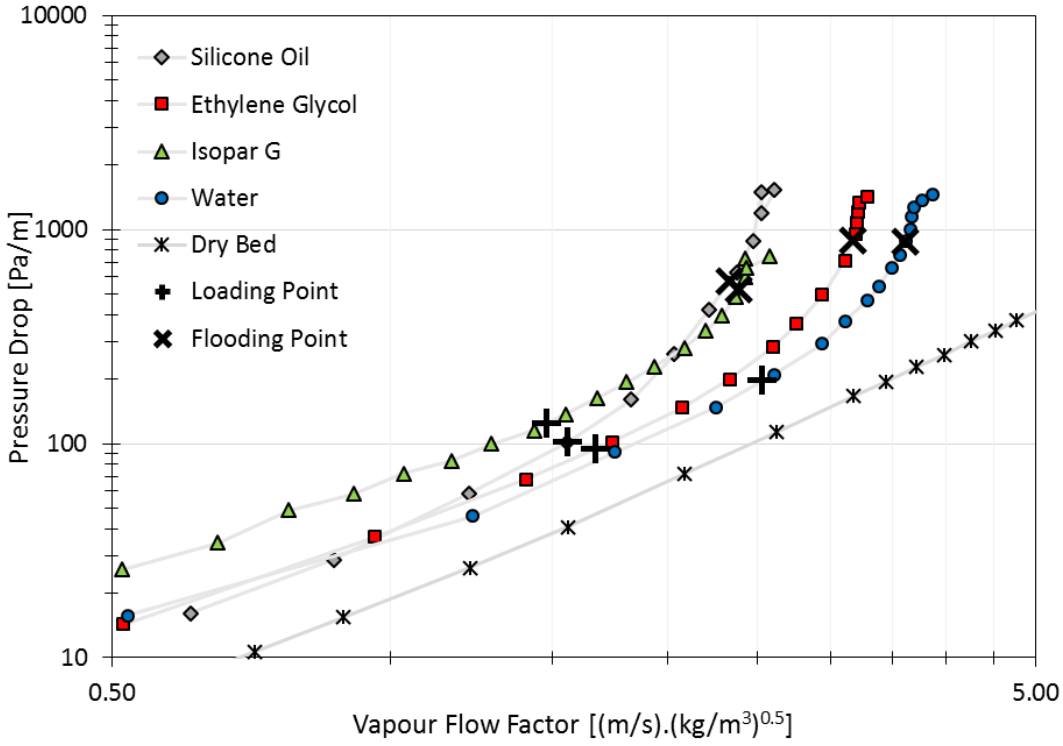

Figure 9.53: Pressure drop, CO_2, 2.5" Intalox Ultra A at 73 $m^3/(m^2.h)$

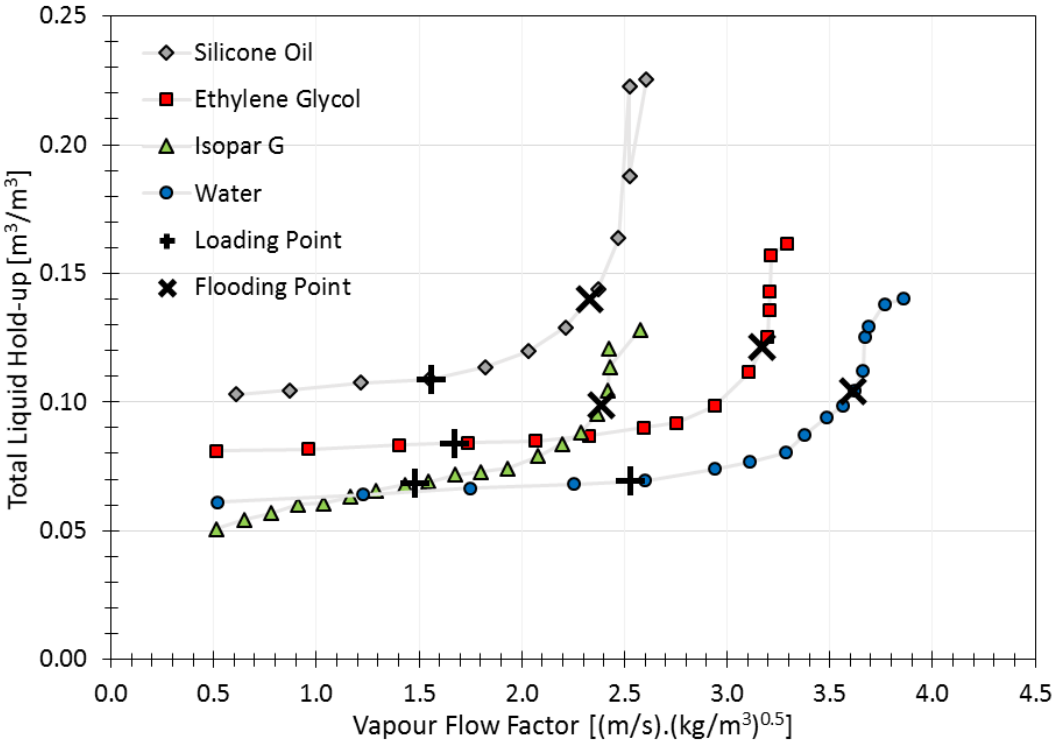

Figure 9.54: Liquid hold-up, CO_2, 2.5" Intalox Ultra A at 73 $m^3/(m^2.h)$

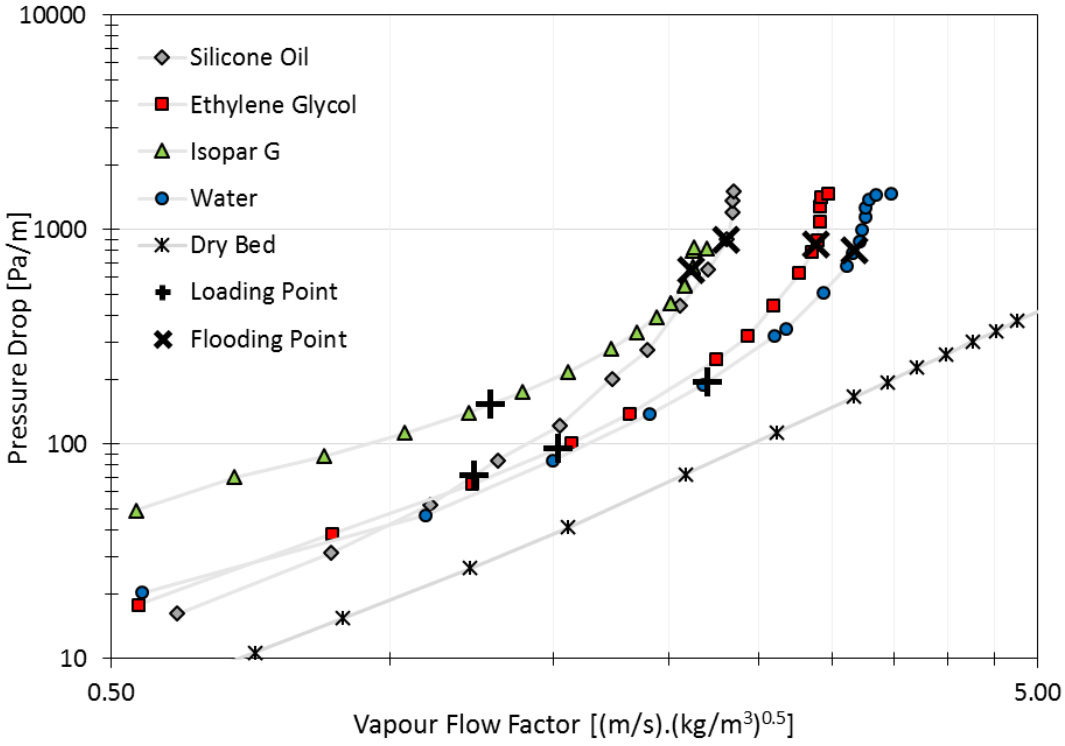

Figure 9.55: Pressure drop, CO_2, 2.5" Intalox Ultra A at 98 $m^3/(m^2.h)$

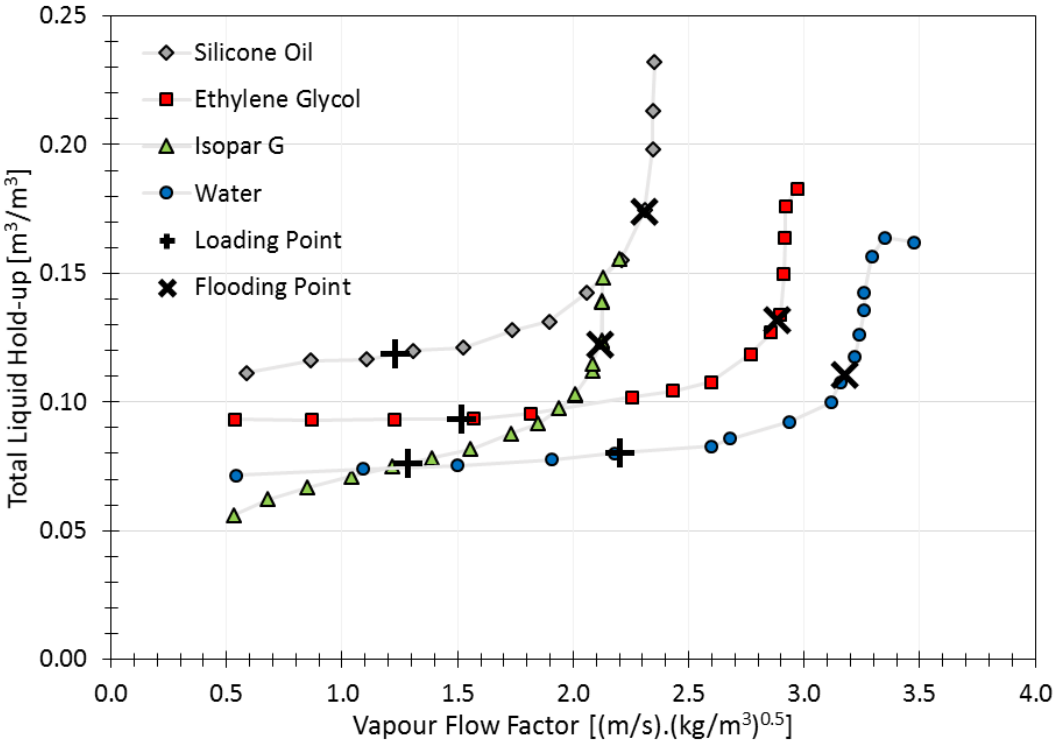

Figure 9.56: Liquid hold-up, CO_2, 2.5" Intalox Ultra A at 98 $m^3/(m^2.h)$

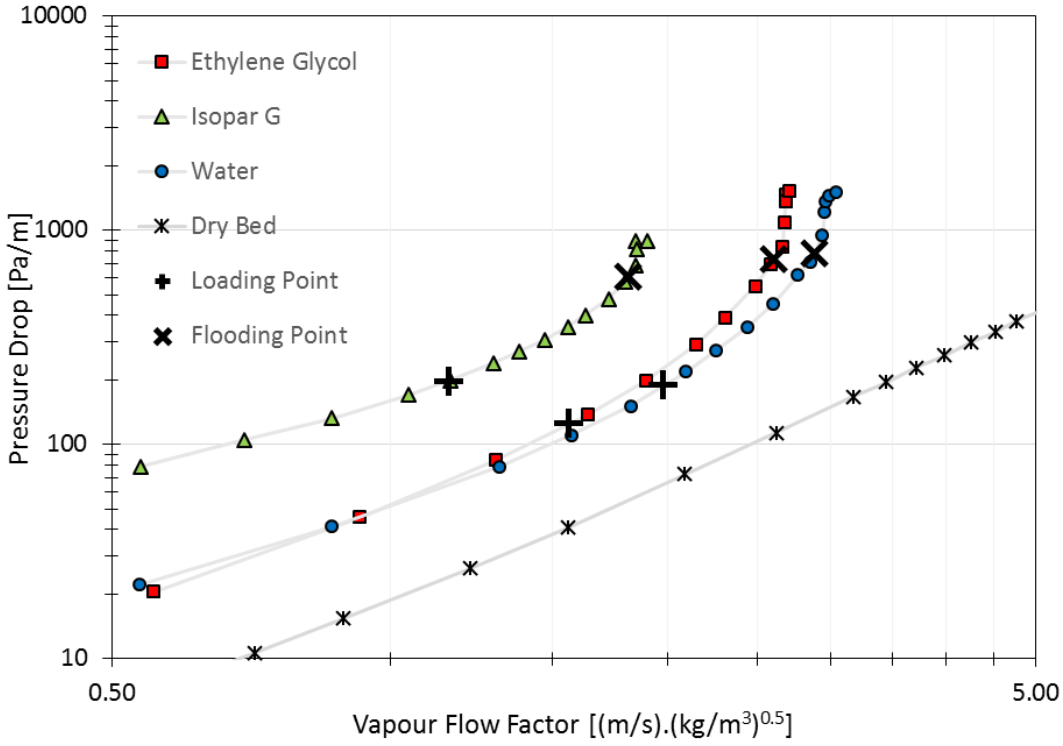

Figure 9.57: Pressure drop, CO_2, 2.5" Intalox Ultra A at 122 $m^3/(m^2.h)$

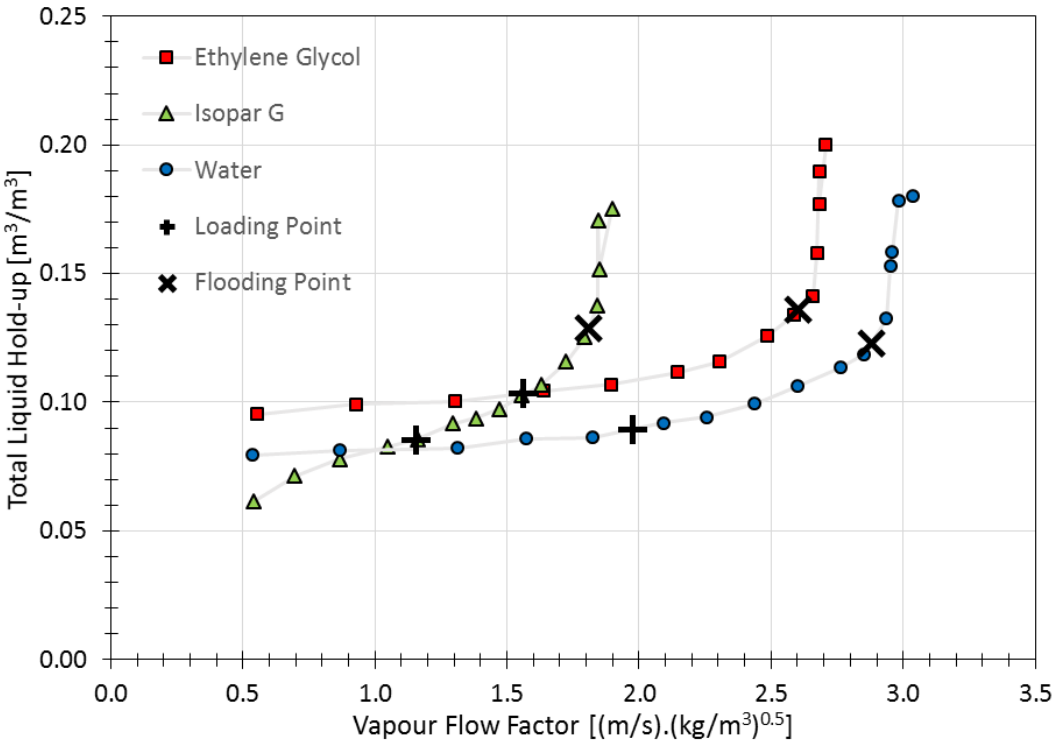

Figure 9.58: Liquid hold-up, CO_2, 2.5" Intalox Ultra A at 122 $m^3/(m^2.h)$

9.11.4 2.5” Intalox Ultra O Entrainment

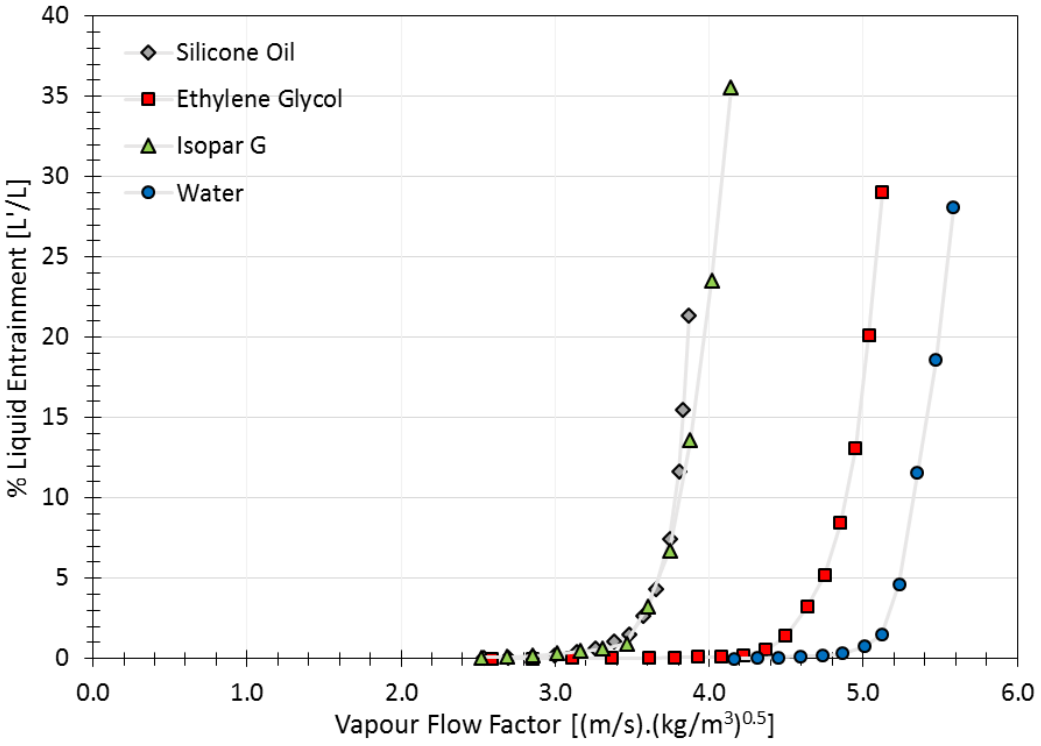

Figure 9.59: Entrainment, air, 2.5" Intalox Ultra A at 6 $m^3/(m^2.h)$

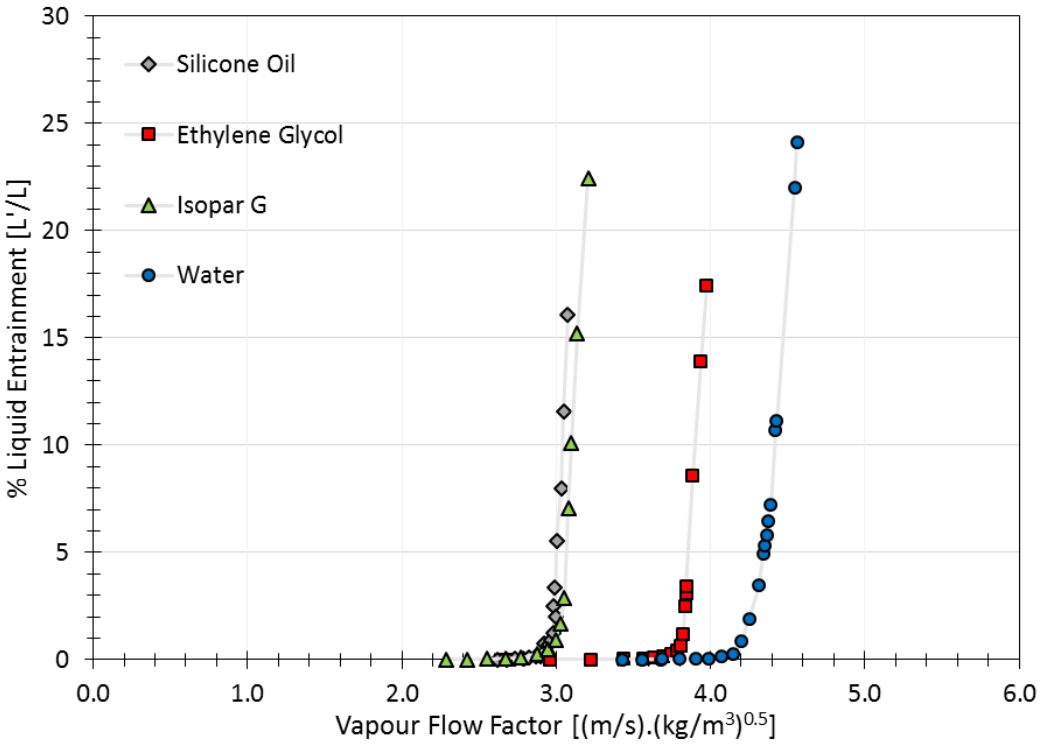

Figure 9.60: Entrainment, air, 2.5" Intalox Ultra A at 37 $m^3/(m^2.h)$

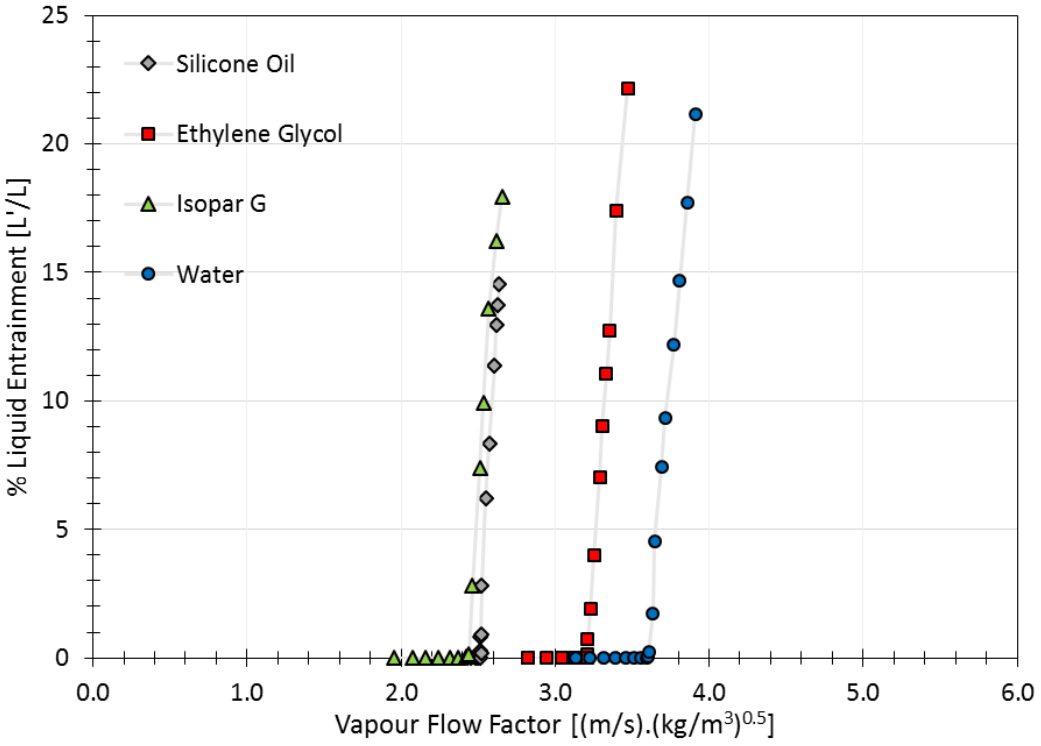

Figure 9.61: Entrainment, air, 2.5" Intalox Ultra A at 73 $m^3/(m^2.h)$

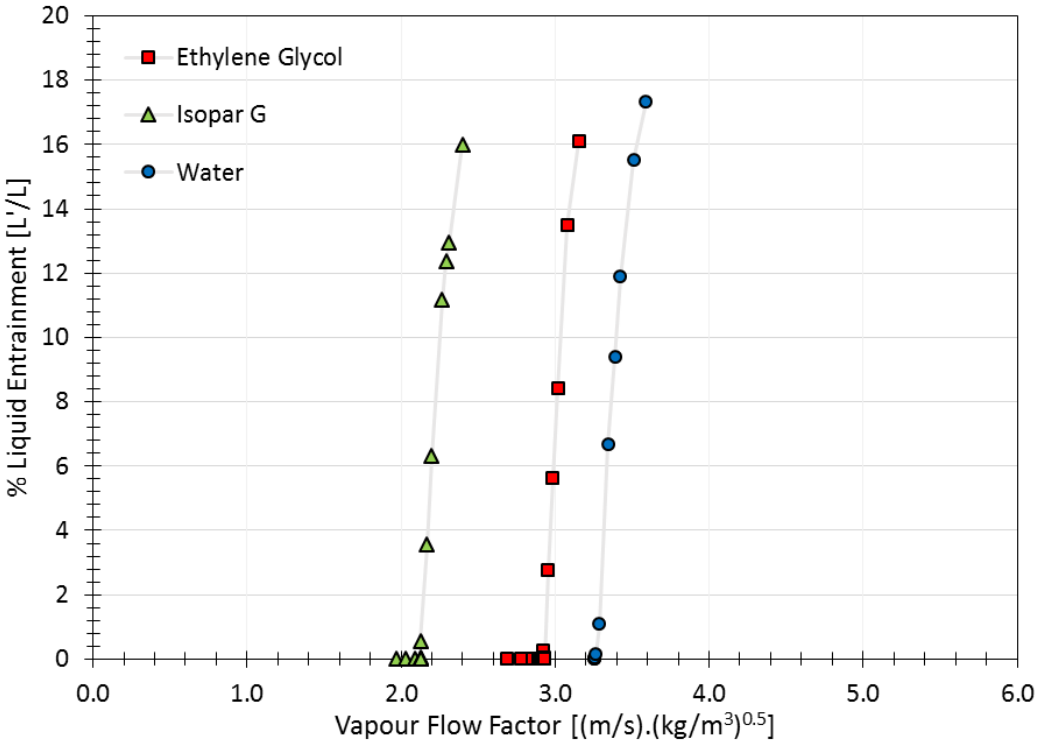

Figure 9.62: Entrainment, air, 2.5" Intalox Ultra A at 98 $m^3/(m^2.h)$

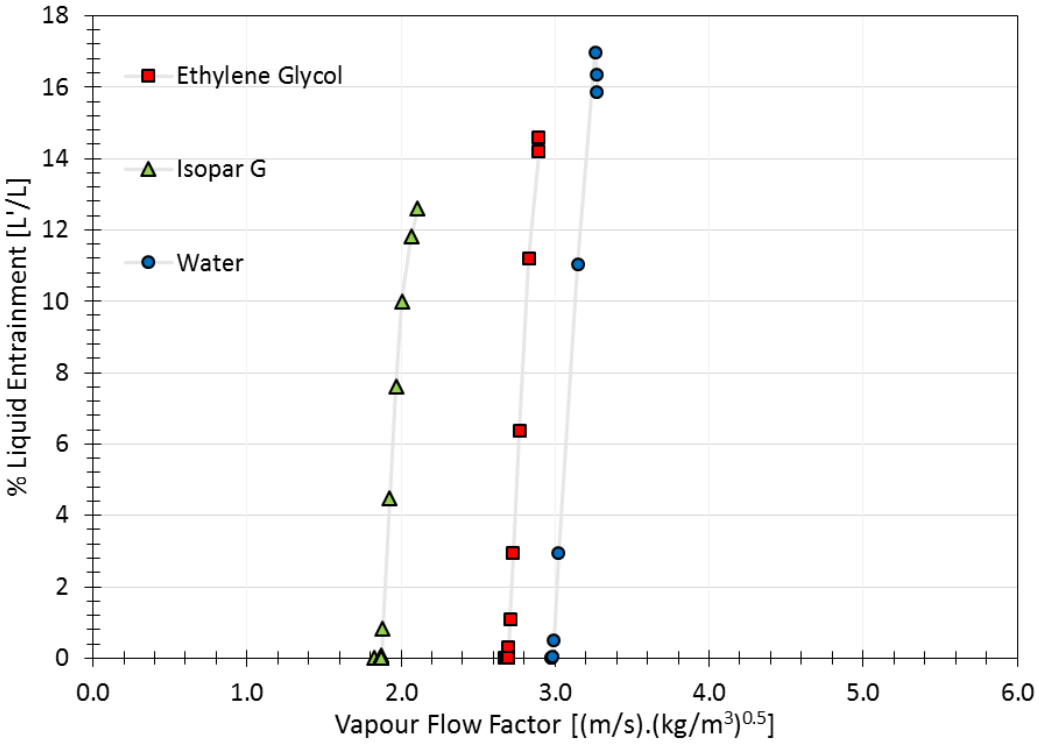

Figure 9.63: Entrainment, air, 2.5" Intalox Ultra A at 122 $m^3/(m^2.h)$

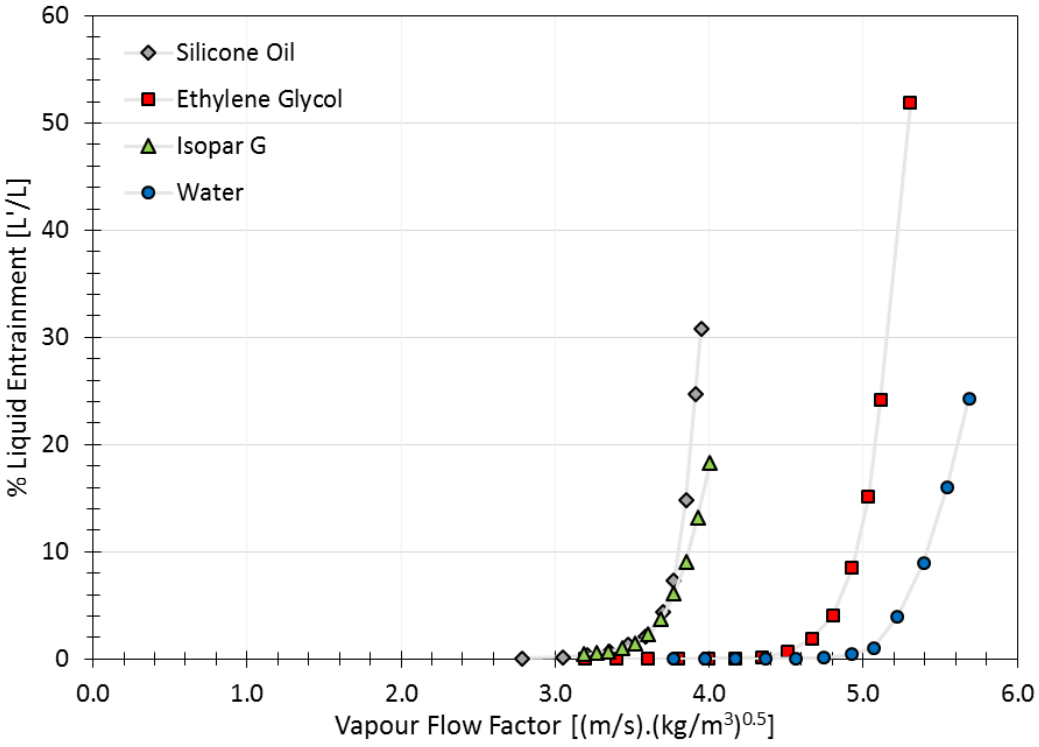

Figure 9.64: Entrainment, CO_2, 2.5" Intalox Ultra A at 6 $m^3/(m^2.h)$

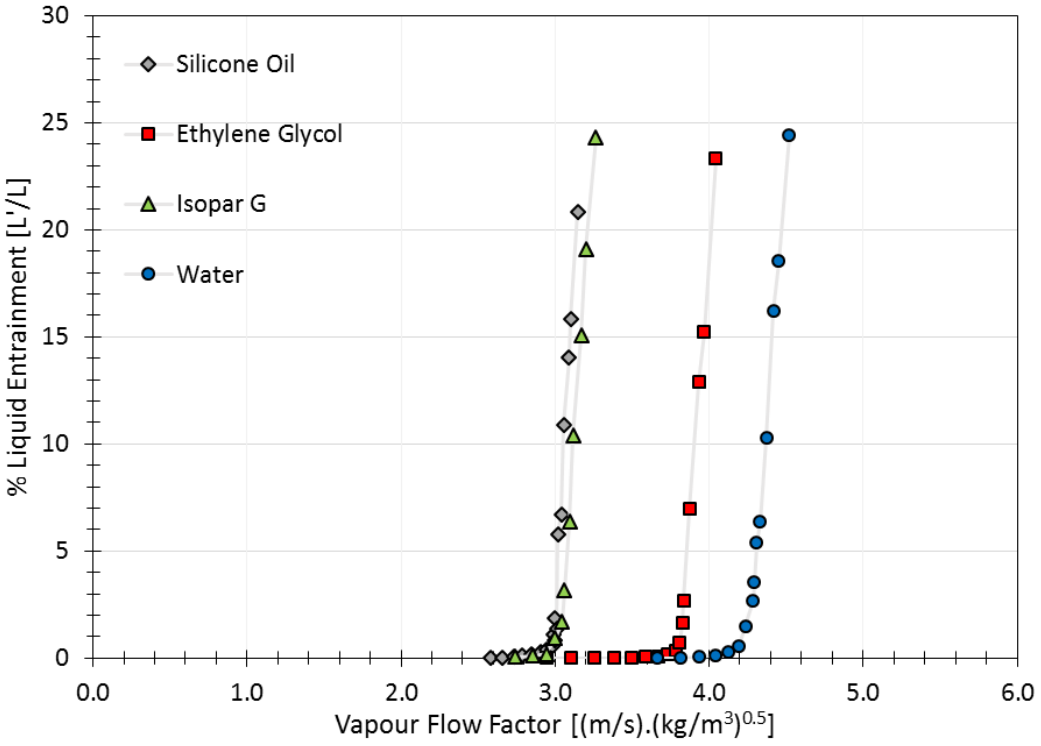

Figure 9.65: Entrainment, CO_2, 2.5" Intalox Ultra A at 37 $m^3/(m^2.h)$

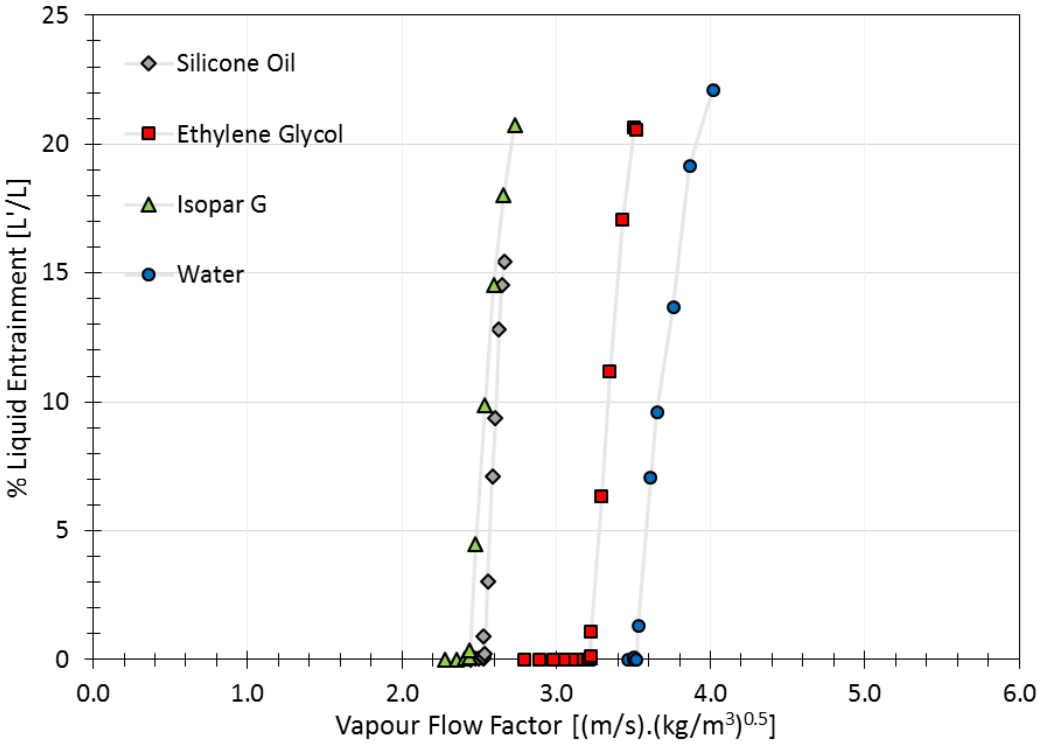

Figure 9.66: Entrainment, CO_2, 2.5" Intalox Ultra A at 73 $m^3/(m^2.h)$

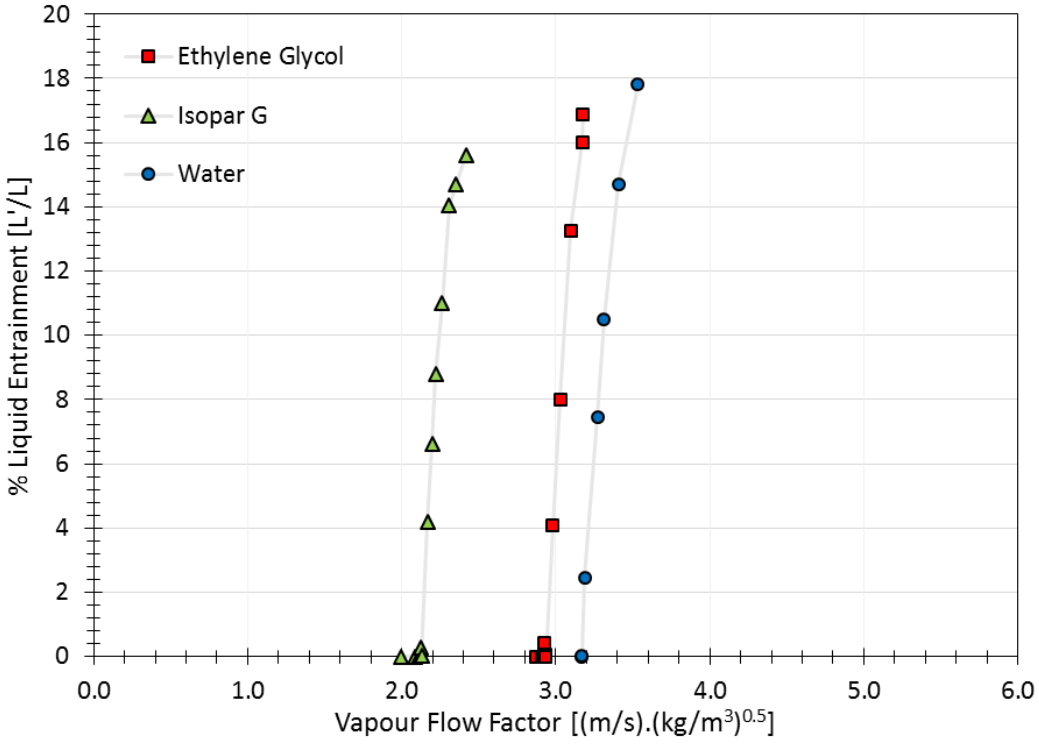

Figure 9.67: Entrainment, CO_2, 2.5" Intalox Ultra A at 98 $m^3/(m^2.h)$

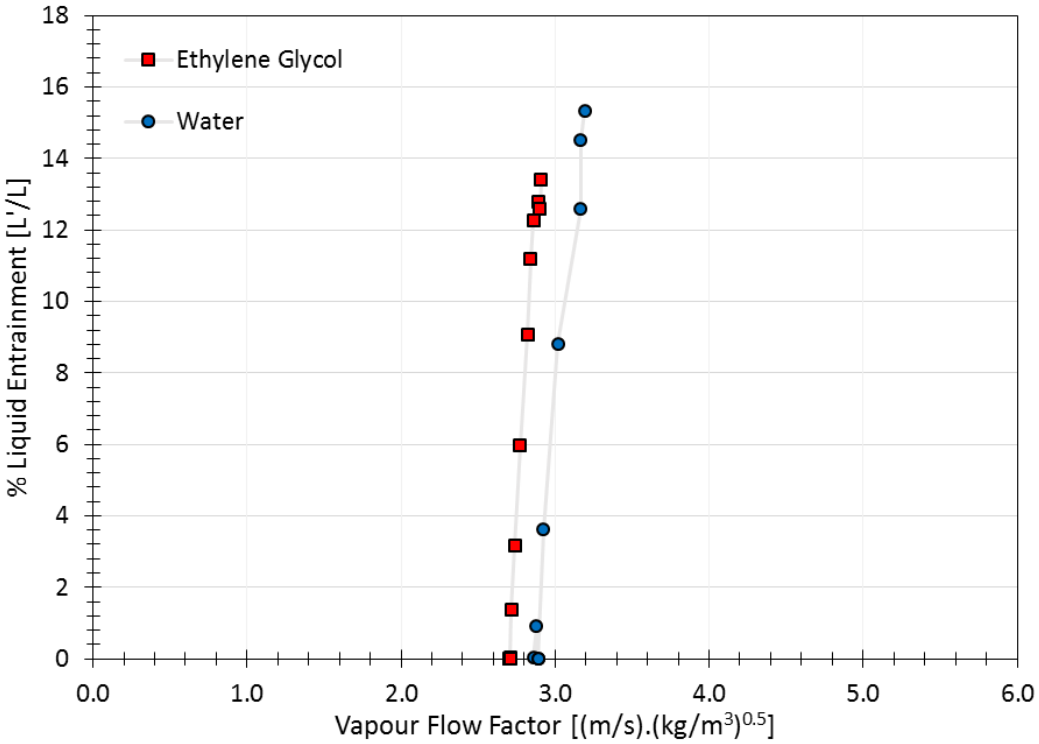

Figure 9.68: Entrainment, CO_2, 2.5" Intalox Ultra A at 122 $m^3/(m^2.h)$

9.12 Hydrodynamic Models Graphs

9.12.1 1.5” Intalox Ultra A

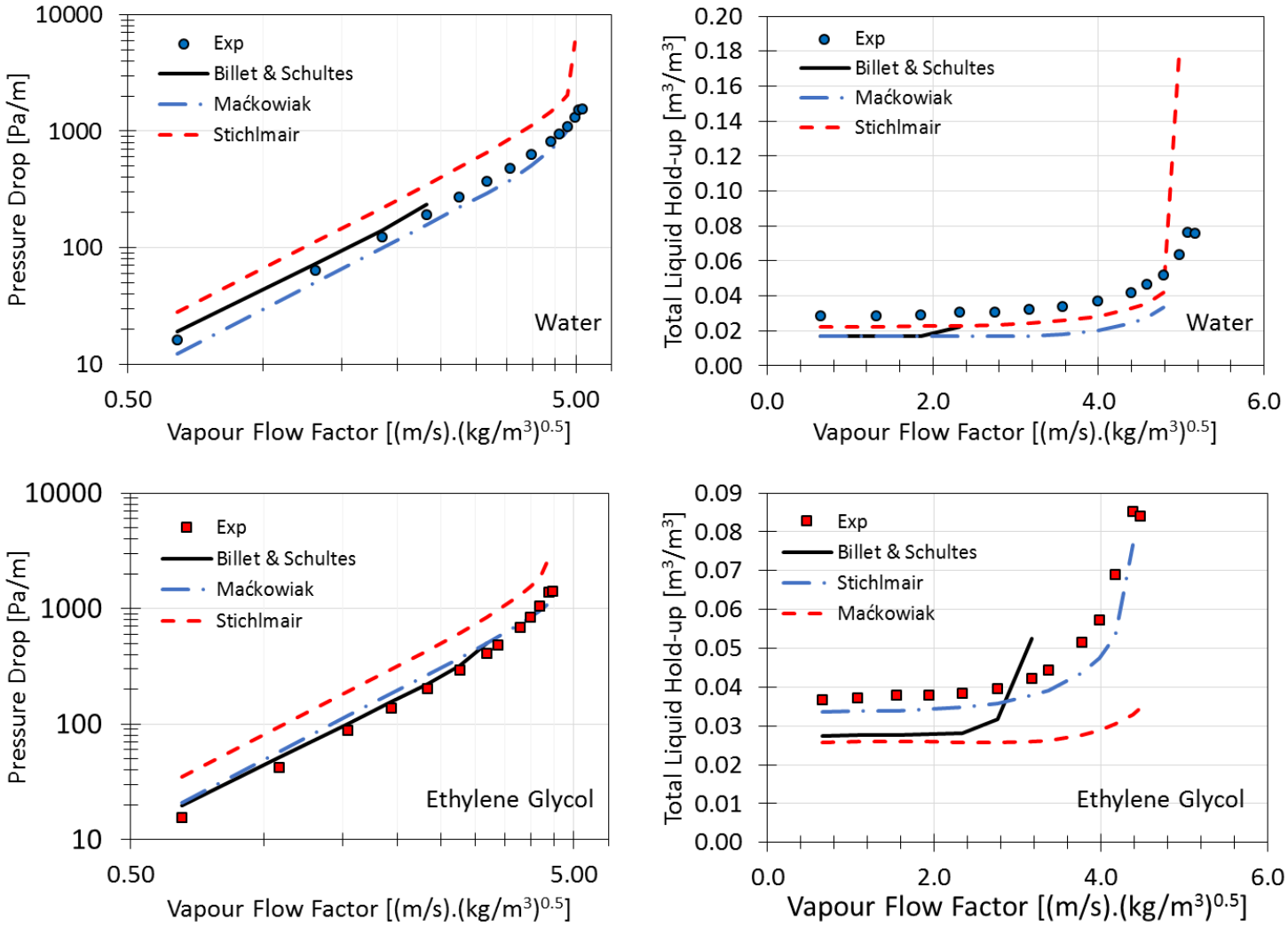

Figure 9.69: Billet & Schultes, Maćkowiak and Stichlmair models, 1.5" Intalox Ultra A, air, water & ethylene glycol at 6 $m^3/(m^2.h)$

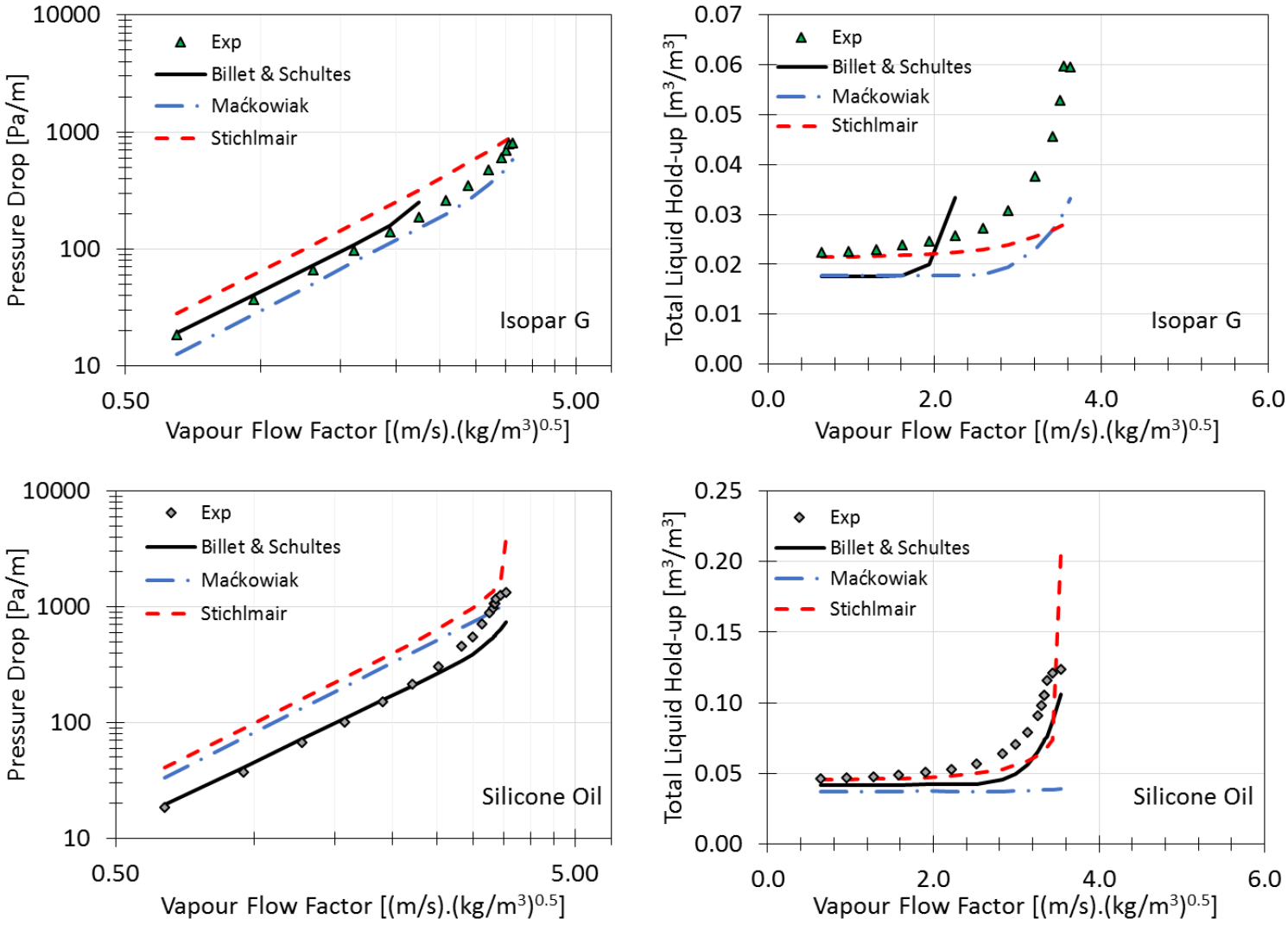

Figure 9.70: Billet & Schultes, Maćkowiak and Stichlmair models, 1.5" Intalox Ultra A, air, Isopar G & silicone oil at 6 $m^3/(m^2.h)$

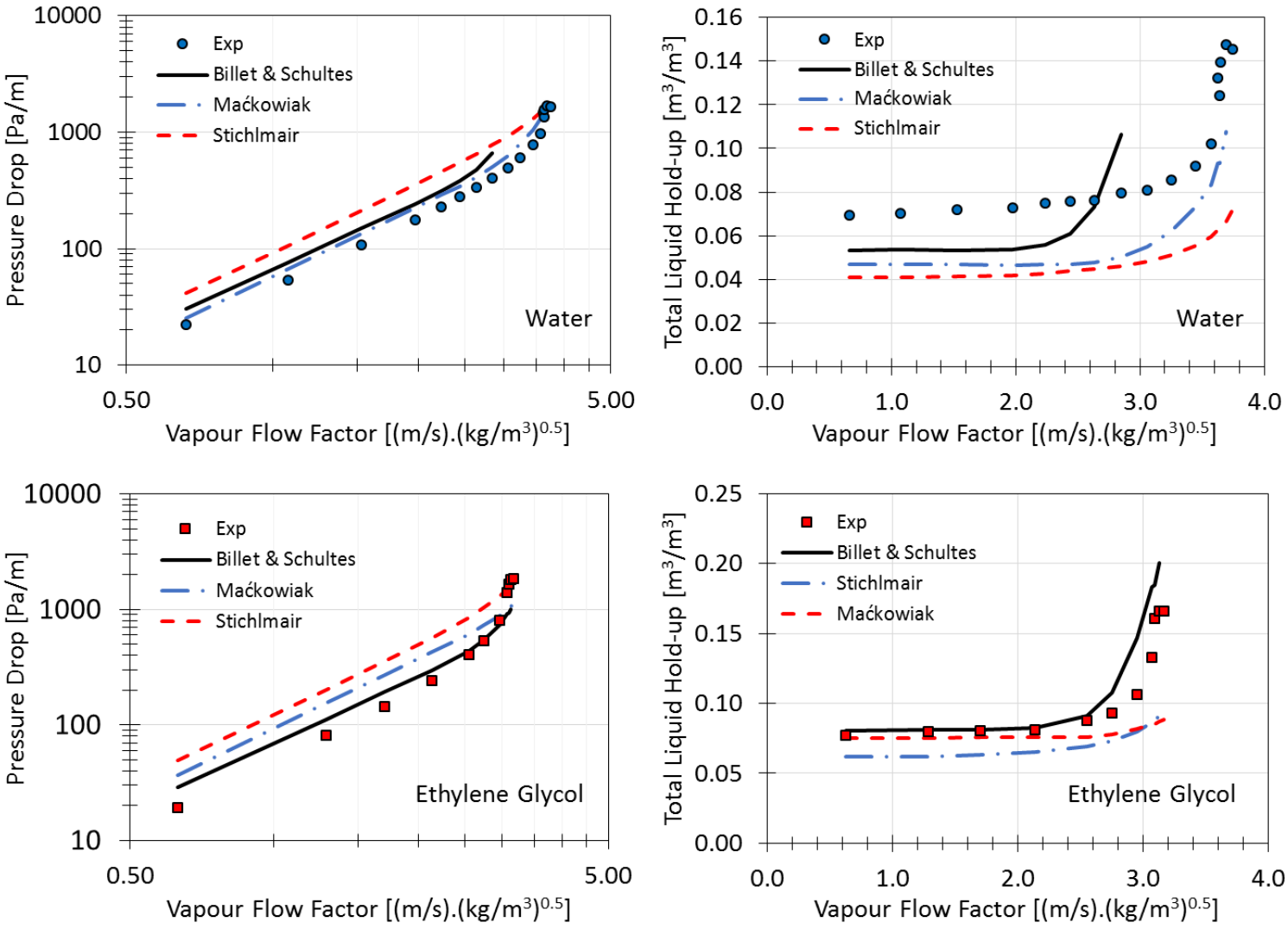

Figure 9.71: Billet & Schultes, Maćkowiak and Stichlmair models, 1.5" Intalox Ultra A, air, water & ethylene glycol at 37 m³/(m².h)

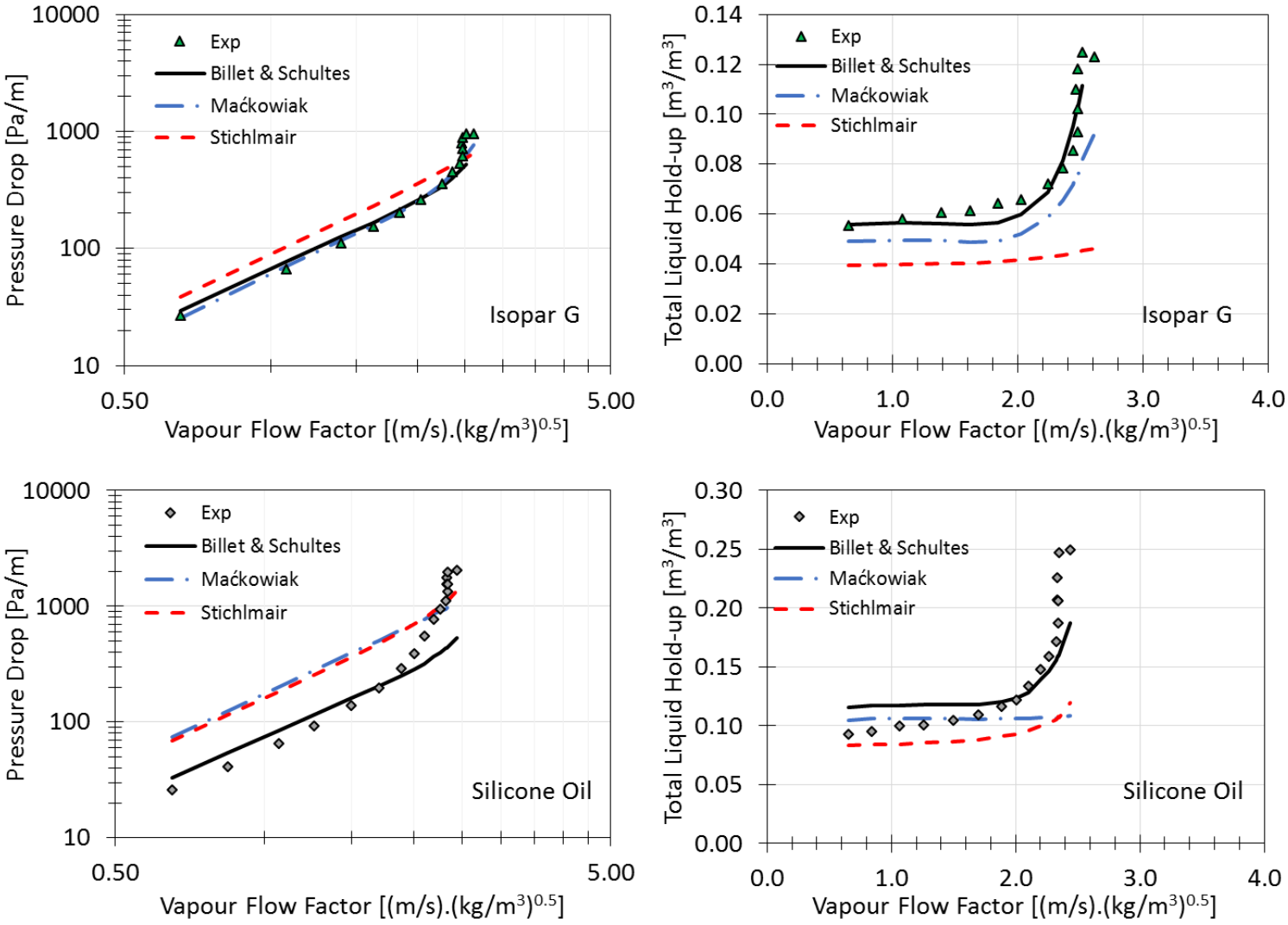

Figure 9.72: Billet & Schultes, Maćkowiak and Stichlmair models, 1.5" Intalox Ultra A, air, Isopar G & silicone oil at 37 $m^3/(m^2.h)$

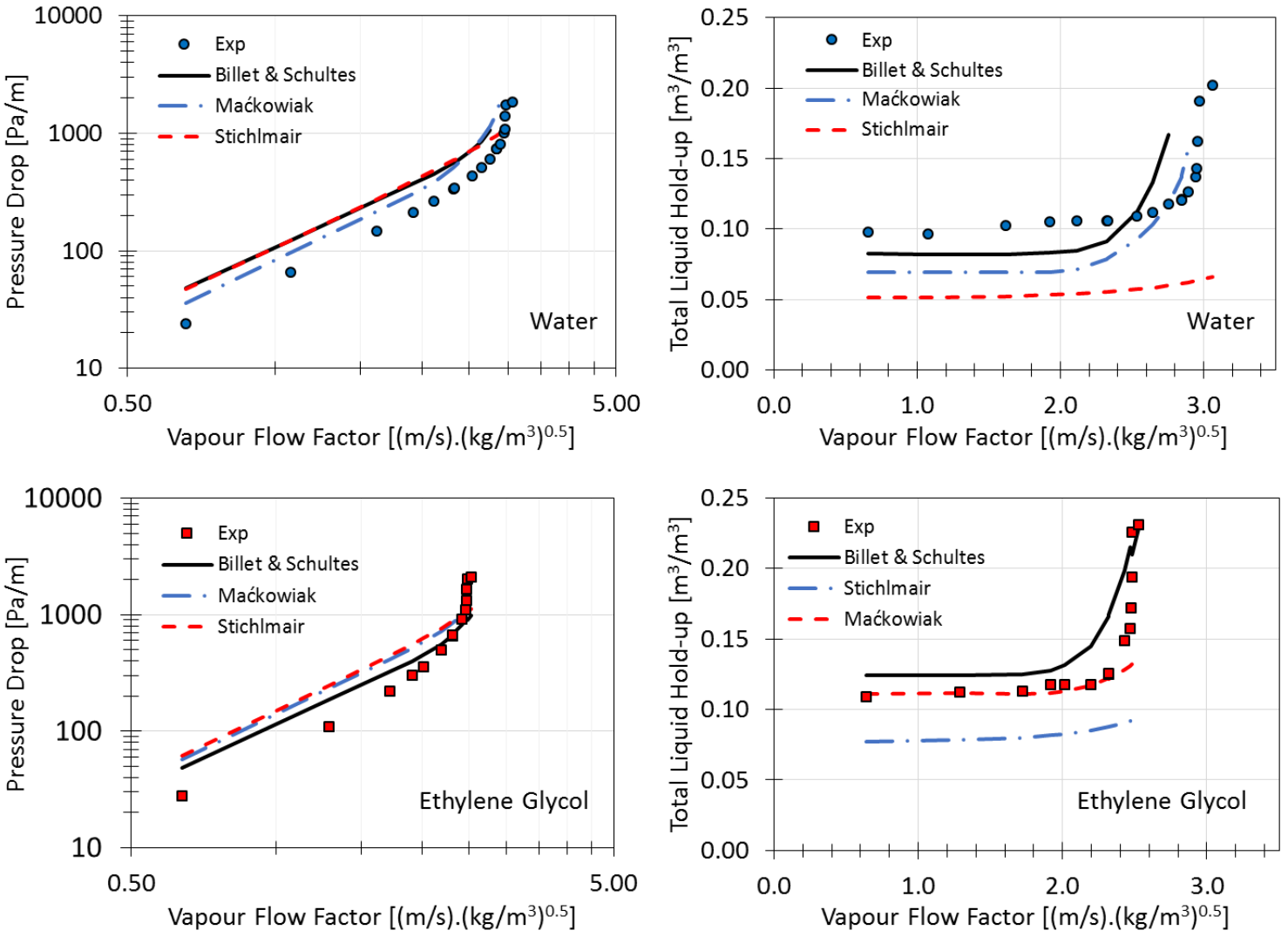

Figure 9.73: Billet & Schultes, Maćkowiak and Stichlmair models, 1.5" Intalox Ultra A, air, water & ethylene glycol at 73 $m^3/(m^2.h)$

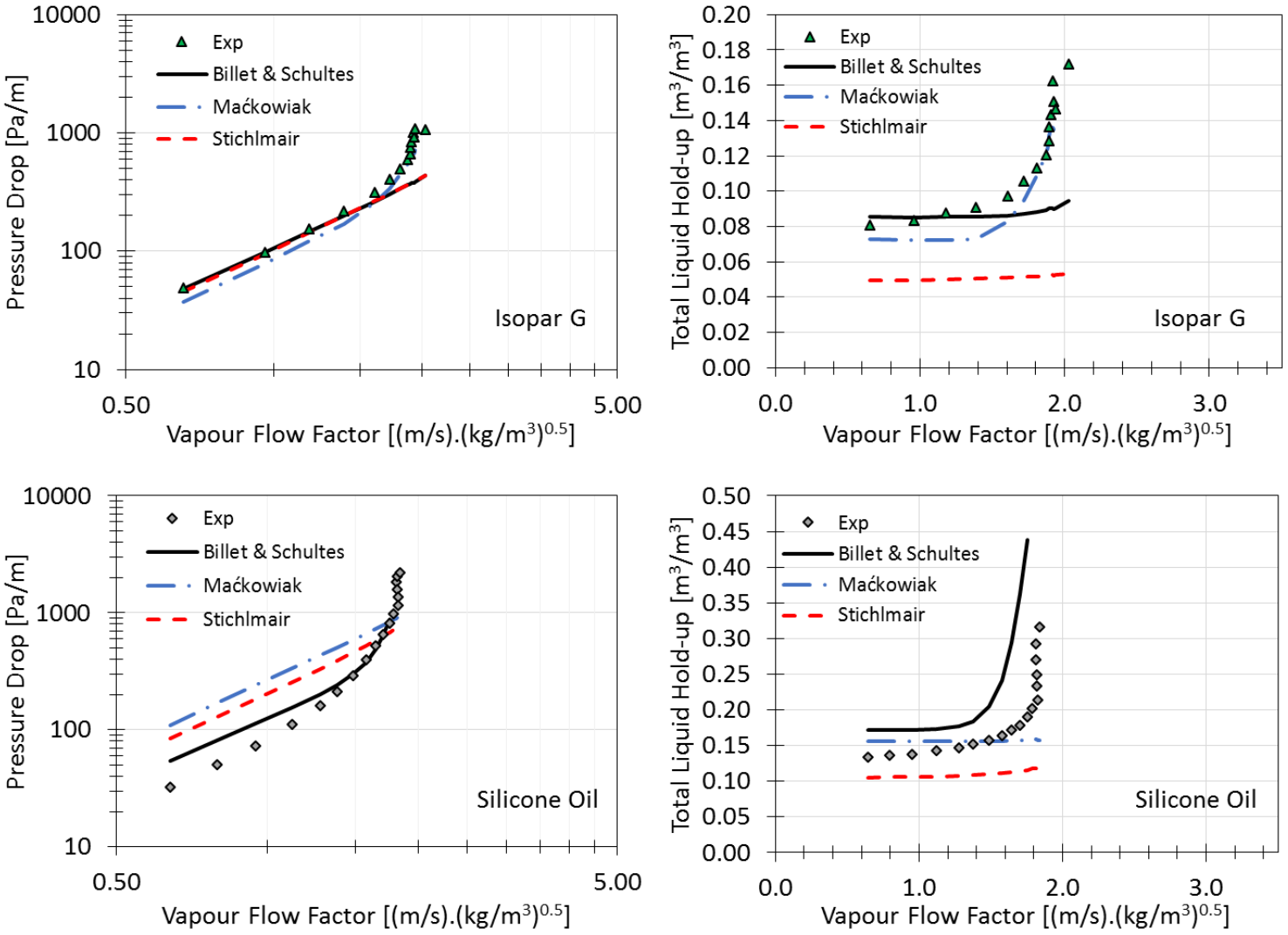

Figure 9.74: Billet & Schultes, Maćkowiak and Stichlmair models, 1.5" Intalox Ultra A, air, Isopar G & silicone oil at 73 $m^3/(m^2.h)$

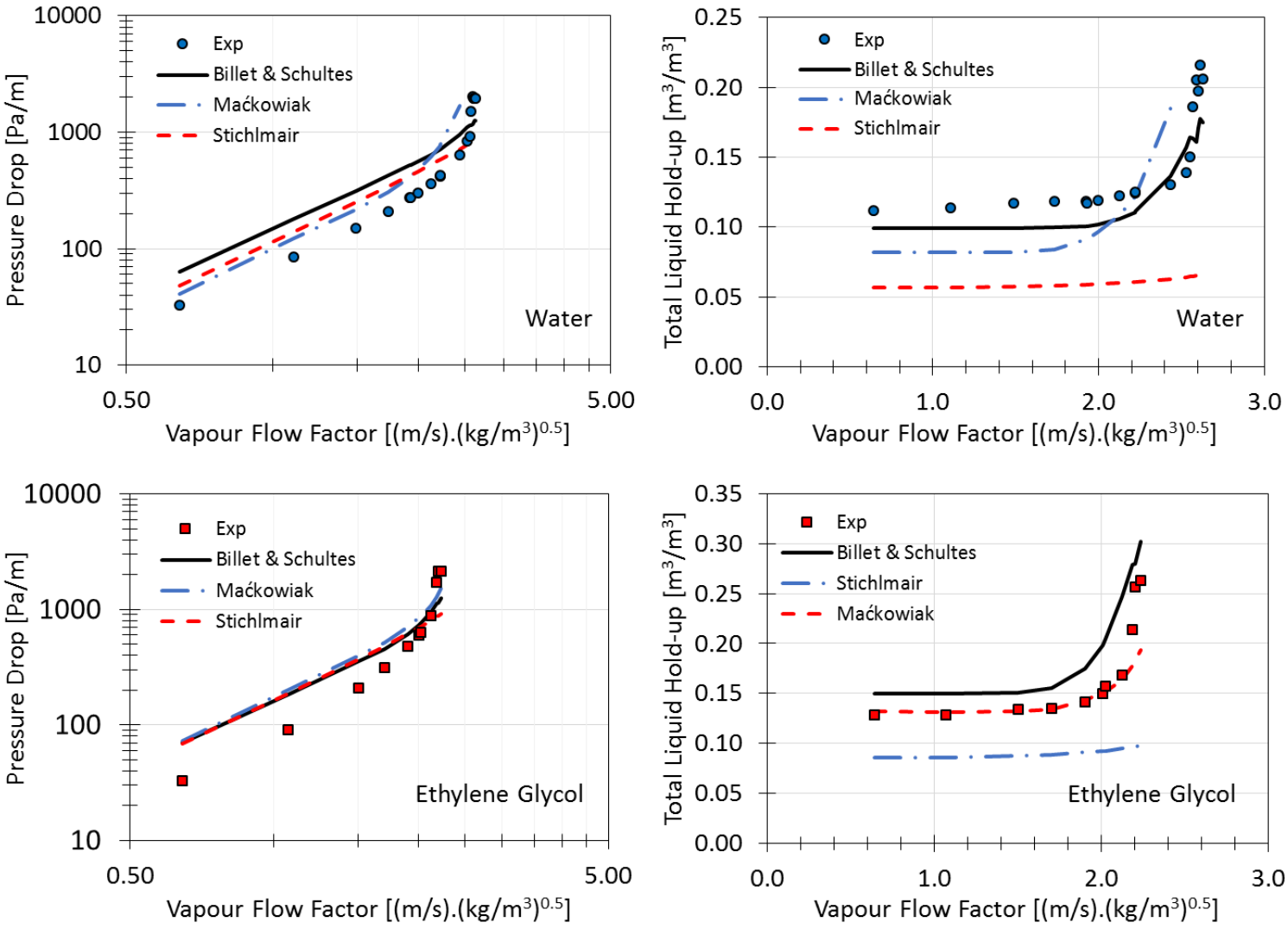

Figure 9.75: Billet & Schultes, Maćkowiak and Stichlmair models, 1.5" Intalox Ultra A, air, water & ethylene glycol at 98 $m^3/(m^2.h)$

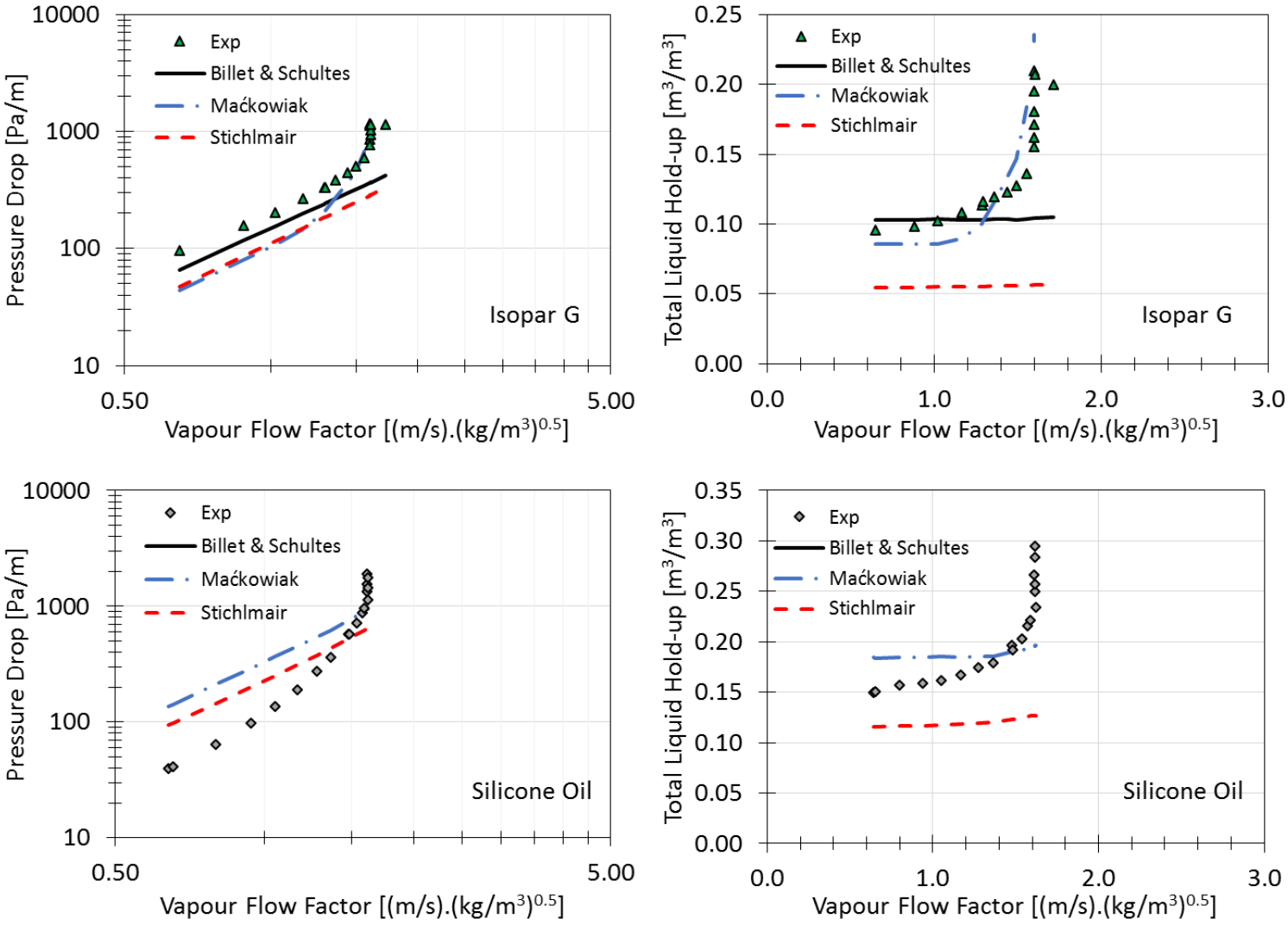

Figure 9.76: Billet & Schultes, Maćkowiak and Stichlmair models, 1.5" Intalox Ultra A, air, Isopar G & silicone oil at 98 $m^3/(m^2.h)$

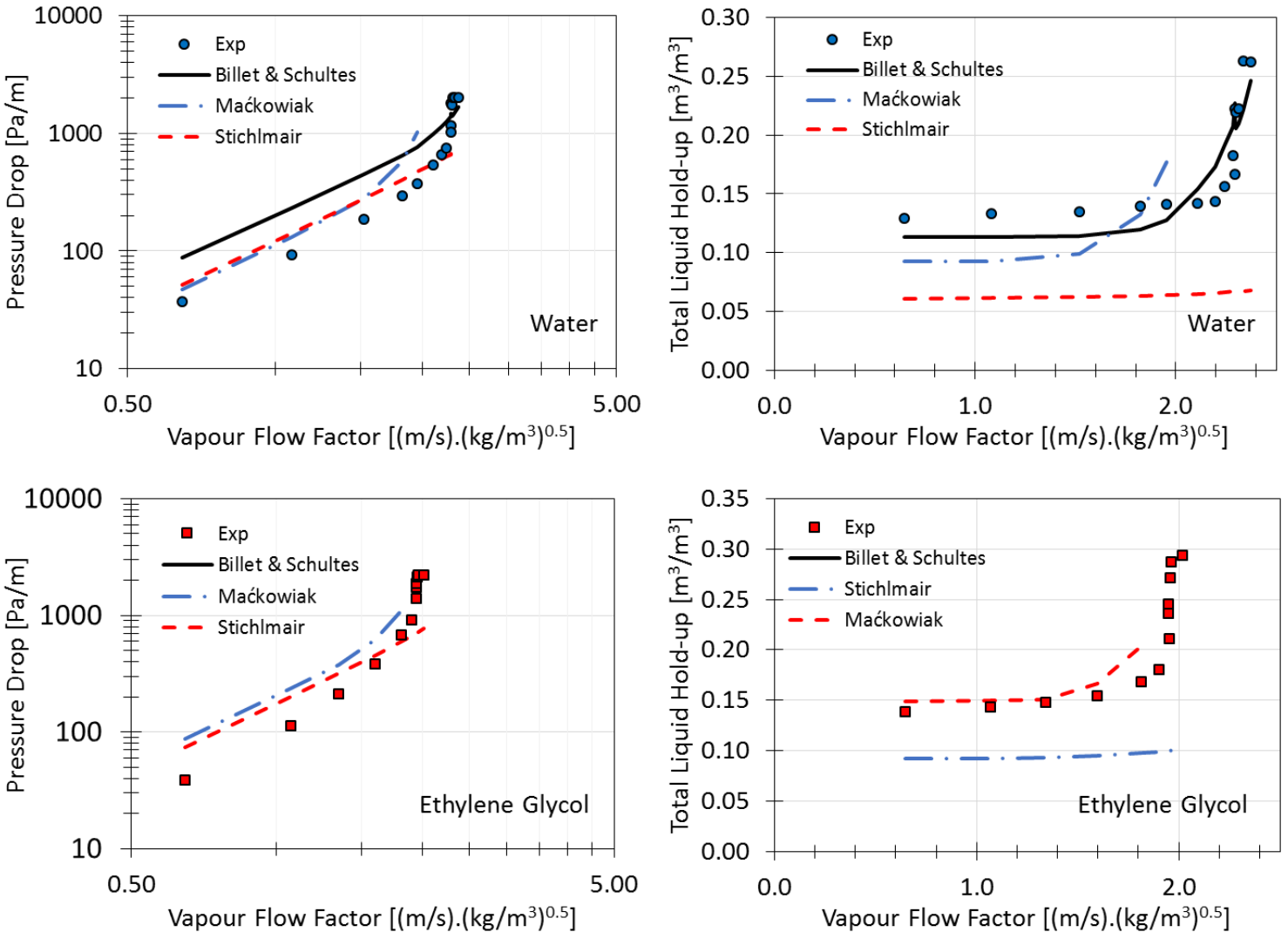

Figure 9.77: Billet & Schultes, Maćkowiak and Stichlmair models, 1.5" Intalox Ultra A, air, water & ethylene glycol at 122 $m^3/(m^2.h)$

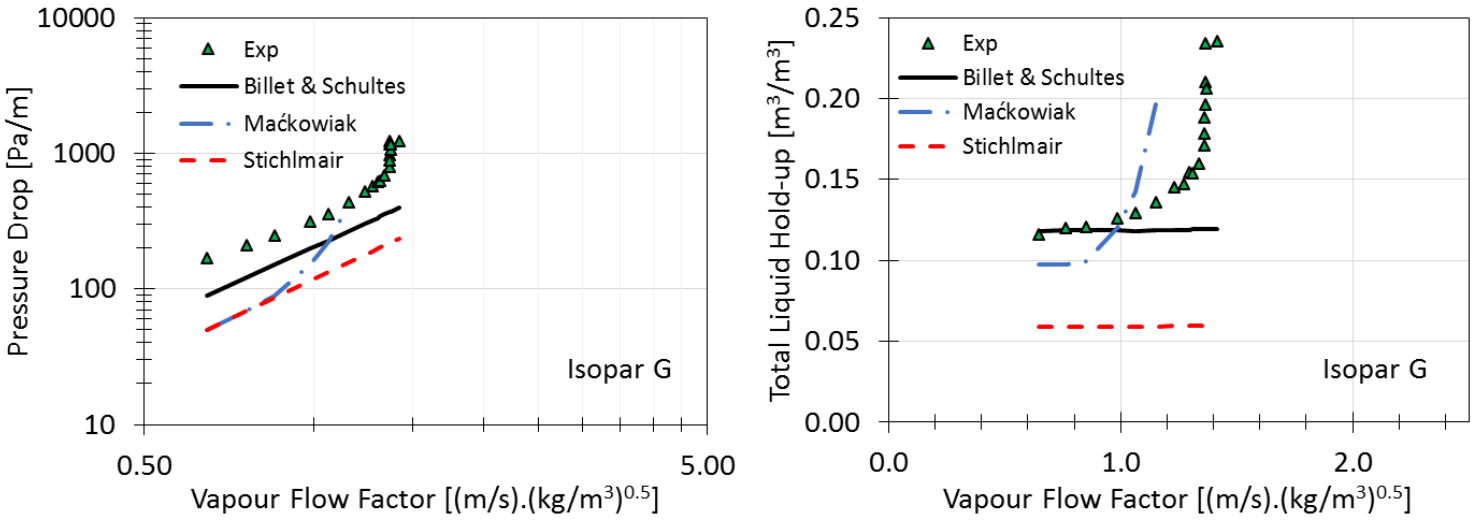

Figure 9.78: Billet & Schultes, Maćkowiak and Stichlmair models, 1.5" Intalox Ultra A, air, Isopar G & silicone oil at 122 $m^3/(m^2.h)$

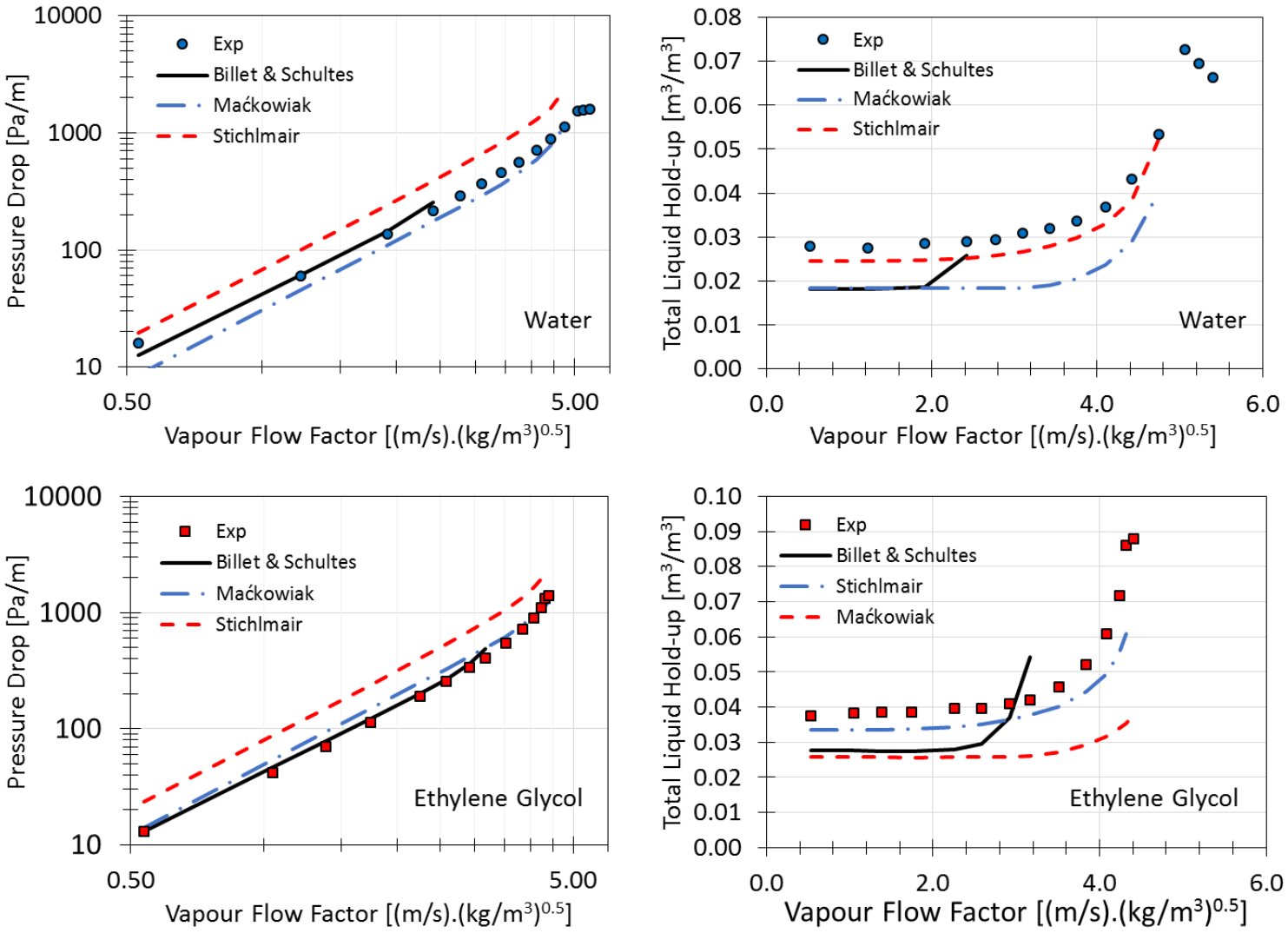

Figure 9.79: Billet & Schultes, Maćkowiak and Stichlmair models, 1.5" Intalox Ultra A, CO_2, water & ethylene glycol at 6 $m^3/(m^2.h)$

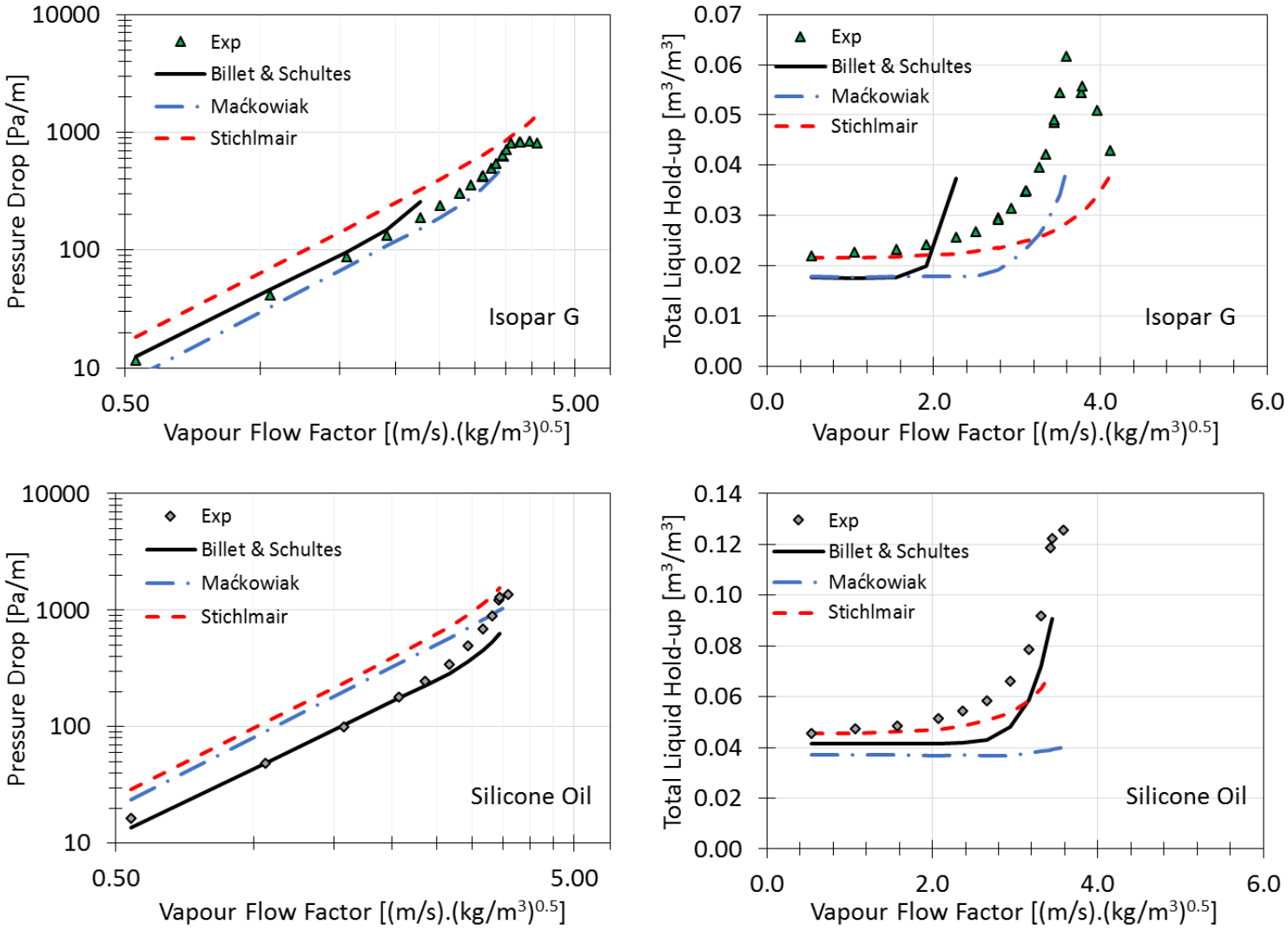

Figure 9.80: Billet & Schultes, Maćkowiak and Stichlmair models, 1.5" Intalox Ultra A, CO_2, Isopar G & silicone oil at 6 $m^3/(m^2.h)$

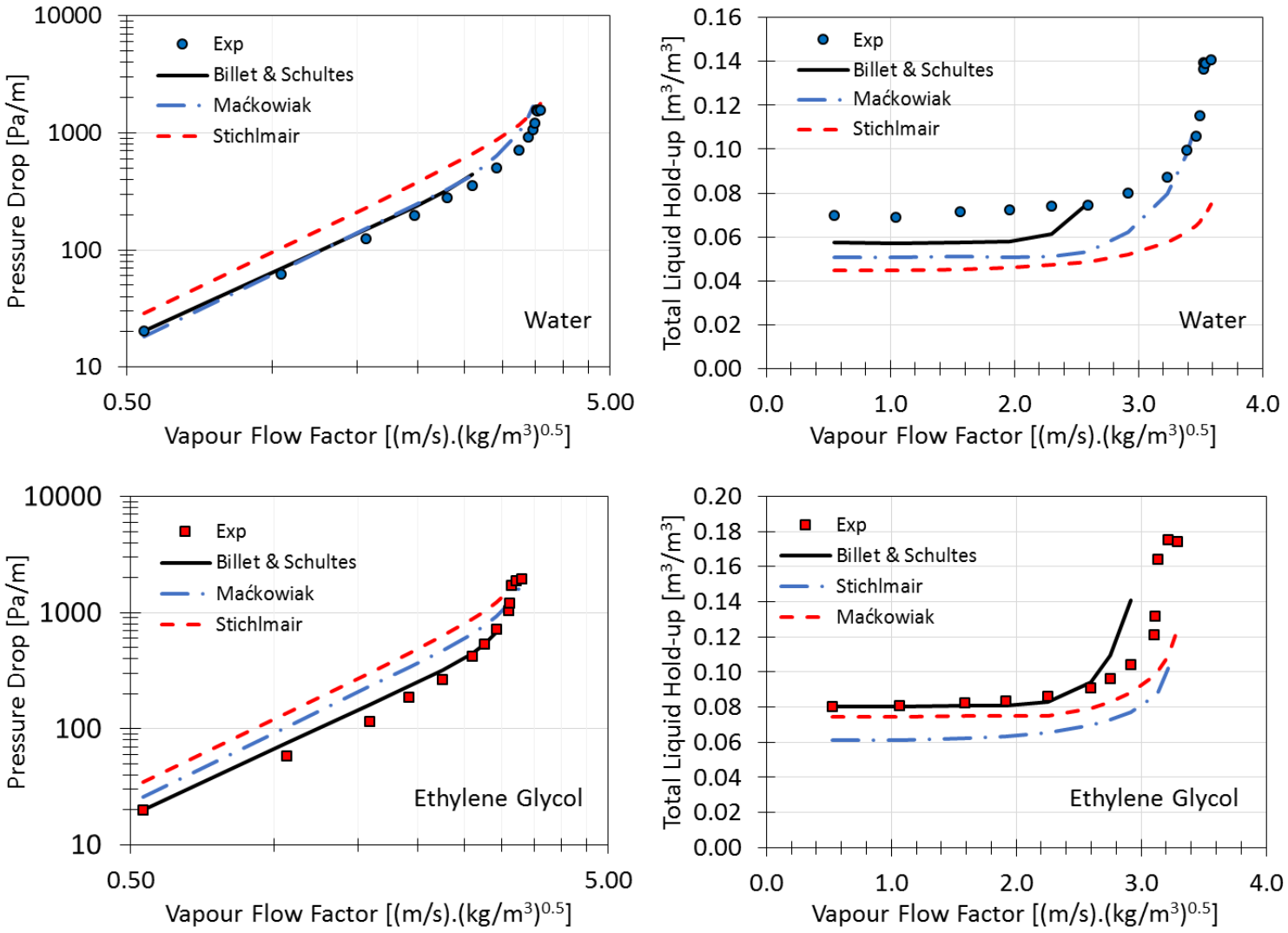

Figure 9.81: Billet & Schultes, Maćkowiak and Stichlmair models, 1.5" Intalox Ultra A, CO_2, water & ethylene glycol at 37 $m^3/(m^2.h)$

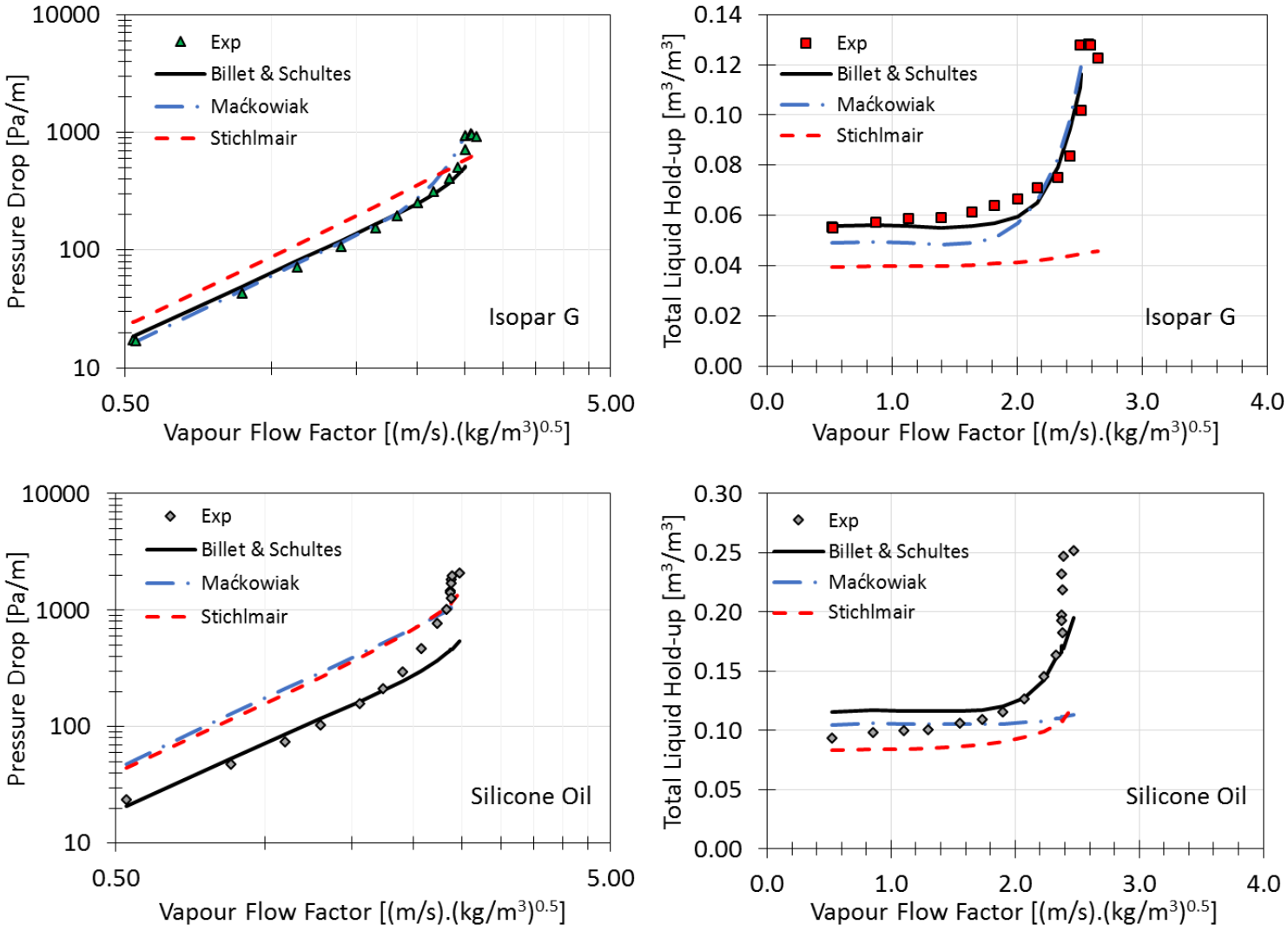

Figure 9.82: Billet & Schultes, Maćkowiak and Stichlmair models, 1.5" Intalox Ultra A, CO_2, Isopar G & silicone oil at 37 $m^3/(m^2.h)$

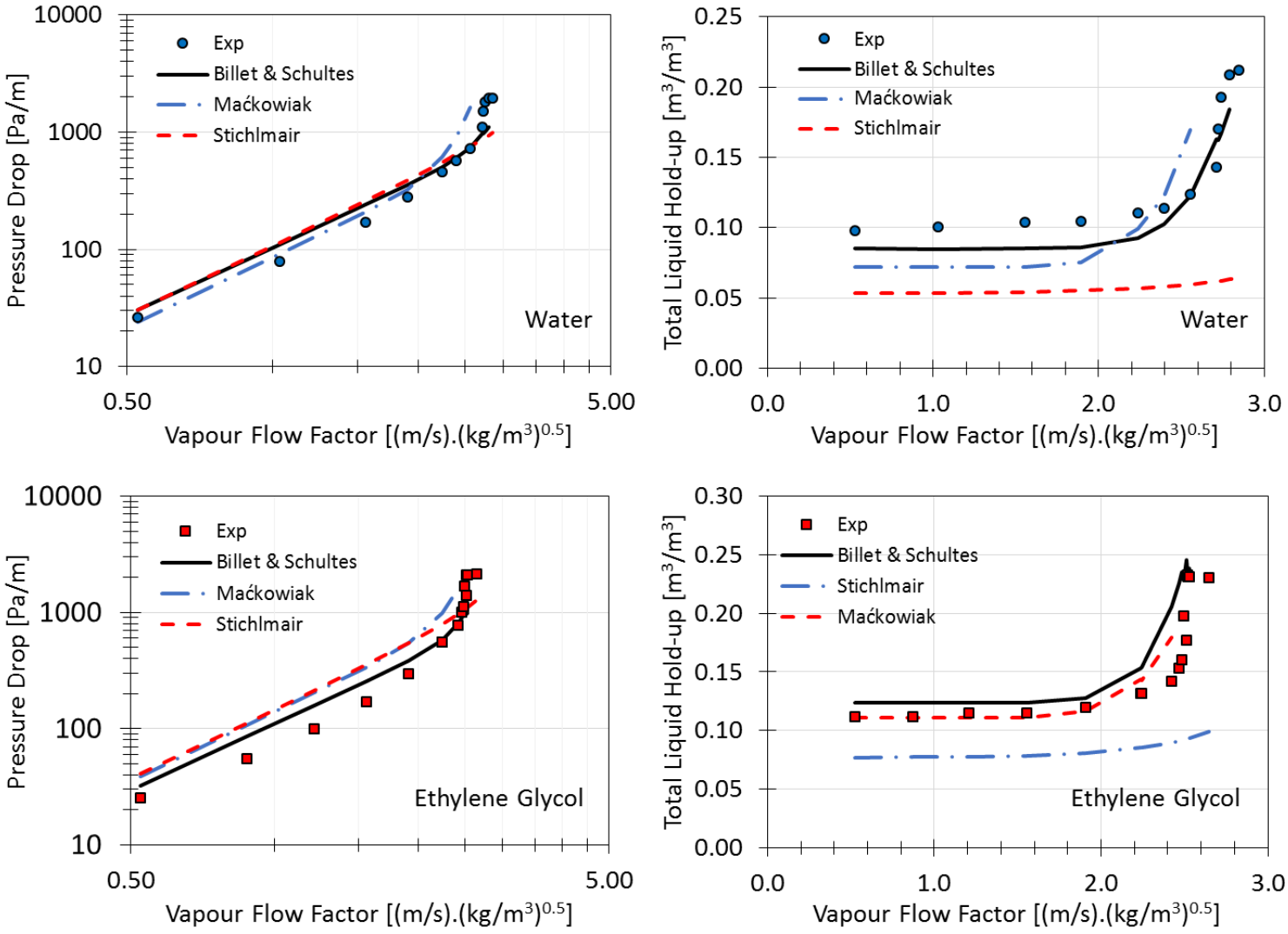

Figure 9.83: Billet & Schultes, Maćkowiak and Stichlmair models, 1.5" Intalox Ultra A, CO_2, water & ethylene glycol at 73 $m^3/(m^2.h)$

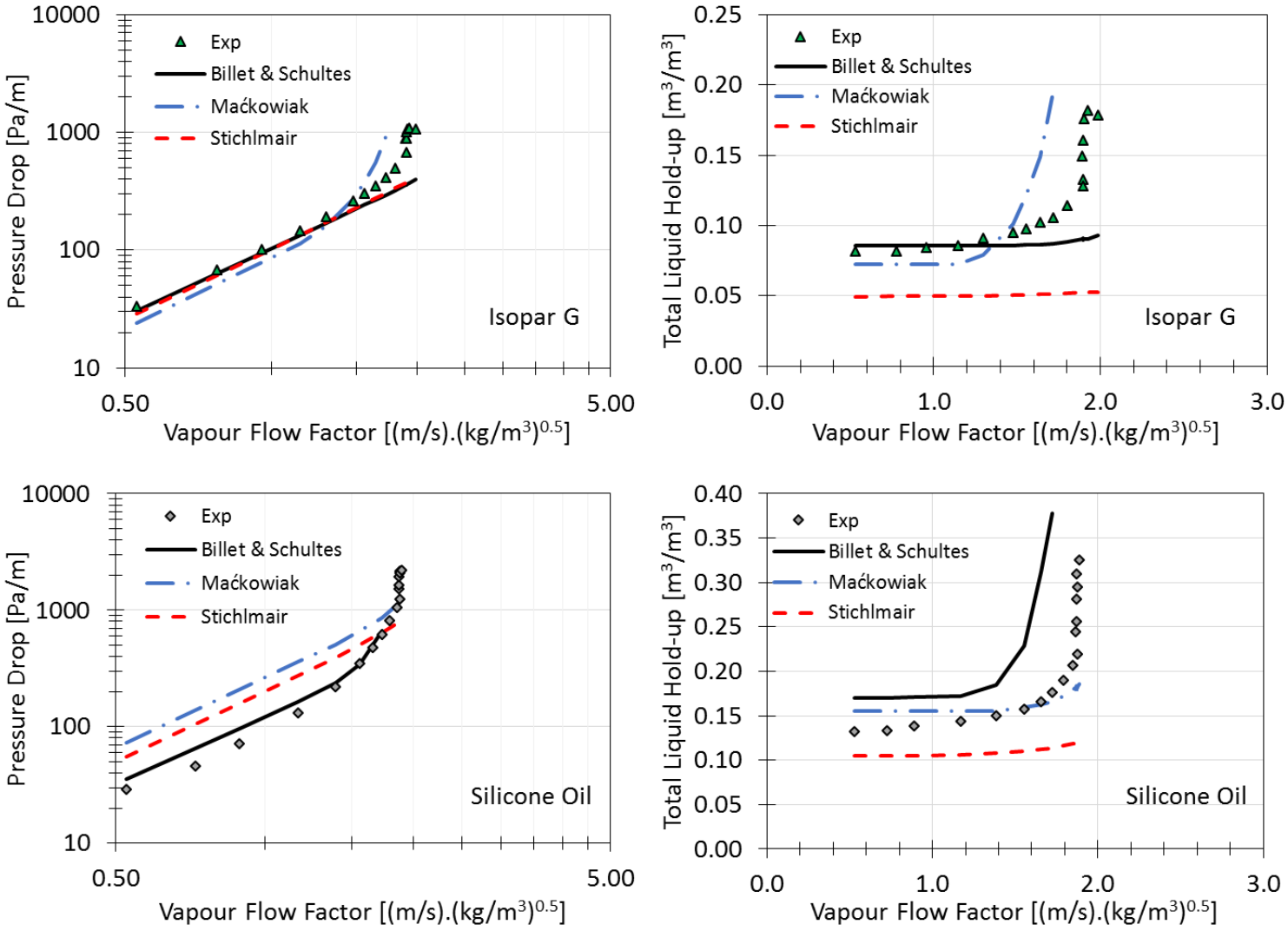

Figure 9.84: Billet & Schultes, Maćkowiak and Stichlmair models, 1.5" Intalox Ultra A, CO_2, Isopar G & silicone oil at 73 $m^3/(m^2.h)$

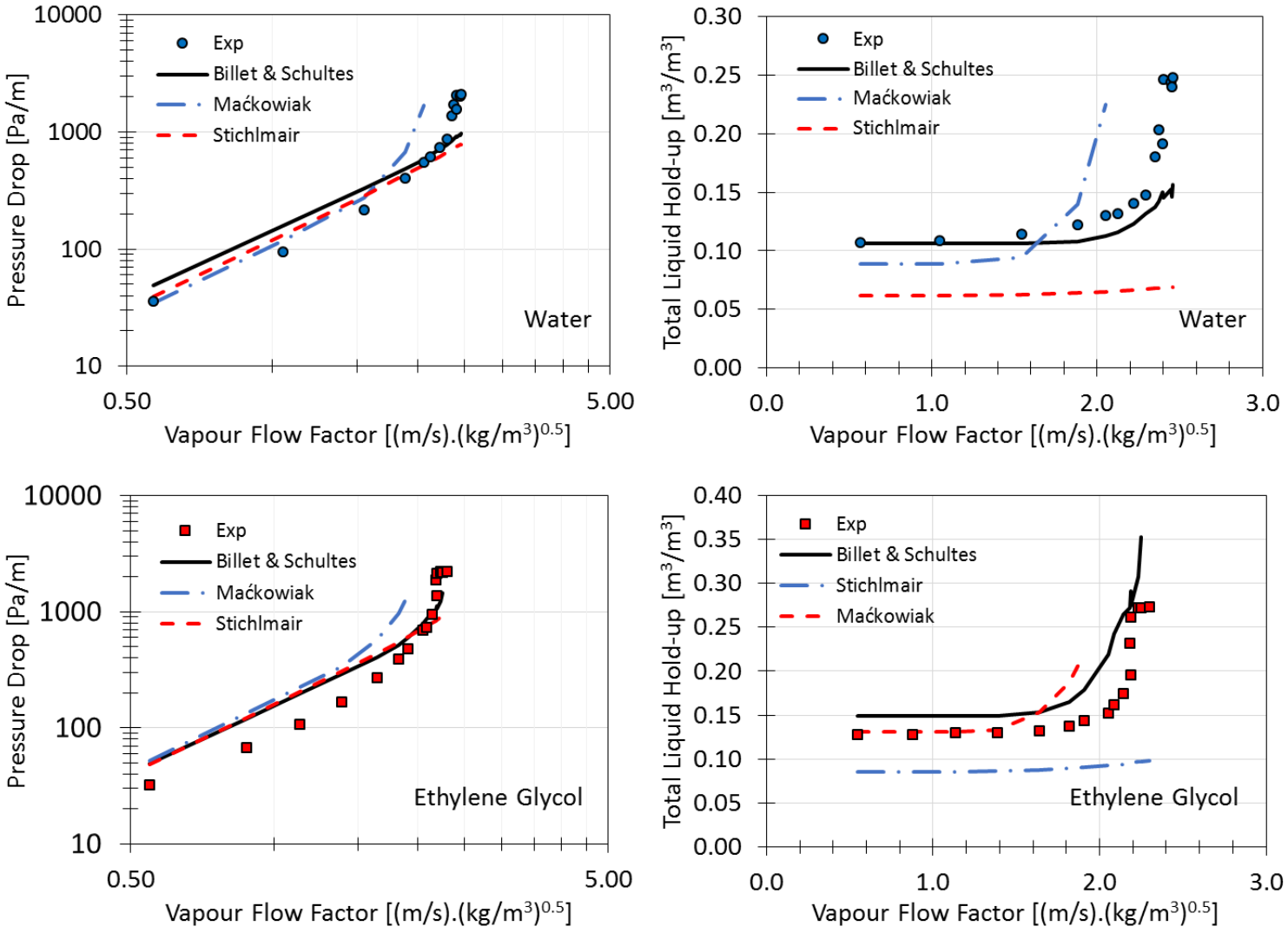

Figure 9.85: Billet & Schultes, Maćkowiak and Stichlmair models, 1.5" Intalox Ultra A, CO_2, water & ethylene glycol at 98 $m^3/(m^2.h)$

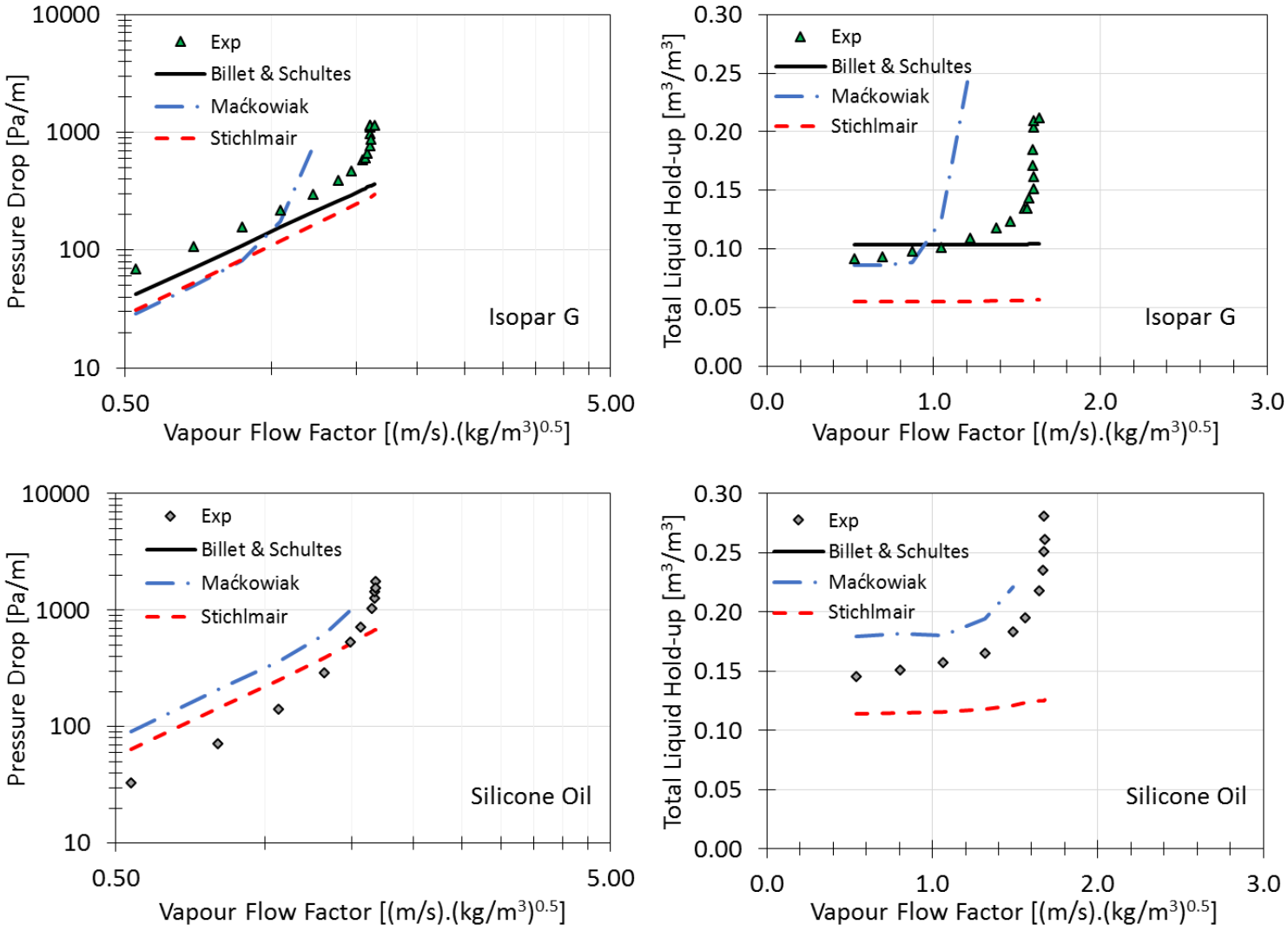

Figure 9.86: Billet & Schultes, Maćkowiak and Stichlmair models, 1.5" Intalox Ultra A, CO_2, Isopar G & silicone oil at 98 $m^3/(m^2.h)$

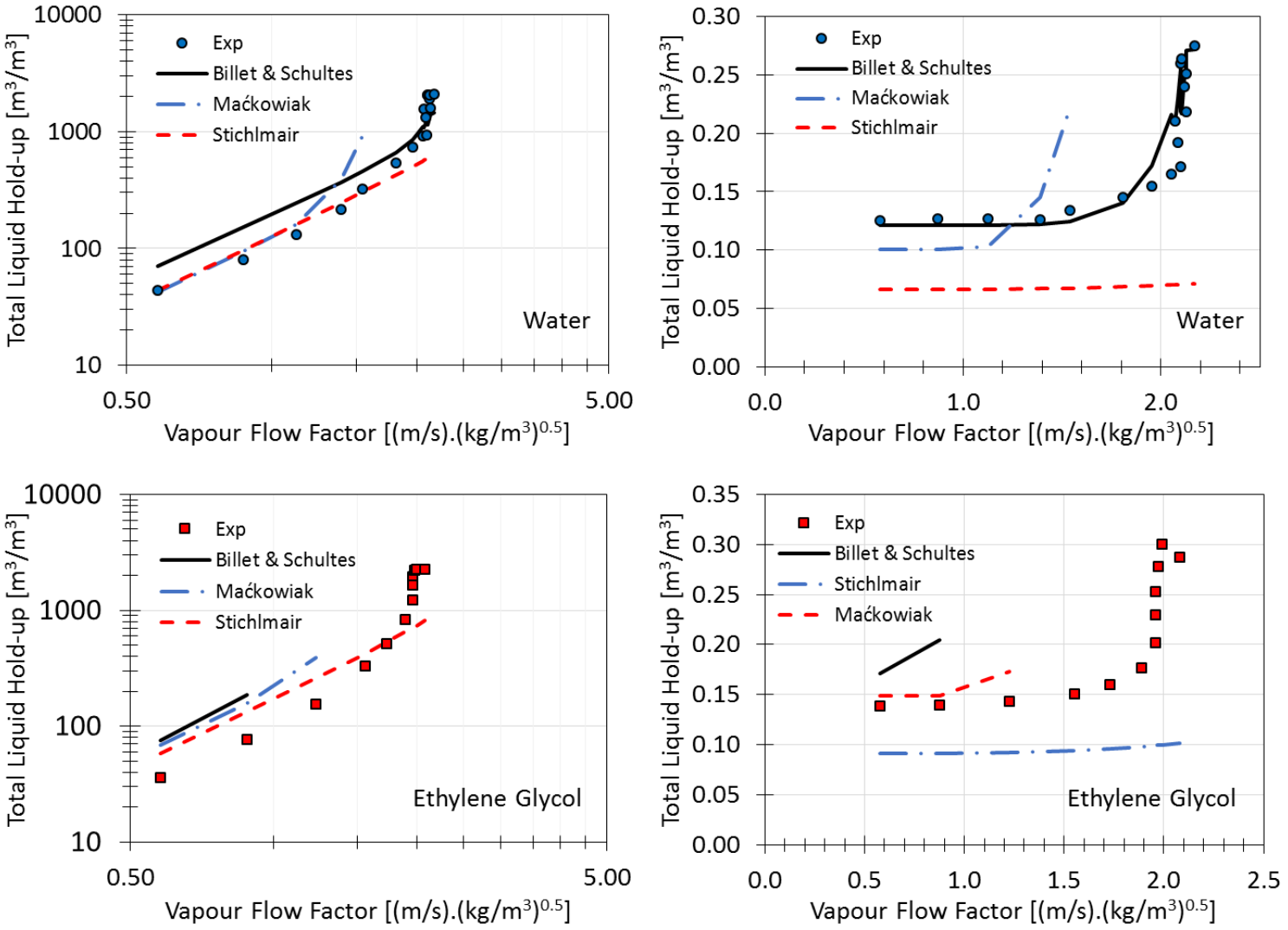

Figure 9.87: Billet & Schultes, Maćkowiak and Stichlmair models, 1.5" Intalox Ultra A, CO_2, water & ethylene glycol at 122 $m^3/(m^2.h)$

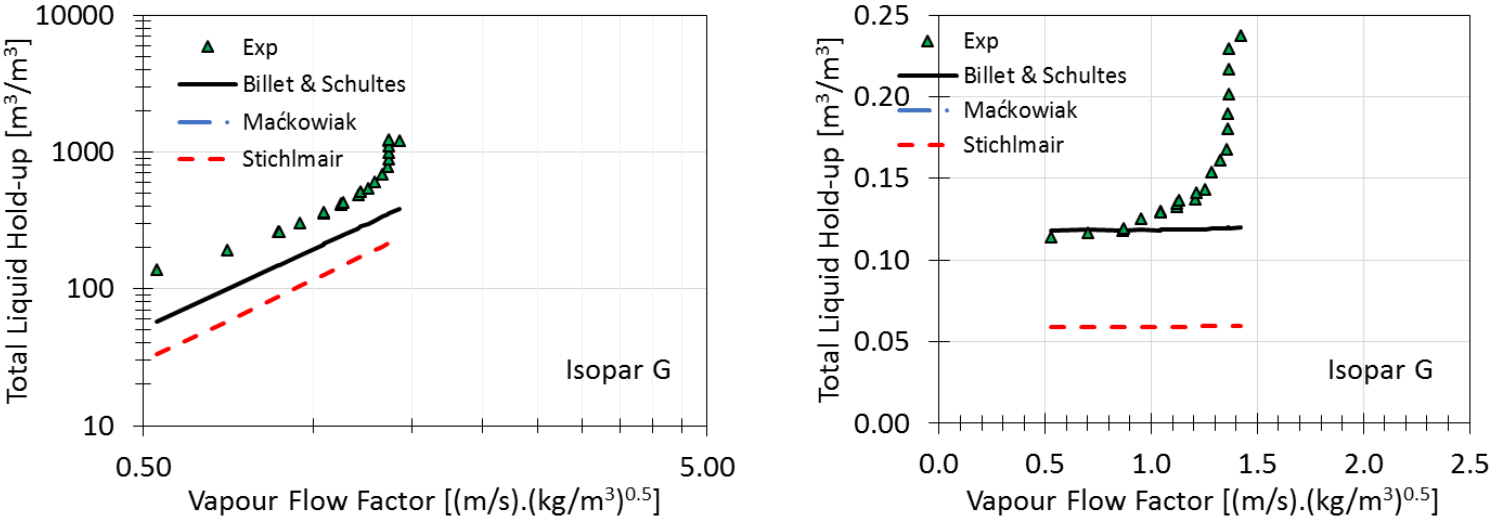

Figure 9.88: Billet & Schultes, Maćkowiak and Stichlmair models, 1.5" Intalox Ultra A, CO_2, Isopar G at 122 $m^3/(m^2.h)$

9.12.2 2.5” Intalox Ultra O

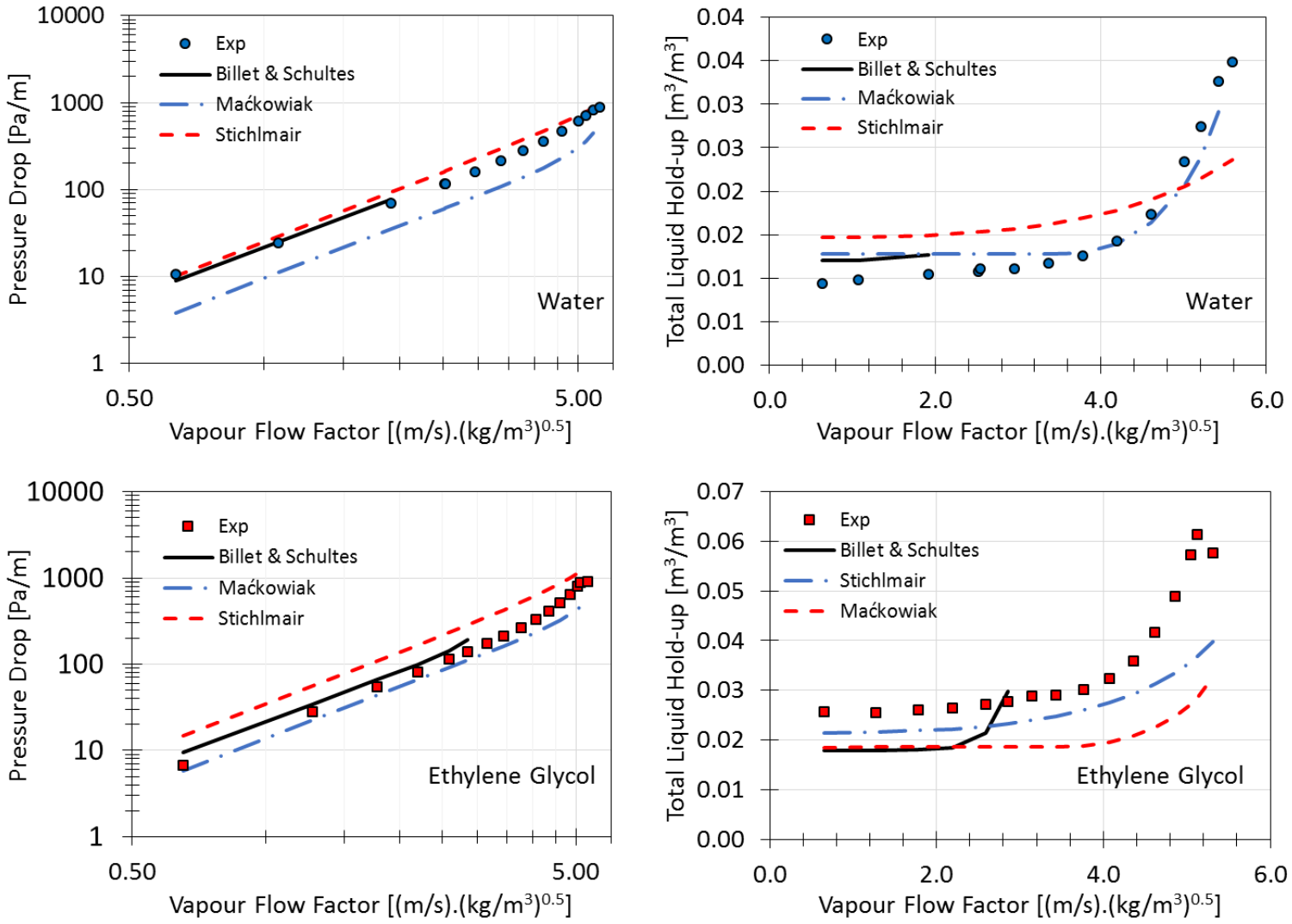

Figure 9.89: Billet & Schultes, Maćkowiak and Stichlmair models, 2.5" Intalox Ultra A, air, water & ethylene glycol at 6 $m^3/(m^2.h)$

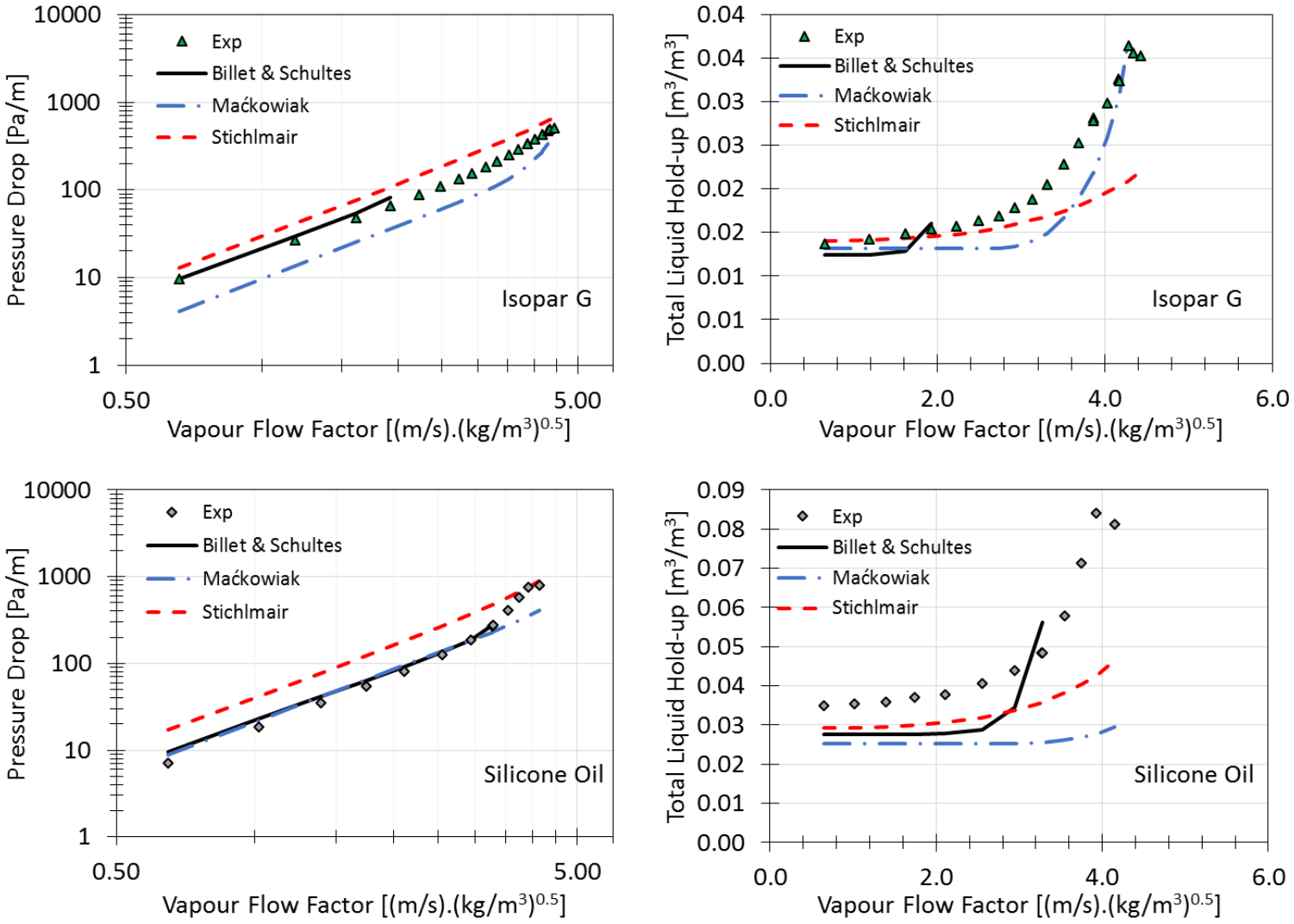

Figure 9.90: Billet & Schultes, Maćkowiak and Stichlmair models, 2.5" Intalox Ultra A, air, Isopar G & silicone oil at 6 $m^3/(m^2.h)$

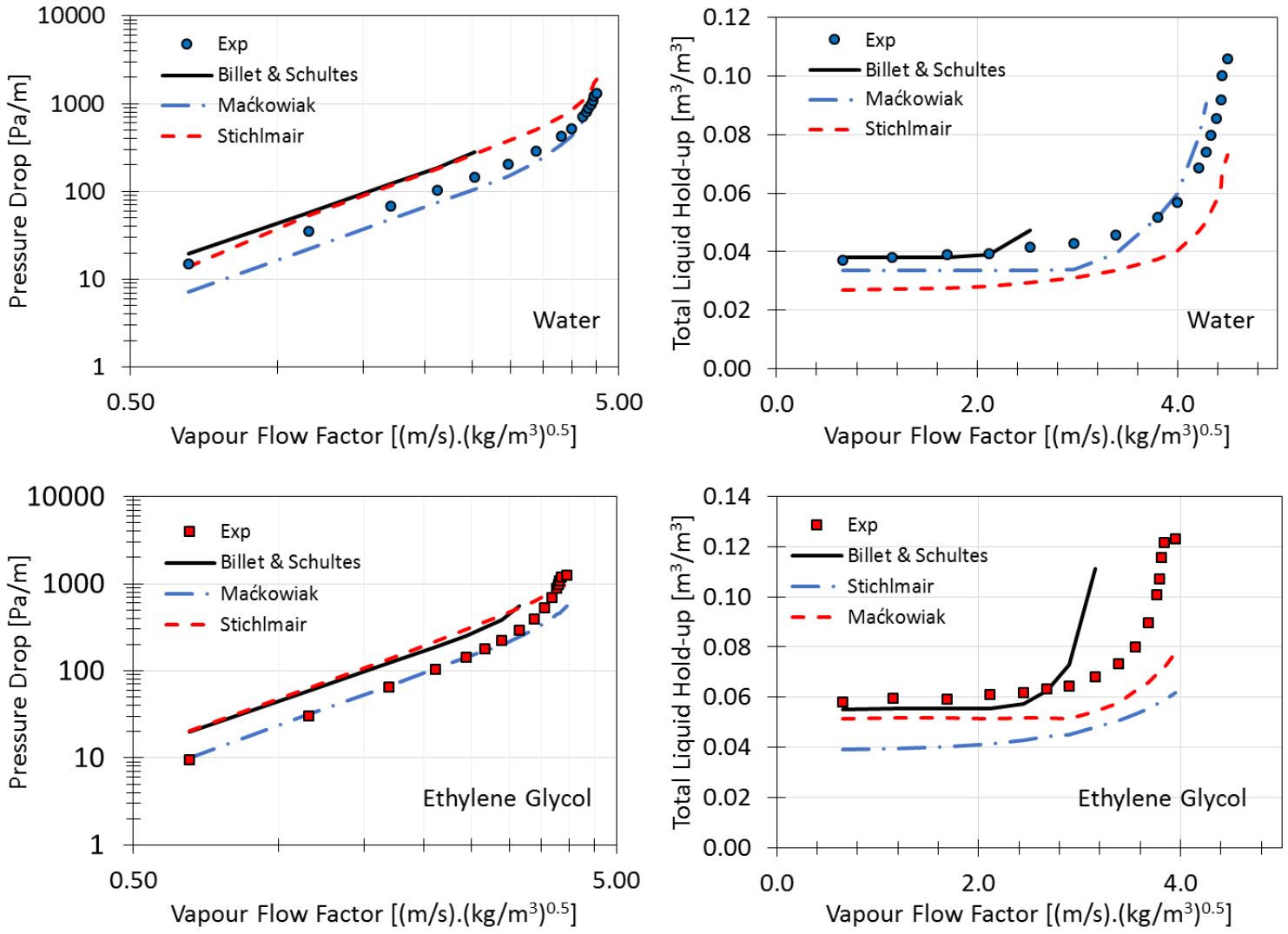

Figure 9.91: Billet & Schultes, Maćkowiak and Stichlmair models, 2.5" Intalox Ultra A, air, water & ethylene glycol at 37 $m^3/(m^2.h)$

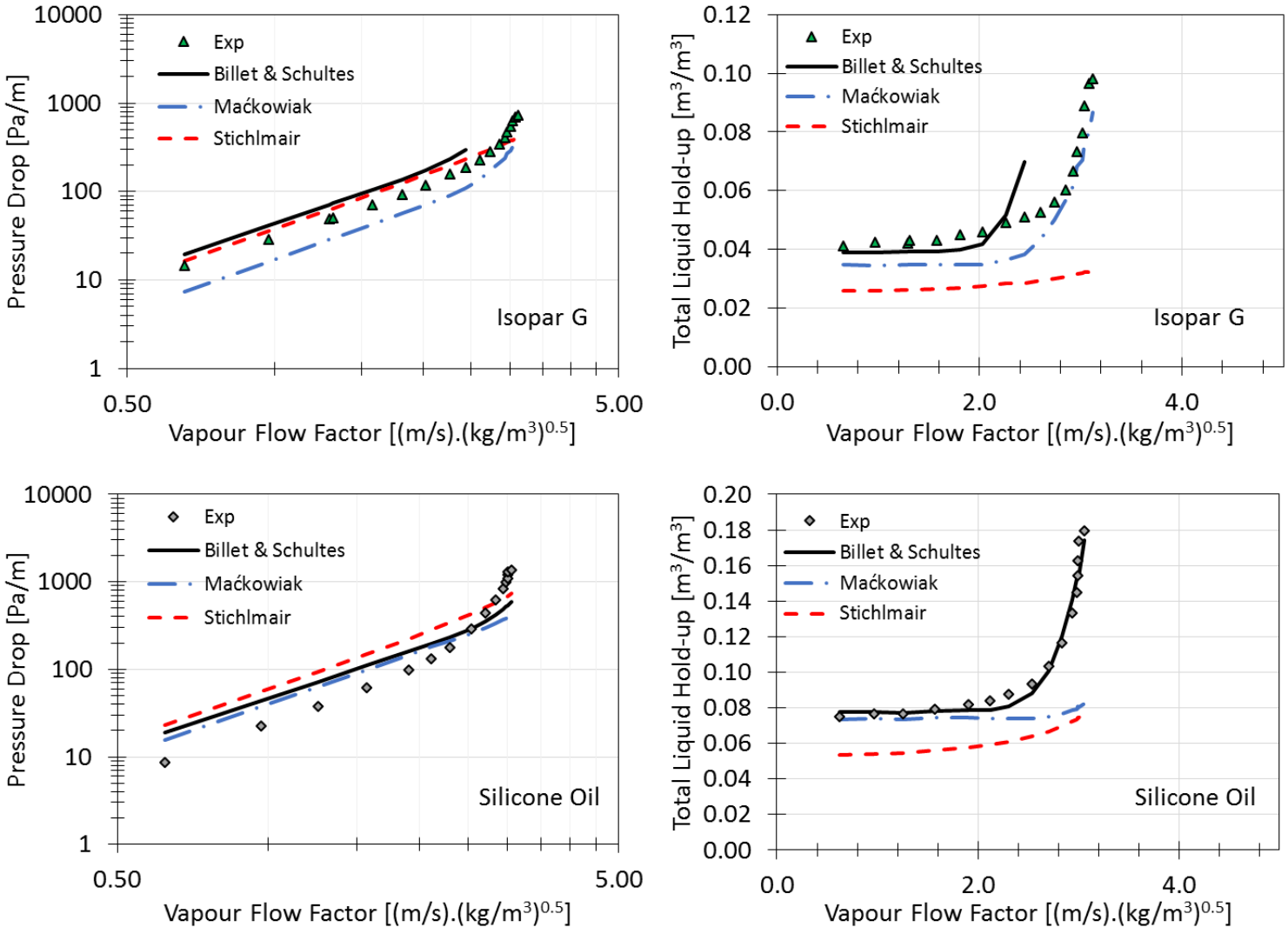

Figure 9.92: Billet & Schultes, Maćkowiak and Stichlmair models, 2.5" Intalox Ultra A, air, Isopar G & silicone oil at 37 $m^3/(m^2.h)$

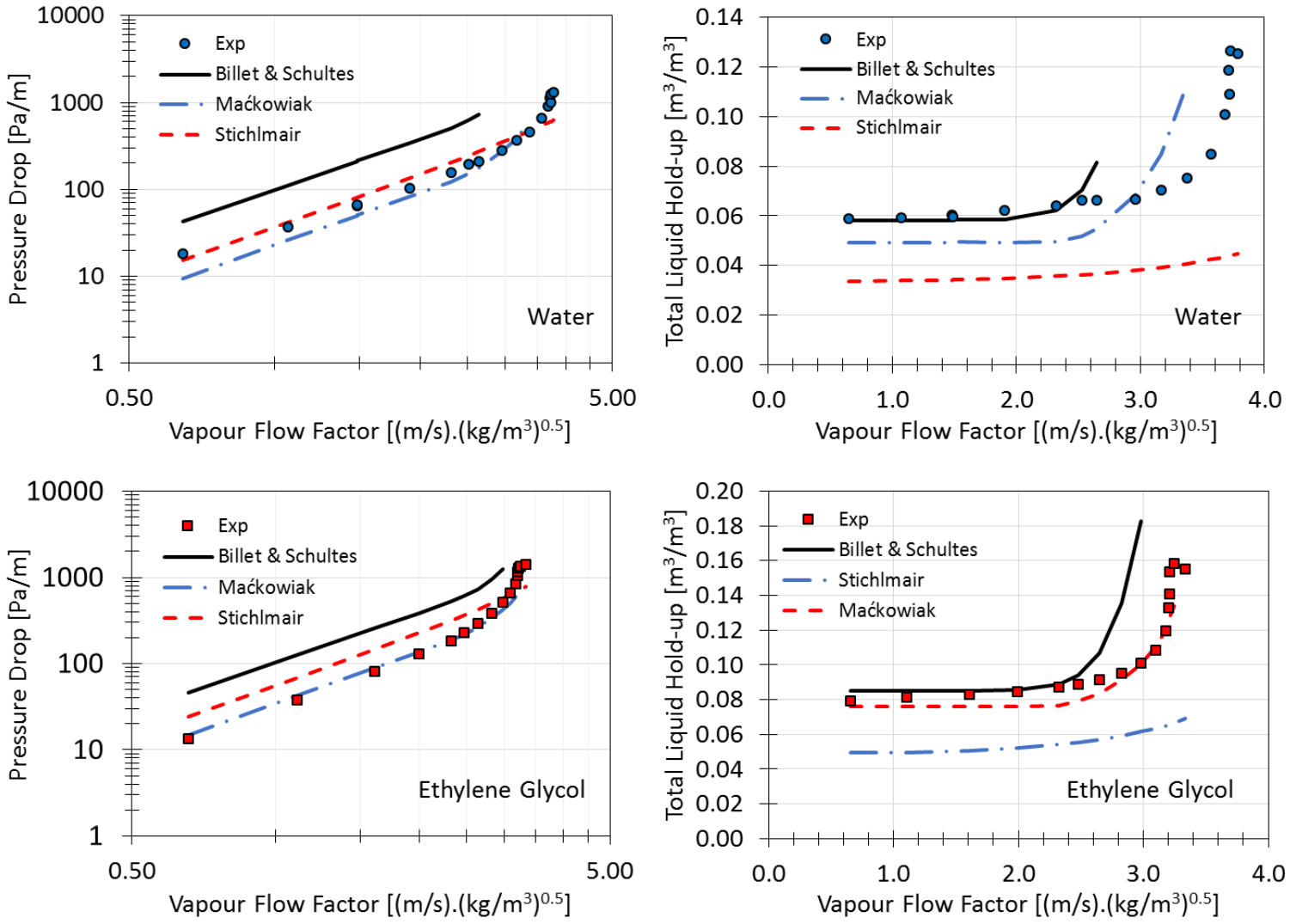

Figure 9.93: Billet & Schultes, Maćkowiak and Stichlmair models, 2.5" Intalox Ultra A, air, water & ethylene glycol at 73 m³/(m².h)

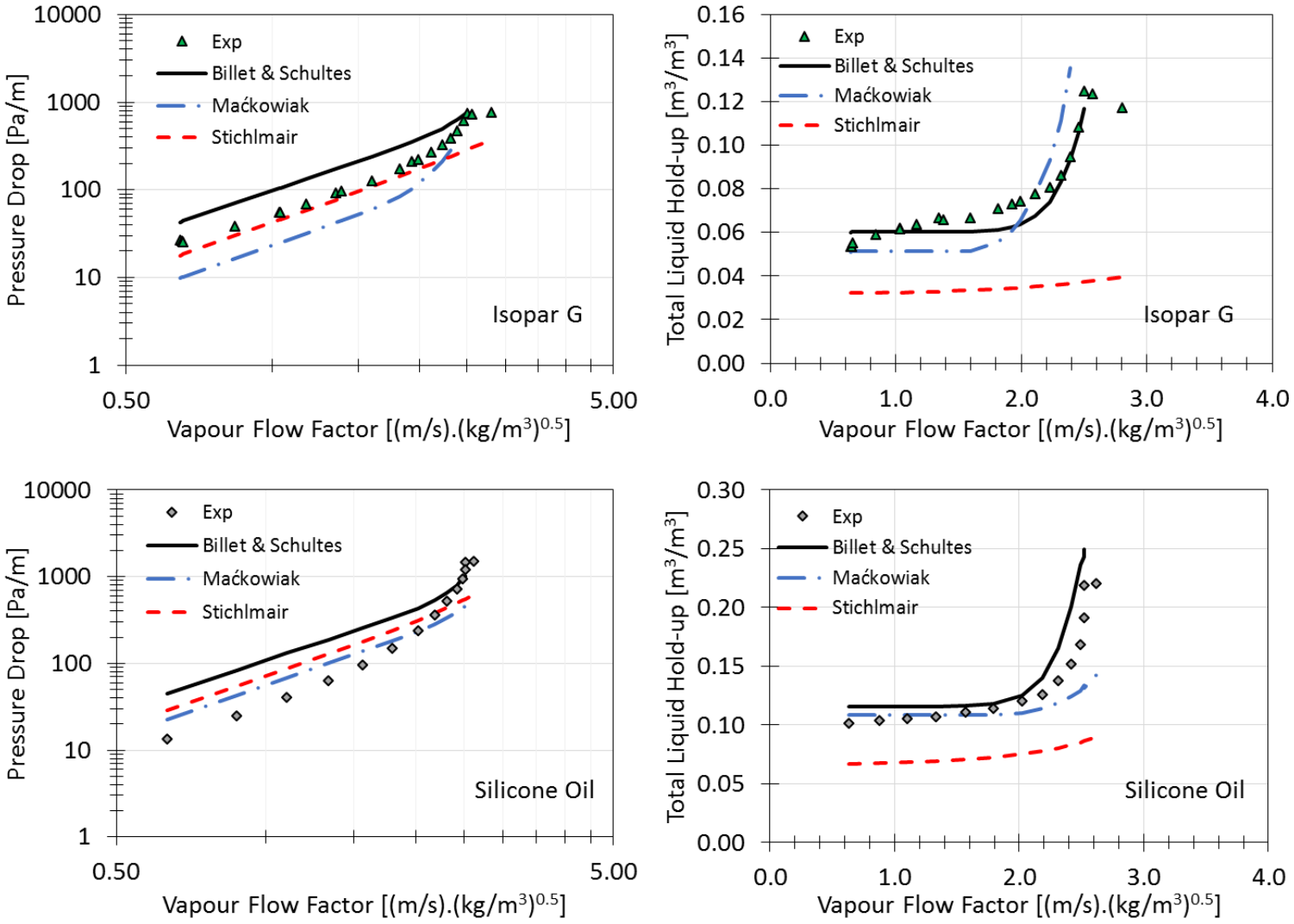

Figure 9.94: Billet & Schultes, Maćkowiak and Stichlmair models, 2.5" Intalox Ultra A, air, Isopar G & silicone oil at 73 $m^3/(m^2.h)$

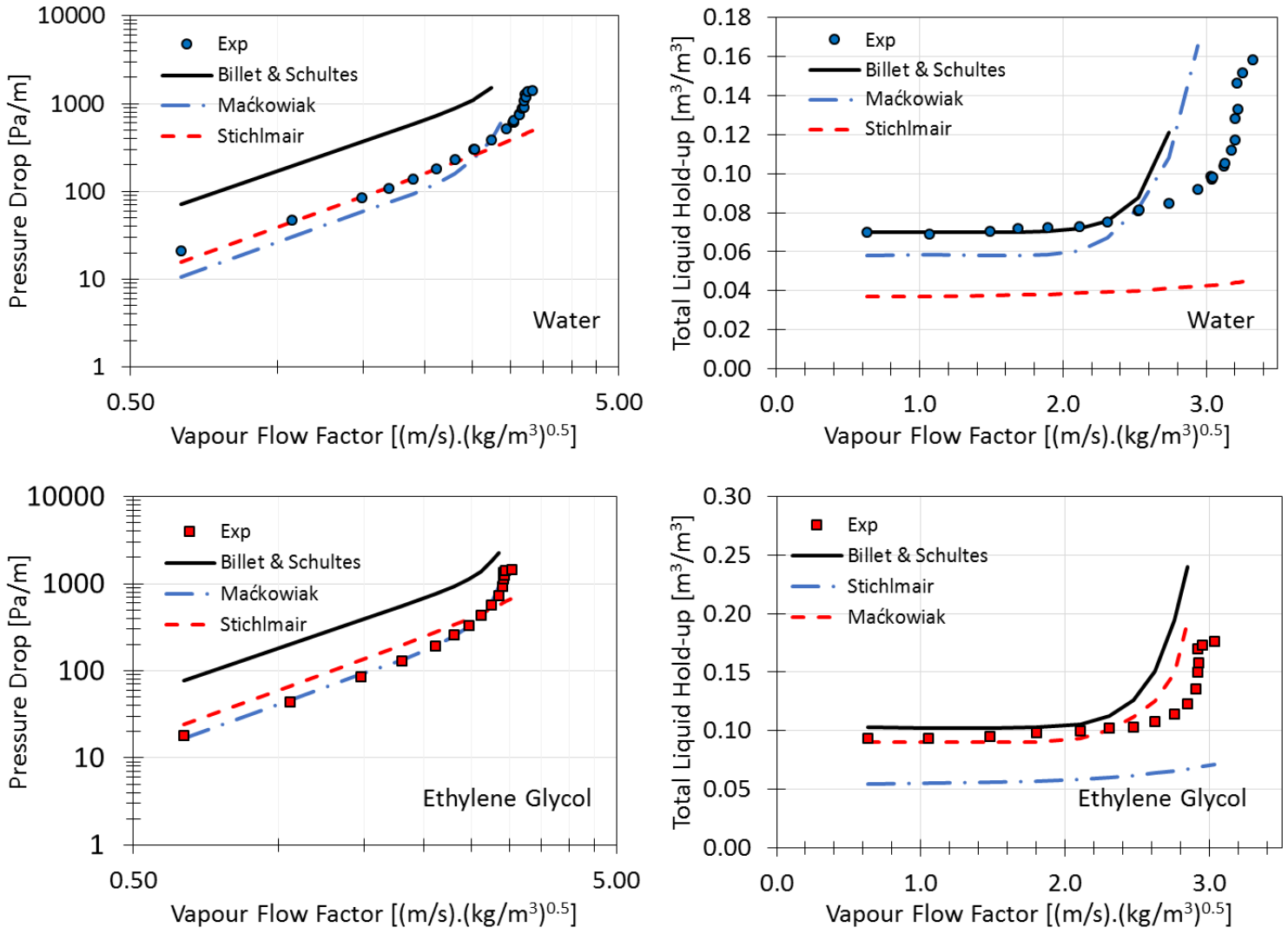

Figure 9.95: Billet & Schultes, Maćkowiak and Stichlmair models, 2.5" Intalox Ultra A, air, water & ethylene glycol at 98 m³/(m².h)

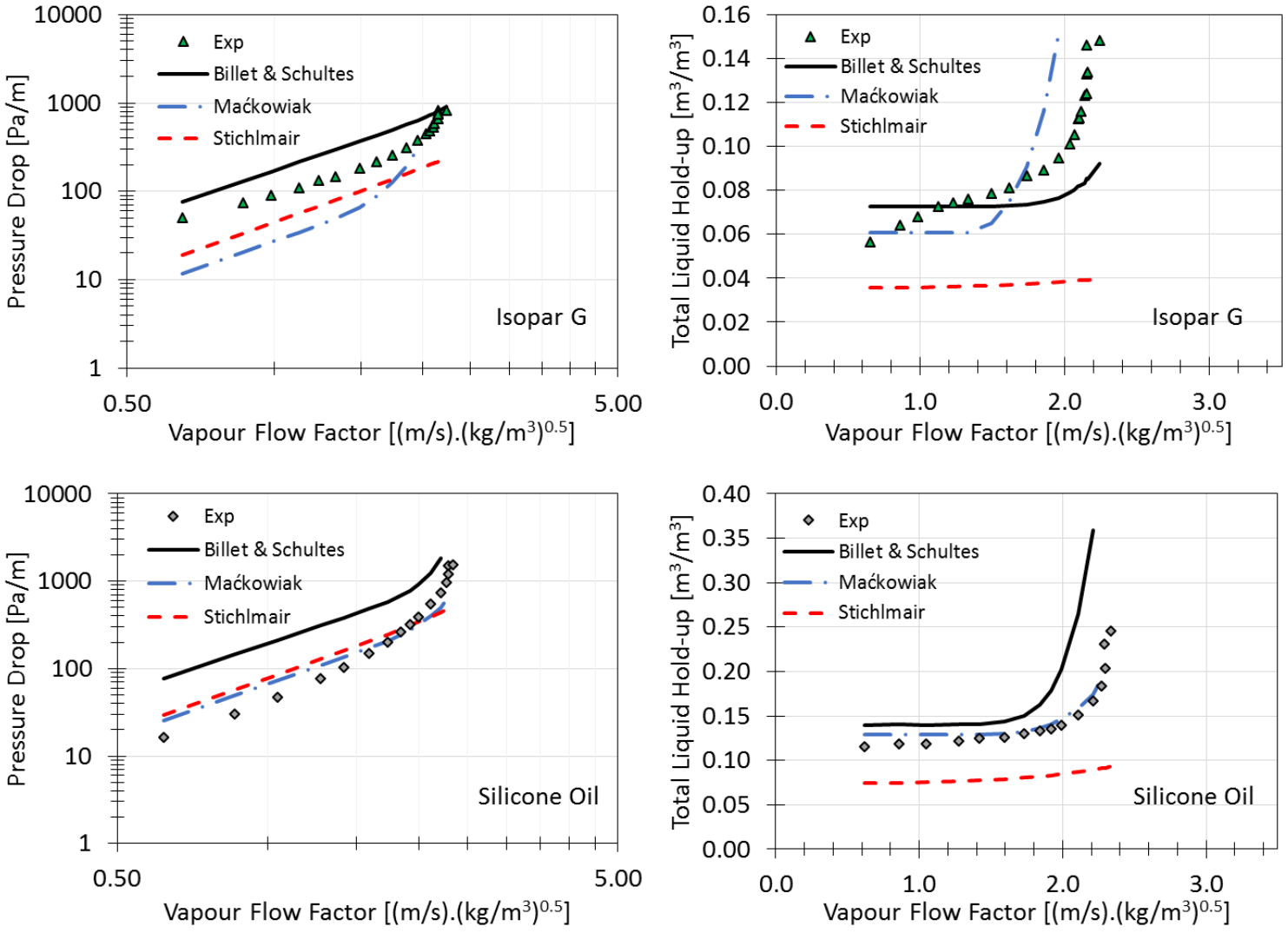

Figure 9.96: Billet & Schultes, Maćkowiak and Stichlmair models, 2.5" Intalox Ultra A, air, Isopar G & silicone oil at 98 $m^3/(m^2.h)$

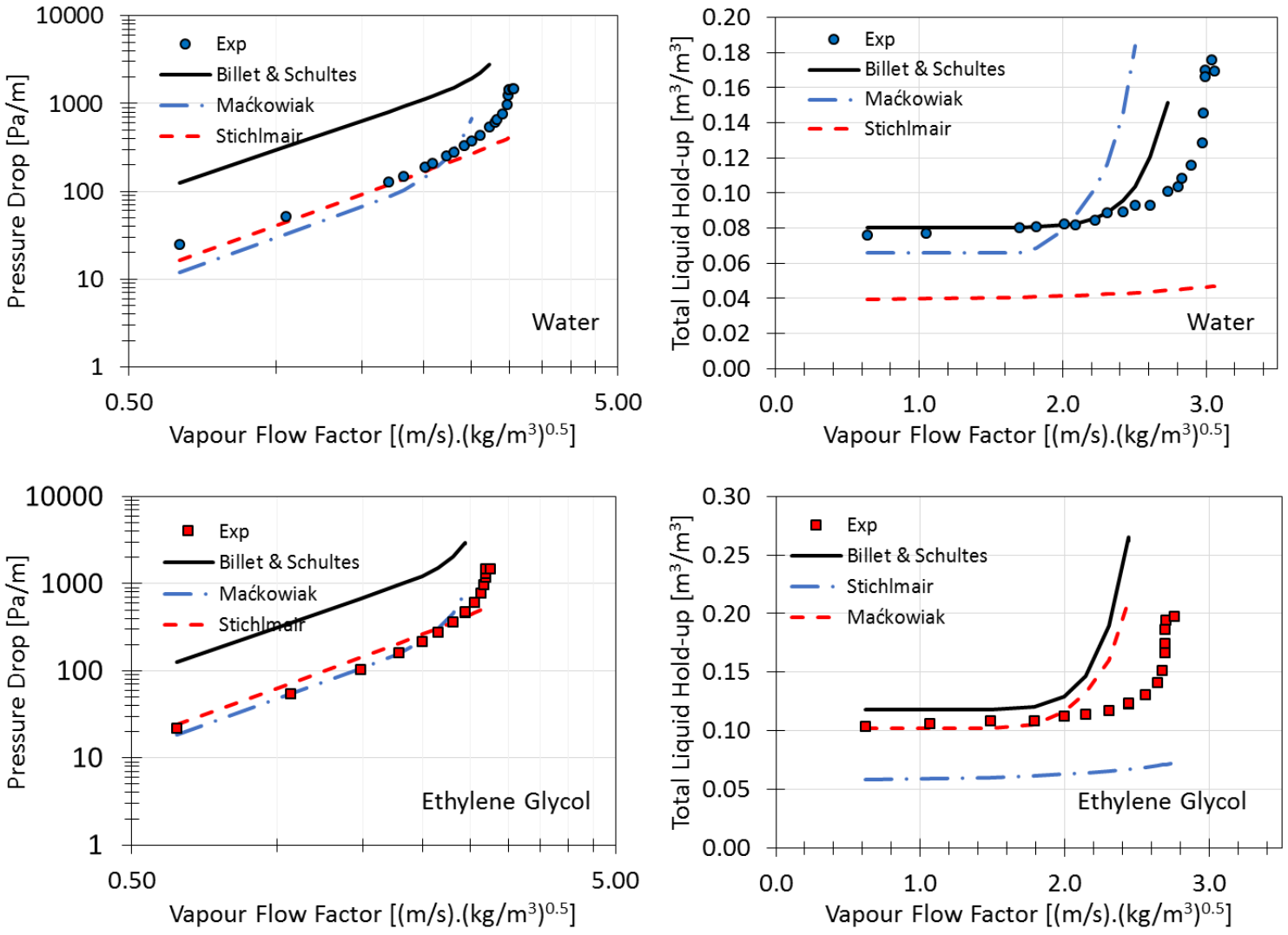

Figure 9.97: Billet & Schultes, Maćkowiak and Stichlmair models, 2.5" Intalox Ultra A, air, water & ethylene glycol at 122 $m^3/(m^2.h)$

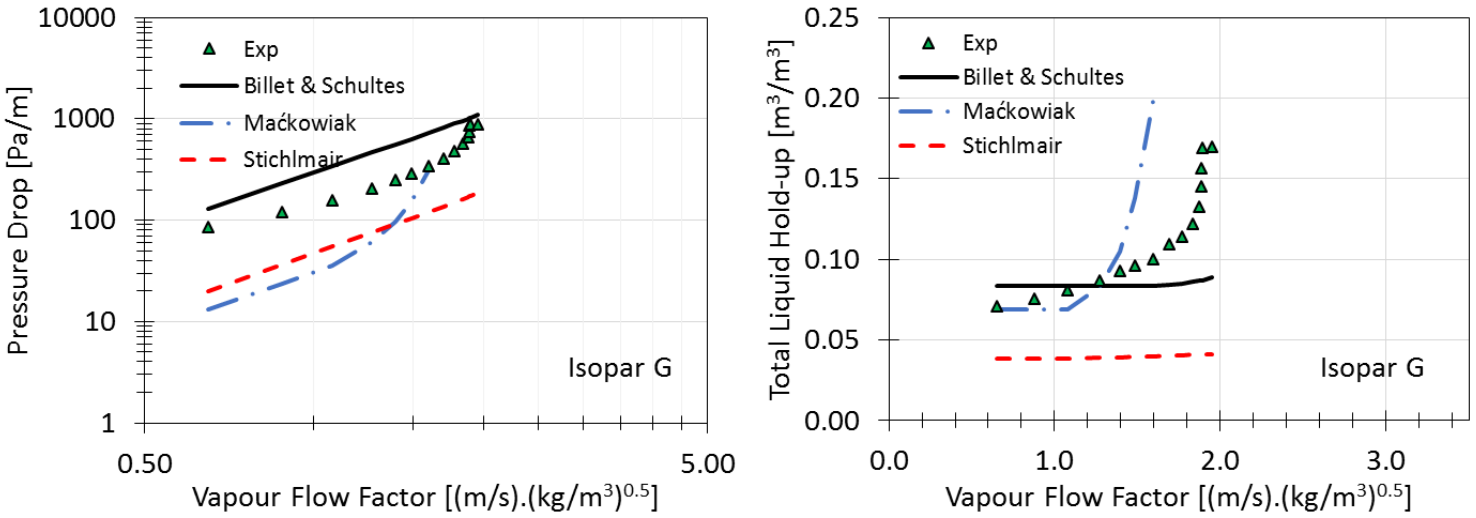

Figure 9.98: Billet & Schultes, Maćkowiak and Stichlmair models, 2.5" Intalox Ultra A, air, Isopar G at 122 $m^3/(m^2.h)$

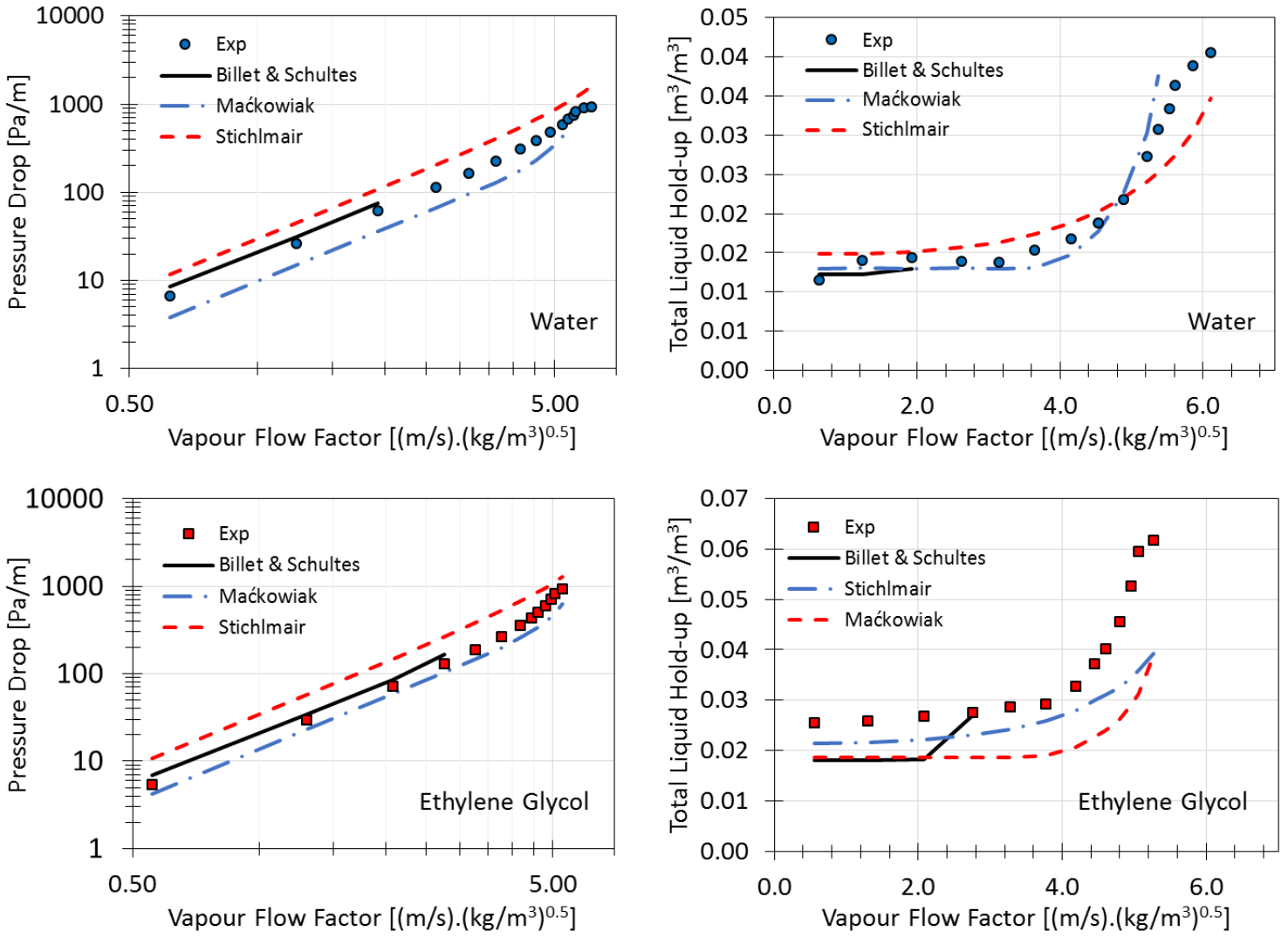

Figure 9.99: Billet & Schultes, Maćkowiak and Stichlmair models, 2.5" Intalox Ultra A, CO_2, water & ethylene glycol at 6 $m^3/(m^2.h)$

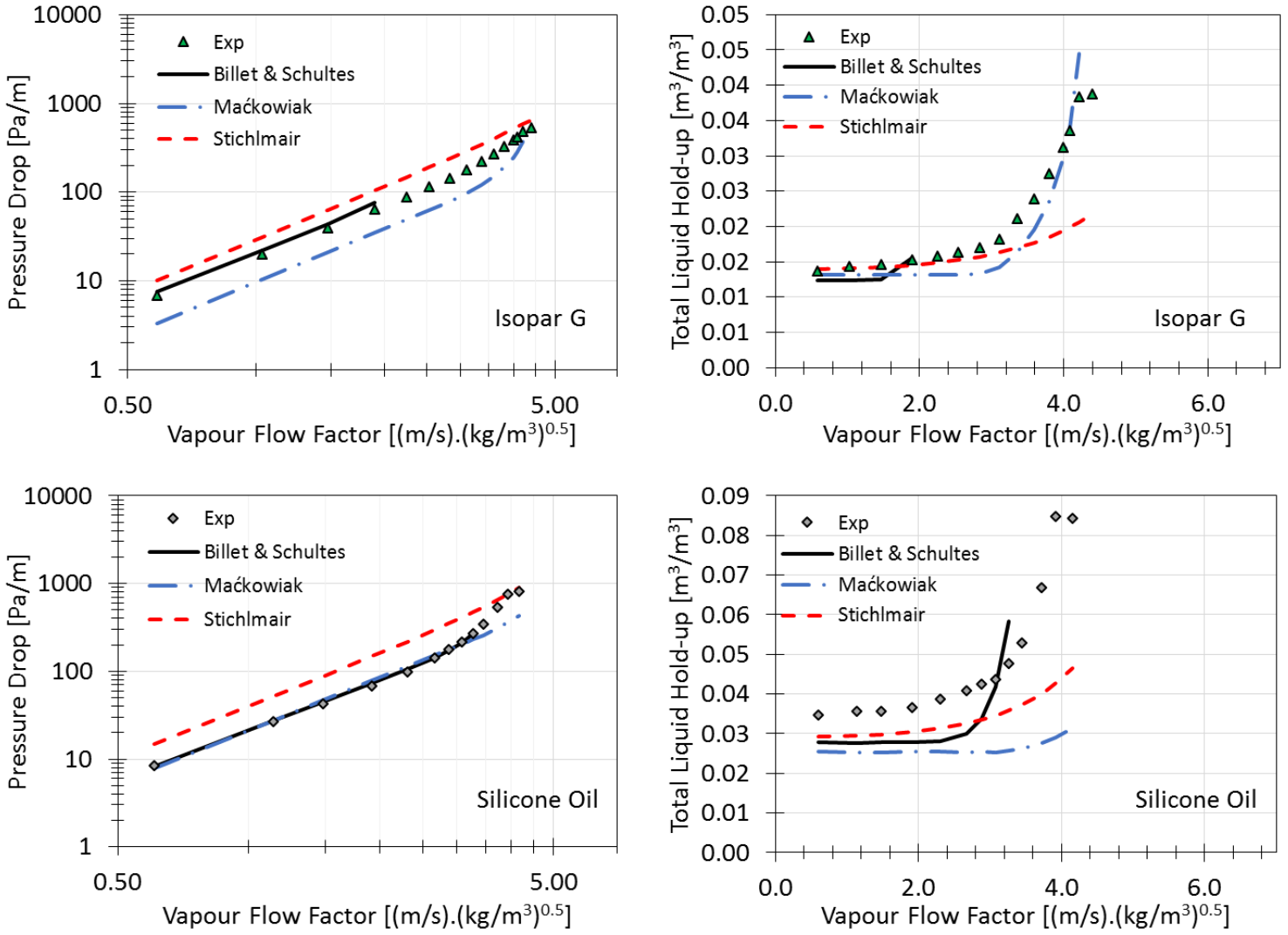

Figure 9.100: Billet & Schultes, Maćkowiak and Stichlmair models, 2.5" Intalox Ultra A, CO_2, Isopar G & silicone oil at 6 $m^3/(m^2.h)$

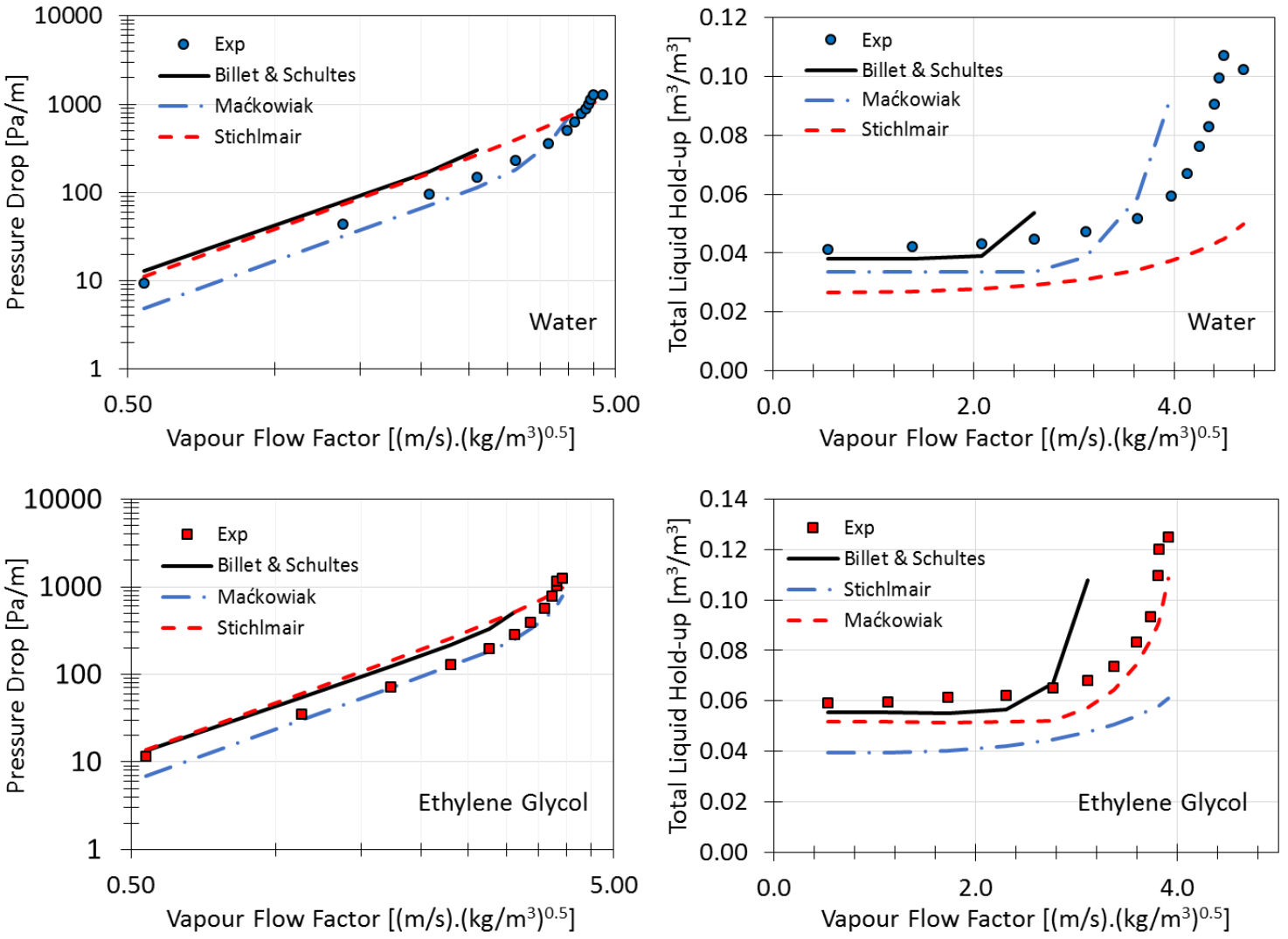

Figure 9.101: Billet & Schultes, Maćkowiak and Stichlmair models, 2.5" Intalox Ultra A, CO_2, water & ethylene glycol at 37 $m^3/(m^2.h)$

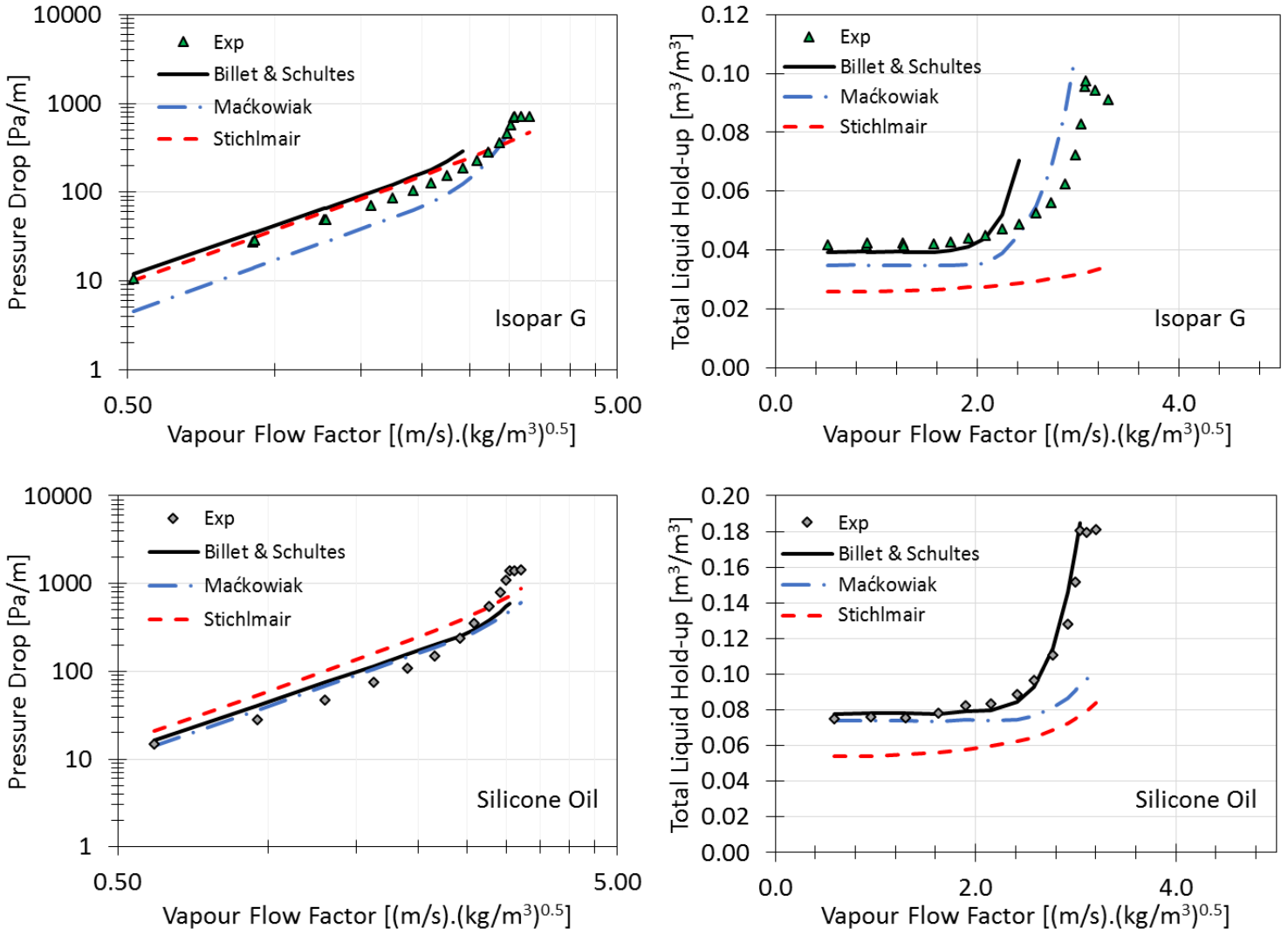

Figure 9.102: Billet & Schultes, Maćkowiak and Stichlmair models, 2.5" Intalox Ultra A, CO_2, Isopar G & silicone oil at 37 $m^3/(m^2.h)$

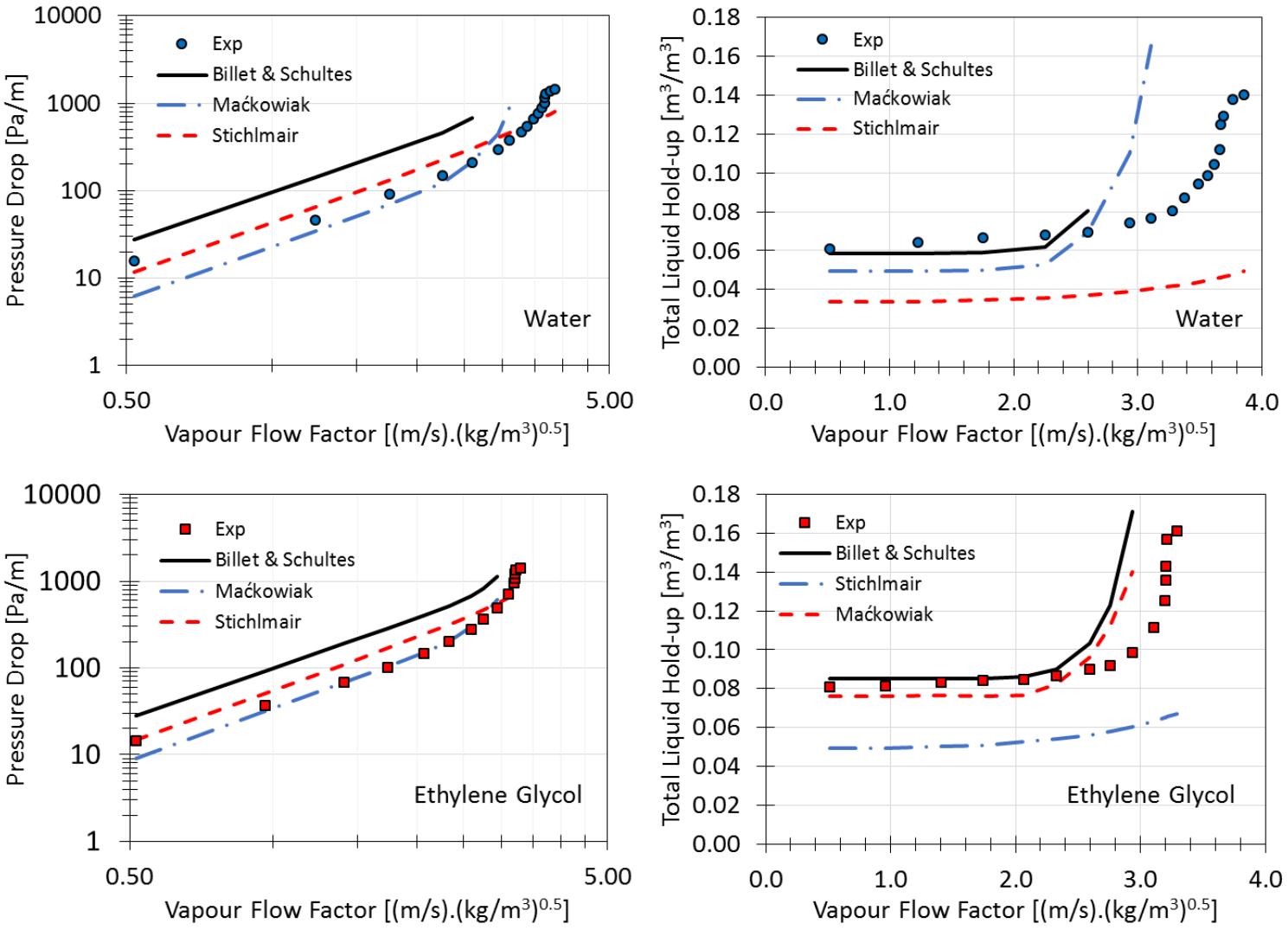

Figure 9.103: Billet & Schultes, Maćkowiak and Stichlmair models, 2.5" Intalox Ultra A, CO_2, water & ethylene glycol at 73 $m^3/(m^2.h)$

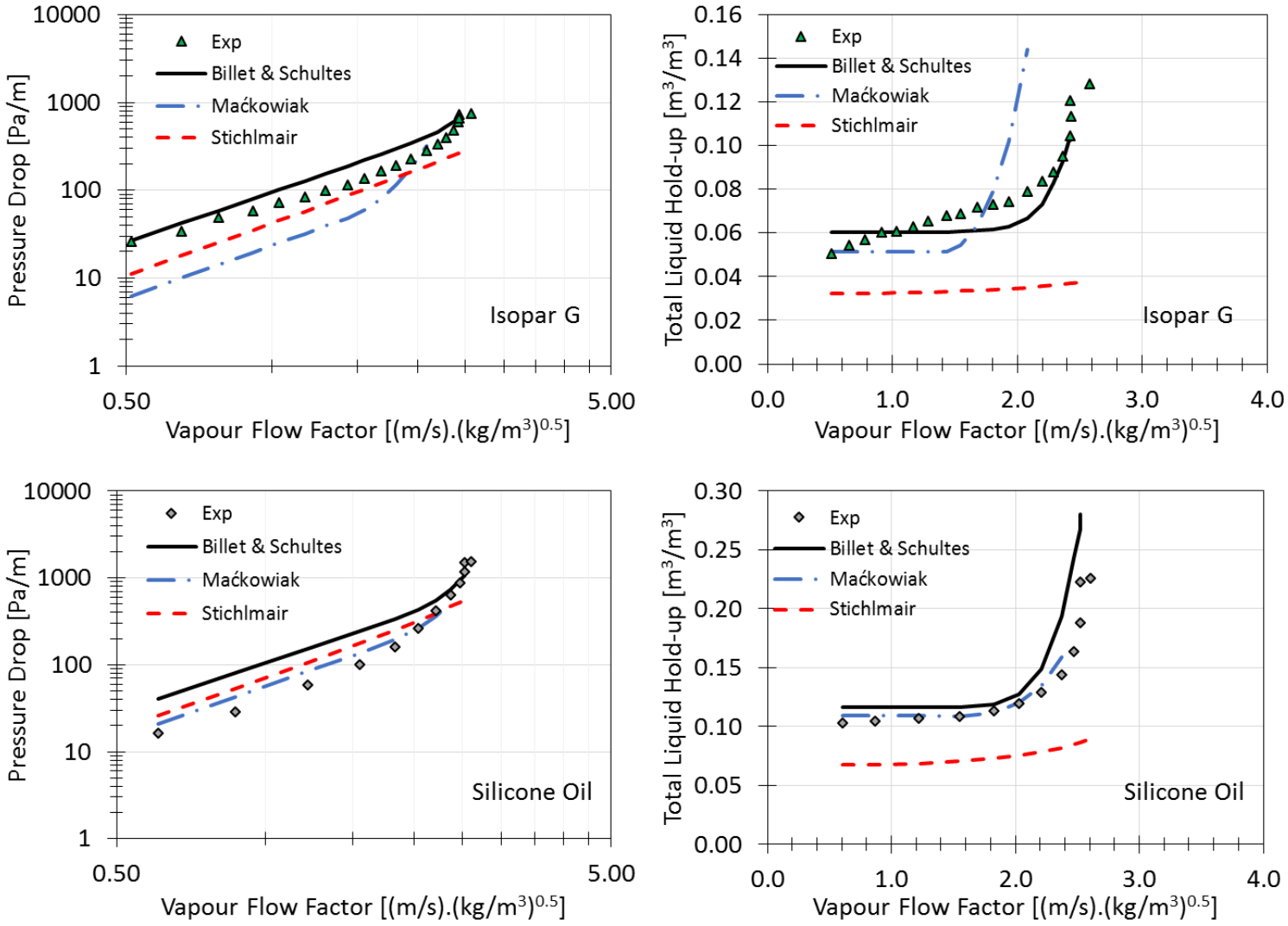

Figure 9.104: Billet & Schultes, Maćkowiak and Stichlmair models, 2.5" Intalox Ultra A, CO_2, Isopar G & silicone oil at 73 $m^3/(m^2.h)$

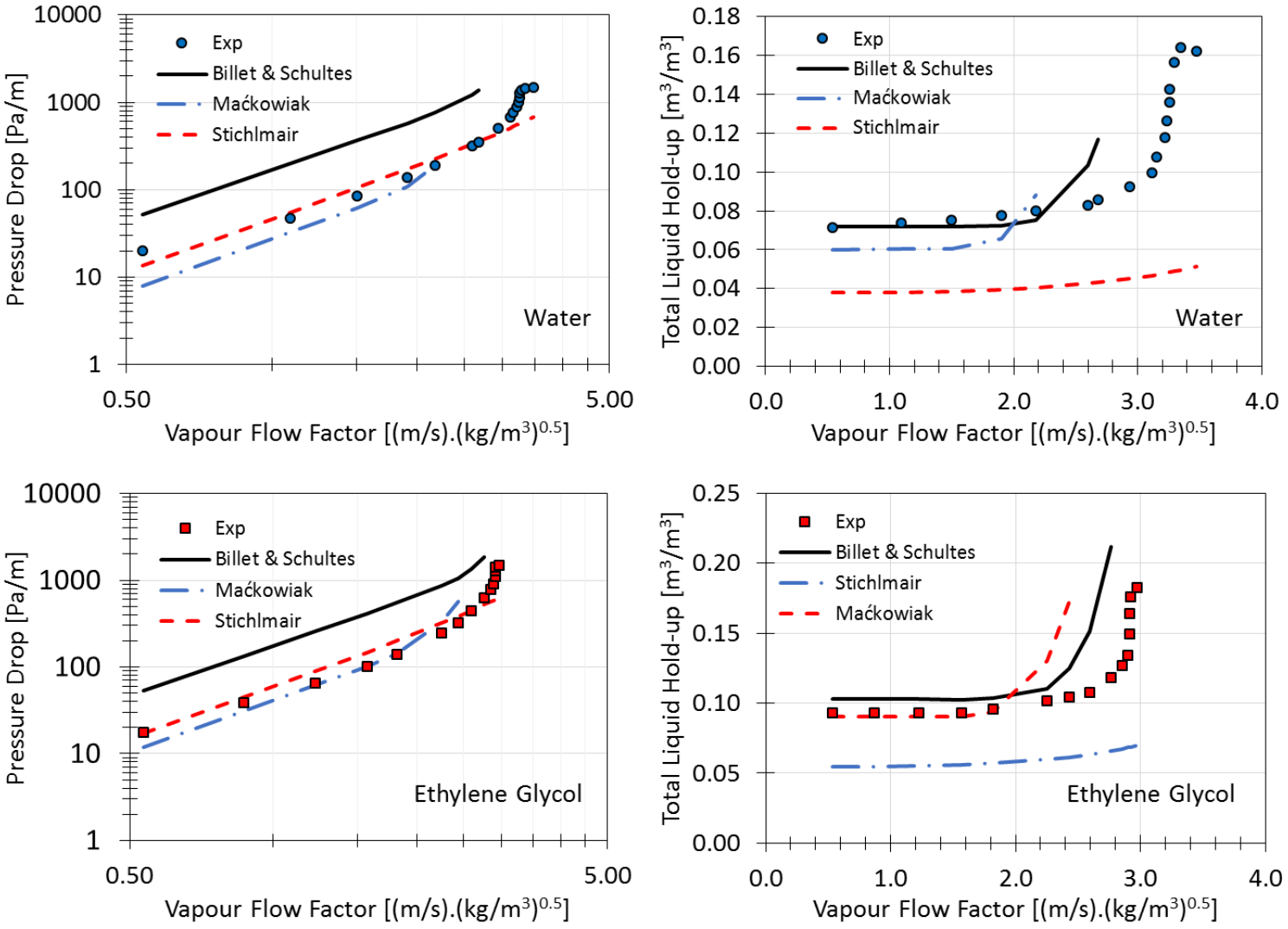

Figure 9.105: Billet & Schultes, Maćkowiak and Stichlmair models, 2.5" Intalox Ultra A, CO_2, water & ethylene glycol at 98 $m^3/(m^2.h)$

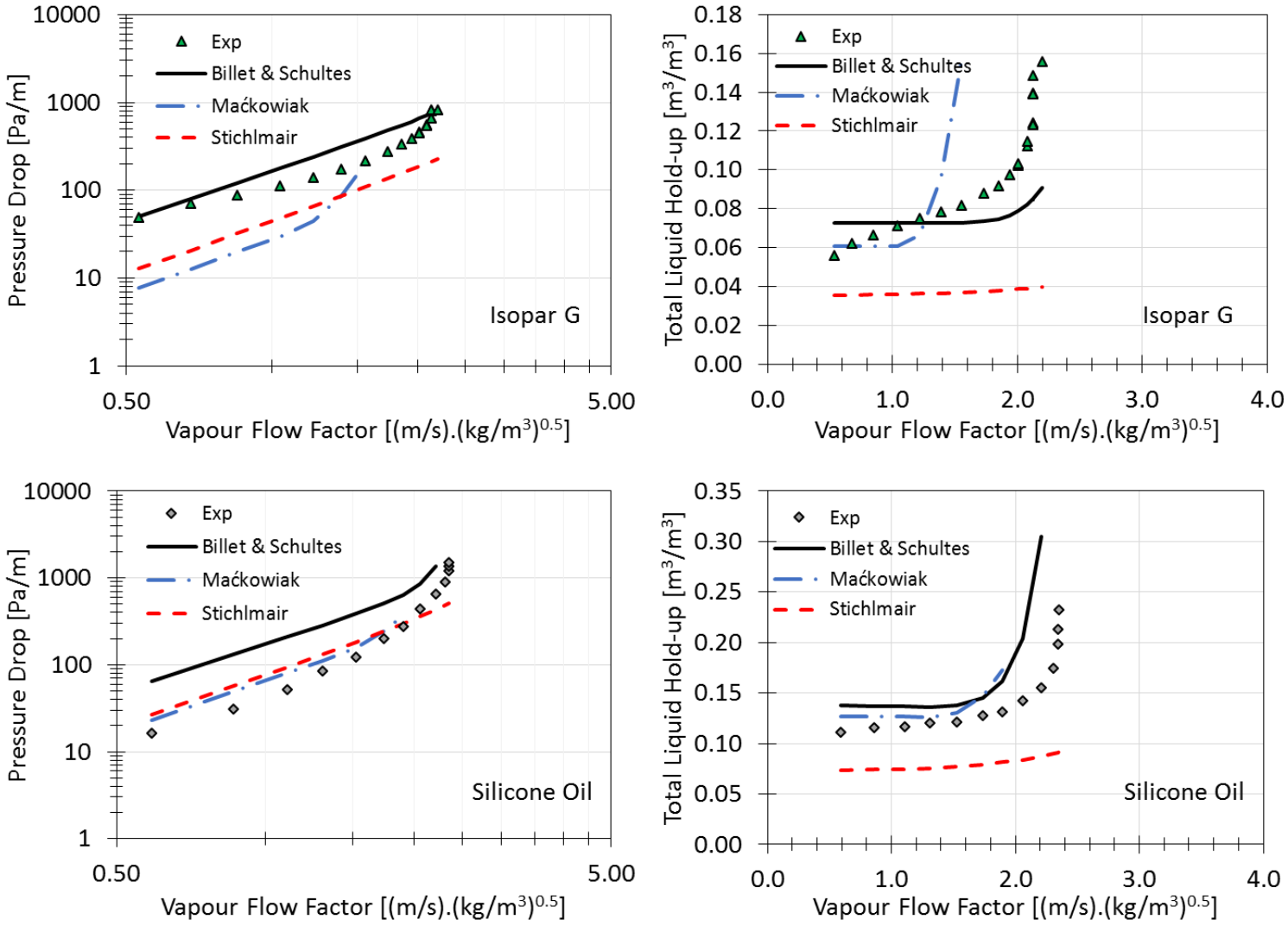

Figure 9.106: Billet & Schultes, Maćkowiak and Stichlmair models, 2.5" Intalox Ultra A, CO_2, Isopar G & silicone oil at 98 $m^3/(m^2.h)$

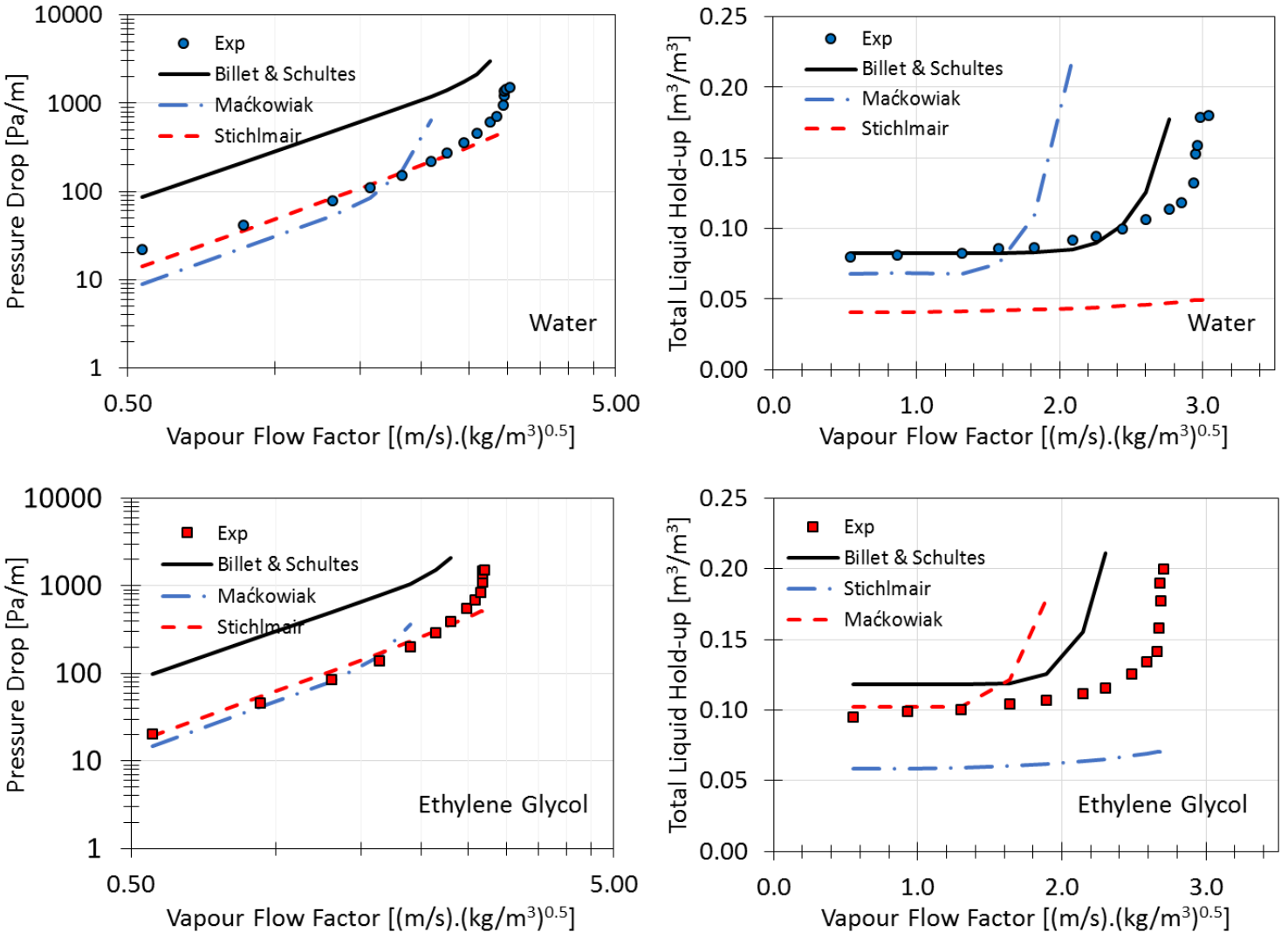

Figure 9.107: Billet & Schultes, Maćkowiak and Stichlmair models, 2.5" Intalox Ultra A, CO_2, water & ethylene glycol at 122 $m^3/(m^2.h)$

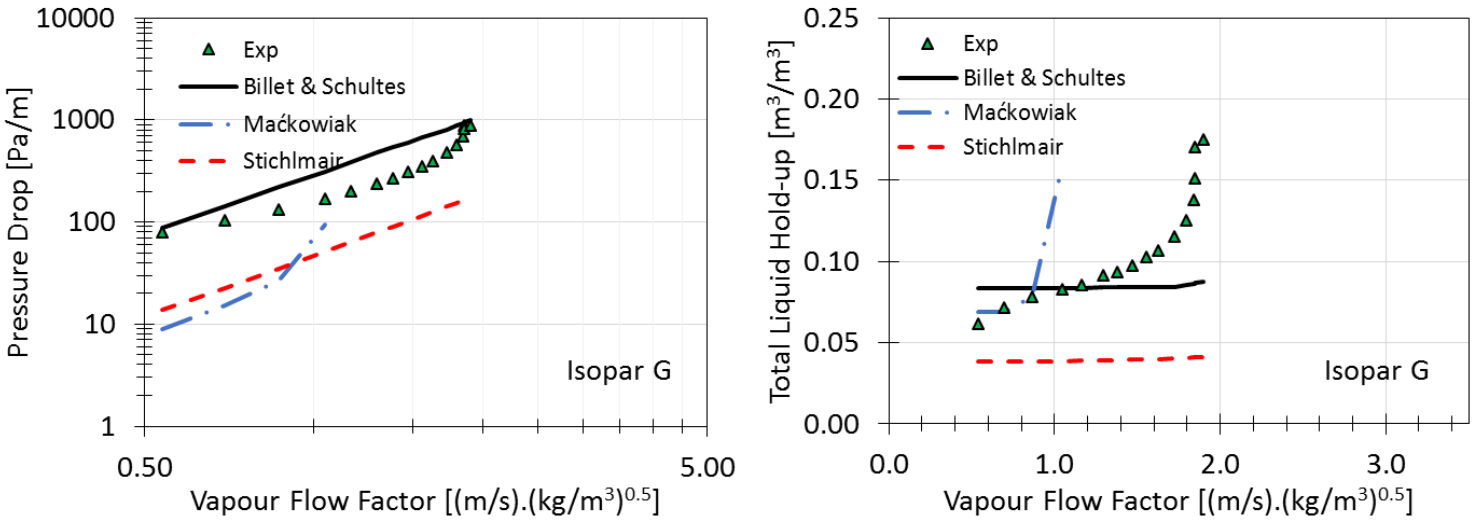

Figure 9.108: Billet & Schultes, Maćkowiak and Stichlmair models, 2.5" Intalox Ultra A, CO_2, Isopar G at 122 $m^3/(m^2.h)$